Evaluation of urban development impacts on the microclimate variations in tropical cities

Thesis

submitted in partial fulfilment of the requirements of the degree of

Doctor of Philosophy

By

Sutapa Bhattacharjee

Roll No: 176104109

Under the Supervision of

Dr. Rishikesh Bharti

DEPARTMENT OF CIVIL ENGINEERING

INDIAN INSTITUTE OF TECHNOLOGY GUWAHATI

GUWAHATI- 781039

Indian Institute of Technology Guwahati

DECLARATION

I, Sutapa Bhattacharjee, declare that this PhD thesis entitled "Evaluation of urban development impacts on the microclimate variations in tropical cities" is carried out by me under the guidance of my supervisor.

I certify that,

1. This thesis is a presentation of my own original research work

2. Any part of this thesis has not been submitted for any degree or diploma or any other qualification either in this institute or in any other university

3. Whenever I have referred to any published things or quotes from other resources, every effort has been clearly accredited by citing them in the text of the thesis work

4. Whenever contributions of others are involved, I have acknowledged to indicate this clearly

5. I confirm that the present thesis is free from plagiarism to the best of my knowledge and I take the whole responsibility if any complaint arises

6. I also affirm that my supervisors are not in a position to check for any possible instance of plagiarism within this submitted work

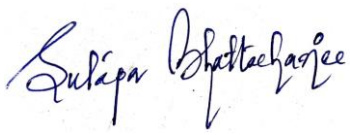

Signature

Date: 10-April-2024

Place: Guwahati

Indian Institute of Technology Guwahati

CERTIFICATE

This is to certify that the thesis entitled "**Evaluation of urban development impacts on the microclimate variations in tropical cities**" submitted by Sutapa Bhattacharjee, in partial fulfilment of the requirements for the award of the degree of Doctor of Philosophy, to the Indian Institute of Technology Guwahati, Assam, India, is a record of the original bonafide research work carried out by her under our supervision and guidance at the Department of Civil Engineering, Indian Institute of Technology Guwahati, Assam, India. The thesis work, in my opinion, is worthy of consideration for the award of the degree of Doctor of Philosophy in Civil Engineering of the Institute. The work presented in this thesis has not been submitted in part or full to any other university or institute for the award of any degree/diploma.

Date: 10-April-2024

Place: Guwahati

RISHIKESH BHARTI

Assistant Professor, Earth System Science and Engineering
Department of Civil Engineering, IIT Guwahati

ACKNOWLEDGEMENTS

I take this opportunity to express my sincere gratitude to a lot many people who supported and helped me to make this dissertation possible.

First and foremost, I express my sincere gratefulness to my PhD supervisor and Dr. Rishikesh Bharti, Assistant Professor, Department of Civil Engineering, IIT Guwahati, for his guidance, encouragement and support in every aspect all through my PhD tenure at IIT Guwahati. I am deeply thankful for his unwavering mentorship, moral encouragement, and the research facilities and atmosphere he provided me in the lab throughout the duration of my PhD.

I am extremely thankful to my doctoral committee members Prof. Subashisa Dutta, Prof. S.N. Joshi, and Dr. Archana M Nair, for their guidance and valuable advice throughout this thesis work. I would also like to thank the Department of Civil Engineering, and the Indian Institute of Technology (IIT) Guwahati for all the necessary facilities provided during my PhD. I would specifically like to thank the Computer Center, IIT Guwahati and the Center for Development for Advanced Computing (CDAC), India for providing and maintaining the High-performance Computing (HPC) facility *Param-Ishan*, in the institute which facilitated the majority of my research. I would also express my gratitude to the Ministry of Human Resources and Development (MHRD), Government of India, for providing financial assistance (as monthly fellowship) during my entire PhD duration.

I would also like to sincerely thank all the data providers for open-source datasets as well as the other secondary information collected from different authorities, which helped in the successful completion of this work.

I would like to thank my family and all my friends who supported me during this entire journey. I shall forever be indebted to my parents Mr. Prodyot Bhattacharjee and Mrs. Anita Bhattacharjee and my siblings Ms. Soma Bhattacharjee and Ms. Pushpita Bhattacharjee for their relentless encouragement and moral support which helped me brave through the lows, and their love to enjoy the highs of this journey. I owe heartfelt gratitude to my senior Dr. Lekshmi K. and my friends Mr. Subham Awasthi, Mr. Siddharth Arora and Mr. Arnab Kr. Pal for always being there for me and also for their constant motivation, guidance and emotional support throughout. I also take this opportunity to sincerely thank all my lab mates, peers, juniors and friends in IIT Guwahati who have added value to my life here and also in general. Last but not least, I would like to thank the Almighty for providing me this opportunity and helping me through every step in the process.

ABSTRACT

Urban forcing on the overlying atmosphere varies over a wide range of scales, developing intense urban-atmosphere interactions resulting in the generation of small-scale, intense, and highly unpredictable climatic systems. A detailed understanding of these interactions, especially in the case of highly heterogeneous and compact cities from the developing regions, which generally coincide with the active tropical climate belts, has remained a formidable challenge in this field of research. The advantages of numerical weather prediction (NWP) models to understand the land–atmosphere interactions and their ability to dynamically downscale coarser resolution global climate products integrated with higher resolution surface parameters has been a widely accepted approach in studying this process. However, the accurate representation of urban morphology is critical in improving the potential of mesoscale NWP models like WRF (Weather Research and Forecasting) to simulate the micro-climatic conditions over the cities more precisely. This study adopted a two-city approach to analyse the urban–atmosphere interactions in the case of the complex tropical region by selecting two dimensionally different cities, i.e., Kolkata and Guwahati, which also differed in terms of urban intensity. Both cities are situated on the most active monsoon belt of the Indian sub-continent, which also has significant influence on their regional climatology. A high-resolution uWRF model was configured considering the general climatology of the region and incorporating improved urban surface characteristics using Local Climate Zone (LCZ) maps. Advanced deep learning-based image classification techniques were applied to derive the LCZ products from high resolution Planetscope satellite images at an overall accuracy of 71.33% and was 78.69% for Kolkata Metropolitan Area (KMA) and Guwahati Metropolitan Area (GMA) respectively. A rigorous set of experiments were performed employing different combinations of the physical parameterizations and urban schemes required by WRF to identify the most optimal configuration of the coupled uWRF-LCZ model. This high-resolution model was further used in analysing different scenarios to understand the nature of micro-scale interaction between urban surfaces and the overlying climate, with the purpose of enhancing the understanding of urban micrometeorology under varying natural and anthropogenic conditions.

The modelled results for important climate variables like T_2 (2m air temperature), T_s (surface/skin temperature), WS (10m wind speed), RF (cumulative rainfall), RH (2m relative humidity), etc. were analysed in detail according to the four predominant LCZ classes, viz. LCZ 2, LCZ 3, LCZ 5 and LCZ 6 (representing the complexity of urban morphology) observed to cover almost the entire built-up extent of the cities. Diurnal as well as seasonal analysis of these variables indicated a significant impact of the city geometry on the immediate meteorological conditions for both cities. The climatic variations from most complex urban areas (overlapping with the city core) towards the outskirts of the city were most prominent during the pre-monsoon season for both cities. The core city with the highest and most compact built-up configuration was observed to be almost 2.5 °C to 3°C warmer than the surrounding

vegetated areas during the day and about 1.8°C to 2.5°C at night in case of KMA and upto 5 °C during the day and 3.5 °C at night in case of GMA revealing the distinct UHI effect for both cities. A gradual decline in T_2 values in a range of 0.2 – 0.5 °C and an increase in WS values in a range of 0.5 – 1 ms^{-1} with each consecutive urban LCZ class was observed, implying the direct impact of compact urban geometry on local climate. Although the other variables like T_s and RF also followed a declining trend in this direction, the transformation did not exactly follow a gradual trend. It was evident from the findings that the micro-meteorological variations were relatively much lesser in the case of monsoons and the least during winter seasons. The analysis further revealed that the dimensions and intensity of urbanization has a definite impact on the synoptic scale weather event such as monsoons, as a gradual increase (3 – 5 mm) in the RF magnitude was visible from LCZ 2 to LCZ 6 which further increased (upto 15 mm) in the non-urban surroundings. However, these variations in RF were more vividly observed in case of the larger and denser KMA region whereas, it seemed to be influenced more by the local topography in case of the relatively smaller and less dense GMA. Moreover, evaluation of the urban-climate conditions according to the changing urban landscape over 20 years also revealed a similar trend. Analysis of these parameters with much reduced anthropogenic functions during the COVID-19 lockdown phase in 2020 showed a considerable improvement in the meteorological conditions compared to the usual trend in 2019. A significant decline in T_2 upto 5 °C for both cities and improvement in WS up to 4 ms^{-1} in case of KMA was observed, which further indicated the role of urban dynamics in altering the local climate. This substantial reduction in the UHI effect could be attributed to the reduced anthropogenic functions leading to improvement in air quality and ultimately the living conditions in these cities, which also provides an opportunity for the planners to devise appropriate UHI mitigation strategies by limiting anthropogenic activities in a controlled manner.

The local geography, along with the urban geometry, roughness length, and urban fabric, play the most crucial role in determining the magnitude of microclimatic variations typical to a city. Thus, an optimal urban micro-climate index (UMCI) was developed to evaluate the combined effects of the different climate variables on the intra-urban climatic conditions. This index can be a helpful tool in assessing the urban meteorological health identifying the most liveable as well as the vulnerable pockets within the cities during different phases of the day. Further, modifications in the existing urban morphology by implementing suitable heat mitigation measures proved to be an important strategy to address the adverse climatic effects on densely populated developing cities by reducing the magnitude of the sensible heat fluxes and latent heat capacity. However, it was found that the same strategy might not be similarly effective throughout the city or in reducing the adverse effects of different climate variables alike; which might help in making more informed decisions to implement suitable techniques in different parts of the city for managing micro-climate variations.

CONTENTS

LIST OF FIGURES

LIST OF TABLES

LIST OF ABBREVIATIONS

ARW	Advanced Research WRF
APHRODITE	Asian Precipitation-Highly Resolved Observational Data Integration Towards Evaluation of the Water Resources
CAPE	Convective Available Potential Energy
CFD	Computational Fluid Dynamics
CMORPH	Climate Prediction Center Morphing Method
CNN	Convolutional Neural Network
GHF	Ground Heat Flux
GHG	GreenHouse Gases
GMA	Guwahati Metropolitan Area
GPS	Global Positioning System
HVAC	Heating Ventilation and Air Conditioning
IGBP	International Geosphere-Biosphere Programme
IMD	Indian Meteorological Department
JAXA	Japan Aerospace Exploration Agency
KMA	Kolkata Metropolitan Area
LCZ	Local Climate Zones
LHF	Latent Heat Flux
LSM	Land Surface Model
LW	Long Wave
MODIS	Moderate Resolution Imaging Spectroradiometer
NCAR	National Center for Atmospheric Research
NCEP	National Centers for Environmental Predictions
NMM	Nonhydrostatic Mesoscale Model
NOAA	National Oceanic and Atmospheric Administration
NWP	Numerical Weather Prediction
PBL	Planetary Boundary Layer
RF	Cumulative Rainfall
RH	2m Relative Humidity
SHF	Sensible Heat Flux
SVF	Sky View factor
SW	Short Wave
T_2	2m Air Temperature
T_2	Surface/Skin temperature
TEB	Town Energy Balance
TRMM	Tropical Rainfall Measuring Mission
UBL	Urban Boundary Layer

UC	Urban Canyons
UCL	Urban Canopy Layer
UCM	Urban Canopy Models
UHI	Urban Heat Island
UMCI	Urban Micro-Climate Index
WPS	WRF Preprocessing System
WRF	Weather Research and Forecasting
WS	10m Wind Speed

Chapter 1

Introduction

1.1 Context

Cities are the epicenters of economic and socio-cultural development attracting a huge magnitude of people and functions which tend to constantly increase with time, further strengthening this process. The rapid expansion of urban spaces and mechanisms are the most distinct anthropogenic activities observed over the last century (Condit 1970; Grimmond 2007; Roth 2007; Seto et al. 2011; Chen et al. 2014), characterized by the evolution of different urban structures and forms and diminishing blue-green spaces (Condit 1970; Oke 1987; Mills 2007; Seto et al. 2011; Song et al. 2014; Fleischmann et al. 2022). Urban areas accommodate about 55 per cent of the global population which is further projected to increase to about 70 percent by 2050, of which majority will be concentrated in the global south (Liu et al. 2014; Zhou et al. 2020; UN-Habitat 2022). However, in contrast, urban spaces constitute a little over 3 per cent of the total area on Earth (Gao and O'Neill 2020; UN-Habitat 2022), reflecting the grave disparity in the arrangement. The process of urban development gained momentum with advancements in technology and its accessibility, remarkably expediting the growth of urban centers both in magnitude and dimensions. However, the versatility and complexity of the urban systems depend on the nature and intensity of the process of urban development as well as urbanism in accordance with the available resources (Oke 1987; Batty 2005; Batty, 2008). The global urban areas contribute to more than 90 percent of the economic output, 65 percent of energy consumption and 70 percent of greenhouse gas (GHG) emissions (Solecki et al., 2013; Zhou et al. 2020). Thus, urbanization is considered indicative of the overall development of a region, making the phenomenon practically inevitable and almost irreversible (Awasthi et al. 2022; Bhattacharjee et al. 2023).

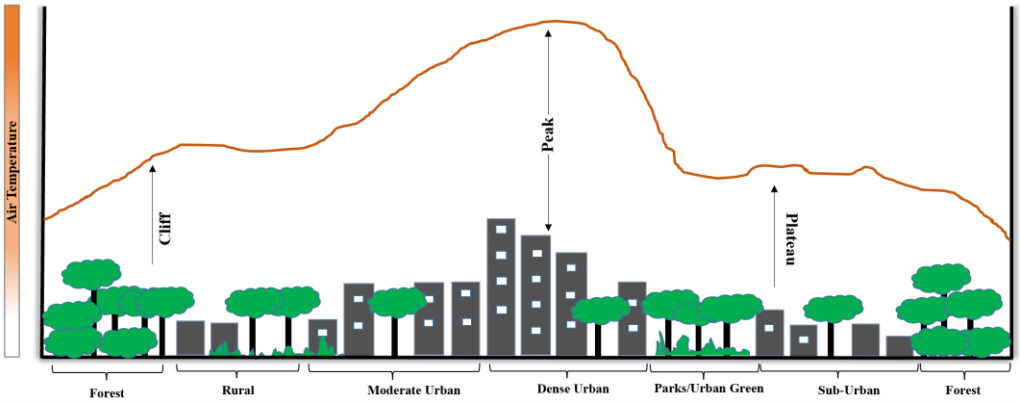

Figure 1.1 UHI Profile (Adapted from Oke, 1982)

These complex urban spaces constantly interfere with the natural systems around them, ultimately developing other complex urban-environmental processes; resulting from the modifications in the surface configuration, atmospheric structure, hydrological and bio-geochemical cycles, etc. (Oke 1987; Imhoff et al. 2004; Ioannides and Rossi-Hansberg 2005; Grimm et al. 2008; McDonald et al. 2008; Batisani and Yarnal 2009; Bhattacharjee et al. 2023). The natural environment works inclusive of all the existing physical, chemical and biological spheres interacting dynamically with each other at different spatial and temporal scales and changes in any aspect of this entire arrangement have a direct or diffused impact on the others (Zhou et al. 2004; Shephard 2005; Grimmond 2007). The interaction between cities and the overlying atmosphere is very intense through different vertical and horizontal levels, defining new atmospheric construct and boundary conditions (Oke 1988; Voogt and Oke 1997; Arnfield 2003). Cities tend to behave as heat source due to their higher potential in storing radiative energy owing to their surface properties; obstruction in atmospheric motion caused by increased surface roughness, further intensified by huge quantities of aerosols and other greenhouse gases (GHGs) from various urban sources; and poor quality of surface or groundwater retention capacity (Lowry 1977; Oke 1978; Becker and Li 1995; Arnfield 2003; Hidalgo et al. 2008; Barlow 2014). This leads to the modification of the atmospheric boundary layer over the urban extent, broadening the gap between urban and rural atmospheres. The constant and rapid interactions with the environmental processes have a significant forcing effect on the weather-climate circulations, resulting in the development of a small-scale, intense and highly unpredictable climatic system enveloping a city (Oke 1982; Voogt and Oke 1997; Hidalgo et al. 2008; Mirzaei and Haghighat 2010). Thus, cities are transformed into important local inducers of atmospheric variability, having an evident influence on the regional

to global climate systems to a considerable extent (Zhou et al. 2004; Shephard 2005; Grimmond 2007; Mills 2007; Roth 2007; Grimm et al. 2008; Zhou et al. 2015).

The concept of urban micro-climate was first scientifically established by Luke Howard in 1833 for London on the basis of definitive observations on the thermal distinction of the city from the non-urban surroundings (Oke 1982; Grimmond 2005). The extraordinary efforts by Howard led to the formation of this new domain within the meteorological studies, which accounted for the increase in the profile of air temperature (T_a), with increasing built-up density and decreasing natural spaces (trees, waterbodies, open scrublands). Since then, it was continuously explored and reinstated by researchers all over the world for cities of varying dimensions and functionalities, and the phenomenon was gradually documented as the Urban Heat Island (UHI) effect (Oke 1982; Arnfield 2003; Shephard 2005; Barlow 2014; Yang et al. 2016; Deilami et al. 2018; Sangiorgio et al. 2020; Du et al 2023). It was observed through space and time that the composition of the atmosphere over urban areas differs from their rural background (Landsberg 1981; Rosenfeld 2000; Ramanathan et al. 2001; Pataki et al. 2003; Heever and Cotton 2006) and the complexity increases with the increase in the level of urban development (Oke, 1987; Kaufmann et al. 2007; Grimm et al 2008; Li et al. 2017). A gradual rise in temperature is experienced from rural to peri-urban (cliff) and then to urban (plateau), with a maximum temperature being reached towards the city center (peak) (Fig. 1.1); i.e., areas with the most complex urbanization, with distinctive high buildings and narrow streets (Oke, 1987; Unger, Sümeghy, Zoboki 2001; Hidalgo et al. 2008). The impact of the cities on the overlying atmosphere is not restricted to the differential temperature profile but also affects the wind system, moisture content, atmospheric pressure, precipitation dynamics etc., which ultimately defines the entire urban micro-climate. With the increasing pace of urban development, these micro-climatic imbalances are gaining momentum and strength, aggravating the already intense process and prompting substantial changes even to the regional climate.

The widening gap between the inter as well as intra urban meteorological conditions has been constantly increasing the scale of associated risks. Urban heating, flood events, wind circulation, pollution load etc. have dramatically increased across all urban spaces, contradicting and heightening the challenges for sustainable development strategies (Ulpiani 2021; Bhattacharjee et al. 2021; Mentaschi et al. 2022). According to the IPCC (Intergovernmental Panel for Climate Change) AR6 Climate Change 2023 report, the past century has experienced significant changes with the rise in number of general heat wave

episodes, which worsens the UHI effect further, posing a threat to not only the health and wellbeing of the residents but also the urban infrastructure, transport facilities etc. (Luber and McGeehin, 2008; Zhou et al. 2020). The frequency of extreme rainfall events and consequent urban flooding phenomena has also increased manifold over the last few decades owing to rampant conversion of natural to built-up surfaces (Dasgupta et al. 2012; Sarmah and Das 2018; Bhattacharjee et al. 2021). Besides, intra-urban climatic variations within small horizonal distances further complicates these processes (Kim and Brown 2021; Bhattacharjee et al. 2021), demanding micro-scale analysis, so that meaningful strategies could be designed to address the specific challenges.

1.2 Scientific Rationale

The depth of the planetary boundary layer (PBL) depends upon the rate of interaction and energy exchange between the earth and atmosphere which also determines its rate of radiative warming or cooling (Oke 1987; Barlow 2014; Das et al. 2014). In the complex urban-atmosphere interface, the urban surface acts as source as well as sink of heat, mass and momentum, which controls the nature of lower atmospheric layers. The urban morphology has higher heat storage potential compared to the surroundings leading to an increase in thermal inertia of the surface, which is notably enhanced by the different anthropogenic heat sources, more apparent in the urban areas (Arnfield 1982; Oke 1988; Barlow, 2014). However, the complexity of urban surfaces attributed to their size, shape, composition and geometrical orientations further complicates the process of energy exchange. The emission of longwave (LW) radiations governed by the temperature and emissivity of the urban surface ultimately increases the surface heat flux and contributes towards stratification of the PBL into two distinct layers, i.e., Urban Canopy Layer (UCL) extending from the ground to roof level of the cityscape and Urban Boundary Layer (UBL) that extends vertically from top of the UCL to the level within PBL until which the influence of urban surface is perceptible, (Oke 1976; Oke 1988; Grimmond 2005; Rasheed 2009; Barlow 2014). The physico-chemical composition of these layers and determining their depth and density alter depending on the city size, physiographic setup, location, and population (Rasheed 2009; Barlow 2014; Crum and Generette 2017); ultimately defining the micro-climatic structure of the urban area.

It is fundamental to understand the concept of scale to grasp the entire process of urban-atmosphere interaction and energy exchange. An individual building with its own design and composition will have varying exposure to the incoming shortwave (SW) radiation, net LW

radiation exchange and ventilation in its different parts, encouraging the development of a building-scale energy budget system (Arnfield 2003). Similarly, the other urban morphological features such as streets, paved and non-paved areas, trees, irrigated gardens and lawns, non-irrigated green spaces have their respective thermal, radiative, aerodynamic and moisture properties, creating individual local-scale systems contrasting their surroundings but constantly interacting with each other by radiative exchange and micro-scale advections (Oke 1989; Grimmond et al. 1996; Arnfield 2003). Thus, to comprehend the total energy budget of these complex urban spaces, the individual features could be hierarchically aggregated to create urban surface morphological units. Urban canyons (UC) consisting of adjacent buildings packed together and the elements lying between them represents the interaction and energy transfer between individual elements at the micro-scale (Oke 1982, 1988; Arnfield 2003; Oke et al 2017) (Fig. 1.2c). Several UCs and the roofs of adjacent buildings at the local scale together form urban blocks which further aggregate to form neighbourhoods, land-use zones, and finally the entire city (Oke 1982, 1988; Voogt and Oke 1997; Arnfield 2003; Hidalgo et al. 2008) (Fig. 1.2 a, b). Therefore, at each level, the urban morphological units build and adjust distinctive energy budgets, representing the area-weighted budget averages of the individual elements and distinctive interactions within themselves, which could be further extended by considering their advective interactions with the adjacent units at the same scale (Arnfield 2003). This highlights the significance of having a complete insight into highly heterogenous urban surface properties governed by the nature of urbanization to understand the urban micro-climate system of a city (Voogt and Oke, 1997).

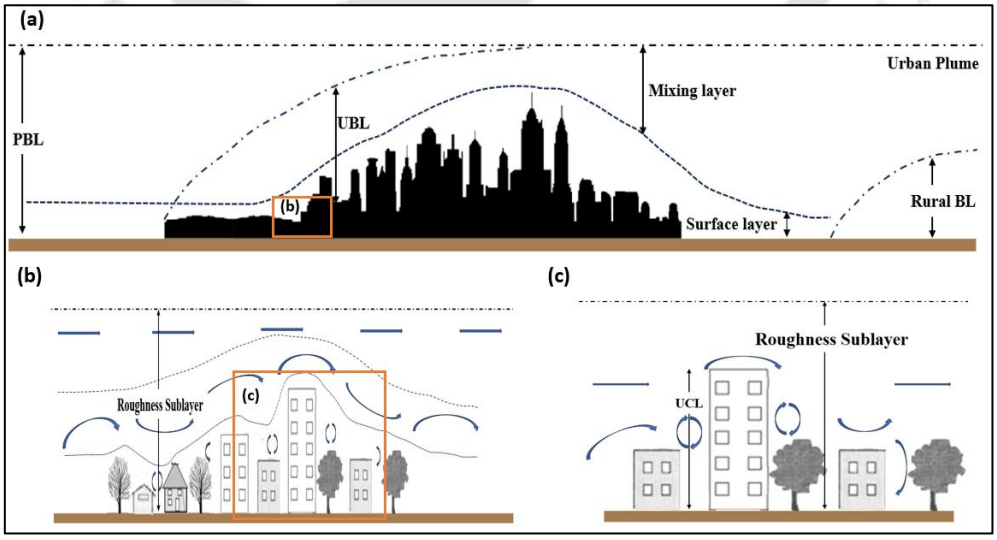

Figure 1.2 Atmospheric processes at different scales in urban areas forming different boundary conditions (Adapted from Oke 1997 and Barlow 2014)

Many observational and experimental studies conducted during the 1960s in the mid-latitudinal cities have analysed the importance of UBL in controlling climatic processes led by the energy fluxes between the atmosphere and urban (Oke 1978; Barlow 2014). However, as evident from the above discussion, energy and mass exchange between cities and their immediate atmosphere develops the more crucial UCL, designated on the basis of horizontal and vertical dimensions of the urban geometry (Oke 1976; Oke 1987; Crum and Generette 2017). The roughness length of cities determined by their aerodynamic properties contributes to the process dynamics as well as pollution dispersion within the vertical layers over the UCs through the UBL depth. Thus, the surface energy balance for a given volume encompassing the UCL can be explained by the following expression (Oke 1988; Arnfield, 2003),

$$Q + Q_F = Q_H + Q_E + \Delta Q_S + \Delta Q_A \qquad 1.1$$

where, Q is net radiation, Q_F is anthropogenic heat release, Q_H is sensible heat flux, Q_E is the latent heat flux, ΔQ_S is the storage heat flux, and ΔQ_A is the advective heat flux (flux here represents flux density).

$$Q = K' + L'$$

where, K' - net SW radiation, $K' = K\downarrow - K\uparrow$
L' - net LW radiation, $L' = L\downarrow - L\uparrow$
$\downarrow$ - incoming radiation
$\uparrow$ - reflected radiation

$$K\downarrow = S + D$$
$$K\uparrow = (K\downarrow)a$$
$$L\downarrow = \varepsilon_a[\sigma T_a]^4$$
$$L\uparrow = \varepsilon_s[\sigma T_s]^4$$

Here, S – direct beam
D – diffuse beam
a – surface albedo
ε_a - air emissivity
ε_s - surface emissivity
σ – Stefan-Boltzmann constant
T_a – air temperature
T_s - surface temperature

The huge magnitude and diverse range of activities of city dwellers that accounts for the emission of heat from vehicles, industries, building HVAC (heating, ventilation and air conditioning systems), metabolism of individuals within the UCs integrates to contribute towards Q_F within this volume. Q_H rises due to surface properties and Q_E dips resulting from diminishing vegetation cover, low transpiration as well as low rainfall interception,

determining the growth rate and depth of the UCL (Oke, 1987; Nakayoshi et al. 2009; Barlow 2014). The ΔQ_S is determined by all the different urban features that absorb and radiate heat within the UC volume including atmospheric particles; and ΔQ_A corresponds to transfer of energy through the sides of the volume (Arnfield, 2003). Several micro-scale processes occurring within the UCL such as surface drag, shearing stress turbulence and wind profile induced vertical motions etc., (Arnfield, 2003) are governed by the above stated parameters. UCL is therefore formed by localized processes induced by the urban land-use type and city function, giving rise to convective plumes and eventually converting to typical UHIs, varying spatially even over the same city (Oke 1987; Arnfield, 2003; Kim and Brown 2021).

UHI is significantly moderated by the city morphology and regional flow characteristics, as multicellular UHI patterns might develop in high-density metropolis with multiple cores and low wind speeds (Oke 1987; Unger, 2004). The city geometry and fabric are responsible for creating heat traps within the urban canopy, affecting the surface and air temperature, air pressure, wind velocity and surface and ground moisture content (Oke 1981, 1988; Coseo and Larsen 2014; Xu et al. 2017). Building height and street width, along with the sky view factor (SVF) and surface albedo, play a major role in the heat fluxes and wind circulation vertically within the city canopies (Oke 1988; Unger 2004). The prevalence of trees, urban green and open spaces significantly affects the energy flux and thermal properties of the atmosphere, regulating the localized effect of UHI (Landsberg 1981; Wong 2005; Morris et al. 2016).

UHI generally follows a diurnal cycle, being more prominent during the night as compared to day, with higher contrast between the urban and rural temperature profiles (Giridharan et al. 2005; Ramamurthy and Bou-Zeid 2016). The UHI condition increases gradually from afternoon and reaches the peak at around late evening persisting through mid-night and diminishing in the early morning hours (Kim and Baik 2002; Kusaka and Kimura, 2004; Shephard 2005; Hamdi and Schayes 2008; Giannopoulou et al. 2010; Ferreira et al. 2013). It is characterized by rura-urban pressure difference and vertical mixing and also due to slower cooling rate of the urban features (Fujibe and Asai 1980; Oke 1981; Lin and Smith 1986; Giannopoulou et al. 2010), resulting from LW radiation emitted throughout the night (Shephard 2005; Hidalgo et al. 2008). In low ambient temperature conditions, the cooling rate increases substantially due to high wind speeds as a result of convective losses. However, in dense urban canopy regions, the wind speed drops (being highly undisturbed), leading to an increase in ambient temperature due to convective gains; further dipping the cooling rate (Giannopoulou et al. 2010). Thus, heat generated by the cities is also one of the main driving forces to initiate

disturbances in other climatic processes such as precipitation, humidity, wind flow etc. (Kurbatskii; 2001; Jin et al. 2007).

A significant number of studies have also reported the influence of urbanization on the precipitation conditions at a local as well as regional scale (Kurbatskii; 2001; Molders and Olson 2004; Shephard 2005; Guo et al. 2006; Kishtawal et al. 2010; Mishra et al. 2012; Rana et al. 2012; Dash et al. 2013). Moisture availability in the environment and the convective circulation are intrinsically related to land-atmosphere interactions. As has been implied earlier, thermal stratification within the urban boundary layer influences the mesoscale circulation, leading to the formation of convective clouds (Akermann et al. 1977; Bornstein and Lin 2000; Shepard et al. 2002; Shephard 2005; Shiraki and Shigeta, 2013). Growth in surface roughness and complexity in urban geometry causes modifications in wind direction and velocity which can divert the precipitating systems (Akermann et al., 1977; Thielen et al., 2000; Burian and Shephard 2005). In addition, the urban functions are highly favourable for the rise in the level of aerosol concentration in the atmosphere, producing abundant hygroscopic nuclei particles (Huff 1986; Rosenfield 2000; Ramanathan, et al. 2001; Shephard, 2005; Heever and Cotton 2006), which enhances the moisture load in the atmosphere leading to short-term high-intensity rain events (Dixon and Mote, 2003). These potential factors instrumenting urban precipitation conditions operate in close correspondence to each other, occasionally one being the initiator or resultant of the other (Huff 1986; Rosenfield 2000); and are required to be observed or analyzed together for a comprehensive understanding of the phenomenon.

Studies from across the globe have drawn connections between the UHI effect and urban precipitation and the feedback mechanism that follows, influencing other climate parameters (Huff and Changnon 1972; Akermann et al. 1977; Sundersingh et al. 1991; Deosthali et al. 1999; Bornstein and Lin 2000; Shephard et al. 2002; Shephard and Burian 2003; Chand et al. 2005Shephard 2005; Ramachandran et al. 2010Ganeshan et al. 2013). The vertical mixing heights of the thermal flux invigorate, and deepen due to high urban temperature accumulation, ultimately increasing the ascending vertical velocity at the cloud base, resulting in downward propagation of the clouds, destabilizing the flow pattern (Akermann et al. 1977; Shephard 2005; Guo et al. 2006; Zhong and Yang 2015). As a result, the squall line breaks and smaller individual convective cells are formed over the urban area (Zhong and Yang 2015), causing spatial variability in precipitation even within the same city. Therefore, downwind rainfall increases over cities caused by UHI-induced unstable boundary layer circulation, reinforcing already existing storms or introducing new convective systems (Huff and Changnon 1972;

Akermann et al. 1977; Bornstein and Lin 2000; Shepherd and Burian 2003; Dixon and Mote 2003; Shephard 2005; Heever and Cotton 2006; Ganeshan et al. 2013). Besides, the urban canopy and high surface roughness also have considerable effect on the local convective systems causing micro-scale variation in downpour pattern (Bornstein and LeRoy 1990; Niyogi et al. 2011; Shiraki and Shigeta 2013).

1.3 Motivation

The degree of complexity in urban climatic processes is determined by the level of heterogeneity of the surface geometry and morphology. Due to the structural versatility of urban areas across the globe owing to differences in their physiographic conditions, level of economic development, anthropogenic functions, built-up and population density, configuration and composition of the surface fabric, nature and extent of UCL also varies substantially (Henderson 2002; Roth 2007; Barlow 2014; Mentaschi et al. 2022; Yan et al. 2022; Du et al. 2023). Although there is considerable variation between cities across the world according to the aforementioned factors, differences are more prominent amongst cities from developing and developed regions (Roth 2007; Grimmond 2007; Kotharkar and Ghosh 2021; Mentaschi et al. 2022), indicating towards the probable difference in forcing mechanism on the urban atmosphere. This emphasizes the importance of critical and minute analysis of the extremely dynamic and intricate urban systems, which are distinct from their surroundings and capable of micro to macro scale transformations.

The urban climate research, since its inception till the present, is highly skewed towards developed cities compared to cities from the developing world, where the observations and analysis of these processes began much later with very slow progression and limited geographical coverage (Roth 2007; Kotharkar and Bagade 2018; Khan et al. 2020a; Marcotullio et al. 2021; Gyimah 2023). However, the percentage of global urban population is higher in the developing world and is expected to rise further. Moreover, due to unplanned and haphazard urban development the morphological composition of these cities is highly heterogeneous, raising the degree of complexity (Henderson 2002; Cohen 2006; Diksha and Kumar 2017; Arfanuzzaman and Dahiya 2019). The developing and underdeveloped regions mostly coincide with the tropical zone where the meteorological processes are inherently more complex and difficult to predict (Sachs 2001; Ramankutty et al 2002; Sobel 2012). Cities located in the tropics and subtropics experience intense UHI compared to higher latitudes; being more pronounced during the summer days as UHI intensity is predominantly driven by

solar radiation heating of the urban canopy at lower latitudes (Jauragui 1997; Arnfield 2003; Roth 2007; Ferreira et al. 2013; Li et al. 2016; Garuma 2023). However, anthropogenic heating is less pronounced in lower latitudes, and the seasonal UHI intensity variation is mostly regulated by the difference of soil moisture between urban and rural (Imamura, 1991; Arnfield, 2003; Roth, 2007). On the other hand, in mid and higher-latitude cities, the anthropogenic energy flux due to air conditioning greatly contributes towards generating and sustaining the UHI, especially during winters and at night (Oke 1982; Morris and Simmonds 2000; Arnfield 2003; Kusaka and Kimura 2004).

The highly developed cities lying in the temperate region with high-rise building canopies and lesser SVF experience lower temperatures at the pedestrian level, as opposed to the lower altitude and irregular urban canopies of the moderately or less developed cities of the tropics (Coseo and Larsen 2014; Xu et al. 2017; Nikolopoulou et al. 2019). The haphazard and unplanned expansion of built-up spaces due to increasing pressure from the growing population takes a toll on the blue-green spaces within cities further deteriorating the urban-meteorological conditions. The abnormal heating effect of the urban surface directly influences the thermal comfort and health conditions of city dwellers along with influencing other weather parameters (Matzarakis et al 2011; Burkart et al 2014; Nikolopoulou et al. 2019). Cases of extreme heat stress are rising throughout the globe, but the situation has worsened especially in the tropical and sub-tropical cities with already hot and humid climatic conditions and prolonged summer periods (Roth 2007; Kubota et al. 2017; Kotharkar and Ghosh 2021; Das et al 2022; Yan et al. 2022; Garuma 2023). The heat exposure of the city dwellers in the metropolises as well as medium-sized cities in the developing region is comparatively higher pertaining to the inaccessibility to adequate living infrastructure for a major section of the urban population (Lapola et al. 2019; Iqbal et al 2022; Laue et al. 2022; Parkes et al. 2022).

But unlike the UHI effect, which is always directly proportional to urban growth; the strength and robustness of urban-induced precipitation dynamics cannot be generalized as drawn from the varied conclusions with respect to it (Molders and Olson 2004; Shephard 2005; Kaufmann 2007). Some studies pointed out that the magnitude and intensity of rainfall events are localized, having distinctly changed with the progressions in urbanization (Ackerman et. al. 1977; Shephard 2005); while some have also reported the signature of urban development on regional convective circulations (Shastri et al. 2015; Liu and Niyogi 2019). The moisture availability and fluxes, location and geomorphological condition, canopy structure influencing the vertical vorticity, heat and aerosol accumulation determine the precipitation pattern in the

cities, which require deeper analysis and understanding. Although increasing thermal gradient in cities is one of the most evident consequences defining the phenomenon called urban climatology, precipitation anomalies over the cities have a short-term but relatively more direct and adverse impact on the living conditions of city dwellers, either leading to high surface runoff or depletion in the groundwater table beneath (Shephard, 2005; Jin et al. 2007; Bhattacharjee et al. 2021; Awasthi et al. 2022). These have become recurring problems in cities from the global south with an extensive rate of built-up expansion catering to the pressing need from escalating growth of the urban population (Bhattacharjee et al. 2021).

This demands a thorough and systematic understanding of the energy fluxes and correlation between the city geometry, which is also a function of the type of data used, acquisition time and weather conditions, procedure and accuracy of analysis (Sheng, Tang, You, Qing and Hao; 2017), other than the surface and meteorological parameters. This broadens the scope of urban climate studies in the tropical and sub-tropical regions with high intensity climate events as well as complex urban structures. Most cities in these regions have similar developmental and structural patterns and experiences almost similar types of hydro-meteorological hazards, which are directly proportional to their rate of urbanization. Therefore, it is important to understand the micro – meso scale variations in the urban climate of such cities according to the surface configuration and also the level of their impact on the synoptic scale climate phenomena.

1.4 Research Aim and Objectives

To widen the spectrum of urban climate research in diverse climatic, geographical, and urban environments, this study aims at "modelling the energy fluxes between the heterogeneous urban surface and the overlying climate to understand the microclimatic variations in tropical cities using a meso-scale Numerical Weather Prediction (NWP) model". Two geographically, dimensionally, and morphologically different cities, Kolkata and Guwahati, lying in the monsoon-dominated belt of India, were identified as study areas to evaluate the process of climate–urban interactions considering the following research objectives:

i. Meteorological downscaling by integrating the mesoscale Weather Research and Forecasting (WRF) with improved urban parameterization to obtain finer-scale urban microclimatic variables.

ii. Simulation of different spatio-temporal scenarios to understand the urbanization impact on the tropical-urban climate.

iii. Comprehensive assessment of the urban climate conditions and possible impacts of heat mitigation strategies on the micrometeorology of the cities.

1.5 Geographical Focus

This study primarily aims to evaluate the impact of urbanization on the micro-climate system of highly heterogeneous and complex urban surfaces, characteristically representing cities from one of the fastest developing tropical zones of the earth. A two-city comparative approach was adopted here to understand the level of interaction and interference of urban with the overlying climate in cities of different dimensions and complexity. Kolkata and Guwahati cities were carefully selected for analysis from the East-North East zone of the Indian sub-continent (Fig. 1.3) as case areas that differ morphologically as well as dimensionally but lie in similar tropical – subtropical zone with hot - humid summer and dry - cold winter. Besides, both cities also lie in one of the most active belts of the south-east monsoon in the region and receive about 80 per cent of the total annual rain during the summer monsoon period, which is critical for hydro-climatic extremes (Mitra et al. 2011; Bhattacharjee and Kar 2022). Following the regional climatology of the Indian sub-continent, these cities also experience four distinct seasons, viz., Pre-Monsoon (Mar–May), Monsoon (June–September), Post-Monsoon (October–November) and Winter (December – February). However, depending on the exact time of arrival of monsoon rains across the sub-continent according to their geographic locations, the length and duration of these different seasons slightly vary.

1.5.1 Kolkata

Kolkata, the largest and third most populous metropolis of India is also one of the historical and most important urban centers of the global south, extending from 22°19’ N to 23°10’ N latitude and 88°40’ E to 88°33’ E longitude over an area of about 1831 km^2 (Census of India 2011; Das et al. 2022). The city functions as the administrative, economic, and cultural hub of the entire eastern India attracting population from the region and also the rest of the country. It is situated about 150 km from the northern coasts of the Bay of Bengal and could be identified as a semi-coastal city with significant influence on the coastal climate (Dasgupta et al. 2012). The city is situated at about 1.5 - 11 m above the mean sea level with an average of 8 m, at the lower deltaic plain of the Ganga River system with insignificant geomorphic variations, surrounded by alluvial flatlands and a large number of small and big water bodies and shallow wetlands (Bose and Mazumdar 2020; Das et al. 2022). Hoogly, a major tributary of the Ganga

flows longitudinally through the city almost dividing it into two equal halves (Fig. 1.3), providing access to the city from the Bay of Bengal making it one of the earliest trade ports in the eastern part of the Indian subcontinent.

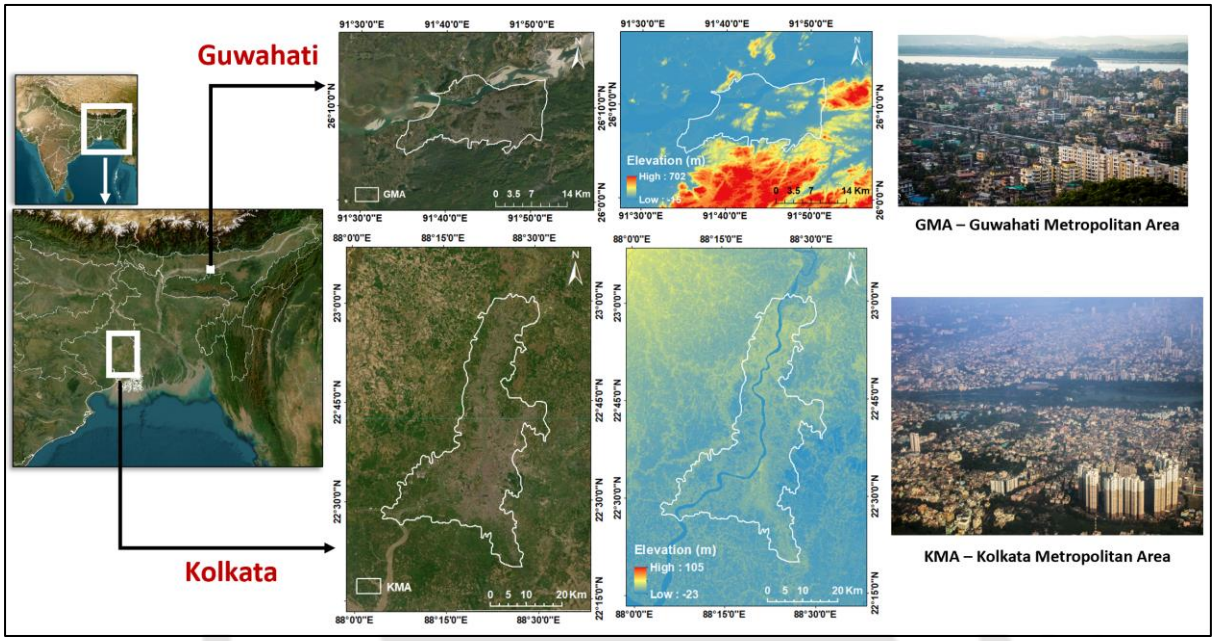

Figure 1.3 Study Region

The Kolkata Metropolitan Area (KMA) under the Kolkata Metropolitan Development Authority (KMDA) includes four different municipal corporations and 37 municipalities, making it a complex administrative unit (Dasgupta et al. 2012). The region has experienced urban population growth since the industrial revolution in the mid-19th century which has increased rapidly since the past century stimulating extensive planned and unplanned development leading to its horizontal as well as vertical expansion. KMA is estimated to accommodate about 20 million population which has increased from 4.5 million in 1951 to 15 million in 2011 at an average of about 8,000 persons per km^2 (Census of India 1951, 2011). As reported by several studies, the city transformed from an urban agglomeration to a metropolitan region over the past century at the cost of the surrounding natural ecosystem (Bhatta 2009; Chakraborty et al. 2021; Das and Jain 2022; Chatterjee and Mazumdar 2022; Bhattacharjee et al. 2023). Extensive conversion of natural surfaces (including forests and scrublands, barren lands waterbodies and wetlands) and agricultural lands into built-up surfaces (Bhatta, 2009; Parihar et al., 2013; Sharma et al., 2015), to accommodate the ever-expanding population and functions of the city has resulted in its areal expansion from 405 km^2 in 1951 to 1851 km^2 in 2021 at a decadal growth rate of 23.7 per cent approximately (Census of India 1951; 2011).

The built-up density of the city is very high with an extremely compact urban form and highly mixed land use land cover (LULC) pattern.

The annual mean temperature of this region is 24.8 °C and the average precipitation is 1600 mm, which is mostly received during the South-West Indian Monsoon period from June to September (Dasgupta and De, 2007; Mitra et al., 2012). Kolkata experiences prolonged summer season which almost begins from the early pre-monsoon and extends until the late monsoon period (Dasgupta et al. 2012; Khan et al. 2020b). The pre-monsoon season Kolkata region is a little longer than the average, extending from March to almost mid-June when the monsoon rains generally arrive, making the season a little longer than the average (Bhattacharjee et al 2023). The heat stress in the city is particularly severe during this period with extremely high temperatures ranging between 38 – 44 °C, due to the heat accumulated from higher insolation (the solar power) and LW radiation from the surface trapped by the higher concentrations of GHGs and lower wind speed (Khan et al. 2020b). After the advent of the monsoon season, T_s reduces substantially and the wind velocity increases which improves the heat wave episodes, but due to the higher level of relative humidity (RH), i.e., above 80 per cent the average drop in T_a is only 2 – 3 °C. The monsoon season experiences high-intensity rain episodes, the frequency of which has increased since the last decade leading to urban flood hazards across many parts of the city (Dasgupta et al. 2012; Malik et al. 2020), degrading the living conditions of the city dwellers.

1.5.2 Guwahati

Guwahati, one of the oldest urban centers of India, occupies the most dominant position in administration and trade in entire North-East India. The city lies between 25° 5’ N to 26° 12’ N latitude to 91° 34’ E to 91° 5’ E longitude and covers a large part of the Kamrup Metropolitan district of Assam. The Guwahati Metropolitan Area (GMA) sprawls over an area of 328 km^2 and accommodates more than 1 million people living within its administrative boundary (Census of India 2011). Guwahati lies at an average altitude of 55 m above the mean sea level (MSL) and lies on the south bank of the river Brahmaputra, making the river its northern boundary. On the south, it is bounded by the hills of Meghalaya state, and the tributaries of Brahmaputra, Khanajan and Bondajan line it along the west and east respectively (Bhattacharyya 2001). It contains some scattered hill ranges, reserve forests and a number of wetlands, which are shrinking with time due to the pressure of urbanization (Bhattacharyya, 2001). Guwahati city is adorned with tropical rainforest, which mainly includes semi-evergreen

and mixed deciduous types with three reserve forests lying within its territory. Besides, there are some other important natural vegetation units and wildlife sanctuaries that lie within the close vicinity of the city, having a definite impact on its climate system (Bhattacharyya 2001).

The spatial expansion of Guwahati has been caused by a huge population explosion over a short period of time. It enjoys a prime status in the region with the largest area and population base. According to the Census records, the population increased from 43,615 in 1951 to 9,68,549 in 2011, which is estimated to be around 1.3 million in 2021 (Census of India 1951, 2011). The average density of the population of the city is as high as 4468 persons per sq. km as per the 2011 census. The city center, old city, business centres as well as the newly developed residential areas show highest population density. This is indicative of the growing compactness and complexities in the LULC pattern of the city with time (Bhattacharyya, 2001; Pawe and Saikia 2018; Nath et al. 2021). The highly heterogeneous functional characteristics of the city have led to the excessive population influx and rapid urban development.

The average annual temperature of Guwahati city ranges from 24 - 30 °C and the annual rainfall received lies within 1600–2000 mm. The maximum amount of rainfall occurs during the monsoon months and it is lowest during the winter season following the general trend of the region (Bhattacharjee and Kar, 2022). The summer season coincides perfectly with that of monsoon when T_a is the highest with higher percentage of RH. The region used to receive lower magnitude rainfall for longer durations during the monsoon season, which has changed into high intensity shorter spells off late, leading to recurrent flood episodes within the city, also owing to its undulating topography and improper urban planning (Bhattacharjee and Kar, 2022). There has been a remarkable rise in the UHI effect and urban flooding episodes in Guwahati (Borbora and Das 2014; Sarmah and Das 2018; Mohammed and Goswami 2022; Bhattacharjee and Kar 2022), both in terms of intensity and spatial extent, pressing the requirement of hydro-meteorological analysis of the region.

1.6 Organization of the Thesis

The thesis comprises total of 7 chapters, the first being Introduction, providing the context and background of the topic and the motivation for pursuing the study. It also includes the objectives and the geographical focus of the study. The second chapter includes a detailed review of relevant literature including a brief introduction to the WRF model and its underlying principles. Chapter 3 corresponds to the first objective and discusses the methods adopted to

achieve high-resolution urban parameterization by generating and identification of optimum model parameters to calibrate the WRF model according to the present surface as well as meteorological conditions and obtain improved microclimate parameters. The fourth chapter deals with the second objective, which highlights the performance of the coupled WRF-Local Climate Zone (WRF-LCZ) model to simulate diurnal as well as seasonal variations in the micro-scale climatic conditions for both cities. Chapter 5 consists of scenario-based analysis to further understand the impact of urbanization on the local meteorology of both cities. The sixth chapter is associated with the final objective to explore the potential of heat mitigation measure to transform the existing urban climate and also to prepare a micro-climate index to ultimately analyse the overall micro-meteorological health of the cities. Finally, the seventh chapter provides the concluding remarks, limitations and recommendations of the study.

Chapter 2

Literature Review

2.1 Introduction

The chapter attempts to provide a systematic review of important studies related to urban climate research and discusses the variety of approaches, techniques and data that have been used over time to understand the associated processes. Due to the vast magnitude of available literature in this domain, this section was streamlined by recounting the most relevant studies significant towards understanding the evolution, concepts and approaches of the important urban climate indicators relevant to this particular investigation. A special emphasis was given to understand the capabilities of the meso-scale Weather Research and Forecasting (WRF) model to perceive the climatic structure of urban areas and recognize the micro-scale variations using high-resolution surface parameters across different climatic zones and urbanization levels.

2.2 Important Urban Climate Indicators

2.2.1 Urban Heat Island (UHI) Effect

The inception of the phenomenon called urban climate was synonymous with the UHI effect, i.e., the thermal distinction of cities from their surroundings. The concept was established by very important studies during the 19th and 20th centuries inspired by the monumental works of Luke Howard in London in 1833 (Oke 1989; Arnfield 2003; Barlow 2014; Stewart 2019). Careful and consistent observations of air temperature for over a 20-year period at the city center and three sites outside the city led Howard to conclude that difference in air temperature between London and the surrounding countryside is directly proportional to urban density and development (Stewart, 2019). He also acknowledged the contributions of increased

anthropogenic activities, including the transport systems, industries as well as human and animal metabolism within compact urban spaces, towards the heating intensity. This was followed by similar studies over the next century based on long-term observations of temperature differences in different cities such as Paris (Renou 1868; Hann 1885), Mexico City (Moreno 1895; Jauregui, 1973), Berlin (Perlewitz 1890), Vienna (Topolansky 1924), Moscow (Bogolepow 1928), Bath (Balchin and Pye 1947), London (Chandler 1960, 1965); Vancouver (Oke 1976) etc. which established the foundational concepts in urban climate research and ultimately the phenomenon called the UHI effect (Oke 1974; Stewart 2019). However, urban climate research gained momentum during the last quarter of the 20th century with the advent of sophisticated technology and communications (Oke 1976; Changnon et al. 1977; Landsberg 1981a; Voogt and Oke 1997; Arnfield 2003; Grimmond 2005). This next phase of the urban climate research contributed towards revealing the complex physical mechanisms in developing these isolated small-scale climate systems engulfing the urban areas (Oke 1978, 1981, Landsberg 1981a; Oke 1987, 1988a, 1988b; Immamura 1991; Voogt and Oke 1997). Thus, UHI studies, since its inception to the present, have been a convincing focus of climate research in built-up areas, as it displays diverse characteristics and is controlled by different facets of the energy exchange processes (Voogt and Oke; 1997; Kurbatskii; 2001; Arnfield, 2003; Jin et al. 2007; Barlow, 2014; Ren et al. 2017; Mughal et al. 2020).

Comparison of the mean annual temperature recorded by the weather stations in the urban and their non-urban surroundings, or between different cities, has been an important indicator for estimating the UHI intensities (Changnon et al. 1977; Gallo and Owen 1988; Ren et al. 2003; Gaffin et al. 2008). Comparison in historical and recent weather records have proved that UHI intensity varies spatially within the city, plummeting and escalating during different parts of the day with changes in the sun angle, with the core city recording a sharp increase of about 2 to 6.5°C (Giridharan et al 2004; Gaffin et al, 2008; Giannopoulou et al 2010; Mohan and Bhati 2011; Ferreira et al. 2013). Studies based on ground observations were conducted for cities like Mumbai (Kumar, et al. 2001), which estimated the difference in urban and rural temperature to be around 8.5°C on clear days; mean daytime and night time temperature to be 1.5 and 1.3°C for Hong Kong (Giridharan et al. 2004, 2005); maximum temperature difference between urban and rural to be 4.01°C for Singapore (Wong and Yu 2005); mean temperature difference of 7°C in Colombo (Emmanuel and Johansson, 2006); and 2.6 – 5.5°C at São Paulo (Ferreira et al. 2013). Significant variations were also recorded in the seasonal UHI conditions both in the tropical and temperate regions, depending on the solar insolation and other anthropogenic

functions. It was observed the heating potential of the tropical cities increased extensively during summers due to the higher intensity of the incoming solar radiation in the already warmer climate, which is further deteriorated by the compact urban structures (Emmanuel and Johansson 2006; Roth et al. 2007; Mohan and Bhati 2011; Mohan et al. 2013; Giridharan and Emmanuel 2018). The temperate cities experiences higher UHI during winter as compared to summer due to the contribution of air conditioning systems used almost in all building in the extreme cold climate, according to studies conducted in various cities in the mid-latitudinal region like Vancouver (Roth et al. 1989); Melbourne (Morris and Simmonds 2000); Seoul (Kim and Baik 2002); Atlanta (Dixon and Mote 2003); New York (Gaffin et al. 2008); (Toulouse (Hidalgo et al. 2008); Volos (Papanastasiou and Kittas 2012); Chicago (Coseo and Larsen 2014) etc.

The UHI effect was further categorised into the Surface Urban Heat Island (SUHI) and Atmospheric Urban Heat Island (AUHI) by studies estimating the temperature difference in T_s and T_a of the cities with the surrounding atmosphere (Hidalgo et al. 2008; Mohan et al. 2013; Barlow 2014; Mohammad et al. 2019; Tetali et al. 2022; Jain 2023). The trend of considering T_s as the proxy for T_a to estimate the UHI conditions increased, especially during the past few decades with the easy access to thermal remote sensing data products and lack of uniform means of in situ observation throughout the globe (Tetali et al. 2022; Jain 2023). Further, the concept of LCZ for assessing the UHI distribution in the city has been a convincing approach used by many researchers in the last few years by classifying the city landscape on the basis of urban features into heating zones of different intensities (Stewart and Oke 2012; Lao et al. 2015; Ren et al. 2017; Xu et al. 2018a). Studies conducted for cities like Kiev and Liev in Ukrain, as multiple cities in China and North America, reported the importance of higher resolution or integration of multi-sensor remote sensing data for the improvement in classification accuracy, which ranges from 60 % to 80 % in case of the moderate resolution data (Stewart and Oke 2012; Lao et al. 2015; Xu et al 2017; Xu et al. 2018b).

Similarly, an assessment of the UHI studies in Indian context revealed that like any other part of the world it began with ground observations from surface observatories as well as the mobile observations, either comparing the difference in T_a between the city with its surroundings or between several locations within the same city (Sundersingh et al. 1991; Deosthali et al. 1999; Devadas et al. 2009). However, the fate of AUHI studies suffered greatly due to the lack of systematically maintained network of surface observatories and also due to the lack of adequate resources which could authorize independent research bodies to undertake such mobile

observation missions more frequently (More et al. 2014: Kotharkar et al. 2018). This prompted the use of T_s as an important proxy in many of the initial UHI studies in India, as access to the these datasets were easier, flexible as well as cheaper compared to T_a and gained significance (Chand et al. 2005; Ramachandran et al. 2010; Bajaj et al. 2012; Mohan et al. 2012; Borthakur et al. 2013; Agarwal et al. 2014). Thus, it was observed that the SUHI studies could be located from all over the country since its inception (Veena et al. 2020) and is widely used even during the recent times (Gogoi et al. 2019; Mohammad et al. 2019; Jain et al. 2023).

The intrinsic relationships between the different climatic variables led to the inclusion of other climatic parameters such as wind systems, moisture availability, rainfall pattern, air quality etc (Fujibe and Asai 1980; Arnfield, 2003; Dixon and Mote 2003; Grimmond 2005; Barlow 2014) into this domain. Many of the UHI studies attempted to understand the wind velocity and moisture concentration in different parts of the urban areas along with the temperature distribution, which further explained the UHI variations. It was observed that the decrease in wind velocity with the increase in surface roughness had a definite impact on the temperature accumulation, further enhancing the UHI impact (Voogt and Oke 1997; Roth et al. 2007; Hidalgo et al. 2008; Bhati and Mohan 2016). Similarly, an increase in moisture concentration in the atmosphere had an additional implication on the feel-temperature and discomfort due to the UHI effect (Patel et al. 2020; Banerjee et al. 2022). Thus, the scope of UHI studies further expanded to include the dimension of thermal discomfort associated with the acute increase in the city's temperature, which has serious implications on the health and well-being of the city dwellers (Höppe 1997; Matzarakis et al. 2011; Ketterer and Matzarakis 2014; Banerjee et al. 2020). The specialized branch of biometeorology thus evolved, which studied the impact of urban heat accumulation on the indoor as well as outdoor ambient temperature using various indices such as Physiologically Equivalent Temperature (PET), Universal Thermal Climate Index (UTCI), Discomfort Index (DI) etc. (Höppe 1997; Matzarakis et al. 2011; Ketterer and Matzarakis 2014; Yin et al. 2023) These studies provided a deeper understanding of the UHI phenomenon and the need for its accurate evaluation and analysis.

2.2.2 Urban Precipitation Anomalies

The capability of urban surfaces to alter precipitation dynamics began to be explored more carefully in the latter half of the 20th century with the development of refined instruments and other techniques. Changnon (1968) was one of the first researchers to document an interesting anomalous behaviour of the convective precipitation a little downwind of Chicago at a place

called La Porte. This observation, also known as the La Porte anomaly, later motivated many such studies of precipitation anomalies over or downwind of large urban agglomerations around the globe (Shephard 2005; Han et al. 2014). The Metropolitan Meteorological Experiment (METROMEX) was one of the pioneering studies that was carried out in the United States during the 1970s to investigate the modification of mesoscale and convective rainfall by major cities (Changnon et al. 1977; Huff 1986). The results from METROMEX experiments revealed that urban developments led to increased precipitation during summer months, typically observed within and also 50–75 km downwind of a city, estimating an increase of 5–25% above normal (Changnon, et al. 1977). Huff and Changnon (1972), recognized an increase in the urban precipitation during the late afternoon and early evening periods by analysing the diurnal rainfall characteristics of the St Louis metropolitan area using data from the METROMEX network of 225 recording rain gauges. It was further analyzed that the rainfall peaks were due to increased rainfall magnitude rather than the initiation of new rainstorms. Analysis of the METROMEX data by various experts over and 15 – 40 km downwind of St. Louis revealed about 10 % increase in cloudiness, about 30 % increase in total rainfall, and absolute increase in extreme storm events (Changnon et al. 1977; Ackerman et al. 1977; Huff and Changnon, 1972). The METROMEX experiment was also one of the first studies to indicate a positive relationship between UHI and rainfall increase as a result of enhanced convergence within the PBL and increased surface roughness (Ackerman et al. 1977).

Several other important works that concretized the foundation of this domain were reported from cities like New York (Bornstein and LeRoy 1990); Bucharest (Tumanov et al. 1999); Atlanta (Bornstein and Lin 2000) Houston (Orville et al. 2001) etc., relating the impacts of urban development on the structure and movement of cloud systems and moving thunderstorms. With the advancement in technology, the capability of the mathematical models to relate the different climate variables within the UBL from regional to micro-scale enables researchers to improve the understanding of urban precipitation dynamics, which was difficult to achieve using only observational datasets (Han et al. 2014). Therefore, this domain of urban climate research particularly gained momentum in the past couple of decades and more analyses exploring the changes in distribution pattern, frequency and intensity of rainfall from cities all around the globe were undertaken (Shephard 2005; Han et at. 2014). The most important causes of precipitation anomalies in the urban areas as identified by different researchers could be directly related to i) changes in urban morphology and surface roughness

(Ackerman et al., 1977; Bornstein and Lin 2000; Thielen et al., 2000; Burian and Shephard 2005; Shastri et al. 2015; Liu and Niyogi 2019), ii) UHI effect (Huff and Changnon 1972; Ackerman et al. 1977; Shephard et al. 2002; Shephard and Burian 2003; Shephard 2005; Han and Baik 2008; Lin et al. 2011; Ganeshan et al. 2013; Zhong and Yang 2015), and iii) increased concentration of hygroscopic nuclei in the urban atmosphere due to anthropogenic activities (Huff 1986; Rosenfield 2000; Ramanathan, et al. 2001; Dixon and Mote, 2003; Molders and Olson 2004; Shephard, 2005; Heever and Cotton 2006). The intensity of rainfall was reported to have increased in a range of 12 – 30 % in these studies, which impacted the other aspects of the urban environment. Thus, UHI influence on precipitation and the importance of air pollutant concentration in its enhancement has been the basis of many recent studies, which established the relationship between urban expansion and in situ or downwind rainfall enhancement (Heever and Cotton 2006; Ganeshan et al. 2013).

The relationship between the urbanization and precipitation has been explored for the Indian cities, but the frequency of such studies is much less compared to the UHI studies. Similar to that of the temperature the impact of urbanization on rainfall in the beginning was dependent on ground observations mainly acquired from the Indian Meteorological Department (IMD) and a comparison between the magnitude and intensity of urban and rural rain episodes were drawn (Kishtawal et al. 2010; Mishra et al. 2012; Rana et al. 2012; Dash et al. 2013). However, the availability of gridded data products from Tropical Rainfall Measuring Mission (TRMM), IMD, Asian Precipitation-Highly Resolved Observational DataIntegration Towards Evaluation of the Water Resources (APHRODITE), have increased the frequency of studies emphasizing on urban precipitation due to the advantage of constant monitoring (Kishtawal et al. 2010; Vittal et al. 2013; Shastri et al. 2015). In the recent period, many studies have indicated the relationship between urbanization and extreme rainfall episodes, the trend of which has been increasing (Patel et al. 2020; Nadimpalli et al. 2022). Some studies have also corelated urbanization with the modifications in the summer monsoons for some Indian cities (Shastri et al. 2015; Bisht et al. 2017; Patel et al. 2020). However, such studies are relatively fewer and due to the complexity of the processes more such studies are required to concretize the concepts.

2.3 Approaches and Methods of Urban Climate Analysis

Urban Meteorology is a complex subject which can only be explained by methodical observations, experiments and mathematical simulations. Thus, on the basis of the approaches

adopted for analysis, urban climate studies can be broadly classified into two categories: *Observational or experimental*, which include physical measurement of the change in climate parameters over cities; and *Modelling or numerical simulation* of these anomalies, depending on the interactions between different parameters as well as with the surrounding environment (Imamura 1991; Grimmond 2005; Mirzaei and Haghighat 2010; Barlow 2014; Toparlar et al, 2015). The observational studies have the advantage of measuring the actual process in real-time as opposed to computational studies, which simulate the weather dynamics depending on some key inputs assuming near-real conditions, as the urban microphysical environment is very complex to replicate (Imamura 1991; Rasheed 2009; Toparlar et al. 2015). Observational studies are prominently featured during the early phases of urban climate analysis, while the mathematical modelling of the climate parameters has been gaining importance in the last few decades, although after being accepted and validated by ground-based observations.

2.3.1 Observational & Experimental Studies

2.3.1.1 Instrument-Based Observations and Experiments

In the latter half of the 20th century, more emphasis was laid upon understanding the causes and consequences of the UHI phenomenon observed for over a century inspired mega-scale experiments conducted by different research groups. A thermal anomaly over the urban and peripheral surfaces observed using time series measurements was one of the most viable and valued experimental approaches during that period in urban climate research (Bornstein 1968; Ackerman et al, 1977; Changnon et al. 1977; Ren et al. 2003; Stewart 2011). The concepts of atmospheric stratification above the urban spaces primarily induced by the thermal fluxes and other factors such as wind flow and atmospheric composition were established based on the UBL observations and experimental studies that began as early as 1960s in the mid-latitude region (Oke1978; Landsberg 1981; Oke 1995; Becker and Li 1995; Baik et al. 2007; Barlow 2014). It was noticed that near-surface energy exchange process becomes more complicated due to the presence of different urban features, including buildings, paved areas, streets, open areas, lawns, etc., intermitted by trees and plants of various types, with contrasting thermal, radiative and moisture retention properties (Oke 1988a; Becker and, Li 1995; Grimmond et al. 1996; Voogt and Oke 2003). This led to the temperature differences generating an important boundary condition within the PBL, which has been measured ever since the evolution of high precision instruments which have refined over time (Prata et al. 1995; Pielke et al. 2005). Thus, the key surface parameters like urban surface geometry, heat capacity, thermal conductivity,

roughness parameters, emissivity, albedo, wind velocity and moisture content, etc. began to be monitored parallelly to estimate temperature concentration in the cities using different techniques (Grimmond, 2007; Bechtel et al., 2012; Coseo and Larsen 2014).

Air temperature and emissivity from the urban features began to be recorded using sensors and radiometers placed in air balloons or helicopters flown periodically over the urban sphere of influence to determine the minor transition in energy fluxes (Changnon et al. 1977; Voogt and Oke 1997). Similarly, the BUBBLE field campaign was one of the most successful missions conducted to investigate the detailed boundary layer structure of the city of Basel, resulting in the identification of new parameterizations for canopy turbulence (Rotach et al. 2005). These studies. in spite of being rare, have achieved remarkable results and concretized the concept of micro-climatic variation with the intensification of urbanization. Studies were also reported from various cities where measurements from towers indicated high turbulence in eddy fluxes close to the urban roughness layer interface, as compared to smoother surfaces corresponding to rural terrain (Roth et. al, 1989; Schmid et al. 1991). This evolved the distinct idea of the impact of the heterogeneous urban land use and geometry on the immediate ambient temperature and its change according to the intensity and angle of the sun in clear sky conditions (Imamura 1991; Voogt and Oke, 1997; Kjelgren and Montague 1998; Grimmond 2005). However, the majority of such studies are conducted only as experiments because of being highly cost-sensitive and are limited to massive experimental projects, even for developed countries. Therefore, the trend of these studies persisted mainly for a few developed world cities having access to the experimental datasets (Ackerman et al, 1977; Changnon et al. 1977; Shephard 2005).

Most of the temporal variability in the UHI studies traditionally used observed data from pairs or groups of urban and rural or suburban weather stations (having long temporal records) or using instruments for in situ measurements of T_s as well as T_a (Bornstein 1968; Lowry 1977; Arnfield 2003; Stewart 2011). The installation of a dense network of weather stations throughout the city and its vicinity has proved to be a remarkable initiative in understanding the micro-level spatial variation in climate induced by the micro-scale local systems depending on the geometry of different urban canopies even within the same city (Voogt and Oke, 1997; Mirzaei and Haghighat 2010; Stewart 2011, Mohan et al. 2013; Kotharkar and Bagade. 2018). The significance of ground-observed meteorological products over the mathematical representation of the energy fluxes was recognized even by relatively recent studies from across the globe with the development of cheaper and better-quality instruments over time, which are

also easier to handle. Hardin et al. (2018) conducted a study for four different cities in the US incorporating data from the Observational Surface Research network, 'UrbaNet' operated by NOAA and Earth Networks for 17 different cities in the U.S. at present. Similarly, a study led by Mohan et al. (2013) installed a network of micrometeorological observational stations at 28 different locations according to the different landuse classes across Delhi during March 2008 for continuous measurement of temperature and relative humidity at 1-minute intervals for a period of 5 days. This thorough investigation concluded that horizontal stratification of Delhi UHI could broadly be categorized into three ranges: high UHI (8.6–10.7 °C) observed mainly within dense and commercial built-up areas; medium UHI (7.3–7.7 °C) mostly around low dense built-up areas and the riverside; and low UHI (3.1–6.9 °C) comprising of open and green areas. Similar studies that gathered data from different such already available weather monitoring networks or specifically calibrated instruments to monitor some important parameters were observed for many cities around the world like Toulouse (Hidalgo et al. 2008); São Paulo (Ferreira et al. 2013), Hongkong (Siu et al. 2013); Twin Cities metropolitan area of Minneapolis–St. Paul, Minnesota (Smoliak et al. 2015); Birmingham (Bassett et al. 2016); Nagpur (Kotharkar and Bagade 2018); Taiwan (Chen et al. 2018); Xi'an (Zhang et al. 2021). Due to the unavailability of such a dense network of instruments in the developing cities by the nodal meteorological agencies, most studies reported measurements from self-deployed instruments for a relatively small number of parameters. Such studies could reveal a better picture of urban–atmosphere interaction is fairly less and for a shorter duration in the tropical and developing zone compared to the developed regions.

2.3.1.2 Remote Sensing Based Observations and Experiments

To overcome this limitation, some sophisticated instruments, such as thermal sensors and data loggers which could be temporarily installed, began to substitute weather station data, especially for experiments involving relatively shorter study periods. Real-time and continuous measurements of weather parameters have also been attempted by mounting such portable instruments in cars travelling across a conurbation with Global Positioning System (GPS) loggers and temperature sensors on public buses for better spatial coverage. An innovative study conducted in Geneva called 'Climate urban walk' included the development of a portable monitoring system embedded in a backpack and carried during the walk to measure the real-time ambient temperature and humidity, directional radiation temperature, vertical temperature profiles at pedestrian level, thermal turbulence, wind speed (WS), direction and turbulence, noise level, air quality parameters such as CO2, NOx, ozone, micro particles, along with

hemispherical images of the sky and ground (Gallinelli et al. 2017). Further diurnal as well as seasonal PET was calculated using these parameters to understand the actual feel of heat stress at the pedestrian level. Yokoyama et al. (2018) installed thermometers and GPS loggers in bicycles to measure T_a conditions across Tokyo, considering different spatial resolution grids (10 – 100 m). The study concluded that higher resolution grids (10 m) could capture UHI hotspots for densely built cities, whereas coarser resolution grids (100 m) could only identify the UHI differences roughly. Such surface-level observations also helped in estimating temperature emitted from building facades and roads and were influenced by the presence of trees, open areas and traffic (Voogt and Oke, 1997; Kjelgren ang Montague 1998; Arnfield 2003; Coseo and Larsen 2014).

Such intense experiments helped the researchers to understand and establish the scientific rationale and mechanism of the effect of urban surface properties on the climate, impacting not only the thermal distinction but also the convective circulation regulated by the associated characteristic atmosphere. The METROMEX is one of the best examples of such extensive studies to investigate the modification of mesoscale and convective rainfall by major cities in the United States (Changnon et al. 1977; Huff 1986). Huff and Changnon (1972) analysed the diurnal rainfall characteristics in the St Louis metropolitan area using data from the METROMEX network of 225 recording rain gauges. Measurements from rain gauges have been the most reliable means for quantitative assessment of rainfall but have the disadvantage of limited spatial coverage due to point-scale measurement (Cecil et al. 2005; Petersen et al. 2005). This limitation was updated using weather radars with better spatio-temporal coverage (Bringi and Chandrasekar 2001) which were also instrumental for extensive research in forecasting studies (Bringi and Chandrasekar 2001; Shephard 2005; Cifelli et al. 2018). The precipitation studies have been recognized to cover either multiple cities, undertaking a regional approach (Changnon et al. 1977; Shephard 2005; Ganeshan et al. 2013; Zhong and Yang 2015); or a single city with very high-resolution datasets and detailed analysis (Burian and Shephard 2005; Lei et al. 2008; Niyogi et al. 2011; Cifeli et al. 2018).

Continuous and long-term measurements of meteorological parameters became a reality with the advancement of technology, giving rise to the thermal and infrared revolution of remote sensing techniques for obtaining land surface temperatures (LST) (Prata et al. 1995; Voogt and Oke, 1997, 2003), and spaceborne radar sensors for measuring precipitation magnitudes (Shephard et al. 2002; Cecil et al. 2005; Petersen et al. 2005). Meteorological products derived from satellite, airborne and terrestrial sensors have greatly expanded the horizon of climate

analysis and were continuously exploited and advanced with respect to the foray of climate research (Arnfield 2003; Shephard 2005). Radiative thermometry using thermal infrared sensors placed at the high and medium altitude platforms has improved estimation of urban surface temperature significantly (Voogt and Oke, 1997). Remote Sensing data products accompanied by geospatial analysis have come up as exceptional tools for urban climate studies, as the land surface parameters could be constantly monitored and related with the climate dynamics, non-feasible in case of ground-based measurements (Arnfield 2003; Grimmond 2005; Bechtel et al., 2012; Chrysoulakis et al. 2018). However, these instruments do not always measure the parameters directly and require some mathematical assumptions and transformations to estimate the surface meteorology. However, due to their easy access and application for large-scale spatio-temporal analysis with computations, they have been categorised as observational techniques in the current study.

The thermal Infrared (TIR) remote sensing approach for land surface temperature (LST) estimation, widely applied in UHI studies (Voogt and Oke 2003; Weng 2009), could be considered as an observational technique, although it does not directly measure the surface temperature. The radiant temperature received by the sensors is used to compute the LST after correcting for spectral emissivity corresponding to different land covers (Prata et al. 1995; Voogt and Oke 2003; Tran, et al. 2006). The application of remote sensing data products to estimate LST started from the important cities lying in developed countries like Dallas (Gallo and Owen, 1988), and has been widely applied to many cities throughout the tropical and sub-tropical region, which on validation with available ground observations provided agreeable results. Different algorithms sophisticated numerical and physical models have been developed in due course, such as Mono and Split Window algorithms (Wan 1999; Tang et al. 2008; Qin et al. 2001), energy balance and radiative transfer models (Barsi et al. 2005), Gaussian models (Streutker,2003) etc., for better estimation of LST. This at-sensor radiant temperature was utilized to calculate the LST in many studies either for an individual city like Vancouver (Roth et al. 1989); Seattle (Roth et al. 1989); Paris (Dousset and Gourmelon 2003); Los Angeles (Dousset and Gourmelon 2003); Beijing (Hung and Yoshifumi 2005); Tokyo (Hung and Yoshifumi 2005); Seoul (Hung and Yoshifumi 2005); Tehran (Bokaie et al. 2016) etc.; or as an integral part of several field campaigns including a number of cities in extensive urban climate experiments like BUBBLE (Rotach et al. 2005) and ESCOMPOTE (Mestayer et al. 2005) etc.

These techniques began to be extensively used in UHI studies since the 1990s with the availability of multi senor and temporal data and find their relevance till the present day, especially in developing regions (Beker and Li 1995; Dousset and Gourmelon 2003; Bechtel et al. 2012; Grover and Singh 2015; Mohammad et al. 2019; Sultana and Satyanarayana 2019; Tetali et al. 2022) due to lack of measurement opportunities. Tran et al. (2006) have analysed the UHI effects for 8 major cities (5 from temperate and 3 from tropical regions) of East Asia, using the LST computed from MODIS TERRA/AQUA and LANDSAT thermal datasets. Various thermal infrared sensors, such as NOAA-AVHRR, LANDSAT, MODIS etc., were used to estimate LST and analyse the UHI pattern of cities according to the scale of analysis and concluded that LST is directly proportional to the compactness and intensity of urban development (Mohammad et al. 2019; Tetali et al. 2022; Jain et al. 2023). Due to their consistent availability for a longer time-period, many studies have used these datasets for time-series analysis to establish a relationship between rapid land use transformation driven by urbanization and LST using statistical analysis techniques at regional to micro scale (Weng et al. 2004; Mirzari and Haghighat 2010; Gogoi et al. 2019; Mohammad et al. 2019; Tetali et al. 2022), and have also forecasted the future scenario (Faisal et al. 2021).

Satellites based precipitation measurements with a global coverage along with high temporal resolution have also revolutionized the downside of observations using rain gauges and weather radars with limited coverage, higher cost and non-existence over oceans (Joyce et al. 2004; Chen et. al, 2016). It was observed that the use of satellite-based meteorological information and urban characteristics reflected better feedback of the urban signatures relative to ground-based stations with limited observational capacity. TRMM launched in 1977 was the first satellite mission (joint project between NASA and JAXA) dedicated to high resolution quantification of precipitation using both active and passive microwave instruments and the processing at a low inclination orbit of 35° (Kummerow et al. 1998). Due to its high spatial and temporal resolution, it was widely accepted to monitor precipitation anomalies in the cities and their vicinity (Shepherd et al. 2002; Shepherd and Burian 2003; Shepherd 2005; Swain et al. 2023). Other important satellite observed passive microwave in combination with infrared data for estimation of global precipitation is the Climate Prediction Center morphing method (CMORPH), which also significantly contributed to urban rainfall studies (Joyce et al. 2004). The advantage of high-resolution quantitative precipitation estimation techniques was further solidified using an X-band dual-polarization radar system deployed in Santa Clara, California from February through May 2016 as a collaboration between various institutes (NOAA -

Colorado State University - Santa Clara Valley Water District) which provided 90-second updates with 250 m spatial resolution enabling the capture of low-level rainfall as well as high-end rain rate, and operated much better compared to the rain gauge network of the Santa Clara city (Cifelli et al. 2018).

However, according to an urban climate review by Roth (1989), many studies have reported significant differences between the time, duration and intensity of maximum temperature generated through satellite images from that of the surface measurements, although some have also claimed spatial similarities. The difference is suggested to be a resultant of the 'bird eye' view of the sensors placed at the higher altitude of the urban surface, which on one hand oversamples the building roofs, treetops, open spaces and roads, but on the other fails to identify the vertical surfaces and shaded areas (Roth 1989). In situ observation in any form is absolutely essential in validating the satellite observations (Chen et al. 2016) as a result of being the closest representation of reality; and, therefore, will always hold significance in any climate analysis. However, it was also apprehended that LST derived from satellite-based sensors can be an over or underestimation of reality since it is an average radiant temperature of the surface visible to the sensor across the area of a pixel (Roth, et al. 2007).

2.3.2 Numerical Modelling Studies

2.3.2.1 Energy Balance Models

The thermal energy fluxes of a city modified by its complex morphology leading to temperature differences with the surroundings, as seen in the previous section, began to be modelled by climate experts for cities lying in the temperate region using simple linear models since the early 1970s (Grimmond 2005; Barlow 2014). The numerical approach with careful validation of the results, in meteorological studies has the ability to perform comparative analysis considering different scenarios, and can possibly obtain results for any particular variable introduced in the computational domain (Hidalgo et al. 2008; Barlow 2014; Toparlar et al. 2015). Models can be simulated for comparing the climatic disruption of the city from the surrounding non-urban or even for the minute understanding of the local climatic conditions within intra-urban spaces, in case of unavailability of actual measurements. The insufficiency of a dense network of ground-based stations for cities across the world and the inadequacy of remote sensing based products to monitor the different micro-scale processes at horizontal as well as vertical levels have shifted the attention of researchers towards the application of mathematical models in urban climate studies (Masson 2000; Kusaka 2001; Arnfield 2003;

Salamanca et al. 2012; Barlow 2014). Micro-climate modeling can also serve as an equivalent alternative to the implementation of cost-sensitive weather instruments (Bhati and Mohan 2018), which can provide high-quality observed data if only maintained uninterruptedly for a considerable period. With the passage of time and the increasing gravity of the problem, various types of non-linear two- and three-dimensional surface energy balance models began to be applied for examining the interaction of urban and climate modified according to the prevailing meteorological conditions of a particular city (Taha 1988; Shephard 2005; Mirazaei and Haghighat 2010; Barlow 2014). Different meso to micro to building scale models have been simulated for local to city level structure, under clear and calm as well as unstable atmospheric conditions to estimate the strength of urban properties in modifying the overlying climatic variables (Masson 2000; Kusaka 2001; Hien et al. 2012; Salamanca et al. 2012; Barlow 2014).

The atmospheric models are coupled with land surface models to incorporate the transfer of energy, mass and momentum; from the terrestrial surface to the atmosphere in the Global Climate Models (Mason 2000; Joyce et al. 2004; Kusaka and Kimura 2004a; Jin et al. 2007), producing high temporal but coarser spatial resolution results. However, modelling the urban climate accurately requires very high quality and high-resolution parameterization of the key factors to recreate the energy interaction between the urban and atmosphere and quantify their impact on the entire system (Grimmond 2005; Jin et al. 2007; Stewart 2011). The model input parameters could be derived from observational data for smaller areas of interest, whereas medium to large-scale areas are dependent on different types of output from remote sensing and global models (Hidalgo et al. 2008; Stewart 2011; Liao et al. 2014; Shen et al. 2016). Some studies have also been dedicated to performance evaluation of the climate models of various scales, which have rendered a clear picture of their sensitivity in assessing the different climate variables in comparison to the ground-based observation instruments (Liu et al. 2005; Hamdi and Schayes 2008; Song et al. 2014; Bhandari et al. 2017).

2.3.2.2 Meso-scale Models

The modelling approach also differs according to the data availability as well as the scale and targeted aspect of the entire process. Scale or boundary condition of the model is defining criteria in UHI analysis, with studies ranging from estimation of urban skin temperature to different urban canopy layers further reducing the building level energy exchange process (Stewart 2011; Barlow 2014). It has been clear from the studies that the larger the scale of the

model, the higher the complexity and demand for detail, which endorses extensive and precise information requirements (Kusaka and Kimura 2004b; Salamanca et al. 2018). The meso-scale models are efficient in investigating the large-scale UHI variation of a city using the principles of energy balance and fluid dynamics integrating with radiation, land surface, cloud cover, soil and vegetation etc. models to complete the process (Grimmond et al. 1996; Hamdi and Schayes 2008; Roth et at. 2007; Salamanca et al. 2018). Dynamic Downscaling and Empirical Statistical Downscaling, which enables the climate models to simulate small-scale processes using GCM (Global Circulation Model) and RCM (Regional Circulation Models) outputs have been the major forces in the urban micro-climate modelling. But the highly heterogeneous nature of the urban surface is over simplified in the meso-scale grid, which ultimately underestimates the results. Therefore, dynamic downscaling gained more prominence in this field for being less dependent on time-series data as essential in the case of statistical downscaling, and allowing the incorporation of land surface processes in the model simulation (Lim et al. 2007; Hamdi et al. 2014; Corny et al. 2015)

The Mesoscale Model (MM5) developed by Pennsylvania State University and National Center for Atmospheric Research (NCAR) have been extensively explored to capture the thermal fluxes of the spaces at moderate resolution through time (Grell et al. 1994; Dupont et al. 2004; Otte et al. 2004; Liu et al. 2005). One of the greatest advantages of such models is their capability to study, analyse and estimate a large number of climate parameters at once and also understand their interrelationships, which could influence the overall process (Grell et al. 1994; Barlow 2014), reducing the dependence on individual methods to estimate the different parameters. Thus, these kinds of global or regional scale climate models, which generally underestimated the urban influence providing coarser resolution results, began to be improvised by urban climate researchers ingesting different land surface models (LSMs) for better urban representation since the 1990s (Hidalgo et al. 2008; Barlow 2014; Bhati and Mohan 2018). Urban Canopy Models (UCM) were developed for precise representation of heterogeneous land surface at the subgrid scales, to improve their performance for cities (Taha 1999; Lemonsu and Masson 2002; Martilli et al. 2002; Kusaka and Kimura 2004a 2004b; Chen et al. 2011). Thus, dynamic downscaling of the meso-scale climate models to obtain higher resolution modelled products was achieved by improving the resolution of the land surface as well as meteorological variables to be integrated with them (Kusaka and Kimura 2004a 2004b; Otte et al. 2004). Thus, studies for different cities have considered various physical parameters such as the urban surface geometry, roughness length, anthropogenic heat flux, storage heat

flux etc. to parameterize the mechanisms of urban surface and integrate them into climate models (Jin et al. 2007; Bhati and Mohan 2018). Urban canopy parameterization in a meso-scale climate model for realistic representation of the urban contrast with the surrounding environment have proved to be an excellent approach for many cities like Pennsylvania studied by Otte, et al. (2004), Washington analysed by Zhang et al (2011), Madrid by Salamanca et al. (2012), Taiwan by Lin et al. (2015) etc. However, it is to be noted that not all the urban or meteorological parameters are equally emphasized in each case, which could be regarded as a key cause for variation in the results even in the case of a similar urban setup.

The WRF model was then developed as an update to MM5 with several advantages like high-resolution time patterns, and annual averages (Gsella et al., 2014). The WRF model has become a highly popular choice both in online and offline modes, which could be coupled with various land surface and urban canopy models to incorporate the surface criteria, enabled with appropriate physical parameterization for boundary layer conditions, radiation fluxes, cloud cover, etc. according to the prevailing meteorological conditions of the city (Kusaka and Kimura 2004b; Salamanca et al. 2011). Urban land use classes incorporated in the Noah-LSM, consider the effect of the urban landscape on roughness length to represent the turbulence generated by rough elements and drag created by buildings, soil thermal conductivity, green vegetation fraction etc. (Chen, et al. 2004; Kusaka and Kimura 2004; Salamanca et al. 2012). Finer the resolution of urban parameterizations better is the estimate of the mean thermal and dynamic effects of the cities on the atmosphere. (Salamanca and Martilli, 2011; Corny et al. 2015; Lao et al. 2015; Bhati and Mohan, 2018;). Thus, the transformation of the meso-scale WRF model to a high-resolution model simulating micro-scale weather patterns integrating finer scale representation of the city geometry is an effective but complicated process.

Coupling WRF with UCMs improved the description of lower boundary conditions and provided more accurate forecasts for urban regions. (Chen et al. 2004). These high-resolution urban parameterization models vary in sophistication from simple bulk urban parameterizations (Taha 1999) to single- and multilayer UCMs, such as SLUCM (Kusaka and Kimura 2004a) the Town Energy Balance (Masson 2000) and Building Energy Parameterization (BEP) (Martilli et al. 2002) schemes. Such multi-model coupling had proved to be pertinent in understanding the UHI of multi-core metropolitan areas, which could deliver a range of scales within the same city unfolding macro to micro level interaction (i.e., urban canopies to individual urban entities) with the local climate (Salamanca et al. 2011: Corny et al., 2015; Bhandari et al. 2017; Sharma et al. 2017; Xu et al. 2018b). It was observed that

incorporations of UCMs could successfully produce the climatic parameters such as Ta, Ts, wind circulations, heat and moisture fluxes, rainfall, humidity etc., at a much higher grid-scale of 500 – 1000 m for the entire city and its surroundings, providing a clearer picture of the energy exchange process and meteorological structure (Zhang et al. 2011; Salamanca et al. 2012; Lin et al. 2015; Brousse et al. 2016; Nadimpalli et al. 2022). Thus, downscaling the GCM output (1 – 100 km) to finer scales (0.5 – 1 km) have been a breakthrough in examining micro climatic variation anywhere over the globe (Barlow 2014; Hamdi et al. 2014). The capability of such coupled models to simulate a large number of weather parameters for the past, in real time and also the future, for the entire city at once according to the corresponding surface configuration makes it a very popular choice for developing cities which lack the resources for detailed atmospheric measurements and very high-resolution model simulations (Chang et al. 2009; Bhati and Mohan 2016; Patel et al. 2020; Sultana and Satyanarayana 2023).

2.3.2.3 Computational Fluid Dynamics (CFD) Models

Besides downscaling the regional scale models to achieve finer scale meteorological products, some models were specially developed to simulate microscale conditions considering the specific urban morphological elements in much detail and at very high spatial resolution. Computational Fluid Dynamics (CFD) is one very prominent and widely used modelling approach applied in such micro-scale climate models. Energy fluxes between the individual urban elements and airflow patterns around and within buildings could be resolved using CFD technique, dealing with the governing equations of the flow (Ashie et al. 1999; Toparlar et al. 2015). ENVI-met, is one such model developed by Michael Bruse in 1998 on the basis of CFD and thermodynamics, capable of three-dimensional simulation of airflow around and between buildings, exchange processes of heat and water vapor at urban surfaces, turbulence, exchanges of energy and mass between vegetation and its surroundings, particle dispersion, and simple chemical reactions, all at a spatial resolution of 0.5–5m and temporal resolution of 1–10s (Hien et al. 2012; Salata et al. 2016; Bhandari et al. 2017; Liu et al. 2021; Elraouf et al. 2022). The most important and unique feature of ENVI-met is the detailed representation of the vegetation and its significance in regulating the heat, wind flow patterns and evapotranspiration, which is important to estimate the pedestrian level outdoor heat sensation and also the comparison of multiple scenarios simulations which is otherwise impossible in real-world (Morakinyo et al. 2017; Liu et al 2021).

The nested modelling of meso and micro-scale models has further improved the simulations, as the results derived for canopy level through the meso-scale models could be utilized for building level in the micro-scale models. To overcome the inadequacy of data; the meso to micro to building scale models are coupled, so that the micro-scale response could be integrated to model the meso-scale variability or vice versa (Mason 2000; Baik et al. 2007). Coupling of the meso-scale WRF model with the micro-scale ENVI-met in the case of Chicago (Corny et al. 2015), Oak Ridge (Bhandari et al. 2017) has produced better results compared to ENVI-met results based on observational measurements due to the incorporation of the land surface dynamics in the computation process. However, generating the extremely detailed inputs required in ENVI-met model in terms of individual buildings and their characteristics, the street canyons and structures, etc., is extremely challenging for an entire metropolis, restricting the applicability of the model to neighbourhood scale or specific areas within a city chosen to represent critical situations (Bhandari et al. 2017; Morakinyo et al. 2017; Liu et al. 2021).

Another important model for detailed urban climate analysis is the Town Energy Balance Model (TEB), which is a small-scale model developed to simulate the energy and water exchange between an urban system and the overlying atmosphere at a local scale (Mason 2000; Lemonsu et al. 2003). Similar to ENVI-met, TEB also considers surface roughness and three-dimensional geometry of the city and energy transfer associated with the urban fabric, radiative trappings in the urban canyons and shadows, urban greens, water interception and evaporation, turbulent fluxes etc. thus, incorporating details of the urban system (Mason, 2000; Lemonsu et al. 2003; 2012). However, it has a huge demand for input meteorological parameters and hence is coupled with the MesoNH atmospheric model to accurately simulate the urban micro climate (Mason, 2000). TEB designed to concentrate on the local scale processes of an urban system has been employed by various authors for canopy-level studies or for the entire city coupled with other land-surface models (Mason 2000; Lemonsu et al. 2003). Coupling TEB with the ISBA (Interactions with Soil, Biosphere and Atmosphere) scheme, Lemonsu et al. (2003) simulated the model for the Mediterranean city of Merseille in the offline mode characterized with a detailed urban surface database. The simulated temperature deviated from tower-based observation available for the street canyons in the initial simulations (without coupling), which increased around the road and wall compared to above-the -roof-level air temperature due to the mixing of air in the upper part of the canyon (Nakamura and Oke 1988; Kim and Baik 2002). But when coupled with the ISBA scheme, sufficient and rapid ventilation of the heat released by the urban surfaces within the canyons was enabled, and the results improved

significantly with a maximum error of 2 – 3 K for all three surfaces (roof, road and wall). Various other studies to analyse the neighbourhood or city-scale analysis of urban surface influence on the micro-meteorology using TEB were conducted for the cities like Vancouver and Mexico City (Masson et al. 2002); Sde-Boqer in Israel (Lemonsu et al. 2012); Paris (Pigeon et al. 2014); Toulouse (Bernard et al. 2022) etc.

2.4 WRF for Urban Climate Research

2.4.1 Weather Research and Forecasting (WRF) Model

WRF is a numerical weather prediction (NWP) model and a bundled atmosphere simulation system developed for both research and operational use, with a collaboration of multiple agencies like National Center for Atmospheric Research (NCAR), National Centers for Environmental Prediction (NCEP) under National Oceanic and Atmospheric Administration (NOAA), Earth System Research Laboratory, United States Air Force Weather Agency, United States Naval Research Laboratory, University of Oklahoma - Center for Analysis and Prediction of Storms, and the Federal Aviation Administration. It was built as a next generation meso-scale forecast model and data assimilation system with a vision to succeed the NCAR Mesoscale Model (MM5) and upgrade the understanding of meso-scale climatic processes and enable the transfer of research knowledge in this field to actual applications (Skamarock et al. 2008; Salamanca et al. 2012; Bhati and Mohan 2016). It became a widely used model because of the flexibility and portability of its different components, which could be compiled, configured, and run in systems ranging from massive supercomputers to laptops according to the requirement of the user. It has a community-based structure, facilitating contributions from researchers and experts from across the domain to improve and update the model physics and operations (Skamarock et al. 2005; Salamanca et al. 2012). The model contains two dynamic solver options, i.e., Advanced Research WRF (ARW) and Nonhydrostatic Mesoscale Model (NMM), besides various physics packages and other initialization programs to dynamically construct and resolve the atmospheric structure in relation to the surface conditions. The potential of WRF to

The entire WRF system consists of different components, and the execution begins with the preprocessing unit known as the WRF Preprocessing System (WPS), responsible for integrating geographic and meteorological data according to the user-defined domains (Skamarock et al. 2005). The model provides the opportunity to create nested domains to systematically downscale the model and achieve a finer resolution model run. Nests could be

defined as a second domain covering a smaller portion within a parent domain configured by the boundaries set by it. The child domain could be executed at finer resolution engaging fewer resources compared to the parent domain, and can also accommodate more domains within it, further refining the horizontal and vertical scale of the model. The nesting could be either 1-way i.e., transfer of information from coarse to fine grid or 2-way where the interaction is both ways, enabling the impact of regional climate on the local scale and the local mechanism fed back to the regional scale. Then the geographic information and its different parameters are ingested into the model architecture after being suitably designed for the required simulation followed by rearranging and interpolating the atmospheric fields derived from global or regional models corresponding to the configured domain. Finally, the pre-processed inputs are then horizontally and vertically interpolated and initial and boundary conditions are defined for the model simulation (Patel 2021; Skamarock et al. 2021).

The governing equations that represent the state and evolution of the atmosphere in the Cartesian coordinate system are as follows:

Conservation of Mass: $$\frac{d\vec{V}}{dt} = -a\vec{V}\mathrm{p} - \vec{V}\Phi + \vec{F} - 2\Omega \times \vec{V} \quad (2.1)$$

Conservation of Momentum: $$\frac{\partial p}{\partial t} = -\vec{V}.(\rho\,\vec{V}) \quad (2.2)$$

State of Idea gases: $$pa = RT \quad (2.3)$$

Conservation of Energy: $$Q = C_p\frac{dT}{dt} - a\frac{dp}{dt} \quad (2.4)$$

Conservation of Water Mass: $$\frac{\partial pq}{\partial t} = -\vec{V}.\left(\rho\,\vec{V}q\right) + \rho(E - C) \quad (2.5)$$

Where, $\vec{V}$ = (u,v,w) represents the velocity of air in x, y, and z components, t represents time, a is the specific volume, p is the pressure, Φ is geopotential height, $\vec{F}$ is friction force, Ω is the angular velocity of the Earth, ρ is density, R the gas constant and T is temperature, Q is heating, C_p is the specific heat at constant pressure, q is the water vapor mixing ratio and E and C are evaporation and condensation respectively.

The ARW dynamics solver in the WRF model uses a terrain-following hydrostatic pressure vertical coordinate denoted by η and defined as,

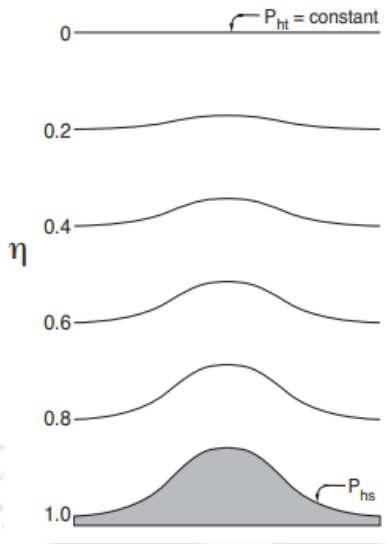

Figure: 2.1 Vertical Coordinate used in ARW

$$\eta = (P_h - P_{ht})/\mu \qquad 2.6$$

where, $\mu = (P_{hs} - P_{ht})$

P_h is the hydrostatic component of the pressure, P_{hs} and P_{ht} refer to the surface and top boundary values, respectively. The values of η varies from 0 at the upper boundary to 1 at the surface of the model domain (Fig. 2.1).

The WRF model uses various physics schemes/models to parameterize the different physical processes of the atmosphere as well as the surface and integrate them into the model to make an accurate representation of the actual land - atmosphere interaction in the region (Skamarock et al., 2005).

i) Planetary boundary layer (PBL): PBL is responsible for vertical sub-grid-scale fluxes caused due to eddy transports in the whole atmospheric column. PBL schemes are one-dimensional, which consider dry mixing, but can also include saturation effects in the vertical stability that determines the mixing. These schemes assume that there is a clear scale separation between sub-grid eddies and resolved eddies and tend to fail at a horizontal resolution of a few hundred meters (resolved eddies).

ii) Cumulus parameterization: These schemes parameterize the sub-grid-scale effects of convective as well as shallow clouds and also represent unresolved fluxes due to vertical movements, which may lead to additional convective precipitation. These models are implemented for the coarser resolution grids (e.g. > 10 km), used to properly release latent

heat on a realistic time scale in the convective columns. However, sometimes, these schemes can be helpful in triggering additional convection in 5-10 km grids.

iii) Microphysics: Microphysics schemes are responsible for explicitly resolving water vapor, cloud, and precipitation processes to parameterize large-scale precipitations at grid-scale. The models can accommodate any number of mass mixing ratio variables.

iv) Radiation: The radiation schemes provide atmospheric heating due to radiative flux divergence and surface downward radiations for the ground surface. LW radiation includes infrared or thermal radiation absorbed and emitted by gases and surfaces and is generally determined by the surface emissivity of different land-use types as well as the skin temperature. SW radiation includes wavelengths that make up the solar spectrum. The processes include absorption, reflection, and scattering in the atmosphere and at surfaces.

v) Surface Layer: This scheme calculates friction velocities and exchange coefficients that enable the calculation of surface heat and moisture fluxes used by the land-surface models and surface stress in the PBL scheme. The schemes provide the information related to the stability of the surface layer.

vi) Land-surface model: LSMs use atmospheric information from the surface layer scheme, radiative forcing from the radiation scheme, and precipitation forcing from the microphysics and convective schemes, together with internal information on the land's state variables and land-surface properties, to provide heat and moisture fluxes over land and sea-ice points. These fluxes then provide a lower boundary condition for the vertical transport required in the PBL schemes

vii) Urban Physics Schemes: The heterogeneous nature of urban land use and its varying spatial distribution has a significant effect on the planetary boundary layer and thus, it becomes important for meso-scale models to capture these effects for better forecasting results. Thus, UCMs are coupled with WRF in order to parameterize the sub-grid scale urban variability and include three urban physics options - Single Layer UCM (SLUCM), Multi-layer UCM (BEP) and Indoor-Outdoor Exchange Model (BEM).

- SLUCM: It was developed by Kusaka et al. (2001) and later modified by Kusaka and Kimura (2004) to represent the two-dimensional geometry of the buildings and roads into the model. This UCM takes into account sensible heat fluxes from roof, wall, and road; and then aggregate them into energy and momentum exchange between the urban surface and the atmosphere.

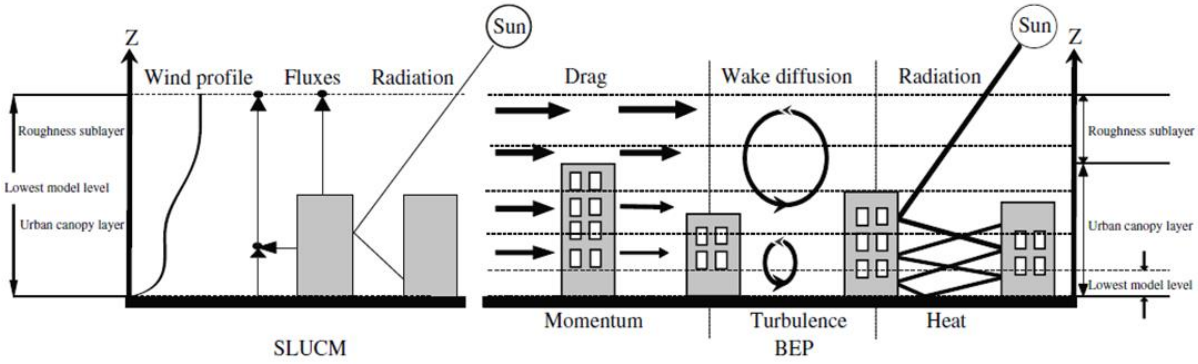

Figure: 2.2. Comparison of the roughness sublayer between single and multilayer UCM models (Source: Chen et al., 2011)

- BEP: BEP was developed by Martilli et al. (2002) in view of the disadvantages of SLUCM due to the fact that interaction of energy in this scheme occurred only at the roof level and interaction between the urban surfaces in terms of energy exchange was null. BEP incorporates and parameterizes the effect of buildings on the urban canopy layer, recognizing the three-dimensional nature of urban surfaces and the fact that buildings vertically distribute sources and sinks of heat, moisture, and momentum through the whole urban canopy layer, which substantially impacts the thermodynamic structure of the urban roughness sub-layer and hence the lower part of the urban boundary layer. It takes into account the effects of vertical (walls) and horizontal (streets and roofs) surfaces on momentum (drag force approach), turbulent kinetic energy (TKE), and potential temperature.
- BEM: In the above models, the internal temperature of the buildings was kept constant and the exchange of energy between the interior of the building and atmosphere was not taken into consideration. Thus, Salamanca and Martilli (2011) developed the BEM scheme as an extension of the BEP scheme, which accounts for the diffusion of heat through the walls, roofs, and floors; radiation exchanged through windows; LW radiation exchanged between indoor surfaces; generation of heat due to occupants and equipment; and air conditioning, ventilation, and heating. Buildings of several floors can be considered, and the evolution of indoor air temperature and moisture can be estimated for each floor.

2.4.2 Application of WRF in UHI Studies

WRF simulations for urban climate studies have gained momentum since the integration of UCMs, enabling proper-scale urban representation. Coupling WRF with SLUCM improved

the model performance significantly since the energy fluxes through the urban canopy could be successfully simulated using this technique (Kusaka and Kimura 2004b; Zhang et al. 2011). The potential of WRF to be built and executed on multi-tier nested domains inspired the researchers to embed the urban areas within the innermost domain with the finest grid scale (Salamanca et al. 2012; Bhati and Mohan 2016; Brousse et al. 2016; Sharma et al. 2017) and utilize the UCMs to resolve the land – atmosphere interactions. It was observed that, in most cases with the incorporation of the two-dimensional urban surface characteristic with the SLUCM urban canopy model, the performance of the model improved and minute effects of urban like diurnal temperature variation, influence of urban roughness, etc. could be captured properly, reducing the error magnitude (Zhang et al. 2011; Sharma et al. 2017; Giannaros et al. 2018). To make the model more rigorous and inclusive of the energy exchange between the three-dimensional and highly heterogeneous urban layers with the lower atmosphere, multi-layer UCM models (BEM and BEP schemes) have been developed and coupled with WRF (Salamanca et al. 2010; Chen 2011). There has been extensive research using the coupled WRF-UCM models; some examples are listed and discussed in brief in this section.

The WRF-UCM high-resolution model was effectively utilized to examine the impact of upstream urbanization on UHI over the Baltimore area by Zhang et al. (2011) applying both surface observations and coupled WRF-UCM with 2001 National Land Cover Data. The advective contribution of upstream urbanization to an extreme UHI event over the Baltimore area was simulated, and it was observed that T_s and T_a differed about 5ºC - 10ºC respectively between the urban and surroundings. The study also concluded that the intensity of the UHI event could be decreased by almost 25 % when Baltimore or its upstream urban areas were replaced with natural vegetation in the model.

Lin et al. (2016) evaluated the impact of urbanization over northern Taiwan using the Weather Research and Forecasting (WRF) Model coupled with the Noah-LSM and a modified urban canopy model (WRF–UCM2D). WRF–UCM was modified to consider the 2-D urban fraction and anthropogenic heat (AH) to overcome the disadvantage of constant urban fraction and AH value, which leads to over-or underestimation of these parameters and further the model-estimated temperature. WRF–UCM2D provided extensive and accurate spatial distribution of urban fraction ranging from 0.01 to 1.0; and AH over the entire area ranging from 0 to 50 Wm^{-2}, giving more detailed information at a finer resolution. The mean bias and RMSE calculated on comparing the modelled results with ground data were: UCM2D - 0.27 and 1.12; and UCM - 1.27 and 1.89 respectively, showing better performance of the modified model.

Salamanca et al. (2012), performed a detailed urban parameterization to evaluate the impact of the air conditioning (AC) system of the buildings on T_a, to assess the existing relationship between energy consumption and the meteorological condition of the city of Madrid. Two different turbulent schemes specially designed for large UHI modelling were used to evaluate the ability of BEP+BEM schemes to describe the surface T_a and WS over the city of Madrid during summer conditions and to generate mitigation strategies for the same. The simulation results for the entire study period showed that, heat fluxes generated by AC systems were responsible for an increase in the air temperature up to 1.5–2°C in some of the denser parts of the city.

The UHI effect and thermal comfort of Delhi was performed using WRF coupled with single as well as multi-layer UCM focusing on T_a and T_s under varying LULC conditions by Bhati and Mohan (2016, 2018). The studies highlighted the importance of appropriate and updated representation of surface characteristics and urban canopies for improving predictive capabilities of the mesoscale models, as the results improved in the later study (2018) where all urban physics schemes (SLUCM, BEP, BEP+BEM) were employed. Urban areas were found to have a higher heat index than non-urban areas, with a difference of about 1.5–2°C and about 2.0–2.5°C at dense built-up stations, validating the fact that the urban canopy effect leads to a rise in thermal discomfort by increasing Heat Index.

Again, the effect of turbulent and radiative fluxes on the near surface temperature was modelled by Brownlee et al. (2017), coupling WRF with SLUCM for Houston to estimate the influence of hydrological processes in the simulation. The results show that the BULK scheme was the least accurate and overestimated the near-surface temperatures and winds over the urban regions. Over the urban land category, the mean temperature is 1.43ºC higher than the observations; for the COI–HIR and LIR categories, the mean temperature is 1.12ºC and 1.87ºC higher than the observations, respectively.

The study by Li et al. (2017) focused on the impact of land use change on the microclimate of the Kolkata Metropolitan Development Area using WRF driven by future land use scenarios. Specifically, two land conversion scenarios were considered including an urbanization scenario; first where all the wetlands and croplands were converted to built-up areas, and an irrigation expansion scenario in which all wetlands and dry croplands were replaced by irrigated croplands, which resulted in the increase in temperature by 1.2 – 4°C. This study

showcased the probable future scenarios in this rapidly developing urban agglomeration which could further worsen the microclimatic conditions.

The WRF coupled with BEP+BEM schemes by Mughal et al. (2018) to simulate the UHI effect of the tropical city of Singapore during April 2016 when a series of heat wave events were experienced by the city; showed that the mean UHI intensity peaked in the early morning at 2.2ºC, reaching 3.6ºC in the compact high-rise areas. The AH was found to play a major role in all the processes studied, contributing 2.2ºC to the mean UHI intensity and 1.3ºC in the compact high-rise. The authors however concluded that the effect of the different land use types was most pronounced during night time and least visible near noon.

Salamanca et al. (2018), evaluated the performance of the recently introduced improved LSM Noah-MP, in estimating the temperature difference over two semi-arid urban environments, Phoenix and Tucson metropolitan areas of Arizona. The WRF model was coupled with 3 urban canopy models (SLUCM, BEP, and BEM+BEP) and the new community Noah with multi-parameterization options Noah-MP-LSM which uses multiple options for key land-atmosphere interaction processes to represent the seasonal and annual cycle of snow, hydrology, and vegetation. The results obtained showed superior performance of only the multilayer BEP model in the metropolitan areas for the daily evolution of surface skin temperature, compared to both the single-layer and bulk urban parameterizations which significantly underestimated the diurnal cycle amplitude. WRF-modeled RMSE was reduced from 2.2°C to 1.8°C for 2 m T_a and from 1.8 ms-1 to 1.4 ms-1 for 10 m WS when Noah-MP was employed. The daytime surface skin temperature corresponding to observations improved significantly with Noah-MP by reducing the cold bias by ~1.4°C and by ~2.0°C (1300 hrs), and by ~0.8°C and by ~1.4°C (1100 hrs) for the Tucson and Phoenix regions, respectively. However, on comparing the nighttime surface T_s with observations it was seen that, the Noah-MP LSM reduced the warm bias by ~0.5°C and by ~0.7°C (2200 hrs), and by ~0.6°C and by ~0.5°C (0100 hrs).

Mauree et al. (2018), attempted to improve the results in meteorological simulations by integrating an additional urban physics option in the Weather Research and Forecasting model. The coupled WRF and CIM when simulated with a high vertical resolution i.e., similar to CIM (5 m) and correction were employed to the CIM calculation to take into account the horizontal fluxes, and the simulated profiles of both models had better coherence. The authors observed that this coupling improves the simulations of the variables in an urban grid and that the

WRF+CIM+BEP–BEM system can provide highly resolved vertical profiles while simultaneously improving the computational time significantly.

Xu et al. (2018) analysed the summertime AC electric loads and their immediate effect on the weather in Beijing city. Coupling BEP+BEM scheme with WRF-Noah-MP LSM reduced RMSE of 2 m T_a by 1.9°C for urban stations and for suburban and rural districts the simulated AC electric load is improved by incorporating urban class-dependent building cooled fraction. Two peaks during 3 pm and 9 pm were noticed in the temperature due to AC electric loads, and the evening peak could be reproduced well by incorporating a realistic AC working system. The authors concluded that if the AC works for 24 hours continuously and vents sensible waste heat into the air, it would impact the evening temperature (1.5~2.4°C) more compared to the afternoon (~1°C). Further, the BEP+BEM scheme coupled with WRF was used by various researchers to estimate the micro-level energy fluxes within the urban canopy for many other cities like Madrid (Brousse et al. 2016); Chicago (Sharma et al. 2017); Osaka (Takane et al. 2017); Beijing (Xu et al. 2018); and Maryland (Gohil and Jin 2019). This scheme could remarkably simulate the anthropogenic heat generated by Air Conditioning (AC) systems employed in the building both during summer and winter as has been observed in the mentioned studies and also assess the effect of this heat on the energy consumption of the buildings.

Another improvement in the high-resolution WRF simulation for urban areas was observed in coupling the WRF with LCZ models which entailed a systematic and detailed urban representation scheme. The incorporation of WUDAPT LCZ into WRF simulation for the city of Madrid (Brousse et al. 2016), obtained better results for building effect and energy parameterization. Ren et al. (2017) incorporated the WUDAPT LCZ product into WRF simulations for urban development impact analysis on the Pearl River Delta Region. LCZ for the area was created using Landsat 5 data. Then two new WRF simulations using the WUDAPT products as input data were conducted and their results were compared with the benchmark one, so that the pure urbanization (1980-2010) impact on local climate conditions of summer time (June-July) can be analyzed; after being validated with in situ data from King's Park station of Hong Kong Observatory which is a representative urban station. As expected, the 2m T_a was observed to have significantly increased due to urbanization during the considered period, from the model simulations, as a result of storage heat. The authors also concluded that the strength of the sea breeze has increased with urbanization as a result of the land becoming warmer which increased the temperature gradient between land and sea.

Hammerberg, et al. (2018), further explored the advantages of integrating WUDAPT LCZ used to identify the complex morphological parameters for the city of Vienna, in the WRF model for climate predictions. WRF model was coupled with BEP+BEM scheme and simulated for five distinct seasonal periods. Results demonstrated that using detailed GIS data to derive morphological descriptions of LCZs for mesoscale studies provided only a marginal overall improvement over using the default WUDAPT parameters based on the ranges proposed by Stewart and Oke (2012); after being validated from weather station data lying within the city.

Molnar et al. (2019), coupled WRF-LCZ and used the SLUCM model to simulate the spatiotemporal behaviour of near-surface T_a and UHI intensity for Szeged city in Hungary, under a 6-day heatwave period from July 2017. The modelled values were evaluated against the observational datasets which showed that the model performed satisfactorily in each LCZ, particularly in LCZ 5 and LCZ 6, with mean absolute error (AE) of 1.3 °C and 1.8 °C and mean spatial correlation coefficients (SCC) of 0.95 and 0.93, respectively. Larger biases of T_a occurred in LCZ 9, with AE of 2.7 °C and SCC of 0.91. The daytime T_a was generally overestimated in each LCZ and during the night, slight underestimations were noticed in LCZ 6, LCZ 9, and LCZ D. The mean ΔT was underestimated in the night-time; however, the daytime ΔT was estimated accurately.

Mughal et al. (2020), integrated WRF with multilayer UCM (BEP+BEM) and LCZ scheme to evaluate the UHI intensity in the tropical city of Singapore and design mitigation strategies. The Singapore LCZ was used as LULC data to account for the intra-urban variability. The simulated results showed that the canopy layer UHI intensity in Singapore can reach up to 5 °C in compact areas during nighttime. The results reveal that city-scale deployment of cool roofs can provide an overall reduction of 1.3 °C in the near-surface daytime air temperature in large low-rise areas. The finding also revealed that increasing the thermostat set temperature to 25 °C from 21 °C in buildings throughout the city can potentially reduce the air temperature due to the decrease in waste heat discharge (~20%) from AC units.

The performance of WRP-BEP/BEM coupled model using LCZ was further evaluated for Barcelona by Ribeiro et al. (2021), The study showed better performance of BEP compared to the BULK scheme; it overestimated the temperature and relative humidity in particular during the night/morning. On the other hand, BEP + BEM performed with the minimum RMSE associated with temperature and relative humidity in the entire domain and is more sensitive than the other scheme over locations where the land use in the model grid differs from the real

one, which is a common consequent limitation of horizontal model resolution. This study also concluded that depending on the synoptic condition, the accuracy of different schemes in determining PBLH might change substantially.

Further Zhou et al. (2022) coupled WRF – BEP/BEM to simulate the influences of vehicle heat (VH) on the urban climate over Sendai in Japan. A novel method was proposed to estimate hourly VH for different LCZs via open-source data. The number of vehicles was counted and the heat release of each vehicle per kilometer in a particular LCZ was calculated. Thus, on the basis of this coupled model integrated with the specific VH values, the effects of various urban heat countermeasures were analyzed at a high spatial resolution. The results indicated that eliminating VH values can contribute up to 0.12°C to urban heat mitigation, and can be considered the most effective countermeasure for the compact areas of the city center.

2.4.3 Application of WRF in Urban Precipitation Studies

The use of high-resolution WRF with a horizontal grid spacing of less than 5 km can improve forecasts for convective-scale phenomena, including explicit information about the timing, intensity, and mode of convection (Hong et al., 2010). Microphysical schemes are explicit, whereas convective parameterizations are implicit. With the decrease in grid spacings, convective parameterizations become more inappropriate, whereas the explicit representation of microphysical processes can be computed for increasingly small clouds, cloud particles, water droplets, and so forth (Hong et al., 2010). Among the microphysics packages for clouds and precipitation, the series of the WRF single-moment (WSM) schemes (WSM3, WSM5, and WSM6 were widely used (Hong et al. 2010; Patel et al. 2020).The WRF model was successfully utilized by many researchers to simulate the characteristic high-intensity storm events in tropical cities and their relationship with the increase in temperature, surface roughness, altered wind directions and pollutant-laden atmosphere as a result of rapid scale urbanization (Roth 2007; Pathirana et al. 2014; Paul et al. 2018). Thus, different numerical predictions and meso-scale climate models have gained significance for simulating tropical and sub-tropical extreme rainfall events.

The extensive use of WRF coupled with different urban canopy models and realistic land use representation has improved the urban-induced convective rain studies (Miao et al. 2010; Zhong and Yang, 2015). The effect of UHI and surface roughness characteristics on the convergence and moisture transport have been simulated for Beijing (Zhong and Yang, 2015), which verified the increased effect of urbanization on urban precipitation. They conducted two

ensemble simulations with real and up-to-date urban land cover data (control experiment) and croplands replaced by urban surface (sensitivity experiment) using the WRF-Noah-UCM coupled system. It was observed that the experiment with urban land cover experienced higher surface temperature and net-wave radiation during daytime with unstable boundary conditions at noon and better reproduced the results for temporal evolution of precipitation including time of occurrence of maximum precipitation rate, as compared to the sensitivity analysis. Other such meso to micro-scale numerical simulations to understand the feedback mechanism of urbanization on rainfall has been performed for Indianapolis (Niyogi et al. 2011), Brussels (Hamdi et al. 2012), Tokyo (Seino et al. 2018) which have obtained positive relationship.

The impact of urban land use processes on the mesoscale circulation has been simulated for an isolated heavy rain event (944 mm in a 24-hour period) over Mumbai during the Monsoon period (July 26, 2005), using WRF-ARW coupled with three different LSMs (SLAB, Noah and Noah-GEM), for evaluating the performance and ability of the model to simulate an event of such extreme intensity (Chang et al. 2009). The authors concluded that WRF coupled with Noah-LSM simulated this highly localized rain fairly better than the other two LSMs; and that the 3.3 km grid spacing performed better compared to 10 and 30 km respectively, indicating better forecasting of heavy rainfall events with finer grid spacing. Similarly, Singh et al. (2015) simulated and investigated a severe thunderstorm that affected Delhi and adjoining regions between 1630 hrs IST and 1730 hrs IST on 30th May 2014 using sensitivity experiments that were conducted with different grid resolutions (9 and 3 km) with terrain resolution 5 min (~10 km) and 1 min (~2 km) respectively and the same microphysics (MPs) and cumulus parameterization (CPs) schemes. The results demonstrated that the model simulates better structure and intensity of the thunderstorm at a higher resolution domain.

Li et al. (2016), investigated the effect of urbanization and urbanization patterns on the thermal environment and local rainfall in the tropical coastal city of Singapore. WRF coupled with SLUCM was employed with 5 one-way nested domains, the highest horizontal resolution being 300 m. It was observed from the model simulations that most of the rainfall (considered cases) occurred from late morning to afternoon when the sea breeze blows north-eastwards, which helped in achieving the conclusion that sea breezes have a stronger influence on the rainfall than the urbanization pattern in this particular case since the downwind part always gets more rainfall than the upwind part. According to the authors', urbanization and associated AH can have two opposite effects on the rainfall amount: increasing rainfall through increasing

buoyancy by AH and decreasing rainfall through reducing evaporation by converting greenery to impervious surfaces depending on the relative strength of either of these two influences.

WRF – BEP/BEM was integrated with LCZ to simulate four very heavy rainfall events over Mumbai by Patel et al. (2020). The results showed that the incorporation of WUDAPT LCZs in WRF results notably improved the model performance for all four heavy rainfall simulations. The changes in the spatial patterns due to the inclusion of WUDAPT data notably contributed to the overall rainfall occurrence over the urban area. The difference in the accumulated rainfall amounts for the control case and BEP/BEM simulated between the paired runs was over 300 mm. These changes in the rainfall distribution and quantity are the result of changes in the urban dynamics and micro/mesoscale convergence/divergence zones within the urban boundary layer. A similar study by Nadimpalli et al. (2022) by integrating WUDAPT based LCZ for Bhubaneshwar in India, enhanced high-resolution forecast from ARW by incorporating the details of building height, terrain roughness, and urban fraction.

2.5 Summary and Conclusion

A detailed analysis of relevant literature in the field of urban climate research from across the globe has revealed the process of conceptualization and the gradual progress in such studies. Two important urban climate indicators were assessed in detail, viz, the UHI effect and the Urban Precipitation Anomalies which have a direct impact on the livability of the cities. It was observed that with time and technological advancements a more detailed assessment was possible in both the cases of temperature and rainfall and their relationship with the process of urbanization. It was possible to study this complex mechanism with the application of more sophisticated techniques which could identify the different aspects of the urban surface characteristics and their influence on the micro – regional scale climatic conditions as well as the near surface to boundary layer meteorology over and around the cities. However, the synthesis of the available literature recognized a clear distinction between the number and frequency of such studies as well as the approaches and techniques adopted for analysis between the cities from the developed world and the global south. It was evident from the analysis that urban climate studies were initiated much later in the tropical and sub-tropical regions which majorly coincides with the developing parts of the world, compared to the temperate regions which mostly accommodates the developed countries. Further, most of the analysis techniques were also adopted the techniques successfully applied in the temperate regions. These could be directly attributed to the lack of adequate facilities and resources in

most the developing countries which has restricted contribution towards innovative research in this field. However, this trend is gradually changing in the recent times with better access to sophisticated techniques in these regions and also the vast scope of research in these climatologically active and vulnerable zones. Besides the complexity of urban surface characteristics in terms of morphological heterogeneity and surface fabric further complicates the process which emphasizes on the urgency and significance of such studies so that a comprehensive understanding could be achieved. Thus, this dearth of adequate number of studies to understand the impact of rapid and unplanned urbanization of the developing region on one of the most important climatological phenomena, i.e., the sub-tropical monsoon motivated the present study. It was initiated with an understanding developed from few studies from the Indian sub-continent and an ambition to contribute in enhancing the knowledge further.

Chapter 3

Meteorological downscaling using high-resolution uWRF Model

3.1 Introduction

The morphological diversity of cities is responsible for micro-scale variations in the urban meteorological environment, causing multiple UHI cores or local convective anomalies within the same city. Thus, the first step towards comprehending this complex system is to develop a detailed understanding of the urban surface characteristics and their inherent properties (Oke 1989; Oke and Voogt 1997). It is important to note that accurate representation of urban surfaces is extremely important to improve the accuracy of the meso-scale WRF coupled with UCMs and transforming into the uWRF (urban-WRF) model, which essentially integrates the urban and atmospheric physics to obtain higher resolution urban climate parameters (Salamanca et al. 2012; Molnar et al. 2018). The UCMs necessarily integrates the urban surface properties into the WRF model defining the general urban characteristics such as the horizontal extent and the nature and composition of the built-up spaces. The very specific details such as the dimensions of the different urban morphological characteristics to the type of the city's fabric etc. could be configured into the model modifying it typically for that city (Kusaka and Kimura 2004). This enables the different physical parameters defining the atmospheric and natural processes of the region to interact with the urban systems at different horizontal and vertical levels, within the WRF framework for a certain case. Further, the uWRF model could be simpler when coupled with SLUCM, i.e, when the cities are considered as two-dimensional artificial spaces almost homogenous throughout its entire extent; or more complex when coupled with Multi-Layer UCM (MLUCM) such as BEP and BEM where the actual three-dimensional urban geometry is taken into consideration (Salamanca et al. 2012). However, the latter is more computationally expansive and requires better quality of input urban

parameterization to achieve better accuracy in estimating urban micro-meteorological variation. Hereby, the uWRF model is configured according to the scope of a particular study coupling with an appropriate UCM for desired level of climatological downscaling.

3.2 Methodology

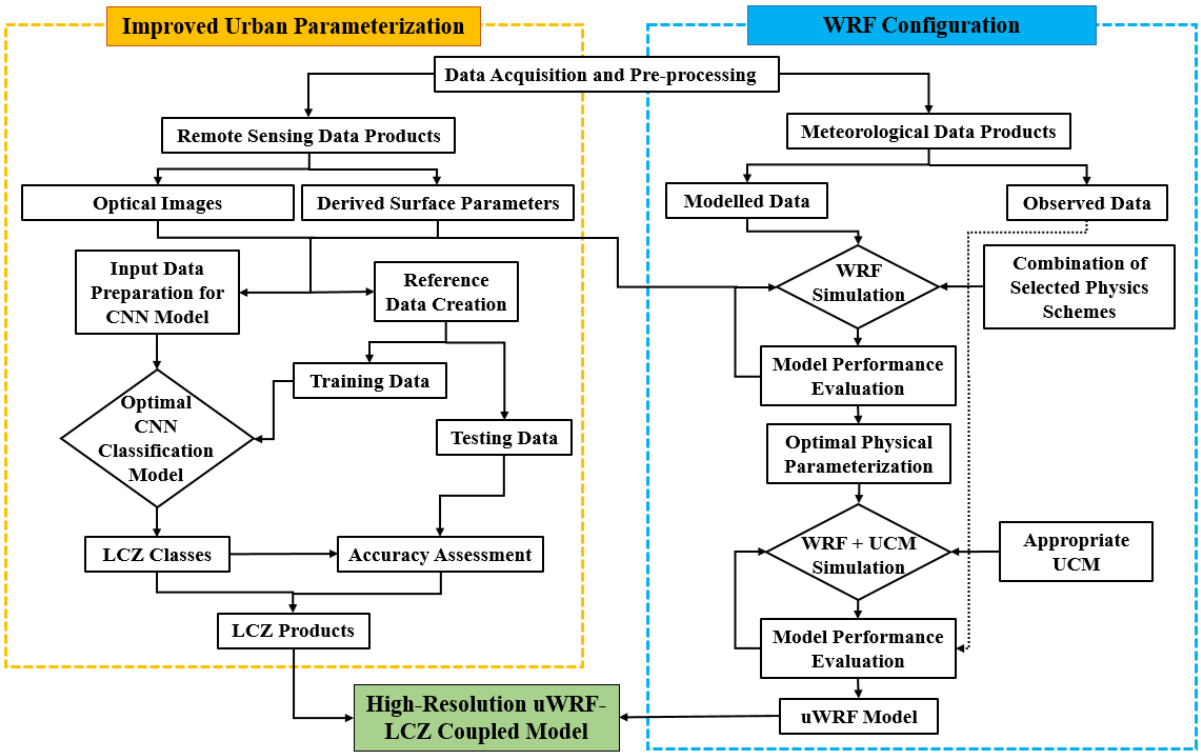

Figure: 3.1 Methodology Implemented; the left-hand section of the figure indicated with orange colour represents input preparation for improved urban parameterization, the right-hand section indicated with blue colour represents the WRF Model Calibration Process, the green box below represents the optimal high-resolution uWRF-LCZ coupled model

The surface geometry of cities from developing regions is extremely complex and dense, which regulates the roughness length, SVF, range of UCL etc, important to determine the temperature and moisture concentration along with wind flow pattern within the compact urban canopies (Chen et al., 2011). Therefore, the globally accepted LCZ scheme of classification with well-defined urban surface characterization, which could efficiently improve urban parameterization when integrated into the WRF model (Ren et al. 2017; Patel et al. 2020) was adopted to generate high-resolution urban parameters. As each LCZ class has distinguishable physical properties, the energy fluxes between the urban elements could be simulated, and micro-scale variations in immediate urban meteorology corresponding to the existing conditions could be captured more prominently. The WRF model highly dependent on model configuration integrates various atmospheric processes with the surface conditions to dynamically downscale

global/regional climate model outputs using suitable physics schemes that could appropriately represent the meteorological structure along with the geographical configuration of the area under consideration. Thus, appropriate physics schemes were identified using a systematic experimental design to augment the model performance. Finally, the model was calibrated using those optimal physical parameterization schemes as well as urban parameterization derived from the LCZ products to develop a high-resolution uWRF model which could ultimately generate different climate variables in required scale (Fig. 3.1). The methods and techniques adopted to obtain the required results are discussed in detail in the following sub-sections.

3.2.1 Improved Urban Parameterization

3.2.1.1 Local Climate Zones (LCZs)

The concept of Local Climate Zone (LCZ) for urban areas was developed based on the satellite observation-enabled classification process of the urban surface using precise information on the morphological and vegetation cover, providing a universal criterion for comparing temperature conditions between different cities (Stewart and Oke 2012; Ren et al. 2017; Xu et al. 2017; Zheng et al. 2017). This classification system helps in characterizing the physical form of urban areas according to built-up fraction, height and compactness of the roughness features, composition of the natural or non-built-up surface, thermal properties of all the elements etc. (Stewart and Oke 2012; Ching et al. 2018). The LCZ classification scheme categorises urban surfaces into 17 different zones considering the geometry and fabric of urban features across the globe (Stewart and Oke 2012). The first 10 classes (LCZ 1 – 10) represent the built-up extent of the cities, and the remaining 7 classes (LCZ A – G) constitute the natural or non-built-up areas such as vegetation, waterbodies, barren lands, rocks and soils etc. (Fig. 3.2). Although LCZs does not quantify temperature accumulation, the spatial distribution and extent of an LCZ class helps in identifying the areas with corresponding expected heating potential (Stewart and Oke 2012; Lao et. al, 2015; Zheng et al. 2017). It has been widely applied as an important input for complex climate models in various studies to determine meteorologically derived surface characteristics in addition to other land surface data (Ren et al. 2017; Mughal et al. 2018; Zheng et al., 2017; Xu et al. 2018).

The World Urban Database and Access Portal Tools (WUBAPT) framework for LCZ generation was widely accepted and used due to its less complicated methodology, which could

be executed using open-source software and datasets (Bechtal et al 2015; Ching et al. 2018). It adopts the random forest algorithm for supervised learning on Landsat images (having moderate spatial and temporal resolution and long-term coverage) using manually created training samples. Although highly popular among urban climate studies, this methodology was not successful in preparing very efficient results in the case of highly heterogeneous cities. Therefore, various other methods were proposed and explored using test cases of different cities and using different datasets to generate robust LCZ products. Different types and resolution remote sensing data base were explored for improved LCZ mapping, including multispectral (Bechtel et al. 2015; Yoo et al. 2019), hyperspectral (Liang et al. 2023), microwave (Bechtel et al. 2016; Zhu et al. 2022), UAV and Lidar products (Koc et al. 2017; Chen et al. 2023) etc. The methods used, differed according to the type of data product, level of detail and also the complexity of the cities. The recent period has seen the application of advanced image classification techniques using machine learning and deep learning algorithms for LCZ creation which have significantly improved the classification accuracy (Yoo et al. 2019; Zhu et al. 2022; Chen et al. 2023).

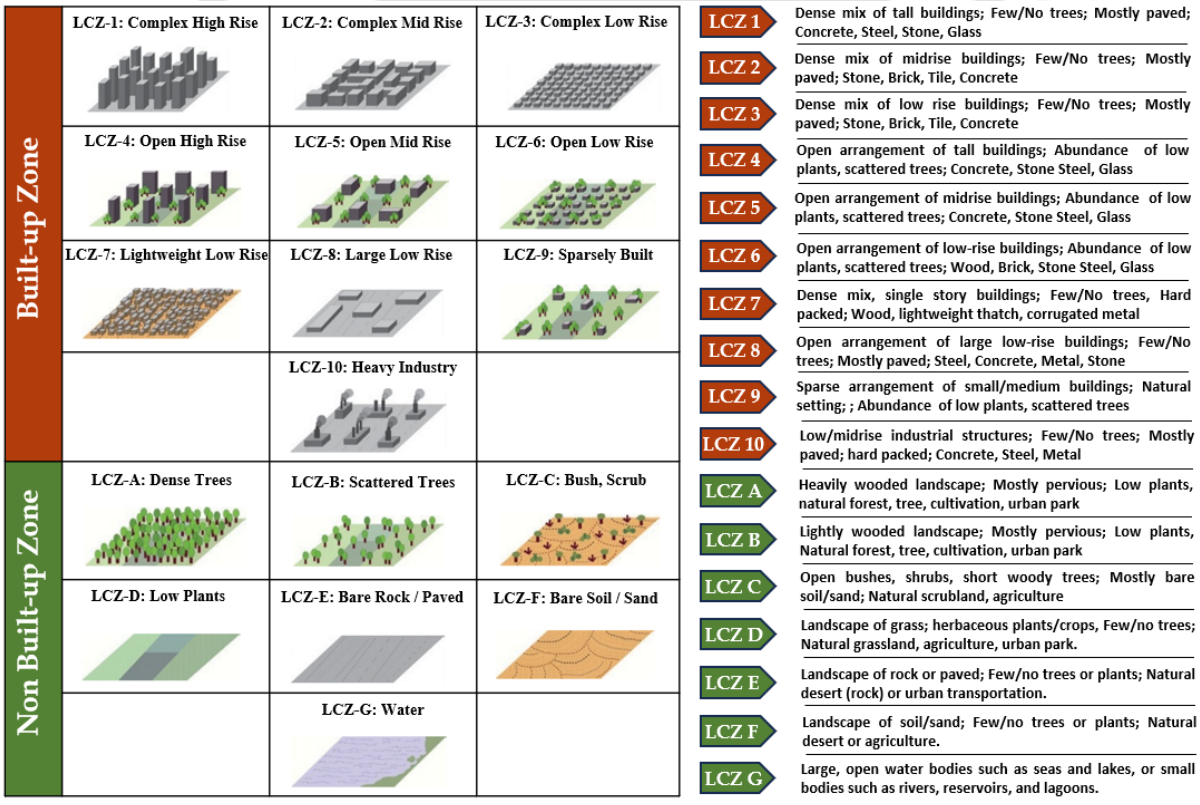

Figure 3.2: LCZ Types and their characteristics (Adapted from Stewart and Oke, 2012)

3.2.1.2 LCZ Generation

This study explored the merit of advanced image processing techniques, adopting deep learning principles using multispectral images and other allied products for LCZ Classification.

a.) Reference Data Preparation

Table 3.1: LCZ-wise training and testing sample size for KMA and GMA regions. The values represent a number of polygons and their corresponding pixels, within parentheses.

LCZ Classes	Kolkata		Guwahati	
	Training	Testing	Training	Testing
LCZ 1	-	-	-	-
LCZ 2	16 (2430)	14(2356)	9(1662)	7(1514)
LCZ 3	9(2087)	8(2023)	14(1923)	12(1850)
LCZ 4	5(1652)	3(1356)	-	-
LCZ 5	17(2497)	12(2326)	7(1257)	5(1083)
LCZ 6	12(2342)	10(2301)	6(922)	5(851)
LCZ 7	8(857)*		-	-
LCZ 8	9(1958)	7(1820)	5(1146)	3(980)
LCZ 9	18(2567)	14(2411)	14(1411)	11(1261)
LCZ 10	5(1847)	4(1324)	7(690)*	
LCZ A	18(2793)	15(2651)	20(2682)	20(2793)
LCZ B	18(2557)	18(2390)	12(1714)	10(1719)
LCZ C	8(1562)	6(1427)	7(961)	6(920)
LCZ D	23(3227)	20(3154)	17(2211)	15(2007)
LCZ E	16(1756)	14(1591)	5(630)	4(529)
LCZ F	12(1547)	11(1580)	8(1101)	5(998)
LCZ G	20(2730)	15(2214)	13(1843)	12(1890)

* is used to denote the red-star classes which represents the training and testing datasets with lesser data samples

The LCZ reference datasets were prepared manually using the technique followed in the WUDAPT framework for LCZ creation individually for both cities. On assessing the ground conditions, it was found that not all the LCZ classes were present in either of the cities. Kolkata accommodated a total of 16 LCZ classes (excluding LCZ 1), and Guwahati had 14 classes (except for LCZ 1, LCZ 4 and LCZ 7). Therefore, reference polygons were manually created for each LCZ class from both cities with the help of google earth datasets and field verifications. Then, the LCZ polygons were randomly divided into two parts: one for training

the model and the other for testing the accuracy of the modelled results. The training and testing samples were carefully divided into 60 % and 40 %, respectively, so that the number of polygons as well as the total area covered by them for each LCZ class is proportional (Table 3.1). However, as some LCZ classes had very few reference polygons due to their lesser prevalence in the study region, and dividing them further into training and testing datasets would bias the model training, the technique established by Yoo et al. (2019) was adopted for those particular classes for both cities. The training and testing data for those classes were extracted within each polygon based on stratified random sampling and they were marked as 'red-star' classes. Finally, all the reference data preparation was completed by converting the polygons into raster layers with a resolution of 3 m to comply with the input data products.

b.) Input Data

The high-resolution Planetscope datasets were used here as the primary input for LCZ preparation which includes the visible and near-infrared (VNIR) bands. The Planetscope products are commercially available satellite images operated by Planet and acquired by a constellation of 130 satellites (https://developers.planet.com/docs/data/planetscope/) which provides daily datasets with 4 bands (which have been updated to 8 bands recently) and at a spatial resolution of 3 m. However, a limited number of images could be non-commercially obtained for research and academic purposes with appropriate justification, and thus was acquired through the Planet API (https://www.planet.com/explorer) for this study. The relatively higher spatial resolutions of these images and their daily availability led to the choice of these products for the analysis and Planetscope scenes with clear sky conditions covering the KMA and GMA and their surrounding regions were acquired systematically. A total of 27 scenes were required to cover the KMA region (more than 2000 km^2) imaged on the 24th of January, 2019 and 9 scenes for the GMA region (more than 500 km^2) imaged on the 28th January, 2019. The 4-band (Blue, Green, Red, NIR) scenes were further pre-processed to achieve the scaled surface reflectance values and mosaicked together after colour assimilation to produce individual images for each region. However, due to the limited spectral range of the Planetscope products, the study further utilized other allied datasets to improve the data volume and consistency of the input datasets required for deep learning-based algorithms. Building footprints for both the cities were downloaded from the freely available Open Street Maps website (https://www.openstreetmap.org), for research and academic activities. The building areas were calculated using polygons and the footprint layers were then rasterized to a spatial resolution matching the planet images and was considered as the next layer.

$$NDVI = \frac{NIR - Red}{NIR + Red} \quad 3.1$$

$$IBI = \frac{\frac{2SWIR}{(SWIR+NIR)} - [\frac{NIR}{(NIR+Red)} + \frac{Green}{(Green+SWIR)}]}{\frac{2SWIR}{(SWIR+NIR)} + [\frac{NIR}{(NIR+Red)} + \frac{Green}{(Green+SWIR)}]} \quad 3.2$$

Normalized Difference Vegetation Index (NDVI) products were generated using the Red and NIR bands of the Planet datasets applying eq. (3.1) and added to the input stack to provide added weightage to the vegetated surfaces. Similarly, the refined Index-based built-up Index (IBI) established by Xu (2008), was used to identify built-up pixels using NIR, Red, Green and short-wave infrared bands (SWIR) (eq. 3.2) of Sentinel-2 images acquired on dates closer to the Planetscope products. The flexibility of Google Earth Engine (GEE) was used to acquire the Sentinel-2 images, process them, create the IBI products and resample them to 3 m resolution to match the Planet products. The elevation profile served as the next layer derived from the ALOS PALSAR digital elevation model (DEM) (12.5 m) obtained from the Alaska Satellite Facility (https://asf.alaska.edu/data-sets/sar-data-sets/alos-palsar/), resampled again according to the other input layers. Therefore, a total of 7 bands including the 3 multispectral planet bands (Gleen, Red and NIR) and the other thematic layers derived through different processes (building footprint layer, NDVI, IBI, and DEM) were stacked together to form the input data bundle.

c.) Convolutional Neural Network (CNN) Classification

The use of different CNN algorithms has become very popular for LULC mapping from remote sensing images over the last decade because of their advantage of extracting important information without any prior knowledge using convolutional layers (Yoo et al. 2019; Zhu et al. 2022). These techniques emphasizes on rather using manually defined features to train the model and categorize the images into the defined classes. 3-dimensional input data (width, height, and channel) could be processed using this process and the output of a convolutional layer could be transmitted to the next layer maintaining the same 3-dimensional shape. The input and output data of the convolutional layer are called feature maps and the convolution process is performed with several filters (or kernels) over the input feature maps (Yoo et al. 2019). However, convolutions reduce the size of the output feature maps, to prevent which they are padded, i.e., filled with specific values before beginning the convolution process so that the spatial dimensions of the output feature maps are adjusted. Mostly 0 values are used for padding, but this could also be determined according to the model. To manage and involve all

the bands of multiple-layer inputs a non-linear activation function is used which could convert the sum of input data into an output result. Following the extraction of feature maps, the model proceeds to the down-sampling stage which is also known as pooling, to reduce the size of data and make the model simpler to avoid the problem of overfitting. This sub-sampling technique is used to locally summarize the output of the previous layer making translation invariance and focusing on the presence of a particular feature rather than the location. These pooling layers also optimize the number of weights to be assigned, making the model less computationally intensive. Then the final feature maps thus produced are transferred to fully connected layers which are used as classifiers to predict the final class with the highest probability using a softmax function, a commonly applied classifier for multi-class classification using neural networks (Yoo et al. 2019). The fully connected layers consist of a set of weights to be optimized for each node and convert the 2-D features into 1-D vectors so that the inputs can be provided linearly to the nodes of the neural network.

A typical CNN architecture including input layers, convolutional layers, pooling layers, and fully connected layer(s), through which the model could learn to identify geometry, spectral properties and distribution in the image, was used for this study. The input layers consist of the data points or image bands which include the 7 layers stacked together with the same dimensions and grid-scale. In the convolutional layer, convolutional filters were iterated as a moving window performing a dot product between the filter kernel and the local region of the previous layer, to find the optimal filter size which could detect the significant spatial features of the input images. The kernel size is one of the most important hyperparameters responsible for creating a group of local regions on the considered inputs, the combination of pixels that provide a hierarchical knowledge of the features it contains. Here, 3 different kernel sizes were tested, i.e., 1×1, 3×3 and 5×5 to find the most optimal layer for both the cities according to their respective surface conditions. Then the next component, i.e., the pooling layer, which provides the representative values (mean or maximum) of the given window was identified. It is to be noted that, on adopting a $k \times k$ pooling layer, the size of the input data is reduced by a factor of k. Here, the max-pooling layer was used which adjusted the scale difference and effect of noise and also reduced the computational requirements.

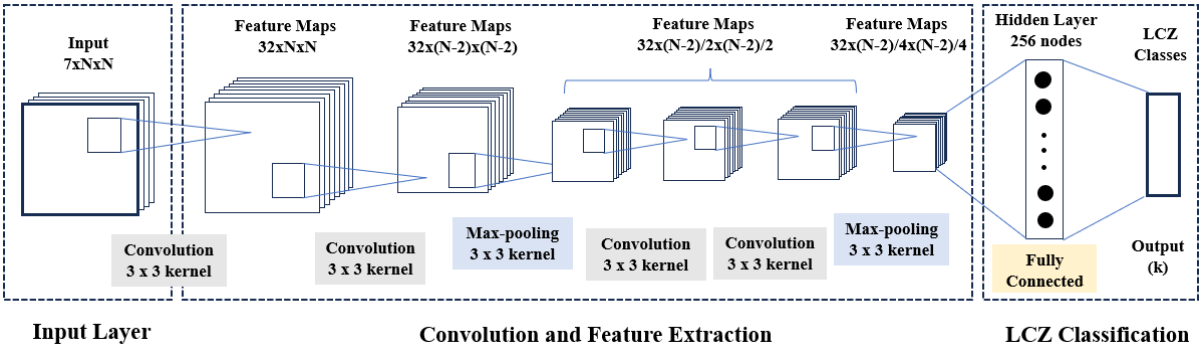

Figure 3.3: CNN structure designed for the study. N is the dimension of input images and k is the last output, i.e, the number of LCZ types to be classified for each city

Therefore, after a number of iterations changing the model structure and the combination of hyperparameters, a four-layer convolutional network with 3 × 3 convolutional kernel, two max-pooling layers (2 × 2) applied after the second and fourth convolutional layers, was found to be the most optimal architecture (Fig. 3.3). The 32 activation maps produced after the first convolution are stacked together and proceeded further to the next stage. To tackle the problem of non-linearity due to multi-layer inputs, the Rectified linear unit (ReLU) activation function was used which performed element-wise activation of the created volume and returned identity function at positive value and zero at the zero/negative values. The choice of ReLU activation function in this case was also due its computational efficiency and better performance on loss convergence. After the second max pooling layer, a 256 node fully-connected layer was used and the softmax function was applied to convert the output of the final fully connected layer which provides the probabilities of the existence of each class. Finally, the output layer thus generated obtained the LCZ classes corresponding to the individual cities. The model was trained at 300 epochs with 256 batch size.

d.) Accuracy Assessment

A randomly selected 90% of the training samples were used to train the CNN model and the remaining 10% used to optimize the weights and biases in the model. Then three different matrices were created to calculate the overall accuracy (OA) of the modelled results in comparison to the test samples using eq. (3.3 – 3.5) (Appendix 3.1).

$$OA = \frac{\sum_{i=1}^{k} N_i^c}{N^a} \quad 3.3$$

$$OA_u = \frac{\sum_{i=1}^{m} N_i^c}{N_b^a} \quad 3.4$$

$$OA_{nu} = \frac{\sum_{i=1}^{m} N_i}{N_b^a} \quad 3.5$$

Where, OA_u and OA_{nu} represents OA of the built-up LCZ classes and the built-up versus non-built-up classes respectively. N_i is the number of pixels classified as the ith LCZ class and N_i^c is the number of pixels correctly classified as the ith LCZ class, N_a and N_b^a are the number of ground truths of all classes and only built-up classes, respectively, and k and m are the total numbers of LCZ classes and total built-up classes. Further, the F1 score was also calculated (eq. 3.6) which is a harmonic mean value of the producer's accuracy (PA) and user's accuracy (UA) for each LCZ class to identify the class-wise classification performance.

$$F1 = \frac{(2\ \mathrm{PA} \times \mathrm{UA})}{(PA+UA)} \quad 3.6$$

3.2.2 WRF Model Calibration

The WRF 4.3 version with ARW dynamic solver was compiled with parallel processing capability in a high-performance computing system using gfortran and gcc compilers. The model was configured with the hybrid vertical coordinate (HVC) and hydrostatic pressure coordinate as the vertical coordinate system and the Arakawa C-grid staggering horizontal coordinate system. The third-order Runge–Kutta scheme was used for time integration.

3.2.2.1 Domain Configuration

The model was configured with three-tier one-way nested domain at horizontal grid spacing (grid points) of 9 – 1 Km (1:3) and 55 sigma vertical levels from the surface to 20 hPa. The outermost or parent domain (D01) consists of the entire Indian sub-continent, including the northern Bay of Bengal in the south and extending a little beyond the Lower Himalayan ranges in the north, responsible for regulating the monsoon currents in this region (Fig. 3.4). The size of this domain is 260 × 268 at a horizontal grid-scale of 9 × 9 km and 2-minute resolution of geographical inputs. The intermediate (first) nested domain (D02) sized 397 × 415 at a spatial resolution of 3 x 3 km, is focused on the East-North East zone of the Indian sub-continent including northern coastline of the Bay of Bengal and stretching till the Eastern Himalayas. Two individual domains D03 and D04 were configured as second nested layer to include the two cities being studied, viz., Kolkata and Guwahati. D03 and D04 contains KMA (94 × 112) and GMA (70 × 58) respectively along with their surrounding regions at a grid-scale of 1 km. Spatial resolution of the geographic inputs for the nested domains was 30 seconds each.

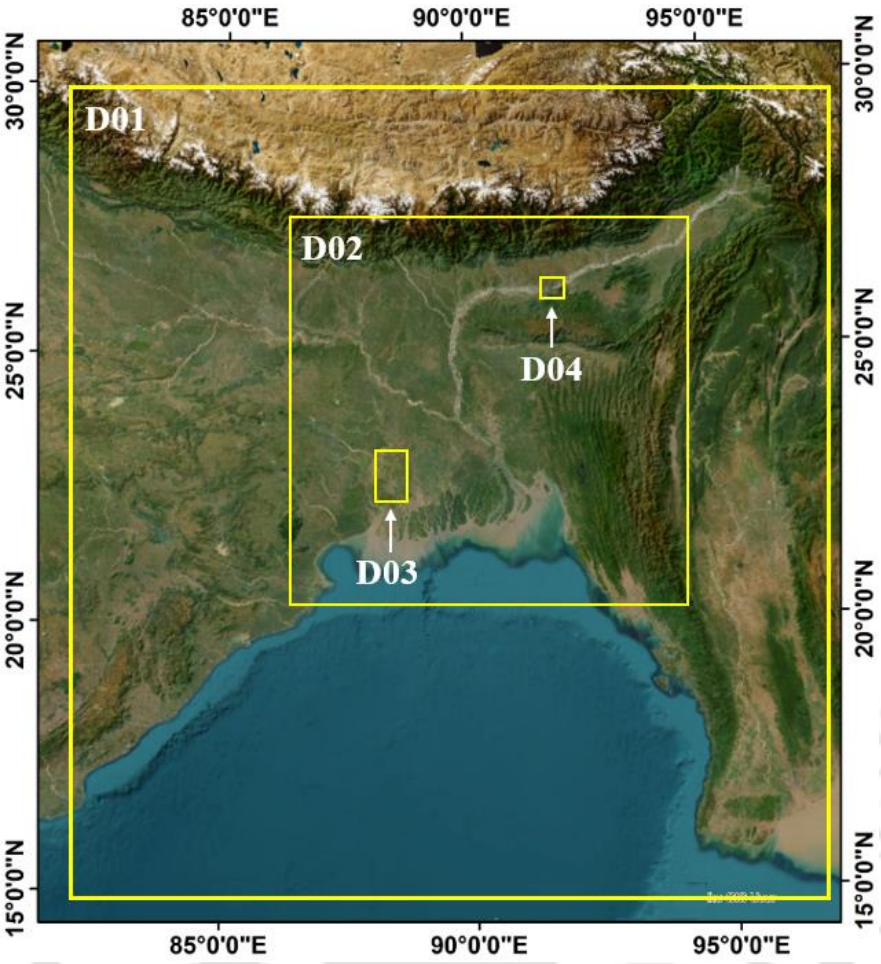

Figure 3.4: WRF Nested Domains covering the study region at different spatial resolution; D01-Outermost Domain (9 × 9 km), D02-Intermidiate Domain (3 × 3 km), D03-KMA (1 × 1 km), D04-GMA (1 × 1 km)

3.2.2.2 Physical Parameterization

WRF was calibrated considering the physical parameters that could adequately represent the regional atmospheric structure of the study region and were selected based on a detailed analysis of the relevant literature (Table 3.2). To define the PBL conditions, the Mallor-Yamada-Janjic (MYJ) scheme was adopted (Janjic and Zavisa, 1994) as it is one of the most suitable schemes to define the boundary conditions of this region. However, synthesizing the relevant literature, three important microphysics schemes (MP) were identified that could properly resolve the water vapour, cloud and precipitation processes in this region, i.e. the Kesseler scheme (Kesseler, 1969); the Lin scheme (Lin et al. 1983) and the WRF Single Moment 6-Class scheme (WSM6) (Hong and Lim 2006). Besides, Kain-Fritsch (Kain, 2004) and Grell-Freitas (Grell and Freitas 2014) cumulus parameterization (CP) schemes were among the best to scale the effects of convective and/or shallow clouds in this region. Rapid-Radiative Transfer Model for LW (Iacono et al. 2008) and Dudhia scheme (Dudhia, 1989) for SW

radiation were selected to configure the atmospheric heating due to radiative fluxes into the model. The Unified Noah LSM was identified to define the lower boundary condition to integrate all atmospheric and surface forcings along with the Monin-Obukhov similarity scheme for the surface layer (Tewari et al., 2004). The model was further integrated with different UCM options to include the dynamics of urban geometry. Both single (SLUCM) and specialized multi-layer (BEP, BEP+BEM) urban physics schemes were individually tested in order to adequately parameterize the sub-grid scale urban variability.

Table 3.2: List of Physical Parameterization Schemes adopted in the study

Sl. No.	Physical Parameterization	Schemes	Selection Criteria	References
1.	Planetary Boundary Layer	Mallor-Yamada-Janjic Scheme	Most widely accepted scheme in case of tropical and sub-tropical regions	Mughal et al. 2020; Bhati and Mohan 2016
2.	Microphysics	Kesseler Scheme	It is used when water is abundantly found in the atmosphere	Singh et al. 2015; Sati and Mohan 2021
3.		Lin Scheme	Can resolve six different types of hydrometeors and useful to resolve precipitation processes in urban areas	Pathirana et al. 2014; Patel et al. 2020
4.		WRF Single Moment 6-Class scheme	It is used to resolve ice-phase along with precipitation, advantageous for Himalayan regions	Hong et al. 2010; Patel et al. 2020
5.	Cumulus Parameterization	Kain-Fritsch Scheme	It rearranges the mass in a column to consume CAPE, useful for shallow convection	Patel et al. 2020; Nadimpalli et al. 2022
6.		Grell-Freitas Scheme	Used for weather and air quality modelling with the advantage of smooth transition to resolve clouds	Patel et al. 2020; Sati and Mohan 2021
7.	Longwave Radiation	Rapid-Radiative Transfer Model	Most widely used LW radiation parameter for tropical and sub-tropical regions	Hong et al. 2010; Bhati and Mohan 2018
8.	Shortwave Radiation	Dudhia Scheme	Most widely used SW radiation parameter for tropical and sub-tropical regions	Hong et al. 2010; Bhati and Mohan 2018
9.	Land Surface Model (LSM)	Unified-Noah LSM	Most widely used LSM model (unless some specific parameter is to be represented into the model)	Molnar et al. 2019;
10.	Surface Layer	Monin-Obukhov Similarity Scheme	Most suitable with the Noah-LSM to calculate the surface heat and moisture fluxes	Patel et al. 2020
11.	Urban Physics/Urban Canopy Models (UCM)	Single Layer UCM	Two-dimensional representation of urban surface parameters	Molnar et al. 2019; Bhati and Mohan 2016
12.		Building Energy Parameterization (BEP)	Three-dimensional parameterization of urban geometry along with the effect of building walls, roofs, roads etc.	Salamanca et al. 2012; Patel et al. 2020
13.		BEP+BEM (Building Energy Model)	Along with BEM it also considers the building indoor – outdoor exchange of energy due to air conditioners etc.	Mughal et al. 2020; Ribeiro et al. 2021

3.2.3 Experimental Design

Three sets of WRF simulations were performed to calibrate the model according to the regional – micro-scale structure of the study area to optimize the model performance and make the experiments more cost and time-effective (Fig. 3.1 and Table 3.3). First, to identify the most suitable physical parameterization schemes, the model was simulated with different combinations of the identified schemes and without integrating with the UCM models (Set – 1). The second set (Set – 2) of experiments were performed by integrating the most suitable physical parametrization schemes with the different UCM models, i.e., SLUCM, BEP and

BEP+BEM individually to test the most appropriate representation of the urban processes into WRF. All the above set of experiments were performed using the same geographical, land surface as well as meteorological forcings. Finally, after appropriate schemes for characterizing the physical as well as urban processes were identified, the uWRF model was integrated with the LCZs thus generated (i.e., the LULC of the innermost domains was replaced by the LCZ products) and the other updated higher resolution land surface products, to improve the accuracy of the model performance (Set – 3). The different urban roughness parameters (Table 3.4) were adjusted according to the study region to calibrate the uWRF-LCZ model. These parameters were either derived from LCZs thus produced (urban, vegetation and impervious surface fractions) or from various secondary sources and certain assumptions (thermal Conductivity, heat Capacity, emissivity and albedo). Some parameters such as building height, roof width, road width and SVF were modified according to secondary information as well as detailed knowledge gathered from field investigations in both cities. The LCZ-wise values of these parameters are provided in Appendix 3.2.

Table 3.3: Experimental Design to identify the optimal High Resolution uWRF model. Parameters shown here are used other than the constant parameters.

Experiment Name	Land Use Land Cover	LS Parameters (Albedo, LAI, Fcover)	Terrain	MP	CP	UCM
Set – 1						
WRF_1	Modified IGBP MODIS NOAH	MODIS	GTOPO_30	Kesseler	Kain-Fritsch	None
WRF_2				Lin	Kain-Fritsch	
WRF_3				WSM_6	Kain-Fritsch	
WRF_4				Kesseler	Grell-Freitas	
WRF_5				Lin	Grell-Freitas	
WRF_6				WSM_6	Grell-Freitas	
Set - 2						
uWRF_1	Modified IGBP MODIS NOAH	MODIS	GTOPO_30	Best of Set -1	Best of Set -1	SLUCM
uWRF_2						BEP
uWRF_3						BEP+BEM
Set - 3						
uWRF_1X	LCZ	CGLS	ALOS-PALSAR	Best of Set -1	Best of Set -1	Best of Set -2

Table 3.4: List of urban roughness parameters modified in the uWRF-LCZ model

Mean Building Height (m)	Emissivity
Roof Width (m)	Surface Albedo
Mean Road Width (m)	Aspect ratio
Sky View Factor	Impervious surface fraction
Thermal Conductivity	Vegetation Fraction
Heat Capacity	Urban Fraction

3.2.4 Datasets for Model Calibration and Validation

The modified International Geosphere-Biosphere Programme (IGBP) Moderate Resolution Imaging Spectroradiometer (MODIS) Noah landcover datasets (1 km resolution) were used to set the geographical boundary conditions and the National Centers for Environmental Prediction (NCEP) FNL (Final) Operational Global Analysis data of 0.25° × 0.25° resolution were used to initialize the meteorological forcings for the initial runs throughout the domain nests. The other land surface parameters such as the albedo, leaf area index (LAI) and fractional vegetation cover (Fcover), were also derived from MODIS products. GTOPO_30, the default terrain model used in WRF 4 version, was used to designate the topographical profile of the domains. These datasets were constant through the first two sets of experiments (WRF_1 – uWRF_3) (Table 3.2). However, in the final set of experiment (uWRF_1X), although the same combination of datasets was used to initialize the coarser domains (D01 and D02), landcover data for D03 and D04 were replaced by the higher resolution LCZ products. To achieve better consistency with the finer scale landcover inputs, the land surface parameters (albedo, LAI, Fcover) were also replaced by higher resolution (500m) and up-to-date products obtained from the Copernicus Global Land Services (CGLS) (https://land.copernicus.eu/global/products). The surface topography for these domains was also replaced by the higher resolution (12.5m) ALOS PALSAR DEMs. The modelled results were validated using higher resolution gridded data products as well as ground observations from meteorological stations under the IMD, for both the cities. Datasets available from three different IMD stations were obtained for Kolkata and one station for Guwahati.

3.2.5 Model Performance Evaluation

Performance evaluation of any model is important to validate its applicability to the intended scenario and to recalibrate it for improved performance. Therefore, some of the most reliable error estimation techniques, such as, Mean Bias (MB), RMSE (Root Mean Square Error) and

Mean Absolute Error (MAE) were used to validate the modelled results, with the observed datasets and compare the accuracy of the different experiments.

$$MB = \frac{1}{n}\sum_{i=1}^{n}(P_i - O_i) \quad 3.1$$

$$RMSE = \sqrt{\frac{1}{n}\sum_{i=1}^{n}(P_i - O_i)^2} \quad 3.2$$

$$MAE = \frac{1}{n}\sum_{i=1}^{n}|P_i - O_i| \quad 3.3$$

where, n is the total number of data points, i is data at a certain time point, and O and P are the observed and predicted values respectively.

3.3 Results and Discussion

This section presents the results obtained from the various experiments conducted to achieve improved urban parameterization as well as sensitivity analysis of the physical parameterization and urban physics schemes to identify the optimal model for high-resolution uWRF simulations, to generate finer scale urban climate variables.

3.3.1 LCZ Maps

3.3.1.1 Accuracy assessment of the classified LCZ Maps

LCZ maps for the KMA and GMA regions using the CNN model was generated for the year 2019 and the OA achieved were 71.33% and 78.69% respectively. However, due to the significance of micro-scale variation in the built-up regions of the cities, OA was also estimated separately for the built-up (LCZ 1 – 10) and non-built-up classes. It was seen that the model performed better in case of non-built-up classes with higher values of OA_{nu} compared to OA_u for both the cities. Further it was observed that the natural as well as built-up land surfaces were better classified for Guwahati compared to Kolkata as evident from the OA_u value of 73.3% and 66.1% and OA_{nu} values of 84.37% and 80.1% respectively.

Thus, on comparing the F1 score for the individual classes, it was observed that classification accuracy showed an increasing trend with the decrease in complexity among the built-up classes (Fig. 3.5). The lowest F1 score was achieved by LCZ2 and LCZ3 for both the cities which lie on the range of 0.5 – 0.6. This can be attributed to the highest chances of mixing in these classes due to the prevalence of higher urban heterogeneity as well as density in case of developing cities. It was further observed that among the natural LCZ classes, the F1 score decreases with decrease in the vegetation density in case of Guwahati but is non-uniform in the

case of Kolkata. However, the natural classes representing non-vegetated areas have higher F1 values for both the regions. The water pixels are most appropriately classified in either case with F1 score above 0.91.

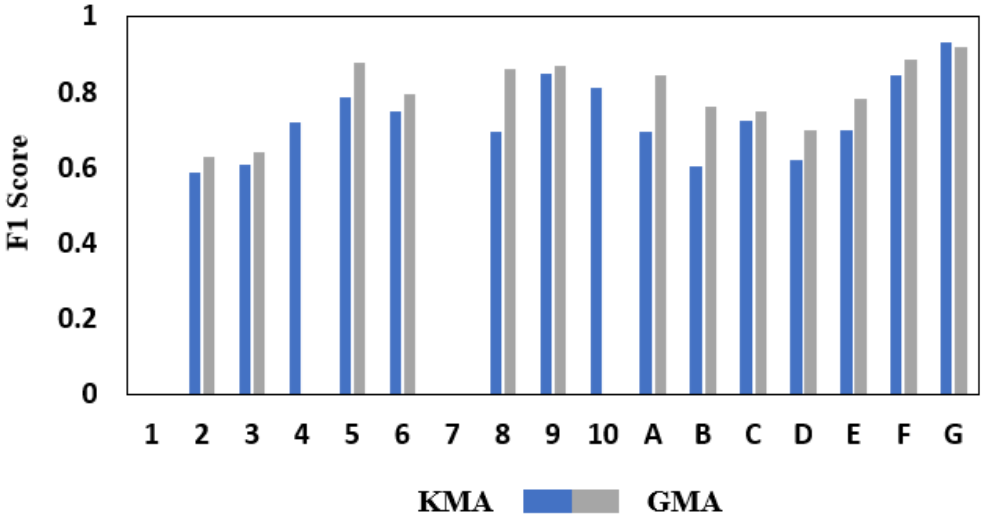

Figure 3.5: F1 score according to the individual LCZ classes for KMA and GMA regions. The 0 values represent either total absence of the LCZ class in the region or absence of testing sample due to lesser area under the particular class

3.3.1.2 Spatial Distribution of LCZ Classes

The detailed landcover conditions depicted by LCZ maps showed the highly heterogeneous nature of the urban surfaces in the case of both cities (Fig. 3.6a and 3.7a). The built-up density, i.e., built-up area to total area calculated for both KMA and GMA regions showed a higher built-up density in KMA (76.7 %) compared to GMA (60.5 %). The core regions of both the cities have high built-up density which gradually declines towards the peripheries following the general trend of the urban expansion. KMA region which is denser and more complex contained almost all the LCZ classes except for LCZ1 i.e., with compact high-rise built-up surfaces. However, the distribution of all other built-up classes however has great variations within the region. It was seen that LCZ2, LCZ3, LCZ5 and LCZ6 are the dominant built-up categories which cover more than 95 % of the built-up extent with the KMA boundary (Fig. 3.6b). The remaining built-up categories like LCZ4, LCZ7 – LCZ10, are more prominent in the surrounding regions outside the KMA boundary. Among all the built-up classes LCZ3, which consists of the compact 1 – 3 floor buildings have the highest areal coverage i.e., 24.4 % and is distributed throughout the KMA boundary from the core towards periphery, with highest density towards the core (Fig. 3.6c – f). The second most significant class is LCZ2 which includes the 3 – 8 floor buildings, covers around 22.6 % of the total area under KMA

and is mostly concentrated in the core city. Although Kolkata is one of the densest cities in India, the presence of compact high-rise buildings (i.e., above 8 floors) is not very common and is found only at a few regions scattered across the city with newly developed residential and commercial complexes.

The LCZ5 and LCZ6 classes with relatively higher green spaces and open areas cover almost the remaining built-up region within the KMA boundary (Fig. 3.6a). LCZ5 (17.9%), with 3 – 8 floor buildings with more open spaces mostly constitute the public enterprises as well as residential units and are observed to feature more prominently away from the compact core. However, some patches of LCZ 5 are also present in the central city which describes the heterogenous nature of urban development in the region. The open low-rises considered as LCZ6 are predominant towards the peripheral range of the KMA boundary with very low concentration in the core city. On the contrary, the density of the non-built-up classes is higher along the edges, which declines when moved towards the center. LCZA and LCZB are the most prominent non-built-up classes with an areal coverage of 6.9% and 8.6 % respectively, followed by waterbodies which covers about 6.72%.

A similar pattern of built-up distribution was observed for the GMA region with LCZ2, LCZ3, LCZ5 and LCZ6 as the most prominently featuring classes (Fig. 3.7b). The LCZ2 and LCZ3 classes constitute about 63.35 % of the total built-up area and is observed to constitute almost the entire core city region following the general rule. Further, LCZ5 and LCZ6 covering 11.5% and 10.2% respectively of the entire GMA territory are mostly concentrated along the city's southern and eastern margins, comprising of the newly developed regions of the city (3.7c – f). The LCZ4 and LCZ7classes are non-existent in the GMA region and the prevalence of LCZ8 – 10 is fairly low within the city boundary. However, LCZ8 and LCZ9 feature prominently on the surroundings of the GMA area, especially towards the north and east. However, unlike Kolkata the distribution of natural surfaces in Guwahati do not follow the general tendency to increase from core to periphery. Due to the unique physiographic set-up of the city, containing high-altitude regions and small hills within the city limits, the built-up expansion is non uniform towards all directions (Fig. 3.7a). These high-altitude parts are mostly covered with dense vegetation and LCZ3 and LCZ6 classes. Thus, the total areal coverage of the LCZA class is 20.9% followed by LCZB i.e., 10.6% which helps in regulating the different climatic variables within the city. Further, the presence of the mighty river Brahmaputra, which flows through the northern reach of the city and many other smaller and larger wetlands, affects the overall climate of the region.

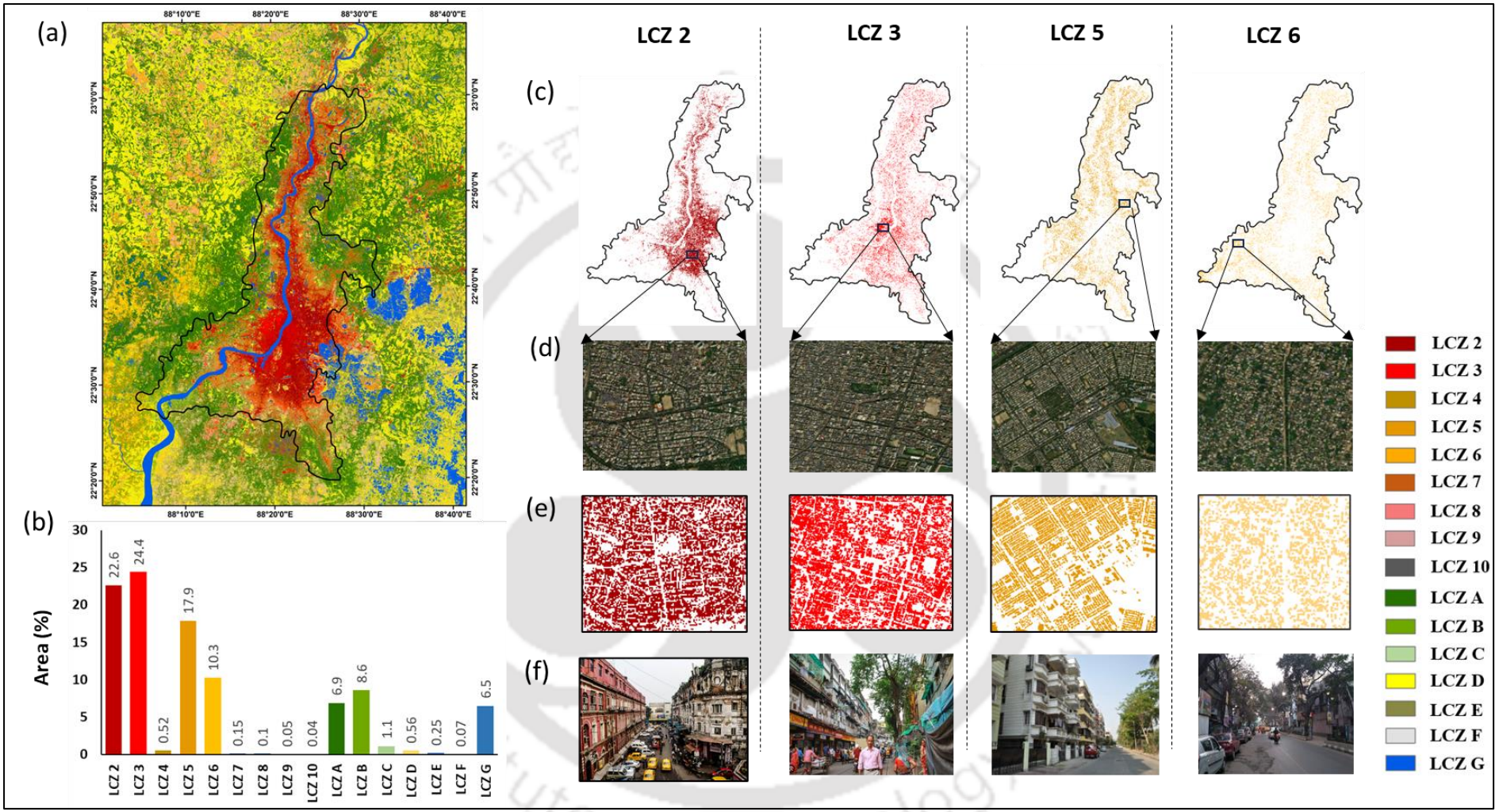

Figure 3.6: LCZ distribution of KMA and the surrounding region. (a) KMA LCZ for 2019; (b) LCZ-wise areal coverage within KMA boundary; (c) Distribution of most prominent built-up LCZ classes with KMA; (d) Satellite Image; (e) Classified result; (f) Field view

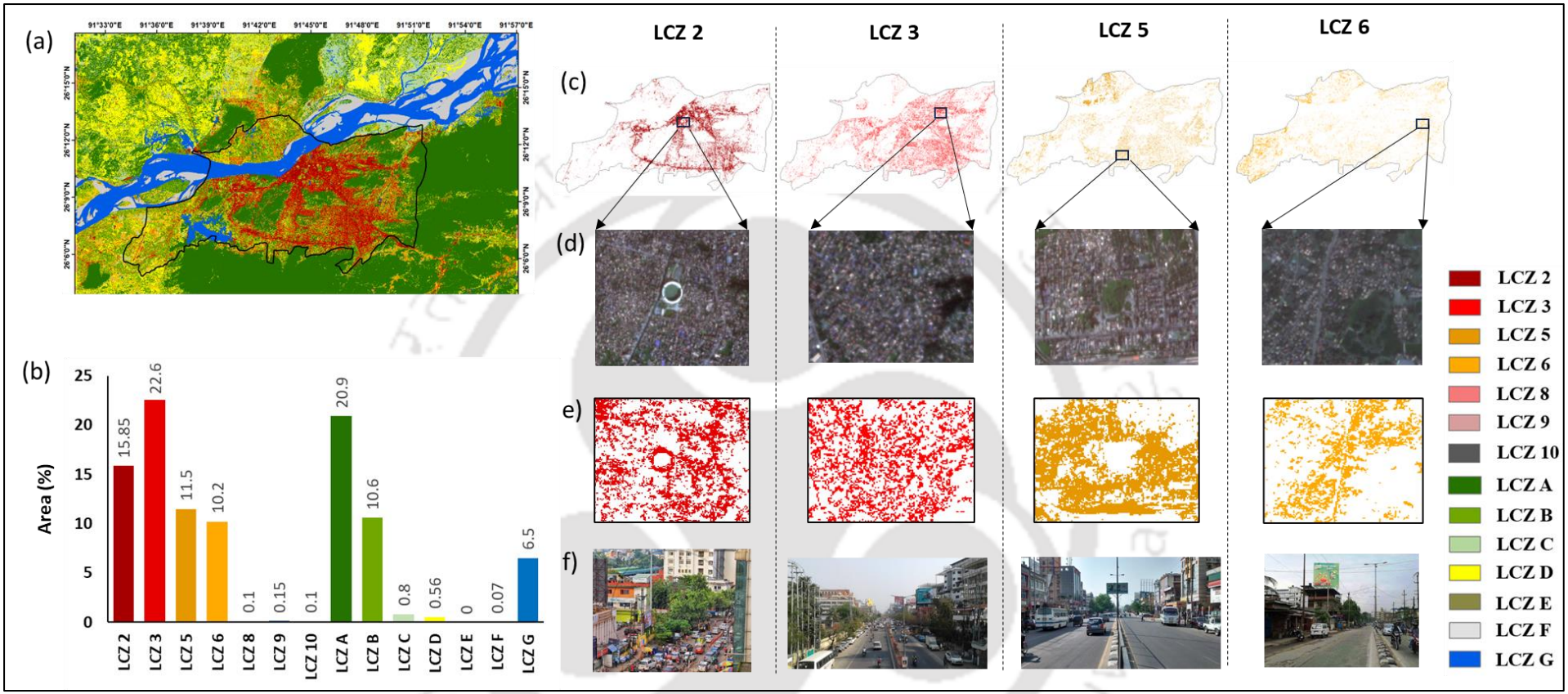

Figure 3.7: LCZ distribution of GMA and the surrounding region. (a) GMA LCZ for 2019; (b) LCZ-wise areal coverage within KMA boundary; (c) Distribution of most prominent built-up LCZ classes with GMA; (d) Satellite Image; (e) Classified result; (f) Field view

3.3.2 WRF Performance and Model Parameter Estimation

Three sets of experiments were performed to determine the ideal WRF configuration, which could appropriately downscale the different climate parameters according to the micro-scale variations in the built-up surface of the city. The model was simulated with a 3-tier nested domain where the innermost domains constituted the cities and had a horizontal resolution of 1 km. Thus, the meteorological variables generated at a resolution of 1 km were compared with the observed datasets for the available sites in the region. The spatial average of data from the three stations available for Kolkata and the data from the single station available for Guwahati was compared with the simulated results to evaluate the model performance in the case of all the designed experiments. The two most important parameters i.e., 2m air temperature (T_2) and rainfall (RF) were the variables chosen to evaluate the model performance due to the reliability of those datasets reported in previous studies conducted for these regions (Dawn et al. 2020; Bhattacharjee et al. 2022).

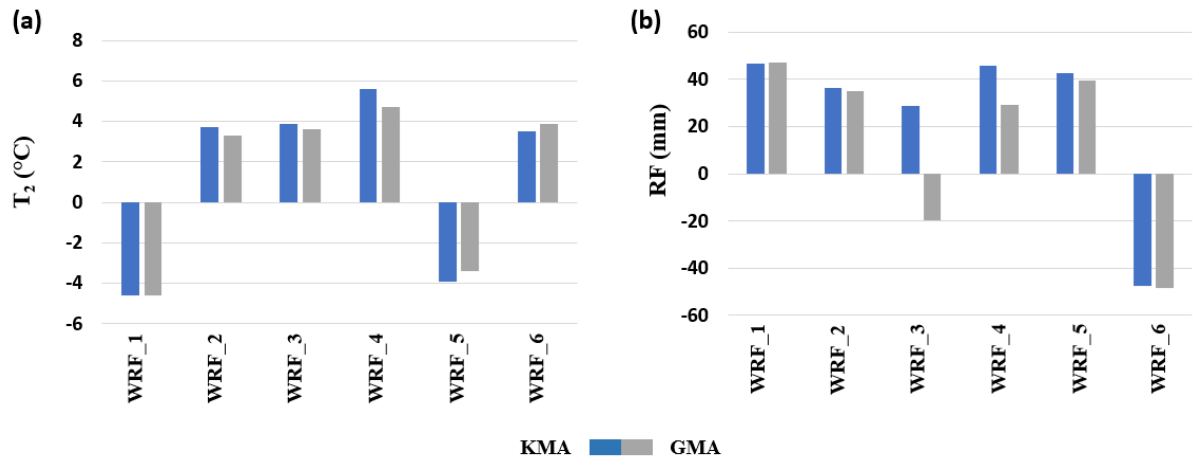

Figure 3.8 MB Estimation of Set – 1 Experiments. (a.) 2m Air Temperature (T_2) and (b) Rainfall (RF)

The first set of experiments was designed to estimate the appropriate cumulus and microphysics schemes which could provide reasonably similar performance for both the regions. A total of 6 simulations were performed by changing the combinations of these two schemes and keeping the other physical parameters constant. On estimating mean bias between the modelled results and observed datasets, it was seen that, experiments WRF_2 and WRF_5 performed most consistently for both parameters over both regions (Fig. 3.8). Although the biasness of WRF_3 simulation was also found to be lower, the acute under-estimation of RF for Guwahati region only made the model unreliable for further use. Thus, it was seen that the Lin scheme, which

was considered in the case of both WRF_2 and WRF_5 experiments, was able to better resolve the water vapour, cloud and precipitation processes in this region. On further comparison, the experiment that produced lower MB value between the two, i.e., WRF_2, was chosen as the final model, which also complied with other investigations in this region (Li et al. 2016; Sabiha and Satyanarayana 2022). Thus, Lin and Kain-Fritsch schemes were identified as the most suitable MP and CP schemes respectively to appropriately parameterize the effects of clouds and convection in this region and were adopted for the next set of experiments.

Table 3.5 Performance Evaluation of Set-2 Experiments

Experiment Name	KMDA					
	T_2 (°C)			RF (mm)		
	MB	RMSE	MAE	MB	RMSE	MAE
uWRF_1	2.9	3.22	4.97	28.11	25.85	17.6
uWRF_2	2.5	2.7	3.7	23.45	21.5	15.7
uWRF_3	1.9	2.5	2.86	20.72	19.89	13.82
	GMDA					
uWRF_1	2.81	2.96	3.2	29.9	24.6	32.7
uWRF_2	2.1	1.78	2.82	23.6	19.23	23.58
uWRF_3	1.69	1.35	2.51	19.81	16.61	21.24

The second set of experiments was conducted to find the most suitable UCM to incorporate the effect of modified energy fluxes due to the heterogeneous and complex surface properties on the urban meteorology. Along with MB, RMSE and MAE were also computed to evaluate the performances of the UCM-WRF coupled uWRF models (Table 3.5). The results show that the SLUCM model (uWRF_1) could substantially reduce the error from the WRF_2 model, which performed best among the Set 1 experiments. The biasness was reduced at a range of 1 – 1.5 °C for T_2 and 10 – 15 mm for RF when a UCM was introduced on the bulk parameterized model. Next, on simulating the model coupled with the BEP scheme (uWRF_2), the error was further reduced as seen from the MB, RMSE as well as MAE values for both the variables, due to the improved ability of the model to comprehend the three-dimensional urban geometry. The effect on T_2 was relatively higher in the case of Guwahati with the difference in RMSE and MAE values being 1.18 °C and 0.5 °C respectively, which could be attributed to the lower built-up density compared to that of Kolkata. However, in the case of rainfall the error margin

reduced by the BEP model compared to SLUCM was almost same for both cities, ranging between 2 – 7 mm.

On introducing the most specialized BEM+BEP (uWRF_3) model which could also resolve the indoor-outdoor energy exchange between the buildings and their surrounding along with their three-dimensional structure, the performance of uWRF was further enhanced. The values of MB, RMSE and MAE of uWRF_3 simulated T_2 reduced by 0.6°C, 0.2°C and 0.8°C respectively when compared with uWRF_2 simulations in case of Kolkata and 0.41°C, 0.43°C and 0.31°C in case of Guwahati. Similar results were also observed in the case of rainfall which shows the capability of near-surface energy transfer to affect the convective system over the region. Error in the simulated rainfall values was further reduced by 2 – 5 mm with the uWRF_3 model. Thus, these three experiments helped in concluding that BEP+BEM is the best UCM to integrate the urban surface properties into the WRF model.

Table 3.6 Performance Evaluation of Set-3 Experiment

Experiment Name	T_2 (°C)			RF (mm)		
	MB	RMSE	MAE	MB	RMSE	MAE
uWRF_1X_KMDA	1.2	1.41	1.52	17.71	17.8	12.2
uWRF_1X_GMDA	0.9	0.91	0.87	15.42	15.1	19.83

The last experiment was conducted in an attempt to further improve the model performance with the introduction of fine-scale urban parameters into the BEP+BEM model. The most capable uWRF model thus estimated from the earlier set of experiments was finally coupled with the LCZ products for both cities, and the model was calibrated by modifying the default urban roughness parameters according to the surface properties of the study region. The simulated results satisfied the hypothesis of the first objective which assumed that, by incorporating finer scale urban parameterization, the meso-scale WRF model could achieve higher accuracy in estimating the micro-meteorological parameters (Table 3.6). The MB, RMSE and MAE values for both cities reduced substantially by a factor of 1.1°C – 1.5°C for T_2 and by 2 – 7 mm for RF. Thus, the above set of experiments systematically helped in identifying the most appropriate physical as well as urban parametrization schemes that could adequately resolve the atmospheric conditions in interaction with the prevailing surface morphology of the Kolkata and Guwahati cities (Table 3.7).

Table 3.7: Optimal physics schemes identified for the final high-resolution uWRF-LCZ coupled model

Physical Parameters	Optimal Physics Schemes/Models
PBL	Mallor-Yamada-Janjic (MYJ)
CP	Kain-Fritsch
MP	Lin
SW Radiation	Dudhia
LW Radiation	Rapid-Radiative Transfer Model (RRTM)
LSM	Unified Noah LSM
Surface-Layer	Monin-Obukhov similarity
Urban Physics (UCM)	BEP+BEM

3.4 Summary and Conclusions

It is important to understand urban meteorology about the surface configuration of the cities, which varies according to the prevailing socio-economic as well as geographical conditions of the region. The cities from developing parts of the world are highly complex due to their dense and heterogeneous nature. It is seen that the meteorological conditions of such cities may vary at very small scale of horizontal distance, which makes the implementation of suitable urban planning and mitigating processes more difficult. Therefore, it is important to develop a detailed understanding of the urban-climate interactions, especially in such cities which are continuously expanding at a much rapid rate compared to cities from developing parts of the world. Therefore, this study tested the potential of a meso-scale NWP model WRF coupled with finer-scale urban parameterization to downscale the coarser resolution NCEP-FNL GCM products to appropriately represent the urban surface meteorology of two dimensionally and morphologically different cities.

Thus, fine-resolution LCZ maps were first derived using higher-resolution satellite images and other geospatial products using a CNN-based model for image classification. The efficiency of CNN models for urban areas with high surface roughness, applying the convolution technique in training the classification algorithm has led to its selection in this particular case. After several iterations, the most appropriate model architecture was identified, which could satisfactorily classify the images and generate 3m resolution LCZ products, at an overall accuracy of 71.33% and 78.69% for the KMA and GMA regions respectively. On evaluating

the LCZ products it was observed that LCZ2, LCZ3, LCZ5 and LCZ6 are the most dominantly featuring LCZ classes for both cities, covering more than 90 % of the total urban area. Also, it was seen that the complexity of the urban landscape gradually decreased away from the city core and the reverse was applicable for the non-built-up classes.

Since WRF is a model highly dependent on model configuration, the second part of the study focused on identifying the most appropriate physical and urban parameterization schemes to be integrated with the WRF model to resolve the atmospheric conditions of the study region properly. Thus, a series of experiments were systematically designed, which could help in building the appropriate high-resolution uWRF model with possibly reduced computation time and cost. Evaluating the performance of all the simulations compared to observed datasets, it was found that Lin and Kain-Fritsch schemes for MP and CU parameterization, respectively were most suitable for the study region, along with the MYJ scheme for PBL, RRTM for LW radiation, Dudhia scheme for SW radiation and Unified Noah LSM for land surface parameterization. Further on integrating different UCMs to resolve the near-surface urban-climate interactions, it was found that the BEP+BEM model when coupled with the high-resolution LCZ products, substantially improves the model performance. Therefore, this high-resolution uWRF-LCZ coupled model thus configured was further used for detailed study of the micro-climate of the considered cities.

Chapter 4

Micro-scale Variations in the Urban Climate of two cities using uWRF-LCZ Coupled Model

4.1 Introduction

The micro-meteorological variations in cities are influenced by a host of different factors such as the geography of the region, built-up area fraction, the complexity of urban structures and forms, the variety of anthropogenic functions, etc., which govern their radiative feedback on the overlying atmosphere. This study adopted a two-city approach to understand the impact-magnitude of these factors on the immediate meteorological conditions of the respective cities. The cities considered for investigation are Kolkata and Guwahati, which reflected similar urban fabric and general climatic structure but differed in terms of the scale of urbanization and local geography. This chapter includes a detailed analysis of the characteristic inter as well as intra-scale meteorological variations and surface energy fluxes defined by the nature of urban dynamics of both these cities.

4.2 Methodology

Apart from the urban physical structure and composition, the micro-meteorological conditions of the cities are also defined by the regional climatology of the area. The uWRF-LCZ coupled model thus configured was used to simulate the diurnal as well as seasonal variations in the micro-meteorology of KMA and GMA regions. Although these regions experience four different seasons, the analyses were conducted only for the pre-monsoon (which overlaps with the hot and dry summer months), monsoon (which covers the hot and wet summer months) and winter seasons. The post-monsoon season, showed lesser significance in terms of meteorological characteristics particular to urban climate from the time-series analysis of temperature and rainfall over the study regions (Appendix 4.1), and was deliberately excluded from this study. It did not possess a distinct or extreme character as that of the other three

seasons such as, lowest temperature and rainfall during winters and highest during the monsoons, highest temperature and dry spells during the pre-monsoons. Since both the study regions experience moderate temperatures and is adequately moist during the post-monsoon season, its impact on the meteorological health especially in the case of an urban area is less significant compared to the remaining three seasons and thus was not included in the detailed analysis.

Table 4.1 Season-wise Simulation time-scale

Season	Simulation Period
Pre-monsoon	21st August – 30th August
Monsoon	5th May – 15th May
Winter	1st January – 10th January

The study was conducted for the year 2019 for a period of 10-days during each season, which could reflect the general climatic trend of the particular season and avoid local biases. The study period was identified by categorically analysing the hourly temperature and rainfall from ERA-5 land reanalysis datasets for 2019 provided by the European Centre for Medium-Range Weather Forecasts (ECMWF). The days reflecting the peak seasonal character, i.e., high temperature and no rainfall during pre-monsoon, high temperature and continuous rainfall during monsoon and lowest temperature with no rainfall during winters were selected for each city individually. Then a 10-day period with such persistent conditions and common to both cities was finally identified so that the study period for both cities could be kept constant to optimize the simulation time and cost (Table 4.1). The downscaled meteorological variables such as T_2, T_s, 10m wind speed (WS), 2m Relative humidity (RH), and cumulative rainfall (RF) along with the surface energy fluxes were then analysed to understand the micro-scale diurnal and seasonal variations.

4.3 Results and Discussion

The detailed spatio-temporal analysis of the different meteorological variables over and around the cities is important to assess the impact of urbanization. Variations from the mean value for all parameters were estimated to effectively depict the differences in spatial as well as temporal distributions.

4.3.1 Micro-meteorological variations in Kolkata

The spatio-temporal distributions of 2m air temperature (T_2), surface/skin temperature (T_s), wind speed (WS), relative humidity (RH) and rainfall (RF); and the sensible heat flux (SHF), ground heat flux (GHF) and latent heat flux (LHF) as shown in Fig. 4.1 – 4.5, determine the variations in the micro-meteorology of Kolkata and its surroundings. The diurnal variability of the parameters was depicted using two distinct local times (LT) i.e., 14:00 hours representing early afternoon and 20:00 hours representing late evening (Fig. 4.1 – 4.2). The spatial distribution was depicted through the simulated results for the monsoon season due to the availability of all variables, including RF. A detailed analysis of the variables was done over the predominant LCZ classes, i.e., LCZ2, LCZ3, LCZ5 and LCZ6, to understand the micro-scale variations within the city. Although the general tendency of these classes is to decline from core to periphery, inter-mixing is still prevalent due to the unplanned nature of urban development in these cities.

Table: 4.2 LCZ-wise selected location across KMA from core to periphery to assess local scale meteorological conditions. Source: Field Investigation and different primary and secondary sources

Sl. No	LCZ Type	Location Name	Selection Criteria
1.	LCZ 2	Dakshineshwar	Core city, very densely populated, residential and commercial
2.		Howrah	Core and oldest part of the city, very densely populated, near the Hooghly river, mostly commercial
3.		Ghusuri	Core city, very densely populated, residential and commercial
4.		Maniktala	Core and oldest part of the city, very densely populated, mostly residential
5.	LCZ 3	Dumdum	Relatively newer part of the city, densely populated, mostly residential, IMD station
6.		Garden Reach	Older part of the city, densely populated, near Hooghly river, mostly residential
7.		Jadavpur	Relatively newer part of the city, densely populated, mostly residential and commercial
8.		Sealdah	Core city, densely populated, mostly commercial
9.	LCZ 5	Alipore	Core and oldest part of the city, relatively lesser population density, mostly public spaces and commercial, green spaces, IMD station
10.		Golf Green	Relatively newer part of the city, relatively lesser population density, mostly residential, green spaces
11.		New Town	Newer part of the city, relatively lesser population density, mostly residential and commercial
12.		Salt Lake	Relatively newer part of the city, planned part of the city, mostly residential and commercial, green spaces, IMD station
13.	LCZ 6	Raypur	Newer part of the city towards the peripheries, densely populated, mostly residential
14		Chandan Nagar	Newer part of the city towards the peripheries, relatively lesser population density, mostly residential and industrial, green spaces, far from the coast
15.		Padampukhur	Newer part of the city towards the peripheries, relatively lesser population density, mostly residential and industrial, green spaces
16.		Garia	Relatively newer part of the city, densely populated, mostly residential and commercial, closer to the coast
17.	Peri Urban (PU)	PU-South	Outskirts of the city, much lesser population density, closer to the coast, mostly vegetated
18.		PU-East	Outskirts of the city, much lesser population density, near water bodies, mostly vegetated
19.		PU-West	Outskirts of the city, much lesser population density, far from the coast, mostly vegetated

Thus, to avoid biases, multiple locations were selected from each class based on field observation and primary and secondary information, and were analysed individually and in relation to the others (Fig. 4.4a). Nineteen different locations were carefully selected from throughout the city and its surroundings, addressing the influence of the local geographic conditions such as the presence of water bodies or closeness from the coast, etc. population and

built-up density, green spaces etc. (Table 4.2). Four locations each were selected from the four urban LCZ classes and three from the peripheral region just from the outskirts of the city. The locations were then arranged from the most complex LCZ class (i.e. LCZ2) to the least (LCZ6) and then further to the urban periphery just outside the KMA boundary (including LCZ8, LCZ9, LCZB and LCZD) according to their individual distances from the central city in increasing order, to analyse the inter to intra urban micro-scale meteorological variations (Fig. 4.4). The diurnal as well as seasonal variations in the micro-meteorological conditions were then shown using a class-wise average of each variable at the selected LT (Fig. 4.5).

4.3.1.1 Near-surface air temperature

The spatial variations of T_2 from its mean during the monsoon season reflect the rural – urban differences in air temperature in KMA and its outskirts by ±1.5°C (Fig. 4.1a, b). T_2 is highest over the core city regions which gradually reduces towards the peripheries and is lowest around the areas with dense vegetation cover around the city. It again increases towards the domain boundaries due to the presence of smaller urban centres, villages, and other settlements. The core city with the highest and most compact built-up configuration is almost 2.5°C to 3°C warmer than the surrounding vegetated areas during the day and about 1.8°C to 2.5°C at night. However, T_2 variations are also visible within the densely built areas of the city in a range of 0.5°C to 1.5°C (Fig 4.1a and Fig. 4.4a). These differences are governed by the diurnal heat exchange between the built-up areas and the overlying atmosphere as represented in Fig. 4.2.

The SHF as well as GHF values are highest during the day due to the higher heating potential of the urban surfaces as well their heat retention capacity. The contribution of SHF is highest in the total heat fluxes both during the day and night, followed by the GHF, which also reflects the heat storage potential of the surface, and LHF, which is mainly induced by evapotranspiration. The value of sensible heat ranges from -40 to 120 Wm^{-2} during the day and -40 to 70 Wm^{-2} at night with the highest values in the core city region. The GHF heat flux is also highest in the core city during the day with values ranging from 0 to 90 Wm-2 which declines at night ranging from 5 to 60 Wm-2 with a lower urban-rural difference. The latent heat, however, is lowest in the core city and highest along the waterbodies, particularly at night. There exists a significant difference in RH between the city and its surroundings, with the values being lowest in the complex urban, even during the monsoon season; which is directly related to the T_2 as well as LHF. It was observed that humidity variations from urban to rural is higher during the day, although the absolute values are higher at night (88 to 100 %)

compared to day (80 to 100 %). The higher temperature conditions within the city and the abundance of waterbodies, and vegetation along with the influence of moist winds from the coasts are responsible for the higher rural – urban contrast in the humidity level.

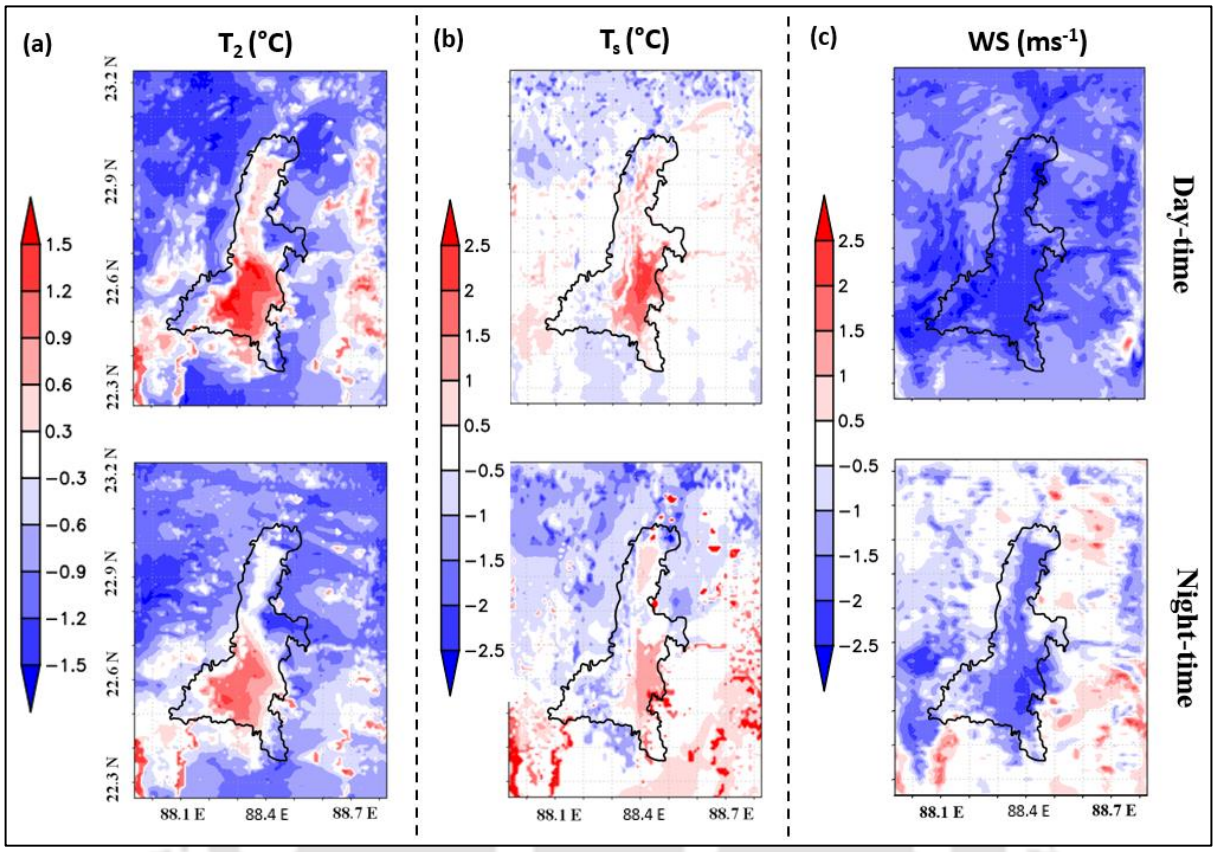

Figure 4.1: Spatial distribution of the modelled meteorological variables (variations from the mean) for the KMA and surrounding regions during a typical monsoon day (24th August 2019). (a) Diurnal Variations in T_2; (b) Diurnal Variations in T_s; (c) Diurnal Variations in WS. Day-time (14:00 LT) and Night-time (20:00 LT)

On analysing the LCZ class-wise hourly T_2 for the 10 day-period during monsoons, the areas covered by LCZ2 classes from different parts of the city were found to be the warmest with a distinct difference of 0.8 to 1.2 °C compared to the locations covered by the next class. i.e., LCZ3 in terms of urban complexity (Fig. 4.4b). However, there also exists inter-class differences due to the distance from the city core. The conditions are almost similar for LCZ3, LCZ5 and LCZ6 classes which could be attributed to the similar pattern of heat retention capabilities. It was seen that the diurnal temperature variations are lowest in the LCZ3 and LCZ5 classes compared to the others, which indicates their consistent UHI potential. The temperature conditions in the surrounding regions are lowest compared to the classes within the KMA area, but the diurnal variation range is the highest.

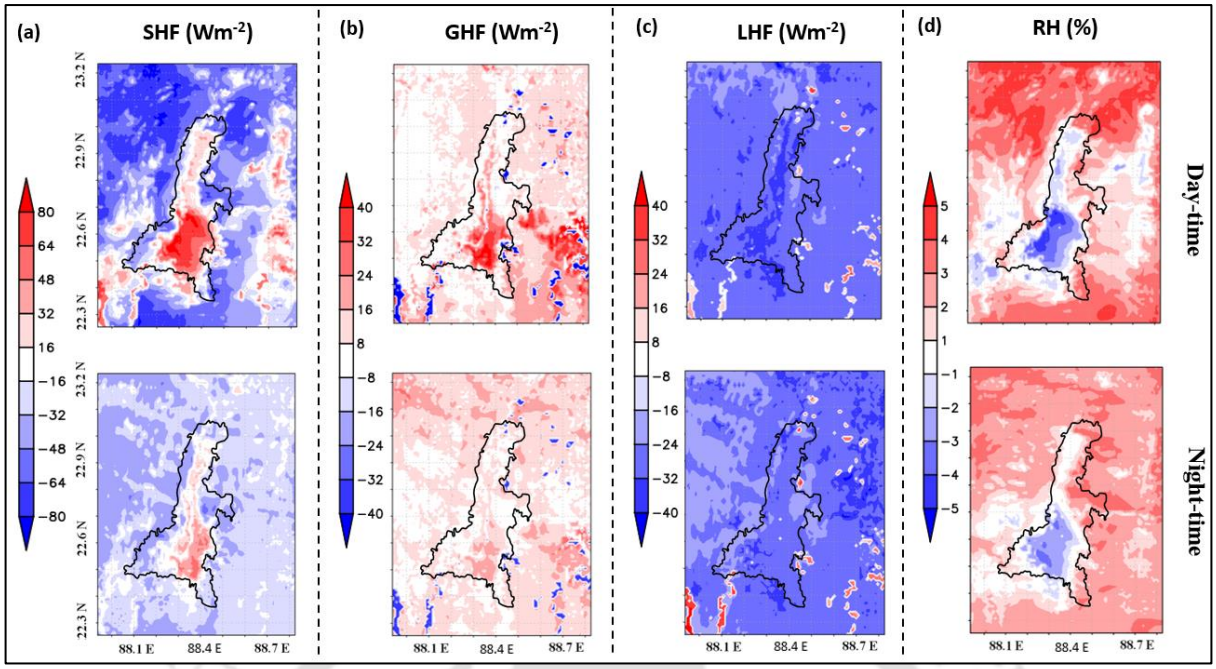

Figure 4.2: Spatial distribution of the modelled variables influencing the radiative feedback mechanism (variations from the mean) for the KMA and surrounding regions during a typical monsoon day (24th August 2019). (a) Diurnal Variations in SHF; (b) Diurnal Variations in GHF; (c) Diurnal Variations in LHF; (c) Diurnal Variations in RH. Day-time (14:00 LT) and Night-time (20:00 LT)

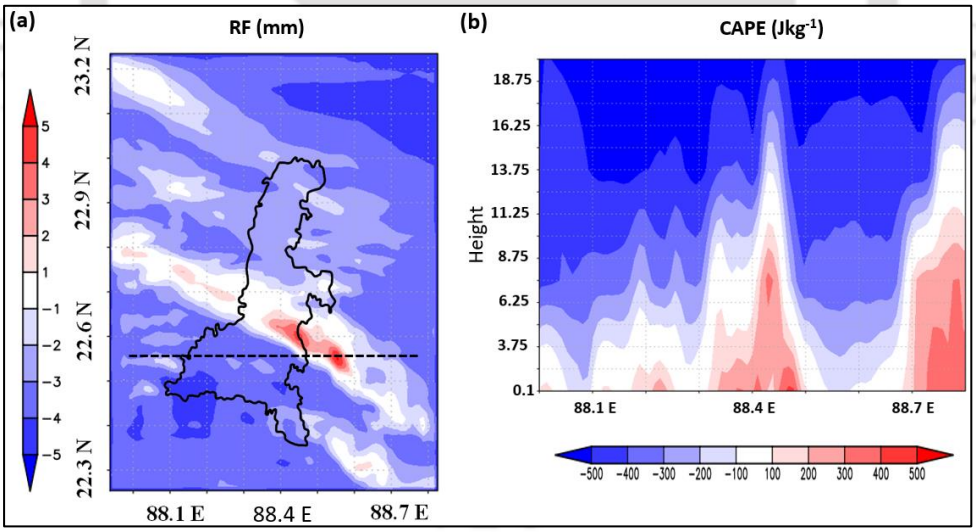

Figure 4.3 Spatial distribution of the modelled RF and CAPE (variations from the mean) for the KMA and surrounding regions during a typical monsoon day (24th August 2019)

The seasonal variations are shown by the average value of all the locations of the individual classes revealing that the potential of UHI is stronger during the pre-monsoon season due to the higher differences in the average, maximum and minimum values of T_2, which could be related to the dry atmospheric conditions (Fig. 4.5a). The daytime analysis is performed considering the modelled results from 06:00 – 17:00 LT and nighttime from 18:00 – 5:00 LT,

which is kept constant throughout the seasons to avoid complexity, irrespective of the seasonal changes in daylight hours. There exists a significant difference between the different built-up LCZ classes with a range of 2 – 4 °C (from LCZ2 – LCZ6) and further up to 5 to 6 °C with the peri-urban classes. On average, the temperature falls within a range of 0.8 to 1.3 °C from the dense urban to the peripheral region (Fig. 4.5a). The min – max variations are also lowest during the pre-monsoons both during day and night, which indicates that the prevailing UHI conditions are almost evenly distributed throughout the day. During the monsoons, the temperature range within each class increases slightly compared to the pre-monsoons, but the inter-class difference declines, which can be an impact of the prevailing rainfall conditions during this season (4.5b). The inter-class variations among LCZ2 – LCZ5 are the lowest during winter, with about 0.5 to 1 °C difference compared to the outskirts both during the day and night. However, the min – max variation during winter is highest for LCZ2 at night, forming cool islands within the city, mainly as the taller urban canopy cover decreases the heating potential of the ground surface (Fig. 4.5c).

4.3.1.2 Surface/Skin temperature

The variations in T_s spatially over the city are almost similar to the air temperature conditions. Still, there exists a higher difference in the range of temperature values, due to the higher heat retention capacity of the surface compared to air (Fig.4.1b), also reflected by the SHF and GHF conditions (Fig. 4.2a & b). It was observed that the rural – urban variation during the afternoon and late evening is 4 – 5 °C with higher differences during the former. However, as the water takes longer to heat up as well as cool due to higher specific heat, the areas covered by water bodies both within and outside the city boundary are cooler during the afternoon compared to the nearby regions and warmer at night. This difference in T_s also regulates the T_2 values of the nearby regions to a certain extent.

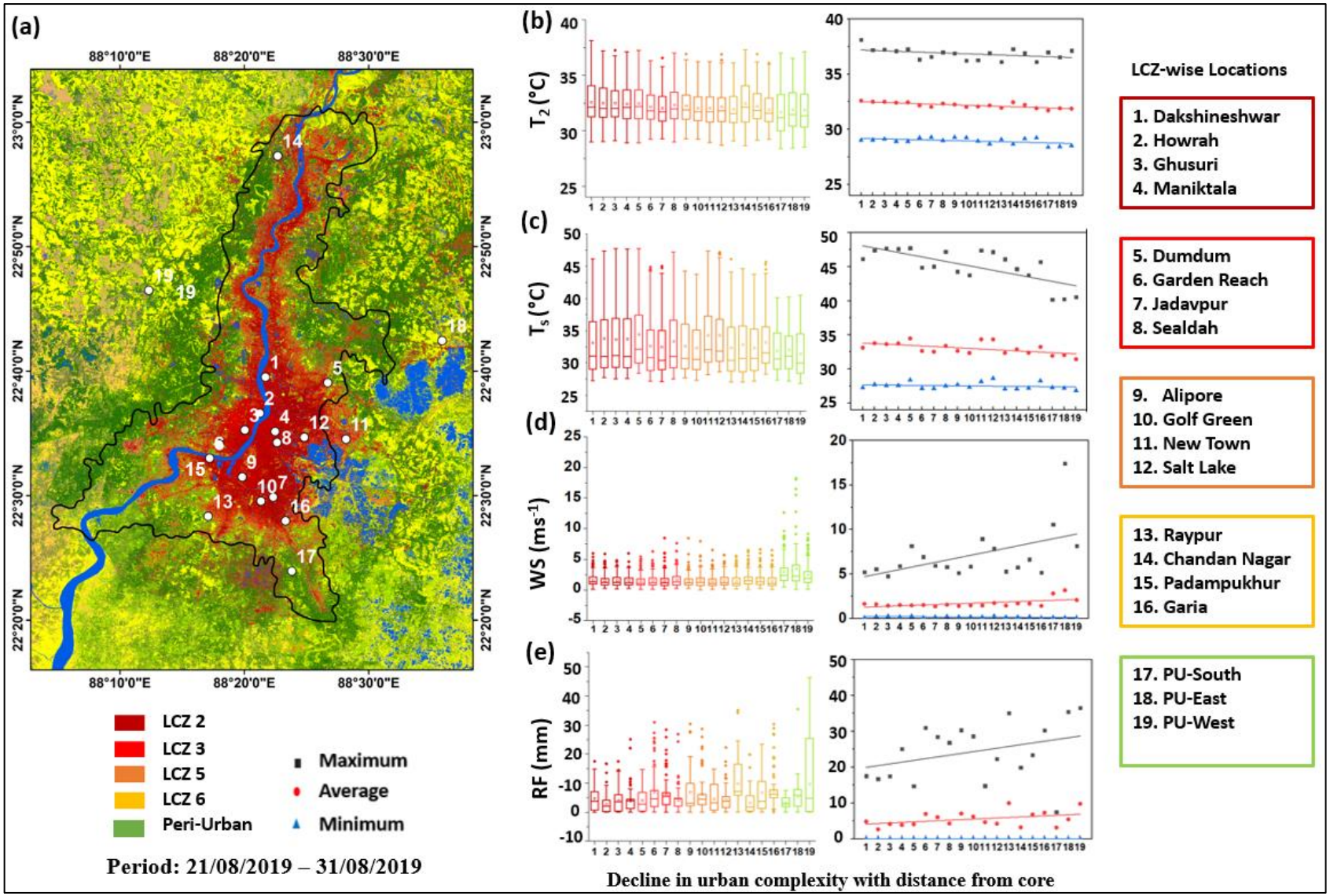

Figure 4.4: Micro-scale variations in the modelled meteorological variables over Kolkata. (a) Selected locations (b) LCZ class-wise variations in T_2; (c) LCZ class-wise variations in T_s; (d) LCZ class-wise variations in WS; (e) LCZ class-wise variations in R

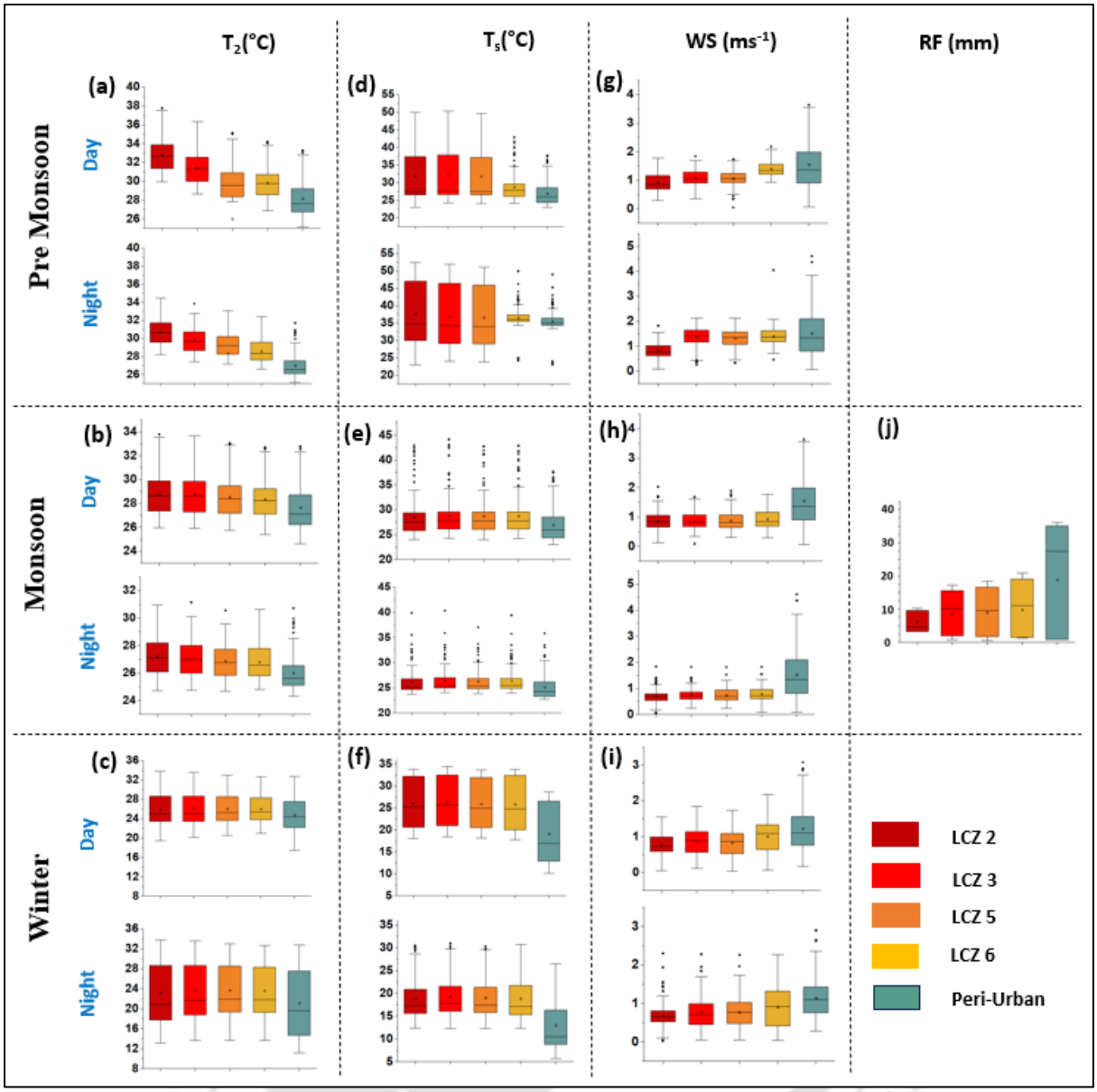

Figure 4.5: Micro-scale variations in the seasonal and diurnal patterns of the modelled meteorological variables over Kolkata. (a - c) LCZ class-wise variations in T_2; (d - f) LCZ class-wise variations in T_s; (g - i) LCZ class-wise variations in WS; (j) LCZ class-wise variations in RF. Pre-Monsoon Period (05/05/2019 – 15/05/2019); Monsoon Period (21/08/2019 – 31/08/2019) and Winter Period (05/01/2019 – 15/01/2019)

Although the LCZ-wise distribution followed the declining trend from the core city to the surroundings, there existed internal irregularities between the individual classes which could be due to the prevailing local surface conditions such as the influence of water bodies, urban green spaces and the general urban fabric (Fig. 4.4c). The decline in the maximum values of T_s for the 10-day average period is higher compared to T_2 which is mainly impacted by the lower temperature conditions of the peri-urban surfaces. However, the variation between the average and minimum values is almost the same. Thus, the inter class variations in surface heating are

not very distinct among the prominent built-up LCZs, which is almost maintained throughout all the seasons, both during the day and night. Furthermore, it could be noticed that, during the pre-monsoon season, the average T_s values are slightly higher in LCZ3 and LCZ4 classes compared to LCZ2, during the daytime and much higher than LCZ6 throughout the day (4.5d). This can be related to the comparatively lower SHF and higher LHF in areas covered by LCZ6 with more open spaces and green cover compared to the others (4.2a and c). The variations are very low for the monsoons and winter between the built-up LCZ classes, although the min – max range is high during winter days compared to nights as opposed to the prevailing T_2 conditions which is a result of this effect (4.5e and f).

4.3.1.3 Wind Circulation

The urban surface roughness conditions and the city geometry greatly influence wind circulations within the cities. This is evident from the spatial variations in WS within the city and surrounding (4.1c). The wind speed could reduce even by 5 ms^{-1} in the core urban areas from the surrounding and the difference is more prominent during the night due to an increase in the coastal breeze. It is noteworthy that the variations between average and minimum WS are very low between the different LCZ classes throughout the city irrespective of the canopy height, but a significant difference exists in the maximum values increasing at an average rate of 1 ms^{-1} through the different classes. The urban structures could greatly reduce the high wind velocity even during monsoons, as evident from Figure (4.4d). However, the seasonal analysis reflected least variations among the LCZ classes during the monsoons as compared to the pre-monsoons and winter during the daytime as well as at night due to the influence of only the local circulations (Fig. 4.5g – i). During both these seasons, the night-time WS in the most complex LCZ class (LCZ2) varies on a scale of 0.2 to 0.5 ms^{-1} from the next (Fig. 4.5g, i). A slight decline is visible in LCZ4 regions compared to LCZ3 which could be directly attributed to the higher building height in the latter.

4.3.1.4 Rainfall Intensity

The response of urbanization to rainfall variations is highly unpredictable, with many studies indicating an increase in extreme rainfall events due to urbanization, change in the storm cycles, delay in the initiation of rainfall periods etc. (Patel et al. 2020; Rath et al. 2022). This study mainly focuses on the influence of urbanization on the synoptic monsoon rains at a local scale (Fig. 4.3a). The vertical distribution of convective available potential energy (CAPE) required to induce rainfall was analysed along the most urbanized transect of the domain, which

has a gaussian distribution of built-up surfaces (Fig. 4.4). It was seen that, the value of CAPE is highest along the densest urban section, varying from 800 – 2000 JKg^{-1} (Fig. 4.3b). However, the lower variations over the non-urban regions indicate that the available energy is already being utilized to enhance the convection, inducing higher rainfall intensity. On analyzing the LCZ-wise hourly RF magnitude over the 10-day period, which experienced light to heavy rain episodes ranging from 0.5 – 35 mm, a considerable increase in the average rainfall intensity was reported along with the decline in LCZ complexity. The results depicted a difference of about 3 – 5 mm in the average rainfall value between LCZ2 and LCZ6 (Fig. 4.5j).

4.3.2 Micro-meteorological variations in Guwahati

The Guwahati city shows almost similar trends as that of Kolkata in the general micro-meteorological context throughout the city. However, significant impacts of the local geography is also evident from the results (Fig. 4.6 – 4.10). Similar to Kolkata, a total of ten different locations were selected with multiple locations in each LCZ class, depending on the areal coverage of each type and the existing geographical conditions (Fig. 4.9a). These locations were carefully selected based on field knowledge and various primary and secondary sources (Table 4.3). One location each was selected from the LCZ 2 and LCZ 3 zones due to the lesser dominance of these areas in the GMA area compared to KMA. Two locations each were selected from the LCZ 5 and LCZ 6 regions due to the local variations within the same broader region. Three different locations were selected from the outskirts of the city in all direction along which the city is expanding and one from near the city center but at a vegetated hill slope (characteristic of Guwahati city, Section 1.5.2), to represent the transformation from core to periphery of a city. The diurnal as well as seasonal analysis was performed with particular emphasis on the monsoon season due to its significance in the region.

Table: 4.3 LCZ-wise selected location across GMA from core to periphery to assess local scale meteorological conditions. Source: Field Investigation and different primary and secondary sources

Sl. No.	LCZ Type	Location Name	Selection Criteria
1.	LCZ 2	GS Road	Core and older part of the city, very densely populated, mostly commercial and public spaces, closer to the Brahmaputra river
2.	LCZ 3	Beltola	Relatively newer part of the city, very densely populated, mostly commercial and residential, closer to the Meghalaya hills and far from the Brahmaputra river
3.	LCZ 5	Hatigaon	Relatively newer part of the city, densely populated, mostly residential
4.		Railway Colony	Older part of the city, densely populated, mostly residential, green spaces
5.	LCZ 6	Dhirenpara	Relatively older part of the city, relatively less densely populated, mostly residential, green spaces
6.		Maligaon	Older part of the city, densely populated, mostly residential, green spaces, closer to the hills
7.	Peri Urban (PU)	Jorabat	Peripheral region of the city, much lesser population density, newly expanded built-up, vegetated region
8.		Regional Meteorological Centre (RMC)	Peripheral region of the city, much lesser population density, newly expanded built-up, vegetated region, IMD station
9.		IIT Guwahati	Peripheral region of the city, much lesser population density, newly expanded built-up, vegetated region, bank of the river Brahmaputra
10.		Kalapahar	Lies near the core city but at higher elevation, much lesser population density, newly expanded built-up, vegetated region

4.3.2.1 Near-surface air temperature

The diurnal variations in the T_2 between the urban and non-urban are higher in the case of Guwahati, especially along the southern boundary due to the abundance of densely vegetated areas (Fig. 4.6a). The temperature difference is as high as 8°C, which reflects the prominence of the UHI effect in Guwahati, irrespective of being surrounded by dense vegetation. The local-scale variations within the LCZ classes also reflect a steady decline from the core city to the outskirts in a range of 0.5 - 1°C between the consecutive classes (Fig. 4.9b). The difference in min-max values, along with the increasing complexity, also shows a gradual decline. On analysing the surface fluxes, it was found that similar to Kolkata, the contribution of SHF is highest in the net radiative forcing varying from -80 to 60 Wm^{-2} (Fig. 4.7a). The urban – non-urban contrast in the SHF values is much higher during the day as compared to night. The spatial distribution of GHF over the entire domain, however, shows relatively lesser variations within the city and outskirts during the day, which rises at night as the heat storage potential of the surrounding natural spaces increases (Fig. 4.7b). There is almost no difference in the LHF magnitude both during the day and night as the presence of the Brahmaputra River dominates the entire region and also as the results are depicted for the monsoon season with higher moisture availability in the atmosphere (Fig. 4.7c). Although there exist significant variations in the RH values between the city core and the northern part of the domain in a range of 0 to 25 %, the difference between the city and its immediate periphery differs within 5 to 10 % during the day which increases at night (Fig. 4.7d). Thus, it can be noted that the radiative

feedback of the prevailing land cover and topographic configuration of the region largely govern the variations in T_2. The seasonal variability in the day and night temperatures reveals an almost similar trend as that of Kolkata with higher variations between the LCZ classes during the pre-monsoon season and very least difference during the winters (Fig. 4.10a -c). However, unlike Kolkata, the variations are not very uniform even during pre-monsoon which generally experiences a significant number of hot and dry days, the frequency of which has increased over time. This reflects the influence of the local topography in regulating the overall trend in the temperature conditions throughout the city.

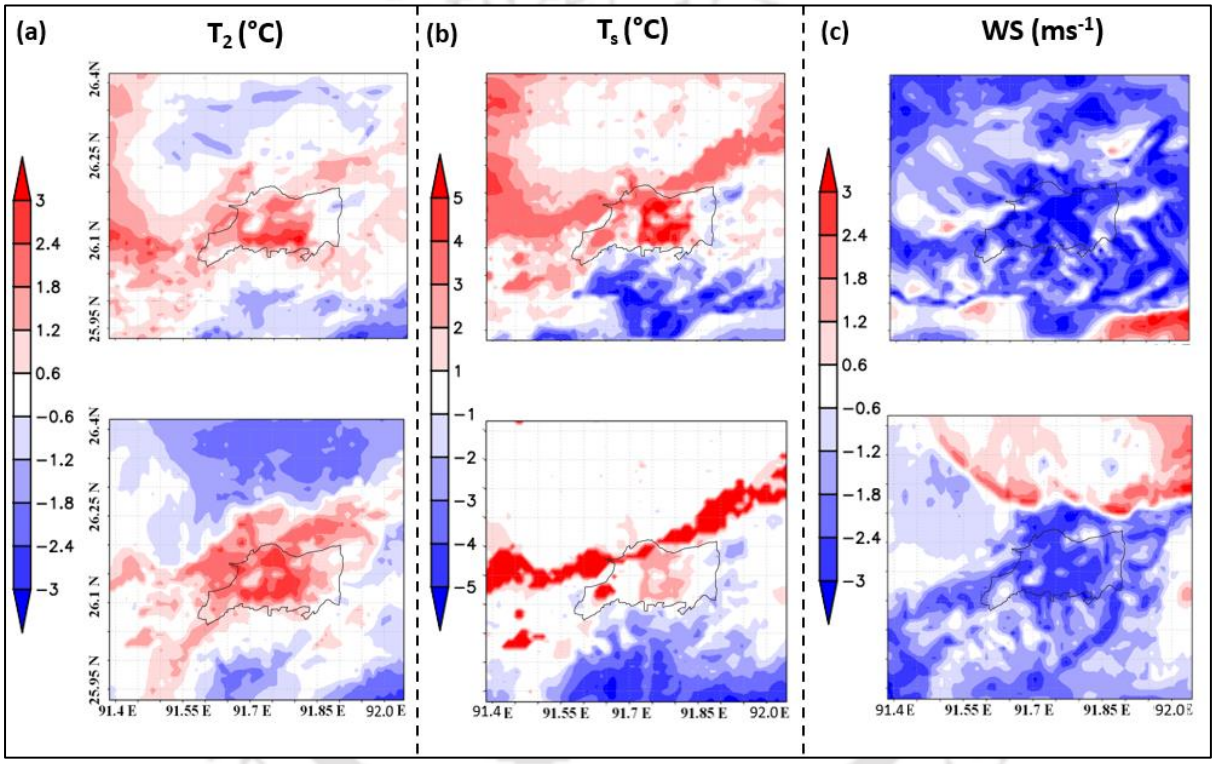

Figure 4.6: Spatial distribution of the modelled meteorological variables (variations from the mean) for the GMA and surrounding regions during a typical monsoon day (24th August 2019). (a) Diurnal Variations in T_2; (b) Diurnal Variations in T_s; (c) Diurnal Variations in WS. Day-time (14:00 LT) and Night-time (20:00 LT)

4.3.2.2 Surface/Skin temperature

The spatial distribution of T_s in the entire domain is also observed to have a crucial relation with the general terrain characteristics of the region. It is observed to be critically high during the afternoon as well as late evening over the river and other larger water bodies existing in the region (4.6b). As the day advances, the water surfaces gradually tend to heat and become even fairly warmer compared to the urban surface during the night. This increases the SHF potential of the surface leading to local-scale rise in the T_s values. Thus, the river acts as a heat source

during the evening hours in the nearby regions, which gradually declines later at night. The influence of the river in cooling the city's atmosphere is prominent from late night (after 00:00) till late morning (8:00) hours when the UHI intensity in the compact urban region closer to the river is lower compared to that of the areas with similar configuration in the inner city.

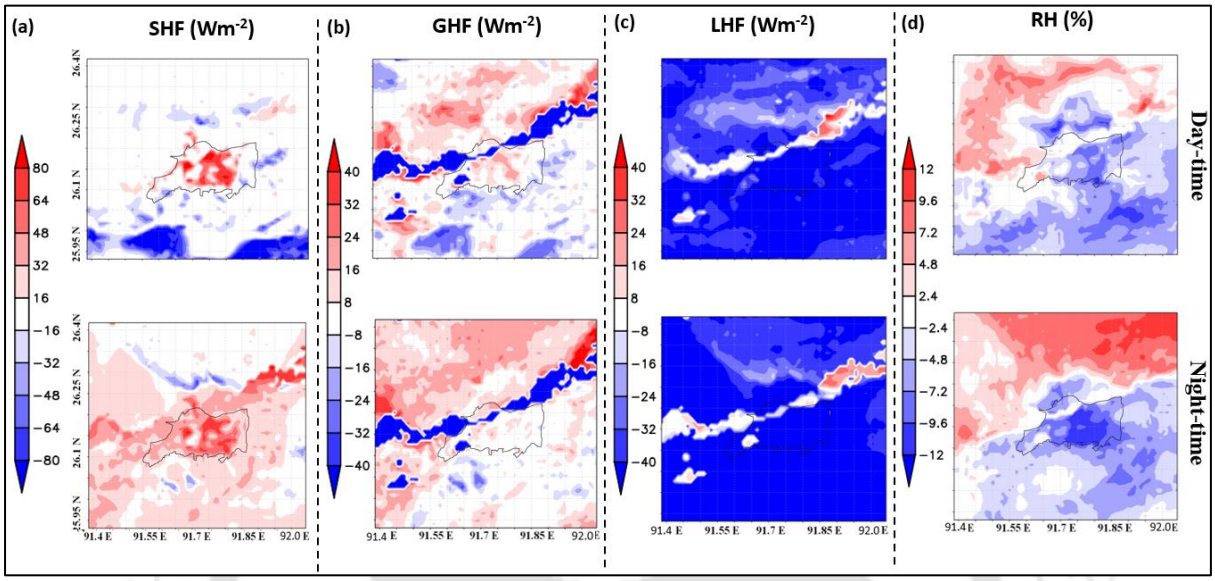

Figure 4.7: Spatial distribution of the modelled variables influencing the radiative feedback mechanism (variations from the mean) for the GMA and surrounding regions during a typical monsoon day (24th August 2019). (a) Diurnal Variations in SHF; (b) Diurnal Variations in GHF; (c) Diurnal Variations in LHF; (c) Diurnal Variations in RH. Day-time (14:00 LT) and Night-time (20:00 LT)

An almost uniformly declining trend is visible from the LCZ-wise analysis of T_s for the Guwahati region with an average variation of 1 – 3 °C in the consecutive classes from core to periphery during the monsoon season (Fig. 4.9c). Further analysis of the conditions during the other seasons also reveals a similar trend except for the day-time T_s values during pre-monsoons, showing a higher range in LCZ5 classes compared to LCZ2 and LCZ3, which could be attributed to the local surface fabric and urban canopy height in the region (4.10d – f). The winter temperatures almost follow a similar trend as Kolkata with highest variations in the min – max range, indicating cooler mornings and warmer afternoons.

4.3.2.3 Wind Circulation

The spatial pattern of wind circulation in the region is influenced more by the local topography and land cover than that of urban (Fig. 4.6c). The variations within the city and its immediate surroundings are almost non-existent or considerably low both during the day and at night. However, the results of micro-scale analysis between the individual LCZ classes show a

gradually increasing trend from the core to the periphery (Fig. 4.9d). The sharp inclination in the maximum WS is biased by the higher number of peri-urban classes considered for the analysis. However, this also indicates the potential of urban surface roughness in decreasing the maximum wind velocity by 5 to 10 ms^{-1} even during the peak monsoons. The gradually declining WS from the core urban to non-urban regions is however more prominent during the pre-monsoon and winter seasons, with highest variation (0.5 to 1.0 ms^{-1} between the consecutive LCZ classes) during the winter nights.

4.3.2.4 Rainfall Intensity

The overall analysis of the influence of urbanization on the monsoonal rainfall in Guwahati however does not reveal a very distinct pattern. The vertical distribution of CAPE along the horizontal transect (extending in the north – south direction) passing along the most urbanized part of the city shows a generally higher trend with highest values along the city centre (Fig.4.8). This follows the pattern revealed by Kolkata of decline in RF with increase in urban intensity. However, the variations within the urban classes do not follow a uniform trend as observed in Figures 4.9 (e) and 4.10 (j) classes. The peri-urban classes greatly influence the gradual rise in the RF intensity. It is seen that the RF intensity declines from LCZ3 to LCZ4 in a range of 3 to 5 mm and again rises in LCZ5 and the peripheral locations. These variations could be driven by the local terrain conditions, such as the natural gradient of the surrounding orography in the southern extent of the city, the influence of the river etc. Also, the presence of small hills within the city boundary may play a significant role in regulating the local scale convections even during the monsoon season.

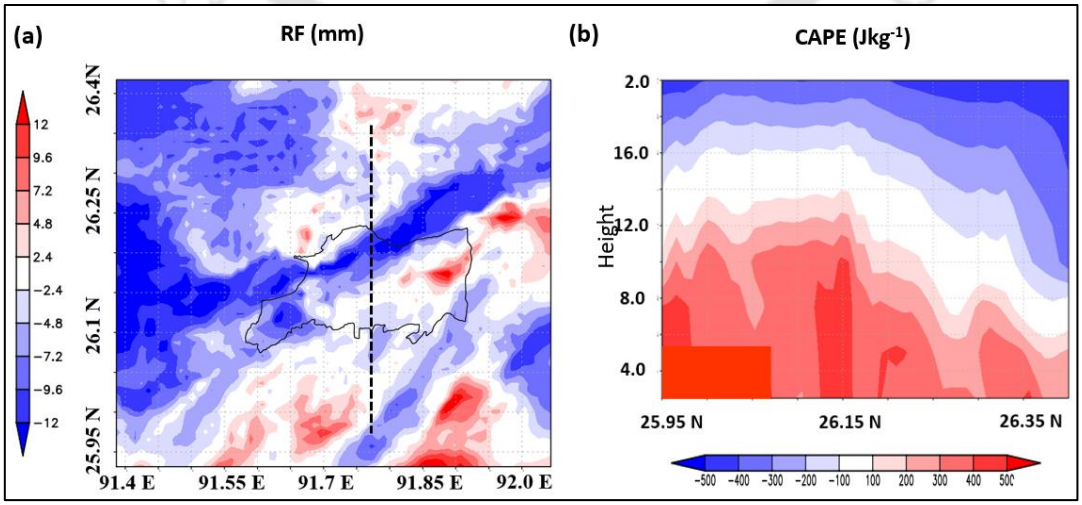

Figure 4.8: Spatial distribution of the modelled RF and CAPE (variations from the mean) for the GMA and surrounding regions during a typical monsoon day (24th August 2019)

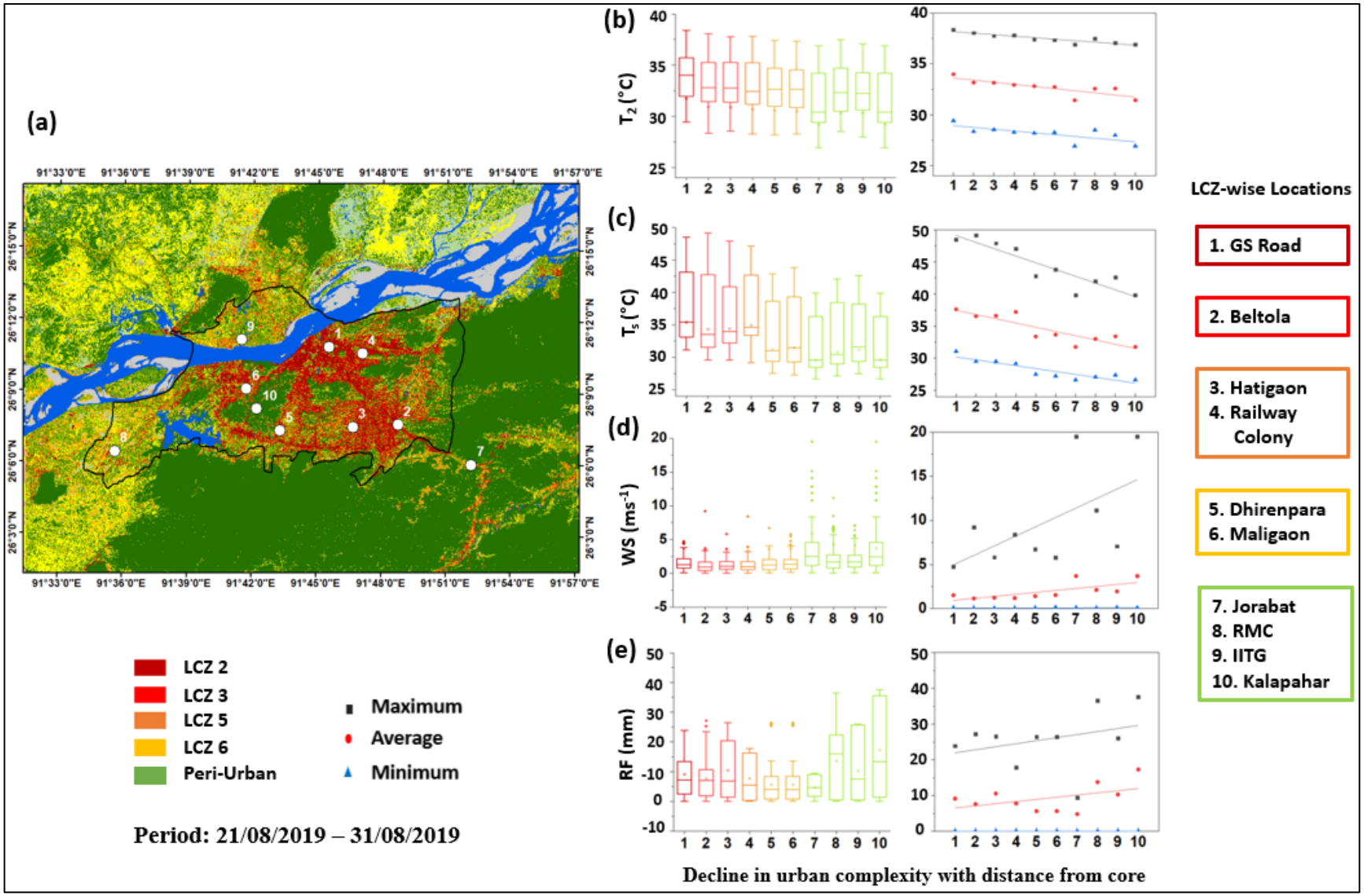

Figure 4.9: Micro-scale variations in the modelled meteorological variables over Guwahati. (a) Selected locations (b) LCZ class-wise variations in T_2; (c) LCZ class-wise variations in T_s; (d) LCZ class-wise variations in WS; (e) LCZ class-wise variations in RF

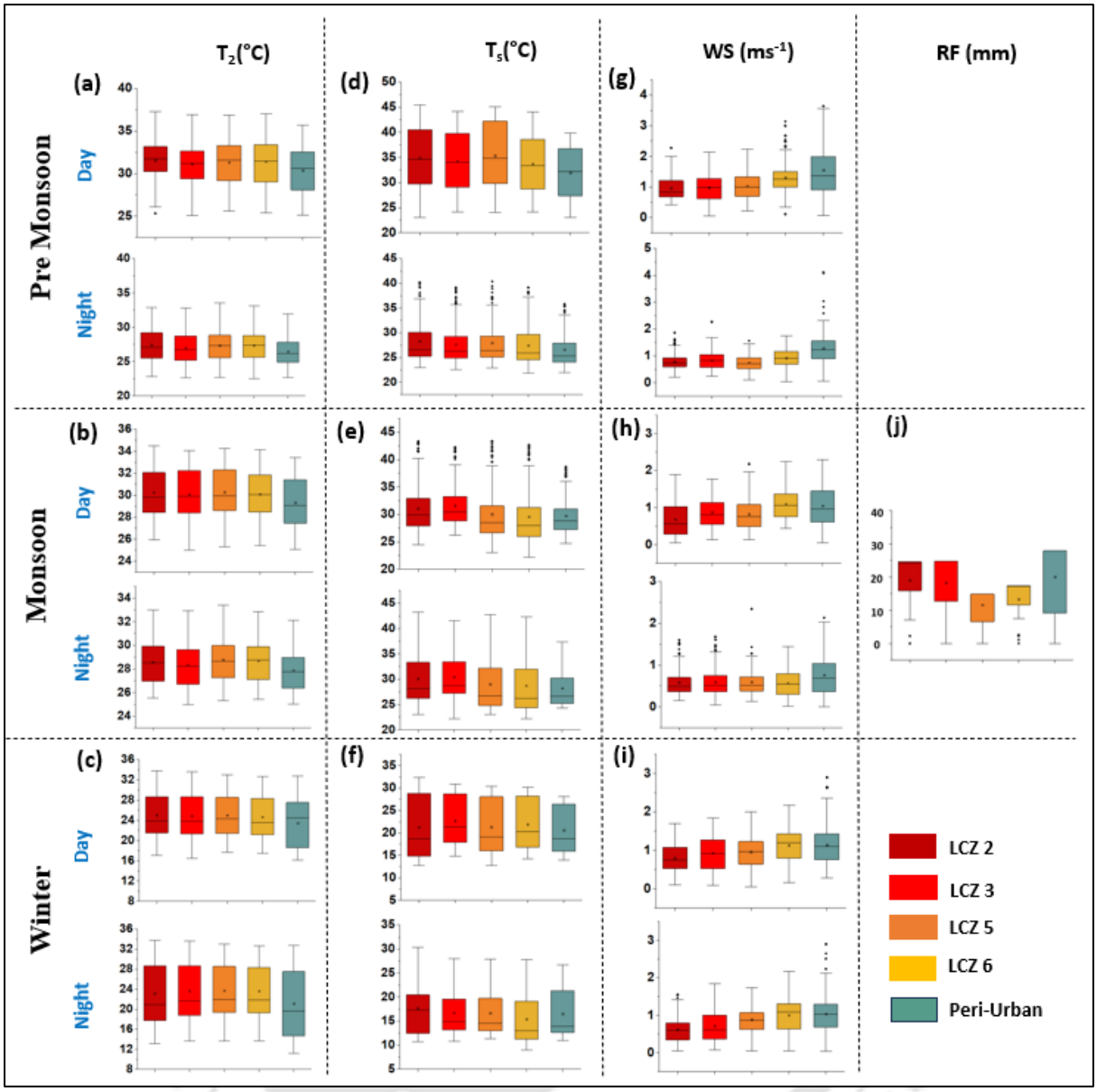

Figure 4.10: Micro-scale variations in the seasonal and diurnal patterns of the modelled meteorological variables over Guwahati. (a - c) LCZ class-wise variations in T_2; (d - f) LCZ class-wise variations in T_s; (g - i) LCZ class-wise variations in WS; (j) LCZ class-wise variations in RF. Pre-Monsoon Period (05/05/2019 – 15/05/2019); Monsoon Period (21/08/2019 – 31/08/2019) and Winter Period (05/01/2019 – 15/01/2019)

4.4 Summary and Conclusion

The high-resolution uWRF simulation using the updated LCZ products notably increased the potential of the model to detect micro-scale variations in the urban-climate structure of two cities differing in dimensions as well as urban intensity but situated in similar climatic contexts. The modelled results show a distinct inter-urban variation in the important climate variables especially for tropical regions which corroborated with the general urban meteorological character. However, since the LULC conditions in cities from the developing regions may vary

with small changes in the horizontal distance, further investigations were carried out across locations representing the dominant LCZ classes (indicating the urban complexity) present in the cities. The results revealed significant intra-urban variations in most of the variables for both cities, diurnally as well as seasonally. However, the variations are higher and more structured in the case of the larger and more urban-intensive Kolkata city compared to Guwahati, especially during the day. The results reflected a gradual decline in the atmospheric as well as skin temperature from the city core with the densest urban configuration to the immediate least urban surroundings. This pattern existed for both cities more prominently during the hot and dry pre-monsoon season, both during the day and at night, indicating the formation of stronger UHIs. The conditions are further deteriorated by a significant decline in the WS during the same season which has the potential to further aggravate the UHI intensity, due to the reduced capacity of the wind system to transport the accumulated heat especially along the most compact urban canopies.

During the monsoon season, the variations are much lower in temperatures as well as wind movements for both cities, indicating the dominance of the synoptic circulations over local meteorology. However, urban signatures are still visible in the overlying climate for both cities in a reduced capacity, more for Kolkata compared to Guwahati. The average air temperature variations among the LCZ classes with decreasing urban complexity are higher in the case of Kolkata. But, the variations in skin temperatures are higher in case of Guwahati due to more prevalence of densely vegetated regions. This is also induced by the highly compact structure of the built-up Kolkata, which leads to smaller variations in the skin temperature. The WS, however, is similar for both cities, with a uniformly declining trend from core to peripheries. It can be understood that the urban structures can even influence the wind movements during the monsoon season, characterised by stronger gusts and higher WS. Moreover, the micro-scale analysis of the accumulated rainfall does not exactly follow a similar pattern. Although there exists evidence of urban – rural contrast for both cases with a gradual decline towards the central city, the intra-urban variations are more prominently characterized in Kolkata, whereas in Guwahati the variations correspond more with the local geography. This reveals that the dimensions of the city and its urban intensity along with the local geographical construct play a significant role in defining the influence of urbanization on the monsoon rains. The micro-meteorology of the urban areas is least affected during winters compared to the other seasons except for the wind circulations both during the day and night.

Chapter 5

Scenario-based Analysis of Urban Micro-Climate

5.1 Introduction

Cities are dynamic entities that tend to grow and expand continuously in the wake of regional developmental change. This process has become faster and more prominent in the case of cities from the global south in the recent times due to several interconnected factors, such as recent economic and technological advancements in these regions, leading to extreme demand from the growing urban population attracted by the opportunities (Gao and O'Neill 2020; Das et al. 2022). This resulted in the vertical as well as horizontal expansion of these cities, accompanied by the growth of a myriad of anthropogenic functions and activities. These changes in the urban systems with time reflected evidently in the corresponding micro-climate structure, which also transformed accordingly (Giridharan and Emmanuel 2018). Thus, analysing and understanding the magnitude of micro-meteorological variability in terms of space and intensity can provide better insights to perceive this process's future, especially in the developing cities in the tropical region with the more complicated meteorological profile.

5.2 Methodology

To develop a deeper understanding of the meteorological transformations with the change in the urban systems, two different scenarios were analysed in this study. First, according to the growth in urban surface and functioning and the second, according to alterations in meteorological forcing due to reduced anthropogenic activities.

5.2.1 Impact of urban growth on the urban-climate pattern

The first scenario, intended to understand the micro-meteorological conditions according to the urban growth pattern over of 20 years (2000 – 2019), was analysed for both cities. The urban growth pattern was assessed by estimating land use land cover (LULC) conditions for three different time periods, 2000, 2010 and 2019 for the KMA and GMA regions. Then, uWRF simulations were performed individually for each case with the same model configuration established in the previous section, replacing the LCZ maps with the new LULC products and keeping the meteorological forcing constant. The 2019 NCEP-FNL datasets were used for all three cases to study the climatic variations only under the impact of changing urban surfaces.

5.2.1.1 Urban Growth Analysis

The LULC products for each time-period were generated using Landsat images (30 m resolution) due to the unavailability of high-resolution Planetscope products for such a longer time scale. Landsat products provided by United States Geological Survey (USGS) are one of the best and consistently available datasets used in different time-series geospatial analysis due to their availability for a more extended time period. Although the WUDAPT method uses Landsat images to generate LCZ, it is tough to achieve higher classification accuracy using automated image classification techniques from these moderate-resolution data products. The absence of ready-made labelled data for model training and the difficulty to categorize the built-up areas according to the fine-scale LCZ framework, especially in the case of a highly dense city like Kolkata from Landsat images, urged using a different classification scheme to derive the time-series LULC maps. A two-class urban classification scheme was adopted for this analysis acceptable by the WRF model using the multi-layer UCM called BEP+BEM. Since it was observed from the LCZ maps that the majority portion within GMA and KMA boundaries consists of the four main LCZ classes, i.e., LCZ2 (compact mid-rise), LCZ3 (compact low-rise), LCZ5 (open mid-rise) and LCZ6 (open low-rise); the two urban classes considered for urban growth simulations were '*high-intensity urban'* U_H and *'low-intensity urban'* U_L which may correspond to the compact and open LCZ classes respectively.

Landsat 5 and 8 products were first acquired for the three time-steps covering the study region, which were then pre-processed for radiometric and atmospheric corrections to estimate the ground surface reflectance values. The non-parametric supervised learning algorithm Support Vector Machine (SVM) was used to classify the images and generate the multi-temporal LULC products. The SVM algorithm is based on the concept of structural risk maximization, which

helps separate the different data classes by determining the hyper plane for class separation with higher accuracy (Gao and Liu 2014; Patel et al. 2020; Talukdar et al., 2020). It is a widely used image classification technique applied for classifying Landsat images with better performance accuracy compared to other machine learning algorithms like random forest, k-means clustering etc. (Pal and Foody 2012; Jamsran et al. 2019; Patel et al. 2020). Further, it is easier and less computationally intensive to train the SVM compared to the neural network-based algorithms. However, as the merit of most machine learning-based classification techniques depends on the quality of training datasets, appropriate training samples were manually created for each class which could most optimally delineate the margin of the hyper plane, also known as the support vector. The samples thus created were randomly divided into training and testing datasets in a ratio of 3:2. Apart from that, a proper type and kernel size is essential, which could further minimize the classification errors by increasing separation between the support vectors. Thus, based on the available literature using SVM algorithms for Landsat data classification, the 3 x 3 kernel size was chosen for this study (Patel et al. 2020; Wang et al. 2020; Prawin et al. 2021). The model was first trained and tested using the most recent images for 2019 for both regions and then the images for the remaining time periods were classified using the trained model. The overall accuracy for the classified products was then estimated using eq, (3.3).

5.2.1.2 uWRF Simulation

The uWRF model configured for the previous analysis with the same domain specifics, physical parameterization and urban physics model was used in this study to simulate the decadal variations in urban meteorology of both Kolkata and Guwahati cities by replacing the default landcover of D03 and D04 with these higher resolutions LULC products for 2000, 2010 and 2019 thus prepared. The urban roughness parameters were re-adjusted according to the urban classes of the updated land cover datasets. The finer scale urban roughness values of LCZ2 classes were used for the U_H class, and the values corresponding to the LCZ5 classes were used for the U_L. Simulations were run for a typical rainy day, i.e., 24th of August, 2019 during the monsoon season for all three time periods by changing the LULC configuration and keeping the meteorological forcing constant. This day was selected as an example of a typical rainy day during the monsoon season with rainfall episodes distributed throughout the day, and was used to show the findings of Chapter 4, so that consistency could be maintained and also comparison could be drawn among the different scenarios.

5.2.2 Impact of reduced anthropogenic activities on the urban micro-climate

The second scenario considered for analysis was to understand the magnitude of changes in the urban-climatology of the cities with the same surface configuration but reduced anthropogenic functions. Although it is almost impossible to reach this scenario in the real-world context for any city worldwide under normal circumstances, the opportunity to experience this kind of situation was presented during the global lockdown as a response to the Covid-19 pandemic, which spanned several months at a stretch. Since extreme restrictions were imposed on the normal functioning of the people, the world experienced a sudden fall in all types of anthropogenic functions in rural – urban alike. As this rare opportunity presented itself, many urban – climate experts tried to understand its direct impact on urban meteorology or air – quality during the said period (Dasgupta et al. 2020; Slezakova and Pereira 2021; Chinnasamy et al. 2023). A drastic improvement in air quality was observed during this period, especially in metropolitan cities from developing countries (Dasgupta et al. 2020). Many studies also revealed significant variations in the meteorological conditions of the cities as well as their surroundings, depicting the impact – the magnitude of daily anthropogenic activities such as transportation, industrial and commercial activities, all kind of jobs that require any energy consumption at a larger scale etc. (Chelani and Gautam 2022; Jallu et al. 2022; Liu et al. 2022; Shephard 2022).

This study was conducted to understand the micro-scale variations in the urban climatology of a huge and dense urban system like Kolkata and a rapidly developing city like Guwahati, which is greatly influenced by fast-paced urban development process. Thus, the high-resolution uWRF-LCZ model was executed for 15 days during the first pandemic lockdown phase in India from 15th April – 30th April 2020. The period was carefully selected in the latter half of the first phase when the initial lockdown days have neutralised the general environment, and the environment has reached a stable stage with as minimum anthropogenic activities as possible following the guidelines provided by the authorities. Since the spatial transformation of urban areas is comparatively slower and less dynamic compared to other physical processes, it was assumed that the LULC conditions remained almost the same in 2020 as it was in 2019. Thus, the same LCZ products produced for 2019 (using the datasets for the corresponding year) were used for the 2020 simulations and using the same model specifics. However, to compare with the general climatic pattern for the same period under normal circumstances, the model was again simulated for the said period during 2019. The modelled results for the critical meteorological parameters were then analysed and compared.

5.3 Results and Discussion

5.3.1 Urban Growth Dynamics

The SVM algorithm for urban classification performed substantially well for both cities with considerable difference in built-up intensity (Fig. 5.1). The overall accuracy in the case of Guwahati, however was observed to be higher (81%) than Kolkata (77.3%). The highest amount of misclassification and over-estimation of urban pixels was observed in the eastern part of Guwahati during 2000 and outside the southern extent of the KMA boundary. Although both cities experienced an increasing trend of urban sprawl and intensification in this 20-year interval, the rates differed considerably. The rate of increase in the total built-up extent is observed to be significantly high for Kolkata (within the KMA boundary) from 2000 – 2010 (52.45 %), which declined to about 39.6% in the consecutive decade (2010 – 2019), as the urban sprawl was more prominent in the surrounding regions of the city during this phase (Fig. 5.1a). Urban intensification was more pronounced in this region with the increasing pressure of population expansion, which resulted in the conversion of U_L into U_H. An almost similar trend was also observed in Guwahati's case, although the urban expansion rate was relatively lower (Fig. 5.2b). The urban sprawl rate in Guwahati was 23.9% in the first decade, which increased to 34.23% in the second. As opposed to Kolkata, the growth of U_H spaces was more prominent between 2000 – 2010 (122.34%) as compared to its increase in the subsequent decade, i.e., 52.76%.

5.3.2 Impact of urban growth on the urban-climate

The modelled results for the important climate variables during the monsoon period revealed a considerable impact of urban growth and expansion on the meteorological conditions of both cities. As the meteorological and physical parameterization was kept constant throughout the simulations, any change in the magnitude and spatial distribution pattern of the different variables could be directly related to change in the urban surface conditions. However, it was again observed that the changes were more prominent in the case of Kolkata, where the rate of urban growth was also more significant compared to Guwahati.

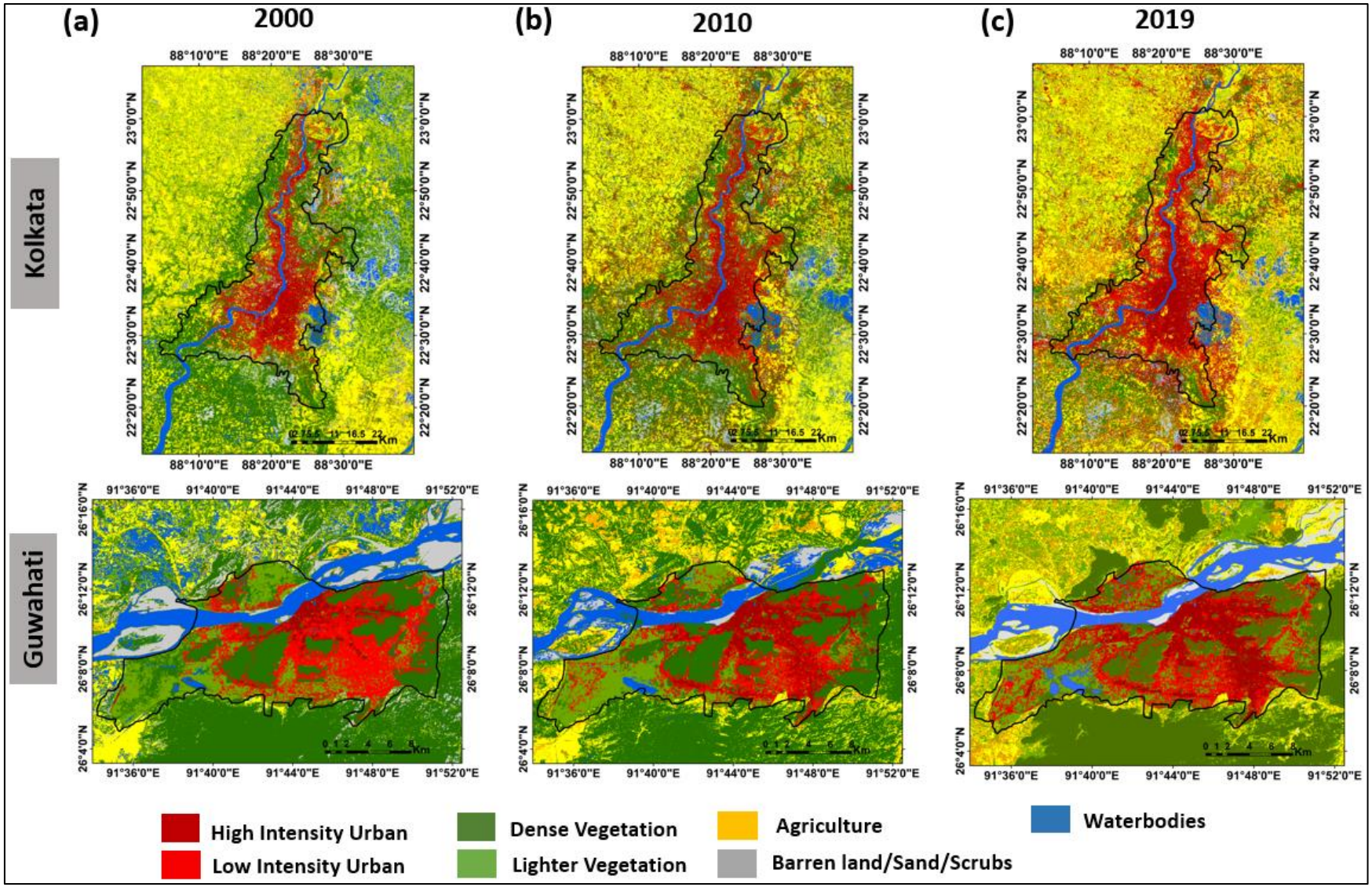

Figure 5.1: LULC variations over Kolkata (KMA) and Guwahati (GMA). (a) for 2000; (b) for 2010; (c) for 2019

5.3.2.1 Variations in T_2

The near-surface temperature condition, which is the major contributor to UHI effect for all the three time periods revealed an increasing trend both in magnitude as well as spatial extent in the case of Kolkata (Fig. 5.2). The rate was observed to have increased from 0.6 to 1.2°C in the core city from 2000 – 2010 both during the day and night. However, the conditions were more critical at night, with a larger extent under a higher temperature range. This indicated that along with the increase in spatial extent of the UHI condition, its intensity has also increased over time. However, a more gradual rise in T_2 conditions was observed in the case of Guwahati during the study period (Fig. 5.3). The expansion in high-temperature conditions was noticed during the daytime simulations, whereas the T_2 magnitude was also observed to rise at night by 0.3 to 1.2°C. Thus, these results indicated an increase in the night-time UHI intensity for both cities.

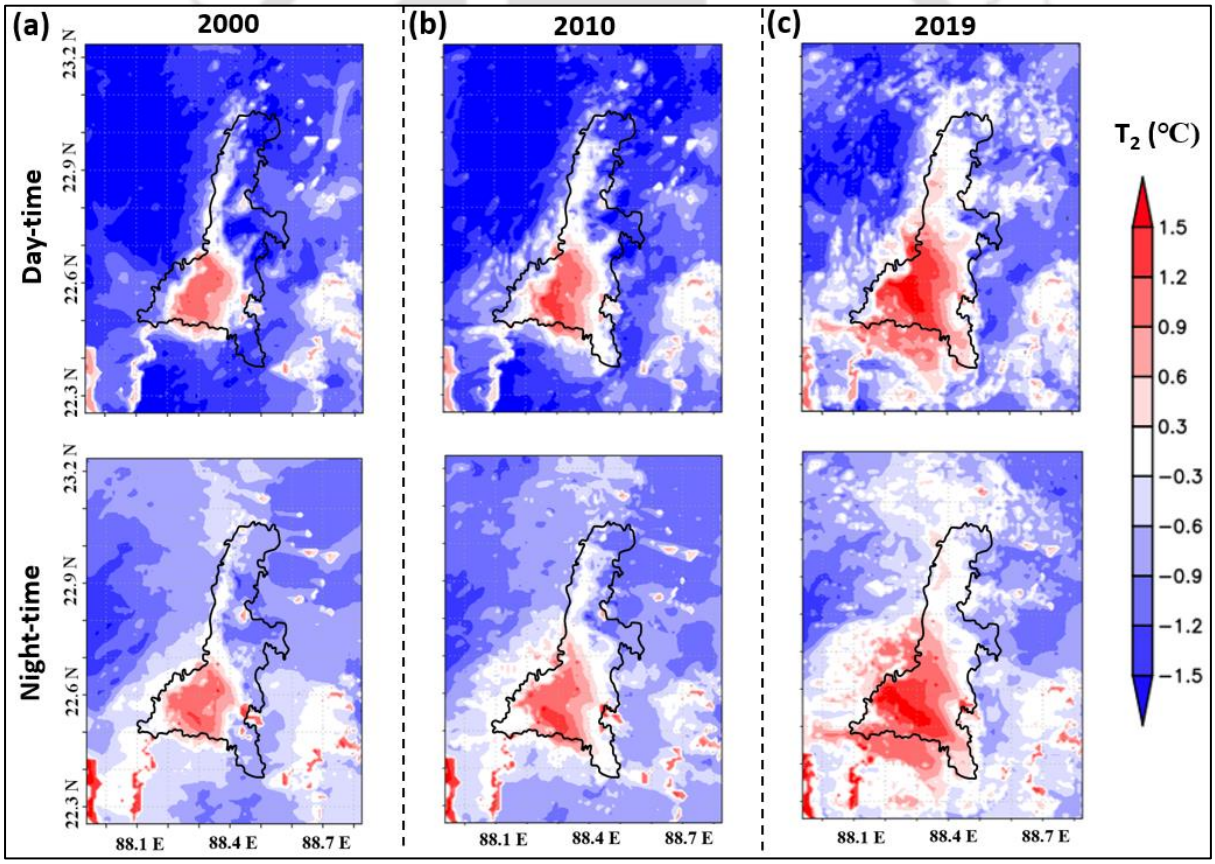

Figure 5.2: Spatial distribution of the modelled T_2 (variations from the mean) for the KMA and surrounding regions during a typical monsoon day (24th August 2019) with three different LULC. (a) Diurnal Variations for 2000; (b) Diurnal Variations for 2010; (c) Diurnal Variations for 2019

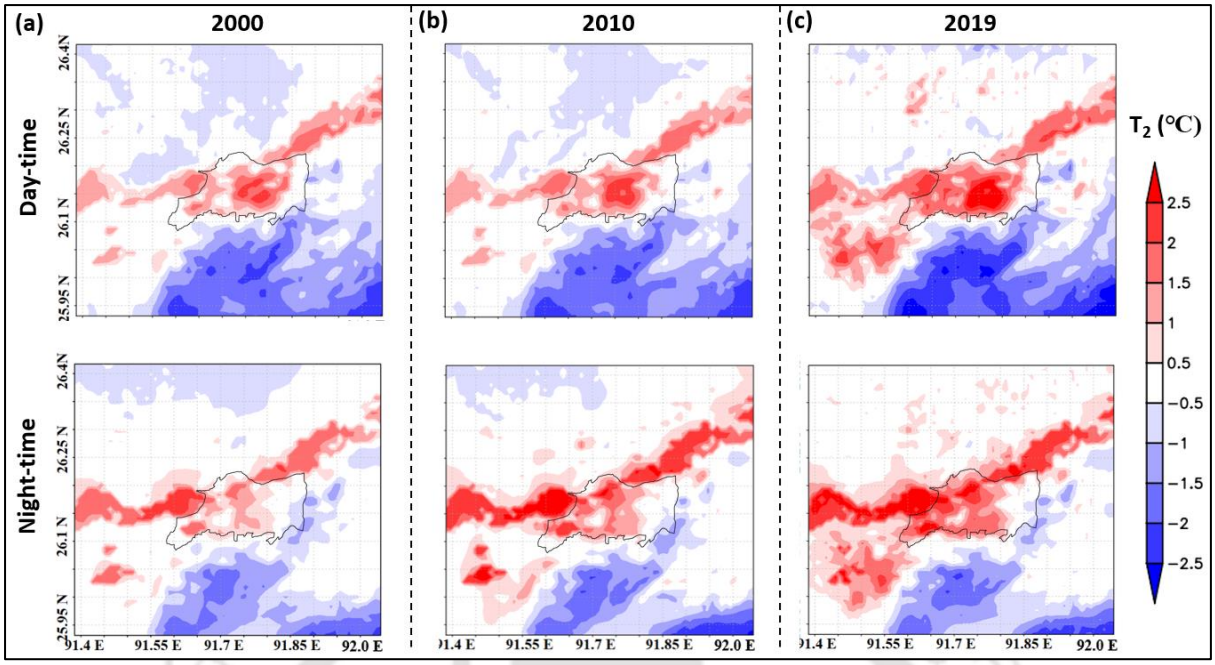

Figure 5.3: Spatial distribution of the modelled T_2 (variations from the mean) for the GMA and surrounding regions during a typical monsoon day (24th August 2019) with three different LULC. (a) Diurnal Variations for 2000; (b) Diurnal Variations for 2010; (c) Diurnal Variations for 2019

5.3.2.2 Variations in T_s

An analysis of the modelled skin temperature during the afternoon as well as late evening however, showed a reverse trend for both cities, with higher variations during the day compared to night (Fig. 5.4 and 5.5). The spatial extent of the area with higher surface temperatures increases at a rate of 1 to 2°C from 2000 – 2010 and another 1°C from 2010 – 2019 during the day. However, the increase in the T_s magnitude is not very significant. Although the spatial distribution pattern followed the nature of built-up expansion and, a notable decline in the rural – urban temperature variation was observed over the period. The modelled results, however, did not show exceptional changes for Guwahati, besides the obvious increase in the spatial extent of higher temperatures conditions controlled by the surface fluxes.

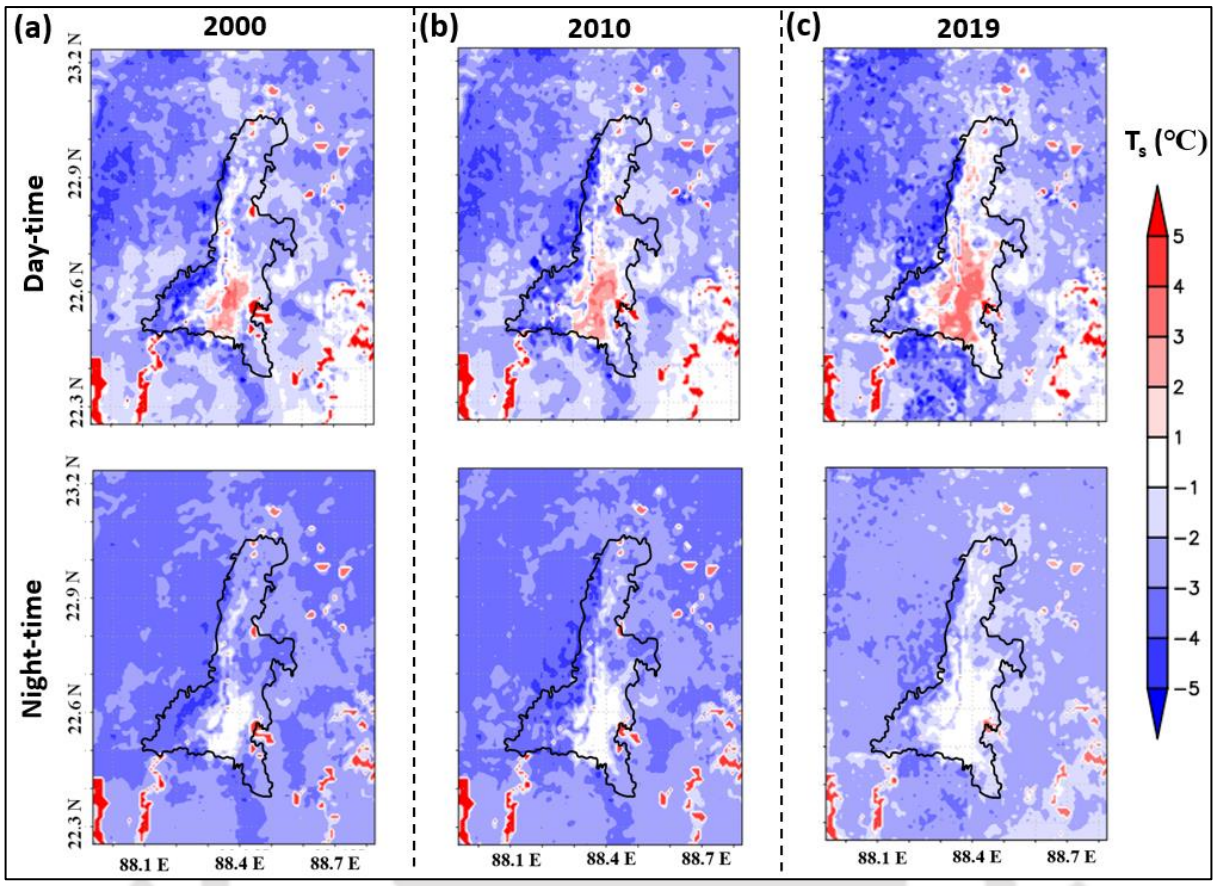

Figure 5.4: Spatial distribution of the modelled Ts (variations from the mean) for the KMA and surrounding regions during a typical monsoon day (24th August 2019) with 3 different LULC. (a) Diurnal Variations for 2000; (b) Diurnal Variations for 2010; (c) Diurnal Variations for 2019

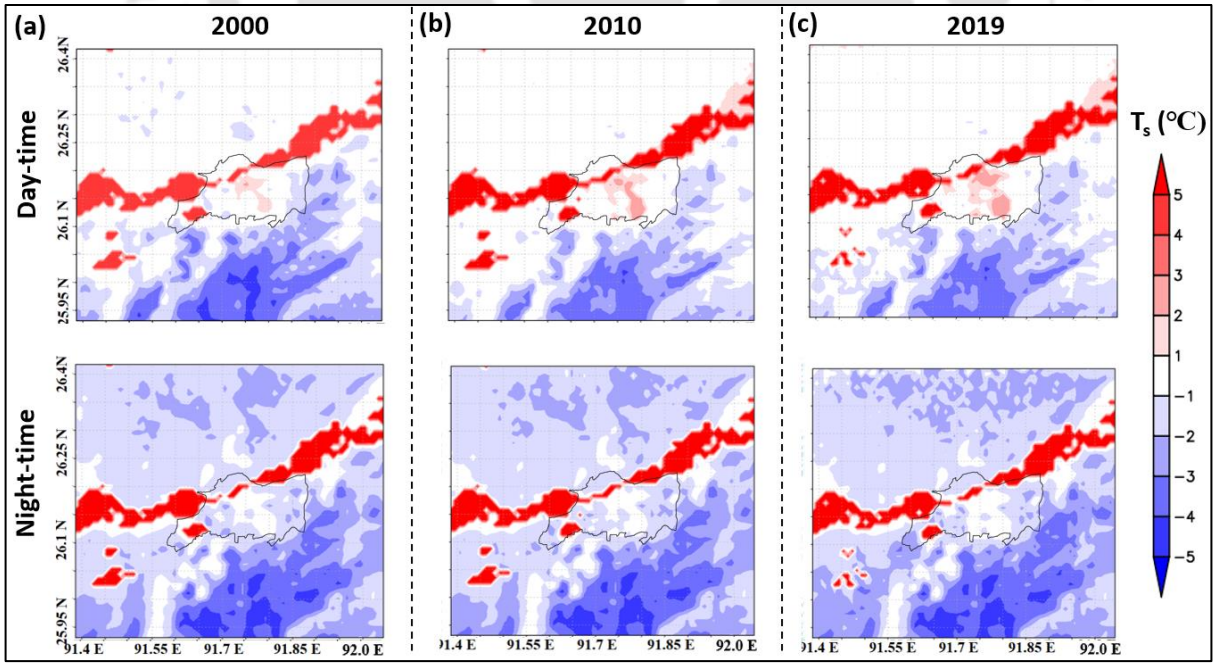

Figure 5.5: Spatial distribution of the modelled Ts (variations from the mean) for the GMA and surrounding regions during a typical monsoon day (24th August 2019) with 3 different LULC. (a) Diurnal Variations for 2000; (b) Diurnal Variations for 2010; (c) Diurnal Variations for 2019

5.3.2.3 Variations in WS

The wind velocity is lowest over the urban areas but, the concentration of higher velocity areas diverged in all directions during the recent time (2019) as compared to 2000 in Kolkata, more prevalent during the day (Fig. 5.6). This process could be related to the increase of U_H conditions along the city boundary which increased the urban roughness contrast in these areas over time. However, the inner city almost remained unchanged. A similar pattern was also observed in Guwahati, with a sudden fall in WS from 2000 – 2010 in the central city, which could be related to the sharp increase in the U_H class in this region (Fig. 5.7). However, the contrast declined in 2019 in the city core, being more prominent in the peripheries. Notably, this effect is more prominent during the day than night, indicating lesser variations in wind circulation during night for Guwahati.

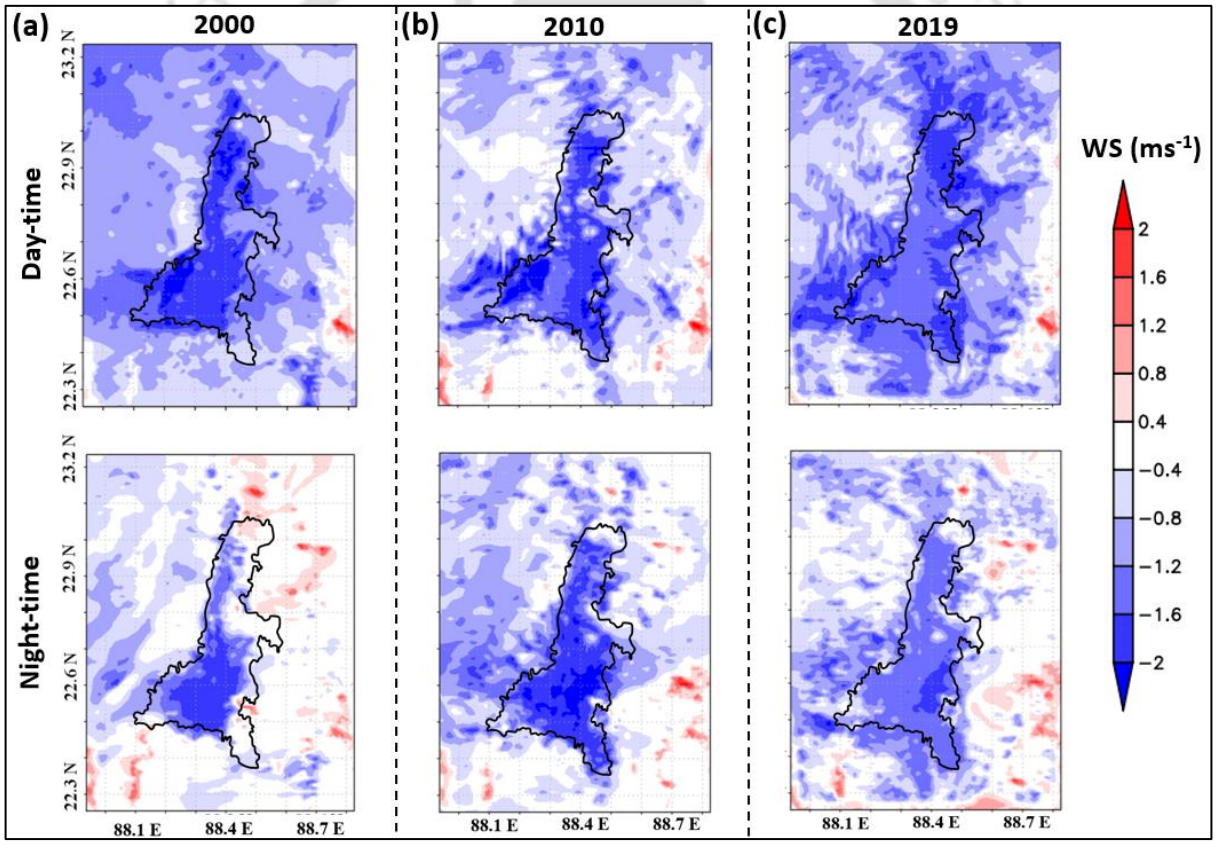

Figure 5.6: Spatial distribution of the modelled WS (variations from the mean) for the KMA and surrounding regions during a typical monsoon day (24th August 2019) with 3 different LULC. (a) Diurnal Variations for 2000; (b) Diurnal Variations for 2010; (c) Diurnal Variations for 2019

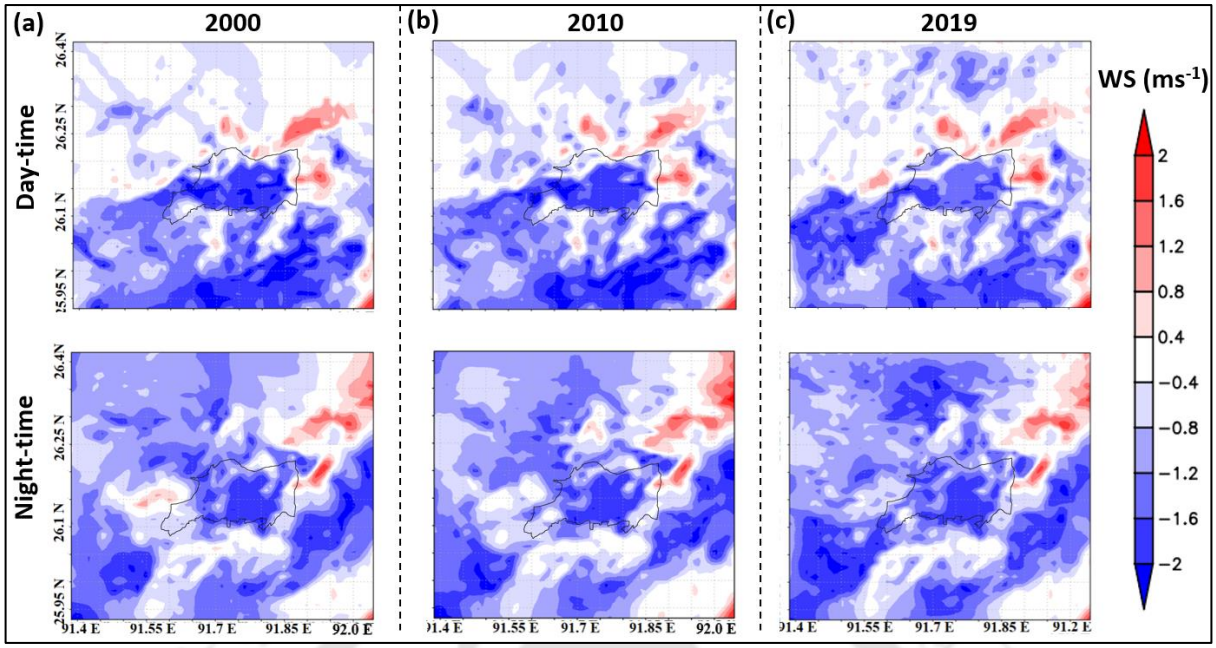

Figure 5.7: Spatial distribution of the modelled WS (variations from the mean) for the GMA and surrounding regions during a typical monsoon day (24th August 2019) with 3 different LULC. (a) Diurnal Variations for 2000; (b) Diurnal Variations for 2010; (c) Diurnal Variations for 2019

5.2.3.4 Variations in RF

The effect of urban expansion on the monsoon rains is more evident in Kolkata's case as compared to Guwahati's. On analysing the spatial distribution of cumulative rainfall over the urban areas, it is seen that the magnitude, as well as spatial extent of rainfall, increased with the increase in urbanization over time within the KMA boundary (Fig. 5.8). The concentration of high-intensity rainfall is observed to have bifurcated with the influence of urbanization and expanded over the northern half of the city. However, the spatial distribution is not very different over the central part of the city with the highest built-up concentration, which remained constant throughout the time period. These variations in the cumulative rainfall could again be related to the sudden change in the urban – non-urban interface towards the north and the peripheries of the KMA region. The vertical velocity of wind increases with the higher contrast, leading to the decline in CAPE over those areas, resulting in the enhancement of local-scale convection. Thus, this evident influence of urbanization on the rainfall pattern results from the energy transfer in the urban – non-urban interface rather than the entire urban extent.

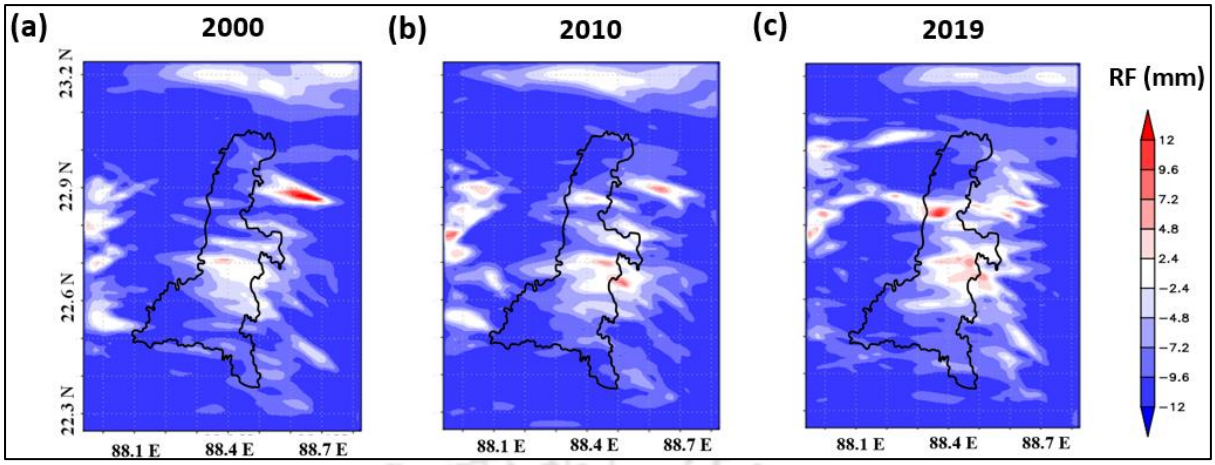

Figure 5.8: Spatial distribution of the modelled RF (variations from the mean) for the KMA and surrounding regions during a typical monsoon day (24th August 2019) with 3 different LULC. (a) for 2000; (b) for 2010; (c) for 2019

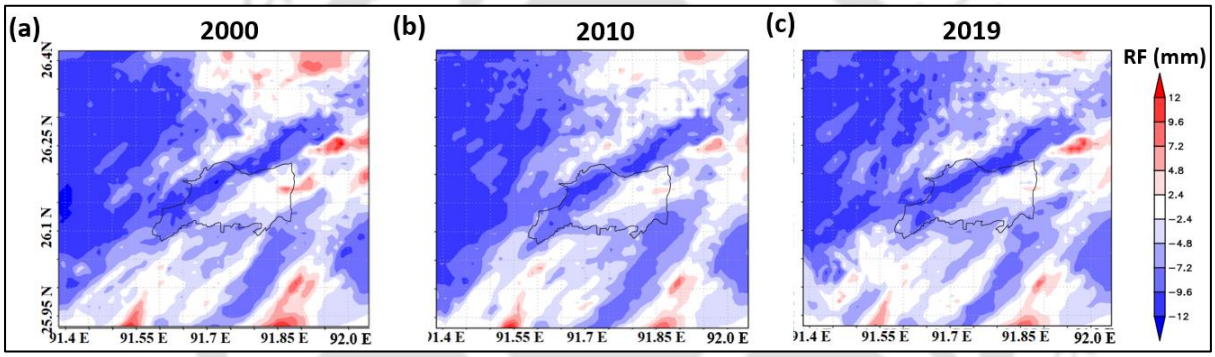

Figure 5.9: Spatial distribution of the modelled RF (variations from the mean) for the GMA and surrounding regions during a typical monsoon day (24th August 2019) with 3 different LULC. (a) for 2000; (b) for 2010; (c) for 2019

The impact of urban expansion on the monsoon convection is not very prominent over Guwahati city, which reflected minor variations (Fig. 5.9). However, variations were observed along the city boundary towards the east, which showed a constantly declining trend over the years, both in terms of spatial coverage and rainfall intensity. These areas also experienced an increase in the urbanization level with the gradual decline of the urban – non-urban contrast, leading to such rainfall variations.

5.3.3 Urban-Climate variations due to reduced anthropogenic functions.

Comparisons of the urban-meteorological conditions for both Kolkata and Guwahati of normal conditions experiencing usual volume of anthropogenic activities (15 – 30 April, 2019); with that of reduced anthropogenic forcings (15 – 30 April, 2020) during the pandemic show significant differences (Fig. 5.10 and 5.11). All three important climate variables, i.e., T_2, T_s and WS (since there was no rain event during the study period), reflected deviations from the

normal condition during this period, indicating the importance of energy consumption and emission due to varied range of anthropogenic activities on the urban atmosphere. During the pandemic, a significant fall in the T_2 values was observed for both Kolkata (1 to 5 °C) and Guwahati (1 to 5 °C). The variations were observed to be highest during the afternoons and lowest during the night, especially for Guwahati. On analysing the diurnal variations of the day with the highest difference, along the four dominant LCZ classes (i.e., LCZ2, LCZ3, LCZ5 and LCZ6), it was observed that the conditions almost remained unchanged throughout both the cities.

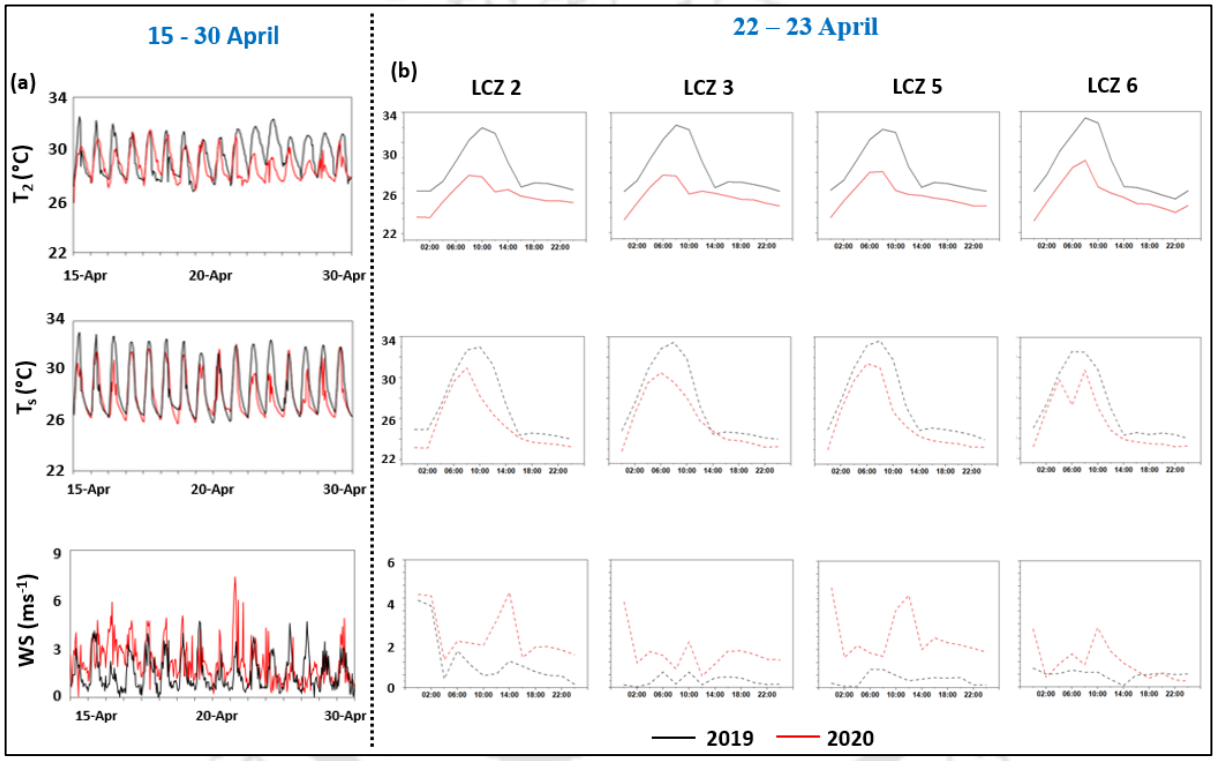

Figure 5.10: Micro-meteorological variations during the Pandemic (2020) and Normal (2019) conditions over Kolkata. (a) Average distribution of T_2, Ts and WS; (b) Diurnal variations in the dominant LCZ classes (LT)

A notable decline was also visible in the skin temperature conditions at a range of 2 – 4 °C, implying that the surface temperature conditions are not only a function of surface configuration but can be impacted by the overlying atmosphere. Variations in the total heat fluxes induced by the reduced air temperature had a feedback impact on the surface heating potential of the built-up spaces, leading to a decline in the T_s values. However, the difference between the normal and pandemic phases was evidently higher in Kolkata than Guwahati due to denser urban structure. Further, an increase in WS was also noticed in the case of Kolkata (1 – 4 ms^{-1}), with the highest effect in the built-up areas with higher urban canopy, which could

again be attributed to the increase in vertical velocity governed by the heat fluxes. However, the differences in WS were not very significant in the case of Guwahati with lesser and non-uniform variations through all the LCZ classes and the average conditions. This could be due to the higher wind velocity during the pre-monsoon season in this region generally experienced by the city (Goswami et al. 2022).

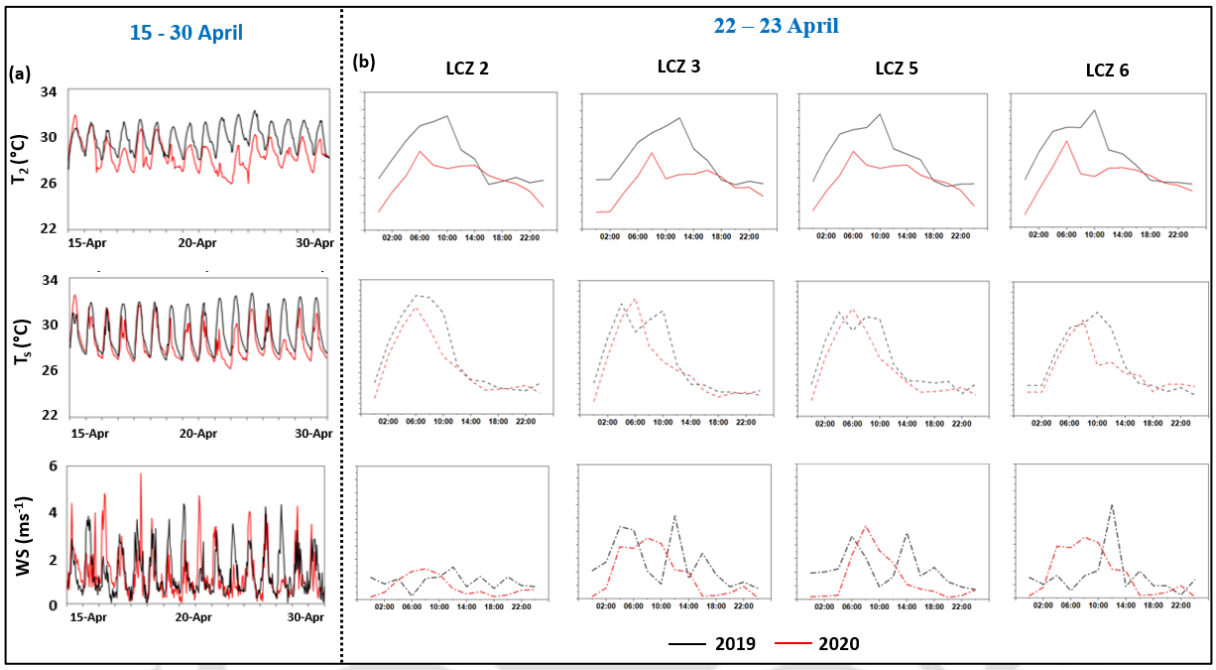

Figure 5.11: Micro-meteorological variations during the Pandemic (2020) and Normal (2019) conditions over Guwahati. (a) Average distribution of T_2, Ts and WS; (b) Diurnal variations in the dominant LCZ classes (LT)

5.4 Summary and Conclusion

This study analysed two important scenarios extremely relevant to the urban climate conditions to understand further the impacts of the urban dynamics on the immediate atmosphere. The first scenario focused on the effect of built-up expansion and densification on the important climate variables that define a city's climatic construct in the tropical-monsoon region. To provide the changing urban configuration information into the uWRF model, the LULC products for three different time periods were created using advanced machine learning techniques for both cities. The simulated results with LULC as the only varying parameter and keeping all the other aspects constant showed that urban expansion and intensification has a definite impact on urban-meteorology, especially for Kolkata, which is larger and more complex. The air and surface temperature variations increased both during the day and night with reducing WS, which reflected the cities' increasing potential for more vigorous UHI

formation. The rainfall concentration was also seen to be impacted by the changing urban cover dynamics with major impact at the urban – rural interface in both cities.

The second scenario emphasized the analysis of micro-climate variations on reducing the anthropogenic functions of a city, which included a huge reduction in traffic (almost 50 - 75 %), various industrial activities (75 – 80 %) and different commercial functions (85 – 90%) depending on the type of city (Chelani and Gautam 2022; Tibrewal and Venkatkumar, 2022). As this rare condition presented itself during the COVID-19 lockdown phase (2020), a 15-day simulation was conducted during the pandemic year with the least concentration of anthropogenic activities possible in the cities and for the same period the previous year (2019) with the usual concentration of vehicular movement, industrial and commercial activities etc. This analysis was motivated due to this chance phenomenon of reduced anthropogenic functions which is extremely difficult to achieve in the present times especially in urban areas, which accommodates the maximum of such functions. A significant improvement was observed from the results in the meteorological conditions of both cities with reduced surface and air temperature and increased wind speed. Further, the variations are again more evident in the case of Kolkata compared to Guwahati, with a higher concentration of anthropogenic functions.

However, it is known that changes in the meteorological conditions especially reduction in temperatures are not solely affected by the heat generated by automobiles, industries or different commercial activities. This reduction is a combined impact of many factors which are directly or indirectly influenced by the decreased anthropogenic functions (Georgii 1969). It was collectively recognized by researchers from across the globe that the reduction in anthropogenic activities decreased the concentration of different GHGs such as the NO2, CO and particulate matter such as PM2.5, PM10 in the atmosphere improving the air quality (Dasgupta et al. 2020; Mishra et al. 2021; Liu et al. 2022; Shephard 2022). Thus, the heat generated by the LW radiations from the urban fabric as well as the stray heat emitted directly by the anthropogenic activities usually trapped within the urban canopy layers dramatically reduced during the pandemic lockdown phase (Ghosh et al. 2020; Bhattacharjee and Bharti 2021; Nanda et al. 2021). Further the wind speed is also increased due to the lesser atmospheric pollutant load which helped in transporting the local scale accumulated heat from the urban canopies further reducing the UHI effect (Abbassi et al. 2022). However, estimating the amount of heat generated from each source could help in utilizing the experience from this rare event in strategizing appropriate measures to mitigate the UHI effect by limiting anthropogenic

activities in a controlled manner. But segregating the percentage impact of each of the above-mentioned urban processes is beyond the scope of the present study and could be addressed in the future. Thus, these results could be important information for urban planners and policymakers for strategizing the deployment of different mitigation measures to improve the urban climate conditions.

Chapter 6

Comprehensive Assessment of Urban Micro-Climate and Impacts of Mitigation Strategies

6.1 Introduction

The type and intensity of urbanization directly influence the various climate-parameters within and around a city, which impacts the health and well-being of the city dwellers. The near-surface temperature conditions, wind circulation patterns, moisture availability etc., collectively determine the thermal comfort of the cities. The micro-scale rainfall variability on the other hand influences the flooding pattern to a certain extent as it is also factored by the hydrological construct of the region and its stormwater management capability. Therefore, it is crucial to understand the collective impact of all the variables to assess the cities' comprehensive micro-meteorological health. This is important to perceive the overall picture of discomfort caused by the different climate variables acting together according to the surface conditions at the local level, which may essentially help in implementing appropriate mitigation strategies. Thus, this study focuses on assessing the combined effect of the important climate parameters towards the thermal comfort of the city dwellers and also tests the potential of different heat mitigation strategies in improving the conditions for those parameters.

6.2 Methodology

6.2.1 Urban Micro-Climate Index Preparation

Composite indices are one of the most widely used techniques to analyse the collective effect of several relevant factors on spatial quality assessment studies (Greco et al. 2019; Liu et al. 2022). This technique has found wide applicability in the case of environmental assessment studies concerning any application such as ecological stress, hazards and vulnerability, water

quality, sustainability etc. (Zou et al. 2006; Wang et al. 2020; Ghosh et al. 2022). Evaluation of different criteria affecting the environment and integrating them using a mathematical or empirical approach, to generate an environmental index have often achieved remarkable results in identifying the overall distribution of environmental hot and cold spots (Hajkowicz, 2006; Oţoiu & Grădinaru, 2018; Gibari et al., 2019). It is to be noted that the environmental hot spots in spatial analysis refer to the areas where the environmental condition in general or concerning a particular quantity is of the highest quality compared to the other areas and the environmental cold spot represents the worst quality. Therefore, a micro-climate index using this technique was designed in this particular study to assess the livability of both cities, including the most important indicators affecting the general thermal environment.

6.2.1.1 Weight Estimation of Individual Criteria

The most important aspect of these composite indices is the assessment of the weightage of each individual criterion, which would assert its importance in the overall scenario (Hajkowicz, 2006; Dobbie and Dail, 2013; Greco et al., 2019). The estimation of proper criteria weight is pertinent for the adequacy of the index to explain environmental health according to the prevailing conditions and also the data that has been used for the analysis (Liu et al. 2022). Here, a hybrid approach of weight estimation was applied which integrated the entropy-based weight estimation (objective) and AHP (subjective) techniques, leading to the derivation of final weights based on the experience and knowledge of the observer as well as the critical aspects of the data used. The detailed process of weight estimation has been explained in Eq. 6.1 – 6.5.

i) Initial normalization of Data

Since each indicator represents a different quantity and is obtained using a different approach, it is essential to standardize them to overcome the impact of their magnitude and units. This is achieved by the step transformation method using the following equations which normalizes each indicator value between 0 and 1, where values close to 0 indicate poorer and close to 1 indicate better liveability.

$$\text{For positive indicators, } X'_{ij} = \frac{X_{ij} - X_{j,min}}{X_{j,max} - X_{j\,min}} \tag{6.1}$$

$$\text{For negative indicators, } X'_{ij} = \frac{X_{j,max} - X_{ij}}{X_{j,max} - X_{j,min}} \tag{6.2}$$

where $X'_{i,j}$ is the normalized value of the indicator in a particular pixel, $X_{i,j}$ is the original value of that pixel, $X_{j,min}$ and $X_{j,max}$ are the minimum and maximum values of each indicator. i = 1 … n, and j = 1 … m, n is the total number of pixels and m is the total number of indicators.

ii) *Weight estimation using the entropy-based approach*

This method emphasizes on determining the weights on the basis of the distribution and relationship of the pixels with each other for each indicator (Liu et al. 2022).

Proportion of ith pixel under the jth indicator: $A_{ij} = \frac{Xij}{\sum_{i=1}^{n} Xij}$ (6.3)

The information entropy of an indicator: $f_j = -k \sum_{i=1}^{n} A_{ij} \ln (A_{ij})$ (6.4)

where, *k* is the Boltzmann constant, $k = \frac{1}{\ln (n)} > 0$

Entropy weight of each indicator: $W_j = \frac{1- f_j}{\sum_{j=1}^{m} f_j}$ (6.5)

iii) *Weight estimation using the AHP method*

This technique reduces the objectivity and estimates the weights based on the observer's judgement on the indicator's importance. It combines the qualitative and quantitative criteria and constructs a judgement matrix on the basis of pairwise comparison of the indicators with each other (Saaty, 2001; Bhattacharjee et al., 2021). Thus, following the 1-9 scale devised for criteria assessment (1 corresponding to equally important and 9 corresponding to extremely important), each attribute was weighted in comparison to every other in a pair-wise manner, according to the effect they ought to have on the eco-environmental condition of the city; and the judgement matrix was formed where diagonal values were 1(a_{ij} = 1 and a_{ik} = 1/a_{ij}). Then each element's eigen vectors were determined, and each criterion's weight coefficients using eq. 6.6. The consistency index was then calculated according to the method discussed in Satty (2001), to check the consistency of the designed decision matrix which should be below 0.1, beyond which the matrix was reiterated.

$$W_l = \frac{1}{a_{ij} * \sum_k \frac{1/}{a_{ik}}} \quad (6.6)$$

where W_l is the AHP weight of each indicator

The final hybrid weights for each indicator were thus estimated by taking an average of the weights derived using the Entropy and AHP methods.

6.2.1.2 Urban Micro-Climate Index (UMCI)

The Urban Micro-Climate Index was then calculated using the following equation (6.7) which integrates the selected indicators according to their respective weights.

$$UMCI = \{(a_1 \times fw_1) + (a_2 \times fw_2) \ldots (a_n \times fw_n) \quad (6.7)$$

where *a* represents the individual indicators and *fw* are the final weights derived for each indicator using the above approach

The UMCI was calculated considering the modelled results during the pre-monsoon season which was identified to have the highest urban - rural temperature variations and capable of increasing the UHI strength in both cities. The previous analysis revealed the direct impact of T_2, T_s, and WS on heat accumulation in the urban systems. Besides, RH is also considered as one of the significant contributors in thermal discomfort, especially in tropical regions. The thermal sensation of the body could be primarily induced by the RH, as wetness of the human skin increases with an increase in humidity due to reduction in the rate of evaporation. (Fountain et al. 1999; Jing et al. 2013). This may increase the perspiration level of human beings, inspiring a perception of discomfort. Therefore, besides the three mentioned variables, RH was also added as an important indicator to calculate the UMCI, specially designed to identify the most vulnerable zones within the cities having the highest potential to enhance thermal discomfort.

6.2.2 Implementation of Heat Mitigation Strategies

Various heat mitigation strategies have been proposed to tackle the UHI effect by different experts according to the local conditions of the city and the feasibility of their implementation. These strategies may range from the use of green infrastructure such as urban lawns, trees, green roofs etc; to the application of biophysical or engineered materials such as, heat resistant cooling materials for pavements and roofs, super-cooled broadband radiative coolers etc. (Akbari et al. 2001; Chow et al. 2012; Georgescu et al. 2015; Khan et al. 2023). Green infrastructures are not always feasible in the highly dense developing cities, which encourages exploring other potential methods depending on their cost – effectiveness. The adoption of

cooling materials is one of the other popular options which is implemented by covering the roofs and walls of the buildings and roads using a combination of cooling materials such as white paints, thermal reflectors, etc., which increases the value of albedo for all the urban surfaces (Morini et al., 2017). The broadband radiative coolers, however are emerging as important alternatives due to their effectiveness even during the evening and night-time (Georgescu et al. 2013; Khan et al. 2023). The building roofs are coated with materials based on titanium dioxide (TiO_2) particles on top of silicon dioxide (SiO_2) or silicon carbide (SiC) nanoparticles, nano porous materials etc. with very high solar reflectivity and sky window emissivity (Bao et al. 2017; Zhong et al. 2020; Feng et al. 2021).

Table 6.1: Numerical Design to implement the heat mitigation strategies

Mitigation Strategies				
Numerical Design	**Type of Roof/Surface**	**Albedo Fraction**	**Emissivity Fraction**	**Roof Top Green Fraction**
Green Roofs (GR)				**75**
Cool Material (CM)	**Cool Roofs**	**Roof 0.65** **Wall 0.60** **Road 0.45**	**Roof 0.90** **Wall0.90** **Road0.95**	
Super Cool Material (SCM)	**Super Cool Roofs**	**Roof 0.95** **Wall 0.20** **Road 0.20**	**Roof 0.95** **Wall0.95** **Road0.95**	
Control Case (CC)	**Conventional**	**Roof 0.20** **Wall 0.20** **Road 0.20**	**Roof 0.90** **Wall0.90** **Road 0.95**	

In this study, three different approaches to mitigate the heating potential of the cities during the hot and dry pre-monsoon season were tested at the city scale using the high-resolution uWRF model, viz. Green-Roof (GR), Cool Materials (CM) and Super-cool Materials (SCM). These strategies were implemented by re-configuring the model with suitable values of albedo and emissivity fractions individually for each case (Table 6.1). The numerical design of the mitigation strategies was adopted after a systematic analysis of relevant literature for such analysis in similar surface as well as climatic conditions (Morini et al. 2017: Mandal et al. 2018; Chatterjee et al. 2019; Zhong et al. 2019; Feng et al. 2021; Khan et al. 2023). Then the

simulated results were compared with the conventional case (CC) to estimate their performance with respect to the controlled simulations.

6.3 Results and Discussion

6.3.1 Comprehensive urban micro-climate analysis

The UMCI index was used to assess the comprehensive effect of the key climate variables on the overall micro-climatic conditions of the city, to identify the vulnerable pockets and the most livable areas. The assessment was done for a hot and humid day during the pre-monsoon season for both cities, which significantly impacted the thermal comfort of the city dwellers. On evaluating the individual indicators, it was found that the spatial distribution of all but RH positively influenced on the core city region due to the lower intensity of RH increasing built-up density (Fig. 6.1 and 6.2). All other indicators showed a negative effect with the increase in urban complexity, the intensity of which varied during the day and at night. Thus, a higher influence of the negative indicators was observed on the comprehensive meteorological conditions of the cities.

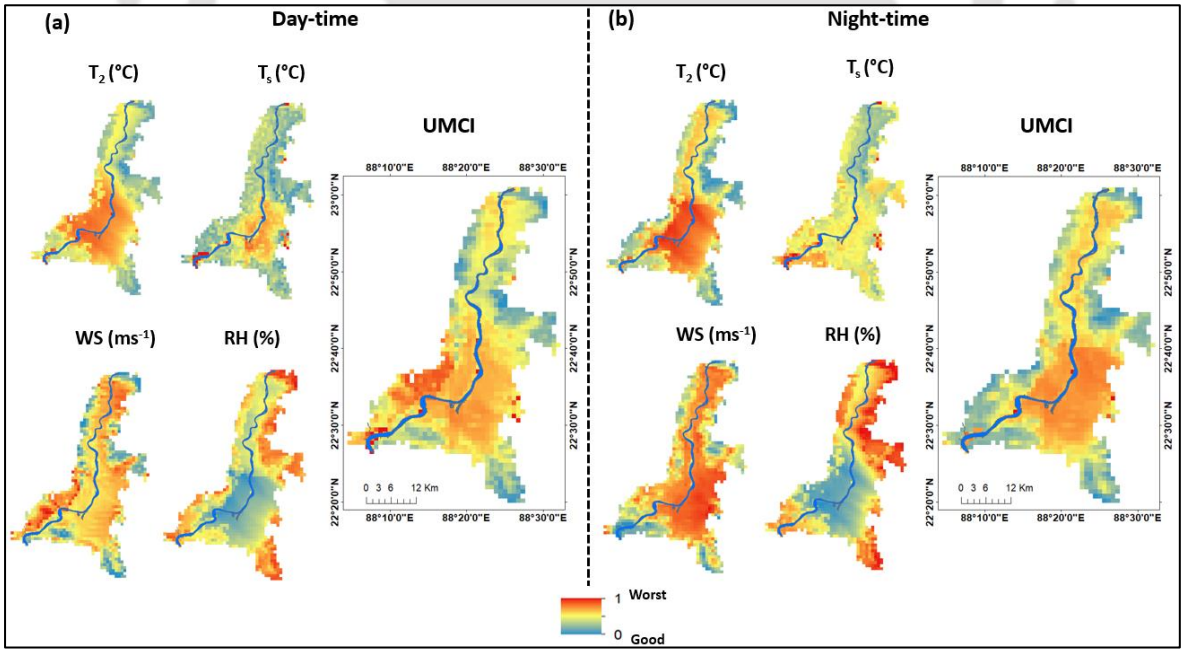

Figure 6.1: Comprehensive assessment of urban micro-climate variations in Kolkata using UMCI

Although the UMCI values have a general tendency to increase from the core to peripheries, the rise in the day-time UMCI on the western part of the city compared to the core indicates the influence of lower wind speed combined with higher T_2 and RH conditions in these areas

of the city (fig. 6.1). This region is dominated by LCZ5 and LCZ6 classes and a combination of dense vegetation and scattered trees which may also play an important role in increasing the surface roughness and increase in RH. However, the conditions are normalised during the night, with most vulnerable zones being concentrated within the highly urbanized sections of the city. Although the T_2 values remained high, the reduction in WS and RH levels in the western city led to the shift in the worst living conditions from the western boundary during the afternoon to the central city at night.

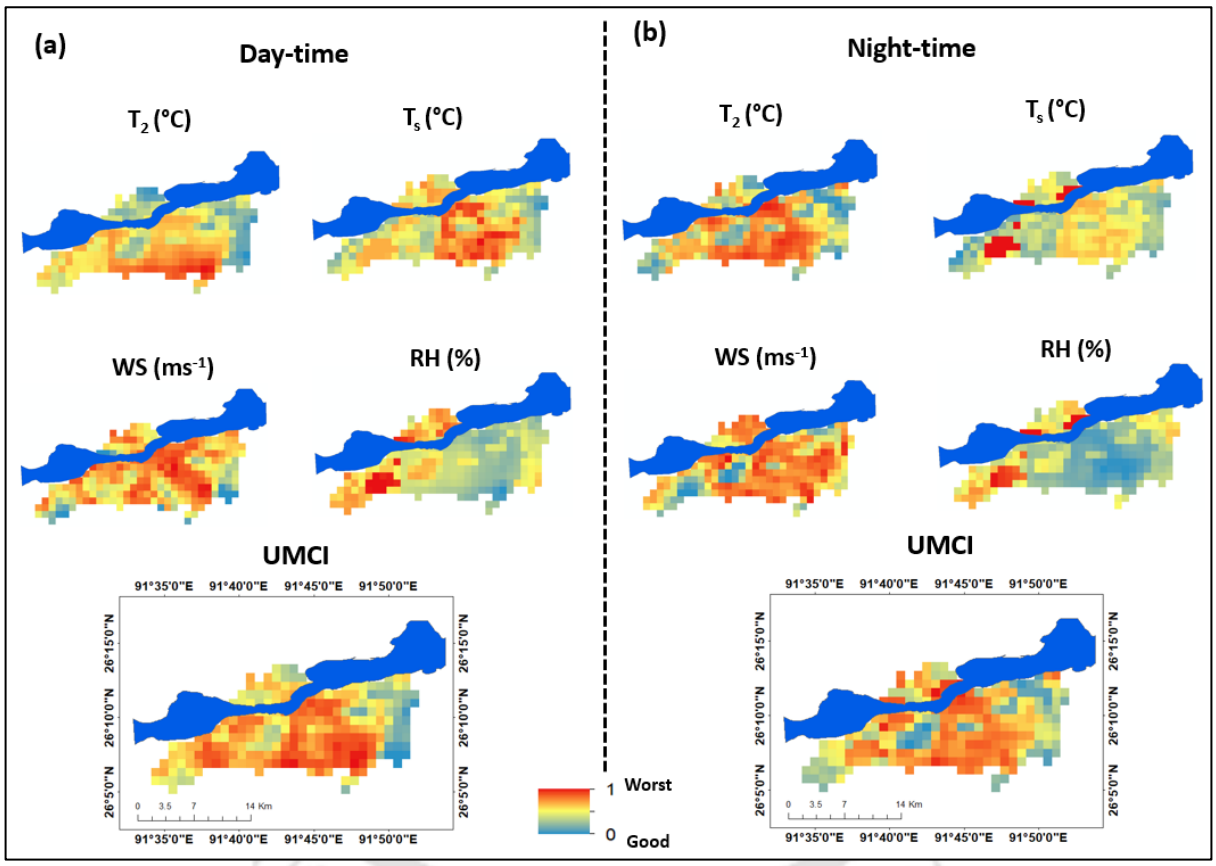

Figure 6.2: Comprehensive assessment of urban micro-climate variations in Guwahati using UMCI

The distribution of UMCI values in Guwahati shows a definitive impact of the local geography on the urban meteorology along with the urbanization pattern (Fig. 6.2). Besides the regions with higher built-up density, the south-eastern parts of the GMA area with lesser urban concentration, also reflected as vulnerable during the day. Despite having relatively lower temperature values, this part of the city could be thermally uncomfortable due to higher concentration of RH governed by the presence of a large lake and numerous wetlands. However, the condition is observed to improve at night slightly. On analysing the UMCI values

during the late evening, it was found that thermal discomfort increases in the vicinity of the river. This could be attributed to the higher Ts as well as RH conditions in these parts which promotes thermal discomfort. This implies the benefit of a comprehensive assessment technique that could assess the combined effect of different climate variables to understand the overall micro-meteorology of the cities.

6.3.2 Impact of heat mitigation strategies

The implementation of heat mitigation strategies on the climatic conditions for both cities was evaluated by assessing the variations in near-surface air temperature as well as wind circulations. The results reflected the efficiency of all these techniques in substantially reducing the T_2 values in both cases especially in the afternoon when the UHI intensity is the highest. (Fig. 6.3). The effect of these strategies was analysed for the different LCZ classes to understand the micro-level variations and also to analyse the differences between their performance according to urban complexity. Thus, the results for Kolkata reveal that, the adoption of different cooling infrastructures performed as expected, with SCM reducing the temperature in a range of 2 – 5 °C, followed by CM and GR, which almost showed similar impact. The results also indicated better performance of these strategies in the most complex parts of the city where the variation is high among the different measures. This variation gradually declines with urban complexity, showing the role of urban canopy configuration in regulating the near-surface temperatures. This condition could also be corroborated by the results obtained from the simulations for Guwahati with comparatively less dense urban structure, where all the techniques performed almost similarly with slight variations in the afternoon. Thus, this analysis could be helpful in finding the most feasible and effective solution for heat mitigation according to the urban configuration. If all the strategies performed similarly in a region, the choice of adopting the best measure could be decided by its cost effectiveness and feasibility of implementation.

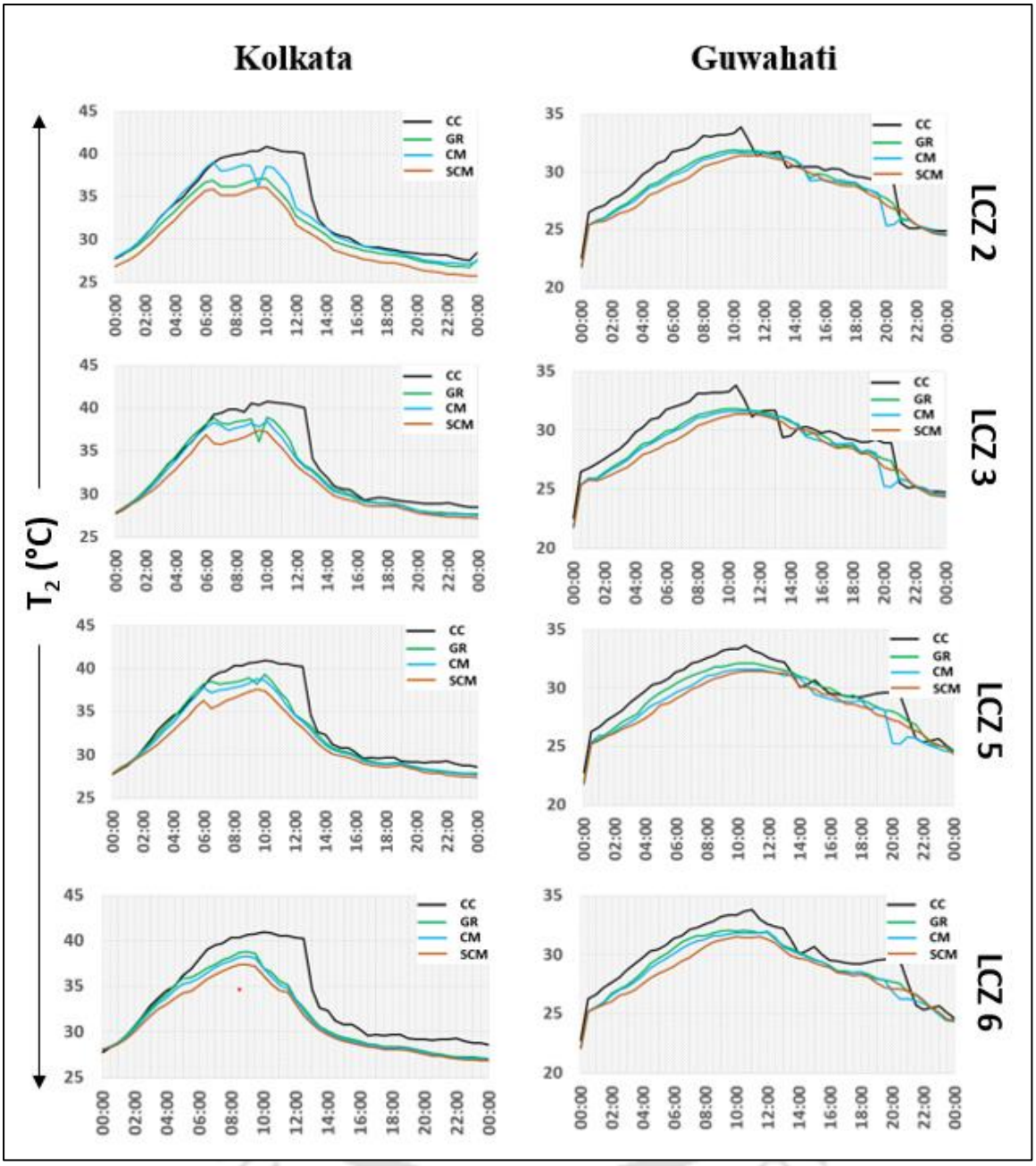

Figure 6.3: Impact of different heat mitigation strategies on T_2 variations for Kolkata and Guwahati

On the other hand, the performance of these techniques in improving the wind circulations are not as effective as temperature (Fig. 6.4). It was observed that the implementation of green roofs could draw better results in increasing the WS compared to the other two techniques based on engineered materials in Kolkata, especially in the less built-up density areas. Notably, the performance of these strategies in the LCZ6 with the least complicated urban profile is maximum as opposed to the T_2 conditions. The results for the Guwahati region, however showed almost no improvement in the wind circulation favorable to urban areas, especially

among the complex LCZ classes. The conditions slightly improve in LCZ6, where GR shows the best results.

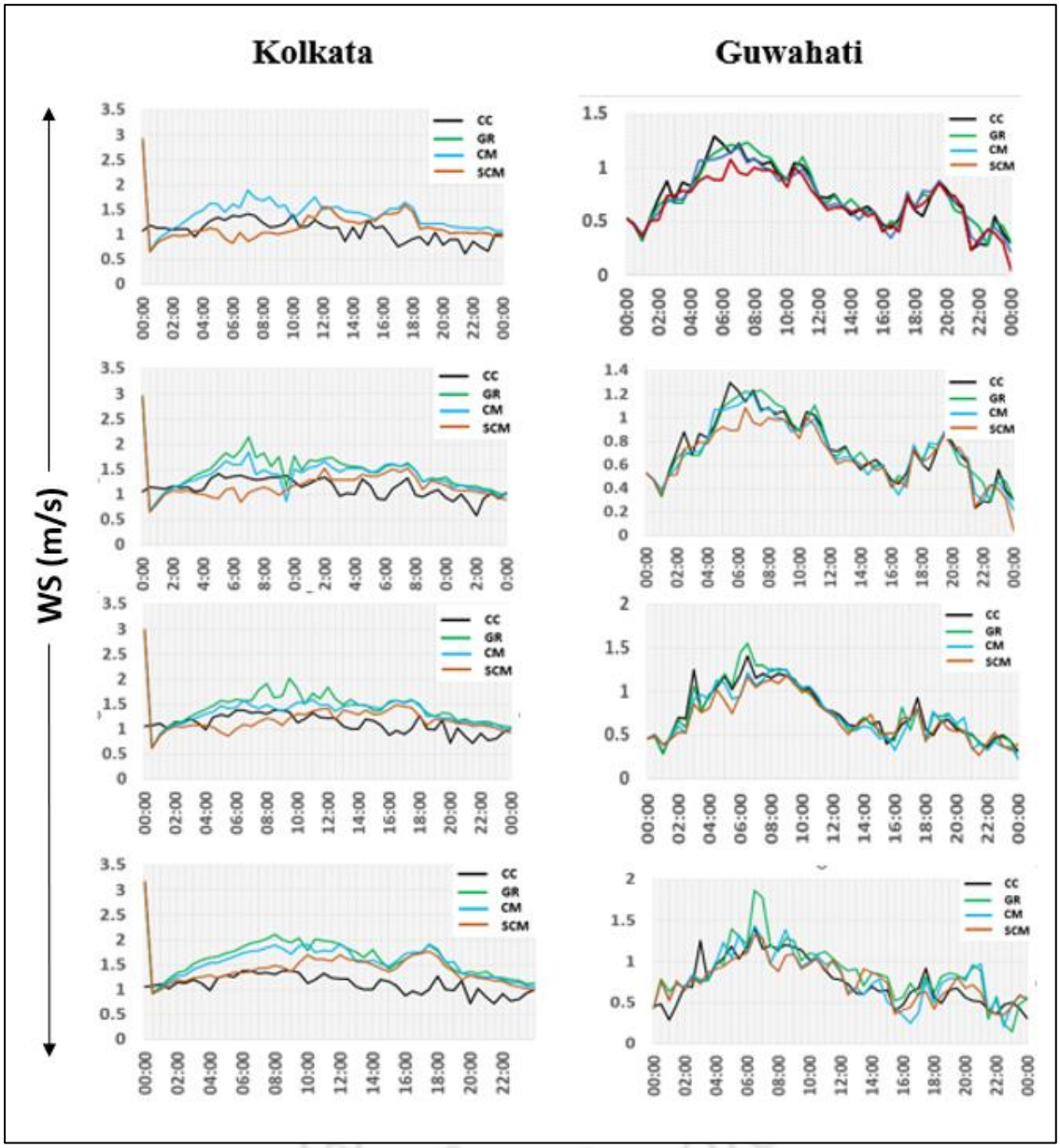

Figure 6.4: Impact of different heat mitigation strategies on WS variations for Kolkata and Guwahati

6.4 Summary and Conclusion

The extensive efforts to understand the micro-scale variations in the urban-climate conditions over the cities can help in developing necessary strategies to mitigate the adverse effects of urban induced climatic risks. UHI effect and urban floods are some of the most important climatic hazards which constantly increase with the rise in urban development. This study focuses on understanding the local variations in urban intensity which could contribute towards

the thermal discomfort of the city-dwellers. This analysis tries to identify the most vulnerable zones within the cities experiencing the adverse effects of all important climate variables which affects the thermal comfort. However, the intensity of thermal comfort sensation of the individuals is beyond the scope of this study. A composite index was built to assess the comprehensive effect of all the variables in inducing thermal discomfort throughout the city within smaller horizontal distances. The analysis revealed that, the direct adverse impact of the prevailing temperature conditions is compounded by the negative effect of other corresponding variables, and could also be improved by their positive feedback. Also, the local land surface conditions might regulate the overall climatology of the area, imposing diverse impacts on the different indicators. A composite index such as UMCI built by careful consideration of the variables and their contributions towards the overall meteorological conditions could prove to be a useful tool for the authorities to quickly assess its spatial variations and identify the most vulnerable pockets of the city. Such an approach to assess the overall meteorological health from the perspective of thermal comfort could not be identified on a careful synthesis of the existing literature and thus could be considered as a major contribution of this study. The findings of this analysis are particularly important since such higher resolution datasets (derived from WRF simulations) for the meteorological parameters considered for the assessment are not readily available, limiting the understanding of the negative impact of urbanization on the comprehensive urban climate at micro-scale (localities or urban canopy level).

Further, on assessing different heat mitigation strategies on the near surface air temperature and wind circulations, notable variations in their performance could be identified in mitigating the different variables. It was observed that although the implementation of SCM is more beneficial in reducing the T_2 especially in the most compact parts of the cities, its relevance is the lowest to improve the wind velocities. WS on the other hand could be improved by using green infrastructure such as green roofs especially in case of bigger and denser urban structures. Besides, it was also evident from the results that a particular mitigation measure is not equally effective for both the cities and across the different types of urban densities. Guwahati, which is smaller, less urbanized and greener in comparison to Kolkata showed lesser variations in T_2 as well as WS employing the different mitigation strategies. Therefore, it could be concluded that the use of comprehensive urban micro-climate assessment in finding the most vulnerable zones could be one step forward in planning suitable mitigation policies. Further an appropriate mitigation measure could be selected according to its effectiveness in the region and feasibility

of implementation. The same mitigation strategy should not be applied throughout any city to avoid wasteful use of the resources and should be strategically planned for optimal results. From the present analysis it can be suggested that, implementation of SCM to mitigate heat as well as improve the wind speed could be more advantageous if implemented in the LCZ 2 LCZ 3 and LCZ 5 regions in case of Kolkata where as a choice between SCM and CM could be made for LCZ-6 depending upon the availability of resources. Further, implementation of GR is more advantageous compared to CM in all the four cases since it performed better and is cheaper and more durable, providing other benefits such as improvement in air quality, regulating wind speed etc. In case of Guwahati mitigating heat by implementing SCM is almost equally beneficial for all the LCZ categories and could be adopted depending on the available resources. However, either GR or CM could be employed for LCZ 2 and LCZ 3, which showed almost similar scale reduction in T_2; and CM was more advantageous in case of LCZ 5 and LCZ 6 compared to GR due to the influence of naturally available green spaces in these zones. Thus, this type of micro-scale analysis in highly advantageous in strategic implementation of artificial heat mitigation techniques in cities of different morphological character and dimensions to achieve better outcome. The combined impact of the improvement in T_2 as well as WS on the thermal comfort especially in the dense urban canopies is particularly advantageous from the urban planning perspective.

Chapter 7

Concluding Remarks

7.1 Conclusions

The study focuses on understanding the micro-scale variations in the meteorological conditions of cities with respect to the local variations in their surface properties. The already complicated nature of this process is further enhanced by the extremely compact and heterogenous surface configuration of cities from the developing regions, which also coincides with the tropical complexities. This study attempted to use the meso-scale NWP model WRF in combination with finer-scale urban parameterization to model the energy transfer between complex urban surfaces and the overlying atmosphere in order to understand this phenomenon. The thesis addresses three major objectives, viz., i.) to optimize the model parameters for high-resolution urban climate simulations; ii) to characterize the micro-scale variations in urban meteorology over two different cities (Kolkata and Guwahati) according to their surface configurations and iii) comprehensive impact of the urban micro-meteorological construct of the cities and possible mitigation strategies. This chapter outlines the work carried out in accomplishing each objective and their overall outcome to contribute towards understanding this complex mechanism.

The first objective, which dealt with finding the optimal physical as well as urban parameterization to configure the WRF model according to the surface configuration as well as general climatology of the study region, is presented in Chapter 3 of the dissertation. To achieve this, at first high-resolution LCZ products were generated using multispectral satellite images and deep-learning techniques for image classification. Then, appropriate physical parameters to resolve the climatic construct were identified by performing a set of experiments with different combinations of suitable physics schemes integrated with the WRF model. Finally, the most successful model configuration was further integrated with the LCZ products

to achieve the high-resolution uWRF-LCZ coupled model which could appropriately downscale the coarser resolution global climate products and obtain finer scale urban climate variables. The major conclusions that could be drawn from this analysis are

1. The classification accuracy of LCZ products for compact and heterogeneous cities most prevalent in the global south could be improved by improving the classification algorithm. The use of a CNN-based model in this case improved the efficiency of classification technique by enhancing the accuracy of the classified products, and could be applied for other such cities.
2. The built-up extent of both cities (i.e., with the KMA and GMA regions) is dominated by the four major LCZ classes namely, LCZ2, LCZ3, LCZ5 and LCZ6.
3. The Kain-Fritsch cumulative scheme in combination with the Lin microphysics models, were identified as most appropriate to scale the effects of convective as well as shallow clouds and resolve the water vapour, cloud and precipitation processes in the study region.
4. The BEP+BEM multi-layer UCM was found to be most effective in modelling the three-dimensional and intricate exchange process of different urban elements with the atmosphere.
5. The uWRF-LCZ coupled model significantly improved the efficiency of the meso-scale WRF model to simulate micro-scale climatic parameters for such a complex urban setup.

The second objective of the study was to analyse micro-scale variations in the simulated meteorological variables for different scenarios, to establish a relationship between the nature of urban surface morphology with the overlying climate. Details of the different scenarios evaluated and the derived results are presented in the Chapters 4 and 5 of the thesis. The different scenarios simulated by the model included i) seasonal variations in the urban micro-meteorology, ii) variations governed by the urban growth pattern, and iii) the effect of reduced anthropogenic functions on the urban climate conditions. The major conclusions from these analyses include the following.

1. Micro-meteorological variations between different parameters according to the dominant LCZ classes representing the most complex built-up extent to the least urban surroundings showed a gradual change, almost for all the simulated scenarios which complied with the general trend of urban complexity distribution.

2. The LCZ-wise seasonal analysis revealed that the pre-monsoon season has the highest variations in the important variables like temperature (including T_2, T_s) and wind circulations between the different LCZ classes according to their declining complexity. This indicated towards the city's higher potential in strengthening the UHI effect during this season leading to increasing thermal discomfort towards the city core.
3. The impact-magnitude of urbanization on the monsoon convections is largely determined by the dimensions of the city and the level of urban intensity along with the local geography of the region.
4. Although the rainfall intensity was lesser in the core city areas compared to the surroundings, its gradual decline with the increasing urban complexity is not constant for both cities
5. A steady relationship was observed in the impact of changing size and urban intensity of the cities on their micro-climate behaviour.
6. Reduction in the anthropogenic functions of the cities could significantly improve their meteorological character, more prominently in case of larger and more complex urban setup.

The third objective undertaken in this study analysed the overall micro-climate behaviour of the cities combining all important meteorological variables during the pre-monsoon season, which experiences most severe climate impacting the health and well-being of the residents, especially in Kolkata. Several heat mitigation measures were also tested to determine a better implementation strategy to address the adverse conditions according to the nature of built-up distribution in the cities. The detailed analysis presented in Chapter 6, helped in deriving the following important conclusions.

1. The creation of the UMCI could help in understanding the compound effect of different climate variables on the micro-meteorological character of a region.
2. The spatial variation in the overall climate of the cities corresponds directly with the urban density and is largely governed by the heat island intensity. Following the general behaviour, the city core with highest morphological complexity is identified to be the most vulnerable zone.
3. The adverse effect of a particular climate variable may be intensified or improved in combination with other variables.

4. UMCI could be an important tool for quick estimation of micro-scale variations in the urban climate and in finding the best and most vulnerable living conditions in a city, also aiding the implementation of suitable mitigation strategies.
5. The use of different heat stress mitigation strategies could potentially reduce the atmospheric as well as surface temperatures along with improvement in wind flow patterns over both cities most significantly during daylight hours.
6. It is not necessary that the same mitigation measure could improve the conditions alike for all parameters and throughout the city.
7. The impact of artificially generated heat mitigation strategies is higher in case of more complex urban setup like Kolkata compared to Guwahati where the role of natural surfaces in mitigating the thermal environment is much lower.

Thus, based on the two-city approach, the entire study comprehended a remarkable influence of the dimensions and nature of urban complexity on the overall and micro-scale urban meteorology.

7.2 Limitations and Recommendations

Some of the major limitations which are recommended to be addressed in future works of this study include

1. The limited period of simulations for each considered case could bias the perceptions regarding the process. Thus, increasing the time scale of analysis by including more days from consecutive years could help in concretizing the conclusions drawn.
2. The impact of urbanization on monsoon rains could be influenced by the local geographical setup of the region and therefore should be tested for other similar urban cases. Simulations for more time periods, along with increasing urban dynamics could also help in establishing a better picture.
3. The micro-scale variables derived from this analysis could be further analysed using robust techniques to understand the urban – atmosphere interaction dynamics at the local scale.
4. The 1 km resolution output could be further downscaled to understand canopy level analysis using more refined and better resolution models for in-depth building-level analysis.

REFERENCES

Abbassi Y, Ahmadikia H, Baniasadi E (2022) Impact of wind speed on urban heat and pollution islands. Urban Climate 44, 101200

Ackerman B, Changnon Jr SA, Dzurisin G, Gatz DL, Grosh RC (1977) Causes of precipitation anomalies: In: Summary of METROMEX. vol. 2. Illinois State Water Survey Bulletin 62:260. CrossRef

Agarwal R, Sharma U, Taxak A (2014) Remote sensing based assessment of urban heat island phenomenon in Nagpur metropolitan area. Int. J. Inf. Comput. Technol 4, 1069-1074

Akbari H, Pomerantz M, Taha H (2001) Cool surfaces and shade trees to reduce energy use and improve air quality in urban areas. Solar Energy 70(3), 295–310. https://doi.org/10.1016/S0038-092X(00)00089-X

Arfanuzzaman M, Dahiya B (2019) Sustainable urbanization in Southeast Asia and beyond: Challenges of population growth, land use change, and environmental health. Growth and Change 50(2), 725-744

Arnfield AJ (1982) An approach to the estimation of the surface radiative properties and radiation budgets of cities. Physical Geography 3:97-122. CrossRef

Arnfield AJ (2003) Two decades of Urban Climate Research: A Review of Turbulence, Exchanges of Energy and Water, and the Urban Heat Island International. Journal of Climatology 23:1–26

Ashie Y, Ca VT, Asaeda T (1999) Building canopy model for the analysis of urban climate. Journal of wind engineering and industrial aerodynamics 81(1-3), 237-248

Awasthi S, Jain K, Bhattacharjee S, Gupta V, Varade D, Singh H, ... Budillon A (2022) Analyzing urbanization induced groundwater stress and land deformation using time-series Sentinel-1 datasets applying PSInSAR approach. Science of The Total Environment 844, 157103

Baik JJ, Kim YH, Kim JJ, Han JY (2007) Effects of boundary-layer stability on urban heat island-induced circulation. Theoretical and Applied Climatology 89:73-81

Bajaj DN, Inamdar AB, Vaibhav V (2012) Temporal variation of Urban Heat Island using landsat data: a case study of Ahmedabad, India. In 33rd Asian Conference on Remote Sensing 2012, ACRS-2012 (pp. 797-804). Asian Association on Remote Sensing

Balchin WGV, Pye N, (1947) A micro-climatological investigation of Bath and the surrounding district. Q. J. R. Meteorol. Soc. 73, 297–323

Banerjee S, Middel A, Chattopadhyay S (2020) Outdoor thermal comfort in various microentrepreneurial settings in hot humid tropical Kolkata: Human biometeorological

assessment of objective and subjective parameters. Science of the Total Environment 721, 137741

Bao H, Yan C, Wang B, Fang X, Zhao CY, Ruan X (2017) Double-layer nanoparticle-based coatings for efficient terrestrial radiative cooling. Solar Energy Materials and Solar Cells 168, 78–84. https://doi.org/10.1016/j.solmat.2017.04.020

Barlow JF (2014) Progress in observing and modelling the urban boundary layer. Urban Climate 10:216-240. http://dx.doi.org/10.1016/j.uclim.2014.03.011

Barsi JA, Schott JR, Palluconi FD, Hook SJ (2005) Validation of a web-based atmospheric correction tool for single thermal band instruments. In Earth observing systems X (Vol. 5882, pp. 136-142). SPIE

Bassett R, Cai X, Chapman L, Heaviside C, Thornes JE, Muller CL, ... Warren EL (2016) Observations of urban heat island advection from a high-density monitoring network. Quarterly Journal of the Royal Meteorological Society 142(699), 2434-2441

Batisani N, Yarnal B (2009) Uncertainty awareness in urban sprawl simulations: Lessons from a small US metropolitan region. Land Use Policy 26(2). doi: 10.1016/j.landusepol.2008.01.013

Batty M (2005) Cities and Complexity: Understanding Cities Through Cellular Automata, Agent-Based Models, and Fractals. MIT Press, Cambridge, MA. CrossRef

Batty M (2008) The size, scale, and shape of cities. Science 319:769-771

Bechtel B, Langkamp T, Böhner J, Daneke C, Oßenbrügge J, Schempp S (2012) Classification and Modelling of urban micro-climates using multisensoral and multitemporal remote sensing data. International Archives of the Photogrammetry, Remote Sensing and Spatial Information Sciences, Volume XXXIX-B8, XXII ISPRS Congress, 25 August – 01 September 2012, Melbourne, Australia

Bechtel B, See L, Mills G, Foley M (2016) Classification of local climate zones using SAR and multispectral data in an arid environment. IEEE Journal of Selected Topics in Applied Earth Observations and Remote Sensing 9(7), 3097-3105

Becker F, Li ZL (1995) Surface temperature and emissivity at various scales: Definition, measurement and related problems. Remote Sensing Reviews 12:225–253

Bernard É, Munck CD, Lemonsu A (2022) Detailed Mapping and Modeling of Urban Vegetation: What Are the Benefits for Microclimatic Simulations with Town Energy Balance (TEB) at Neighborhood Scale. Journal of Applied Meteorology and Climatology 61(9), 1159-1178

Bhandari M, Shrestha S, New J, Allen M (2017) Comparison of Microclimate Simulated weather data to ASHRAE Clear Sky Model and Measured Data. Technical Memo. CrossRef

Bhati S, Mohan M (2016) WRF-urban canopy model evaluation for the assessment of heat island and thermal comfort over an urban airshed in India under varying land use/land cover conditions. Geoscience Letters) 5:27. https://doi.org/10.1186/s40562-018-0126-7

Bhati S, Mohan M (2018) WRF-urban canopy model evaluation for the assessment of heat island and thermal comfort over an urban airshed in India under varying land use/land cover conditions. Geoscience Research Letters 2018:5-27. doi: 10.1186/s40562-018-0126-7

Bhatta B (2009) Analysis of urban growth pattern using remote sensing and GIS: a case study of Kolkata, India. International Journal of Remote Sensing 30(18), 4733-4746

Bhattacharjee S, Bharti R (2021) The Impact of Covid-19 Lockdown on the Urban Micro-Climate of Major Coastal vs Inland Cities of India, EGU General Assembly 2021, online, 19–30 Apr 2021, EGU21-10790, https://doi.org/10.5194/egusphere-egu21-10790, 2021

Bhattacharjee S, Kar BK (2022) Urban Flooding Scenario and Human Response in Guwahati, India. In Climate, Environment and Disaster in Developing Countries (pp. 507-522). Singapore: Springer Nature Singapore

Bhattacharjee S, Kumar P, Thakur PK, Gupta K (2021) Hydrodynamic modelling and vulnerability analysis to assess flood risk in a dense Indian city using geospatial techniques. Natural Hazards 105, 2117-2145

Bhattacharjee S, Lekshmi K, Bharti R (2023) Evidences of localized coastal warming near major urban centres along the Indian coastline: past and future trends. Environmental Monitoring and Assessment 195(6), 692

Bhattacharyya NN (2001) Growth and Changing Face of Guwahati Since 1972. Guwahati-The Gateway to the East 27-34

Bogolepow MA (1928) Über des Klima von Moskau [On the climate of Moscow]. Meteorol. Zeitschrift 45, 152–154. Crossref

Bokaie M, Zarkesh MK, Arasteh PD, Hosseini A (2016) Assessment of urban heat island based on the relationship between land surface temperature and land use/land cover in Tehran. Sustainable Cities and Society 23:94-104

Borbora J, Das AK (2014) Summertime urban heat island study for Guwahati city, India. Sustainable Cities and Society 11, 61-66

Bornstein R, LeRoy M (1990) Urban barrier effects on convective and frontal thunderstorms. Extended Abstracts, Fourth Conference Mesoscale Processes, Boulder, CO. American Meteorological Societ. 120-121. CrossRef

Bornstein R, Lin Q (2000) Urban heat islands and summertime convective thunderstorms in Atlanta: Three cases studies. Atmospheric Environment 34:507–516

Bornstein RA (1968) Observations of the urban heat island effect in New York City. Journal of Applied Meteorology 7:575–582. CrossRef

Borthakur M, Nath BK (2012) A Study of Changing Urban Landscape and Heat Island Phenomenon in Guwahati Metropolitan Area. International Journal of Scientific and Research Publications Volume 2, Issue 11, November 2012 1 ISSN 2250-3153

Bose S, Mazumdar A (2020) IOP Conf. Ser.: Earth Environ. Sci. 505 012022

Bringi VN, Chandrasekar V (2001) Polarimetric Doppler Weather Radar: Principles and applications. Cambridge University Press. CrossRef

Brousse O, Mertilli A, Foley M, Mills G, Bechtel B (2016) WUDAPT, an efficient land use producing data tool for mesoscale models? Integration of urban LCZ in WRF over Madrid. Urban Climate 17:116-134. doi: 10.1016/j.uclim.2016.04.001

Brownlee J, Ray P, Tewari M, Tan H (2017) Relative Role of Turbulent and Radiative Flux on the Near-SurfaceTemperature in a Single-Layer Urban Canopy Model over Houston. Journal of Applied Meteorology and Climatology doi: 10.1175/JAMC-D-17-0088.1

Burian SJ, Shephard JM (2005) Effect of urbanization on the diurnal rainfall pattern in Houston. Hydrological Processes 19:1089–1110; doi: 10.1002/hyp.5647

Burkart K, Khan MM, Schneider A, Breitner S, Langner M, Krämer A, Endlicher W (2014) The effects of season and meteorology on human mortality in tropical climates: A systematic review. Transactions of The Royal Society of Tropical Medicine and Hygiene 108:393–421. CrossRef

Cecil DJ, Goodman SJ, Boccippio DJ, Zipser EJ, Nesbitt SW (2005) Three Years of TRMM Precipitation Features. Part I: Radar, Radiometric, and Lightning Characteristics. Mon. Wea. Rev. 133:543

Census of India (2011). Data on Disability. Office of the Registrar General & Census Commissioner, New Delhi, 27-12-2013. http://censusindia.gov.in

Chakraborty S, Maity I, Patel PP, Dadashpoor H, Pramanik S, Follmann A, ... Roy U (2021) Spatio-temporal patterns of urbanization in the Kolkata Urban Agglomeration: A dynamic spatial territory-based approach. Sustainable Cities and Society 67, 102715

Chandler TJ (1960) Wind as a factor of urban temperatures—A survey in north-east London. Weather 15, 204–213

Chandler TJ (1965) The Climate of London. Hutchinson, London CrossRef

Chang H-I, Kumara A, Niyogi D, Mohanty UC, Chen F, Dudhia J (2009) The role of land surface processes on the mesoscale simulation of the July 26, 2005 heavy rain event over Mumbai, India. Global and Planetary Change 67(1):87-103. doi: 10.1016/j.gloplacha.2008.12.005

Changnon SA, Huff FA, Schickedanz PT, Vogel JL (1977) Weather anomalies and impacts: In summary of METROMEX Vol. I. Illinois State Water Survey Bulletin 62:260 pp. CrossRef

Changnon SA (1968) The LaPorte Weather Anomaly-Fact or Fiction? Bulletin of the American Meteorological Society 49, 4-11. Crossref

Chatterjee S, Khan A, Dinda A, Mithun S, Khatun R, Akbari H, Kusaka H, Mitra C, Bhatti SS, Van Doan Q, Wang Y (2019) Simulating micro-scale thermal interactions in different building environments for mitigating urban heat islands. Science of The Total Environment https://doi.org/10.1016/j.scitotenv.2019.01.299

Chatterjee U, Majumdar S (2022) Impact of land use change and rapid urbanization on urban heat island in Kolkata city: A remote sensing based perspective. Journal of Urban Management 11(1), 59-71

Chelani AB, Gautam S (2022) The influence of meteorological variables and lockdowns on COVID-19 cases in urban agglomerations of Indian cities. Stochastic environmental research and risk assessment 36(9), 2949-2960

Chen F, Kusaka H, Bornstein R, Ching J, Grimmond CSB, Grossman-Clarke S, Loridan T, Manning KW, Martilli A, Miao S, Sailor D, Salamanca F, Taha H, Tewari M, Wang X, Wyszogrodzki AA, Zhang C (2011) The integrated WRF/urban modelling system: Development, evaluation, and applications to urban environmental problems. International Journal of Climatology 31(2):273-288. https://doi.org/10.1002/joc.2158

Chen M, Zhang H, Liu W, Zhang W (2014) The Global Pattern of Urbanization and Economic Growth: Evidence from the Last Three Decades. PLoS ONE 9(8): e103799. doi:10.1371/journal.pone.0103799

Chen S, Behrangi A, Tian Y, Hu J, Hong Y, Tang Q, Hu X.M, Stepanian P.M, Hu B, Zhang X (2016) Precipitation Spectra Analysis over China With High-Resolution Measurements From Optimally-Merged Satellite/Gauge Observations-Part II: Diurnal Variability Analysis. IEEE J. Sel. Topics Appl. Earth Observ. Remote Sens. 9:2979-2988

Chen T, Wang S, Yen M (2006) Enhancement of Afternoon Thunderstorm Activity by Urbanization in a Valley: Taipei. Journal of Applied Meteorology and Climatology 46:1324-1340. doi: 10.1175/JAM2526.1

Chen C, Bagan H, Yoshida T (2023) Multiscale mapping of local climate zones in Tokyo using airborne LiDAR data, GIS vectors, and Sentinel-2 imagery. GIScience & Remote Sensing 60(1), 2209970

Chen F, Kusaka H, Tewari M, Bao JW, Hirakuchi H (2004) Utilizing the coupled WRF/LSM/Urban modeling system with detailed urban classification to simulate the urban heat island phenomena over the Greater Houston area. In Fifth Symposium on the Urban Environment (Vol. 25, pp. 9-11). American Meteorological Society Vancouver, BC, Canada.

Chen YC, Yao CK, Honjo T, Lin TP (2018) The application of a high-density street-level air temperature observation network (HiSAN): Dynamic variation characteristics of urban heat island in Tainan, Taiwan. Science of the Total Environment 626, 555-566

Chinnasamy P, Shah Z, Shahid S (2023) Impact of lockdown on air quality during COVID-19 pandemic: A case study of India. Journal of the Indian Society of Remote Sensing 51(1), 103-120

Chow WTL, Brennan D, Brazel AJ (2012) Urban Heat Island Research in Phoenix, Arizona: Theoretical Contributions and Policy Applications. Bulletin of the American Meteorological Society 93(4), 517–530. https://doi.org/10.1175/BAMS-D-11-00011.1

Chrysoulakis N, Grimmond S, Feigenwinter C et al. (2018) Urban energy exchanges monitoring from space. Scientific Reports 8(11498). doi:10.1038/s41598-018-29873-x

Cifelli R, Chandrasekar V, Chen H, Johnson E (2018) High Resolution Radar Quantitative Precipitation Estimation in the San Francisco Bay Area:Rainfall Monitoring for the Urban Environment. Journal of the Meteorological Society of Japan, Special Issue on Tokyo Metropolitan Area Convection Study for Extreme Weather Resilient Cities (TOMACS) 96A:141−155. doi: 10.2151/jmsj.2018-016

Cohen B (2006) Urbanization in developing countries: Current trends, future projections, and key challenges for sustainability. Technology in society 28(1-2), 63-80

Condit CW (1970) The Evolution of Urban Form. Technology and Culture 11(3), 428-433.

Corny P, Sharma A, Potosnak M, Leo LS, Bensman E, Hellmann J, Fernando HJS (2015) Chicago's Heat Island and Climate Change: Bridging the Scales via Dynamic Downscaling. Journal of Applied Meteorology and Climatology 54:1430-1448. doi: 10.1175/JAMC-D-14-0241.1

Coseo P, Larsen L (2014) How factors of land use/land cover, building configuration, and adjacent heat sources and sinks explain Urban Heat Islands in Chicago. Landscape and Urban Planning 125:117-129

Crum SM, Jenerette GD (2017) Microclimate Variation among Urban Land Covers: The Importance of Vertical and Horizontal Structure in Air and Land Surface Temperature Relationships. Journal of Applied Meteorology and Climatology 56:2531 – 2543. https://doi.org/10.1175/JAMC-D-17-0054.s1

Das Y, Padmanabhamurty B, Murty ASN (2014) Some Parameterizations of Radiative Fluxes at Atmospheric Boundary Layer (ABL). Journal of Atmospheric Pollution 2(1):1-5

Das M, Mandal A, Das A, Pereira P (2022) Land use and land cover change future projection in Kolkata Metropolitan Area, Eastern India. In Mapping and Forecasting Land Use (pp. 299-320)

Das S, Jain GV (2022) Assessment and prediction of urban expansion using CA-based SLEUTH urban growth model: A case study of Kolkata Metropolitan area (KMA), West Bengal, India. Journal of the Indian Society of Remote Sensing 50(12), 2277-2302

Dasgupta P, Srikanth K (2020) Reduced air pollution during COVID-19: Learnings for sustainability from Indian Cities. Global Transitions 2: 271-282

Dasgupta S, De UK (2007) Binary logistic regression models for short term prediction of premonsoon convective developments over Kolkata (India). International Journal of Climatology: A Journal of the Royal Meteorological Society 27(6), 831-836

Dasgupta S, Gosain AK, Rao S, Roy S, Sarraf M (2012) A megacity in a changing climate: the case of Kolkata. Climatic Change 116, 747-766

Dash SK, Saraswat V, Panda SK, Sharma N (2013) A study of changes in rainfall and temperature patterns at four cities and corresponding meteorological subdivisions over coastal regions of India. Global and Planetary Change 108, 175-194

Dawn S, Satyanarayana ANV (2020) Sensitivity studies of cloud microphysical schemes of WRF-ARW model in the simulation of trailing stratiform squall lines over the Gangetic West Bengal region. Journal of Atmospheric and Solar-Terrestrial Physics 209, 105396

Deilami K, Kamruzzaman M, Liu Y (2018) Urban heat island effect: A systematic review of spatio-temporal factors, data, methods, and mitigation measures. International journal of applied earth observation and geoinformation 67, 30-42

Deosthali V (2000) Impact of rapid urban growth on heat andmoisture Islands in Pune City, India; Atmos. Environ. 34 2745–2754

Devadas, MD, Amritham LR (2009) Urban Factors and the Intensity of Heat Island in the city of Chennai. The seventh International Conference on Urban Climate, 29 June - 3 July 2009, Yokohama, Japan

Diksha, Kumar A (2017) Analysing urban sprawl and land consumption patterns in major capital cities in the Himalayan region using geoinformatics. Applied Geography 89, 112-123

Dixon PG, Mote TL (2003) Patterns and causes of Atlanta's urban heat island–initiated precipitation. Journal of Applied. Meteorology 42:1273–1284

Dobbie MJ, Dail D (2006) Environmental Indices. Encyclopedia of environmetrics. CrossRef

Dousset B, Gourmelonb F (2003) Satellite multi-sensor data analysis of urban surface temperatures and landcover. ISPRS Journal of Photogrammetry & Remote Sensing 58:43-54. doi:10.1016/S0924-2716(03)00016-9

Du H, Zhan W, Voogt J, Bechtel B, Chakraborty TC, Liu Z., ... Miao S (2023) Contrasting trends and drivers of global surface and canopy urban heat islands. Geophysical Research Letters 50(15), e2023GL104661

Dupont S, Otte TL, Ching JKS (2004) Simulation of Meteorological fields within and above urban and rural canopies with a mesoscale model MM5. Boundary-Layer Meteorology 113:111-158

El Gibari, S., Gómez, T., & Ruiz, F. (2019). Building composite indicators using multicriteria methods: A review. Journal of Business Economics, 89(1), 1-24.

Elraouf RA, EL Mokadem A, Megahed N, Eleinen OA, Eltarabily S (2022) Evaluating urban outdoor thermal comfort: A validation of ENVI-met simulation through field measurement. Journal of Building Performance Simulation 15(2), 268-286

Emmanuel R, Johansson E (2006) Influence of urban morphology and sea breeze on hot humid microclimate: The case of Colombo, Sri Lanka. Climate Research 30:189–200

Feng J, Khan A, Doan QV, Gao K, Santamouris M (2021) The heat mitigation potential and climatic impact of super-cool broadband radiative coolers on a city scale. Cell Reports Physical Science 2(7), 100485. https://doi.org/10.1016/j.xcrp.2021.100485

Fenger J (1999) Urban air quality. Atmospheric environment 33(29), 4877-4900

Ferreira MJ, Oliveira AP, Soares J, (2013) Diurnal variation in stored energy flux in São Paulo city, Brazil. Urban Climate 5:36–51

Fleischmann M, Feliciotti A, Kerr W (2022) Evolution of urban patterns: urban morphology as an open reproducible data science. Geographical Analysis 54(3), 536-558

Fountain M, Arens EA, Xu T, Bauman F, Oguru M (1999) An investigation of thermal comfort at high humidities.

Fujibe F, Asai T (1980) Some features of a surface wind system associated with the Tokyo heat island. Journal of the Meteorological Society of Japan 58:149 – 152

Gaffin S, Rosenzweig C, Khanbilvardi R, et al. (2008) Variations in New York City's Urban Heat Island Strength Over Time and Space. Theoretical and Applied Climatology 94(1):1-11. CrossRef

Gallinelli P, Camponovo R, Guillot V (2017) CityFeel - micro climate monitoring for climate mitigation and urban design. Energy Proceedia 122:391-396. https://doi.org/10.1016/j.egypro.2017.07.427

Gallo KP, Owen TW (1988) Assessment of Urban Heat Islands: A Multi-Sensor Perspective for the Dallas-Ft. Worth, USA Region. Papers in Natural Resources. 186. https://digitalcommons.unl.edu/natrespapers/186

Ganeshan M, Murtugudde R, Imhoff ML (2013) A multi-city analysis of the UHI-influence on warm season rainfall. Urban Climate 6:1–23; http://dx.doi.org/10.1016/j.uclim.2013.09.004

Gao J, O'Neill BC (2020) Mapping global urban land for the 21st century with data-driven simulations and Shared Socioeconomic Pathways. Nature communications 11(1), 2302

Gao Z, Liu X (2014) Support vector machine and object-oriented classification for urban impervious surface extraction from satellite imagery. In 2014 The Third International Conference on Agro-Geoinformatics (pp. 1-5). IEEE.

Garuma GF (2023) Tropical surface urban heat islands in east Africa. Scientific Reports 13(1), 4509

Georgescu M (2015) Challenges Associated with Adaptation to Future Urban Expansion. Journal of Climate 28(7), 2544–2563. https://doi.org/10.1175/JCLI-D-14-00290.1

Georgescu M, Moustaoui M, Mahalov A, Dudhia J (2013) Summer-time climate impacts of projected megapolitan expansion in Arizona. Nature Climate Change 3(1), 37–41. https://doi.org/10.1038/nclimate1656

Georgii HW (1969) The effects of air pollution on urban climates. Bulletin of the World Health Organization 40(4), 624

Ghosh S, Das A, Hembram TK, Saha S, Pradhan B, Alamri AM (2020) Impact of COVID-19 induced lockdown on environmental quality in four indian megacities using landsat 8 OLI and TIRS-derived data and mamdani fuzzy logic modelling approach. Sustainability 12(13), 5464

Ghosh S, Dinda S, Chatterjee ND, Bera D (2023) Linking ecological vulnerability and ecosystem service value in a fast-growing metropolitan area of eastern India: a scenario-based sustainability approach. Environment, Development and Sustainability 1-31.

Giannaros C, Nenes A, Giannaros TM, Kourtidis K, Meles D (2018) A comprehensive approach for the simulation of the Urban Heat Island effectwith the WRF/SLUCM modeling system: The case of Athens (Greece). Atmospheric Research 201:86-101

Giannopoulou K, Santamouris M, Livada I, Georgakis C, Caouris Y (2010) The Impact of Canyon Geometry on Intra Urban and Urban: Suburban Night Temperature Differences Under Warm Weather Conditions. Pure Appl. Geophys. 167:1433–1449

Giridharan R, Emmanuel R (2018) The impact of urban compactness, comfort strategies and energy consumption on tropical urban heat island intensity: A review. Sustainable Cities and Society 40:677-687. https://doi.org/10.1016/j.scs.2018.01.024

Giridharan R, Ganesan S, Lau SSY (2004) Daytime urban heat island effect in high-rise and high-density residential developments in Hong Kong. Energy and Buildings 36:525–534

Giridharan R, Ganesan S, Lau SSY (2005) Nocturnal heat island effect in urban residential developments of Hong Kong. Energy and Buildings 9:964-971

Gogoi PP, Vinoj V, Swain D, Roberts G, Dash J, Tripathy S (2019) Land use and land cover change effect on surface temperature over Eastern India. Scientific reports 9(1), 8859

Gohil K, Jin MS (2019) Validation and Improvement of the WRF Building Environment Parametrization (BEP) Urban Scheme. Climate 7(9). 109; https://doi.org/10.3390/cli7090109

Goswami BN, Mahanta R (2023) Present and Future of the South Asian Summer Monsoon's Rainy Season over Northeast India.

Greco S, Ishizaka A, Tasiou M, Torrisi G (2019) On the methodological framework of composite indices: A review of the issues of weighting, aggregation, and robustness. Social indicators research 141, 61-94

Grell GA, Dudhia J, Stauffer DR (1994) A description of the fifth-generation Penn State/NCAR Mesoscale Model (MM5). NCAR Tech. Note NCAR/TN-398+STR, 122 pp

Grimm NB, Faeth SH, Golubiewski NE, Redman CL, Wu JG, Bai XM, Briggs JM (2008) Global change and the ecology of cities Science 319:756-760

Grimmond CSB, Souch C, Hubble MD (1996) Influence of tree cover on summertime surface energy balance fluxes, San Gabriel Valley, Los Angeles. Climate Research 6:45–57.

Grimmond S (2007) Urbanization and global environmental change: local effects of urban warming; Cities and global environmental change, Royal Geographical Society 173:83–88

Grimmond, CSB (2005) Progress in measuring and observing the urban atmosphere. Theoretical and Applied Climatology 84(1–3):3–22. http://dx.doi.org/10.1007/s00704-005-0140-5

Grover A, Singh RB (2015) Analysis of urban heat island (UHI) in relation to normalized difference vegetation index (NDVI): A comparative study of Delhi and Mumbai. Environments 2(2), 125-138

Gsella A, De Meij A, Kerschbaumer A, Reimer E, Thunis P, Cuvelier C (2014) Evaluation of MM5, WRF and TRAMPER meteorology over the complex terrain of the Po Valley, Italy. Atmospheric Environment 89, 797-806

Guo X, Fu D, Wang J (2006) Mesoscale convective precipitation system modified by urbanization in Beijing City. Atmospheric Research 82(1):112-126

Gyimah RR (2023) The hot zones are cities: Methodological outcomes and synthesis of surface urban heat island effect in Africa. Cogent Social Sciences 9(1), 2165651.

Habitat UN (2022) World Cities Report 2022: Envisaging the future of cities. United Nations Human Settlements Programme: Nairobi, Kenya, 41-44

Hajkowicz S (2006) Multi-attributed environmental index construction. Ecological economics 57(1), 122-139

Hamdi R, Degrauwe D, Termonia P (2012) Coupling the Town Energy Balance (TEB) Scheme to an Operational Limited-Area NWP Model: Evaluation for a Highly Urbanized Area in Belgium. Weather and Forecasting, 27(2):323-344. https://doi.org/10.1175/waf-d-11-00064.1

Hamdi R, Schayes G (2008) Sensitivity study of the urban heat island intensity to urban characteristics. International Journal of Climatology 28: 973–982

Hamdi R, Vyver V, De Troch R, Termonia P (2014) Assessment of three dynamical urban climate downscaling methode: Brussel's Future urban heat island under an A1B emission scenario. International Journal of Climatology 34:978-99

Hammerberg K, Brousse O, Martilli A, Mahdavi A, (2018) Implications of employing detailed urban canopy parameters for mesoscale climate modelling: a comparison between WUDAPT and GIS databases over Vienna, Austria. International Journal of Climatology 38(Suppl.1):1241-1257. doi: 10.1002/joc.5447

Han JY, Baik JJ (2008) A theoretical and numerical study of urban heat island-induced circulation and convection. Journal of Atmospheric Science 65:1859-1877

Han JY, Baik JJ, Lee H (2014) Urban impacts on precipitation. Asia-Pacific Journal of Atmospheric Sciences 50, 17-30

Hann J (1885) Über den Temperaturunterschied zwischen Stadt und Land [On the temperature difference between town and country]. Österreichischen Gesellschaft für Meteorologie, Zeitschrift 20, 457–462. Crossref

Hardin AW, Liu Y, Cao G, Vanos JK (2018) Urban heat island intensity and spatial variability by synoptic weather type in the northeast U.S. Urban Climate 24:747-762. http://dx.doi.org/10.1016/j.uclim.2017.09.001

Heever SC, Cotton WR (2006) Urban Aerosol Impacts on Downwind Convective Storms. Journal of Applied Meteorology and Climatology 46:828-850. doi: 10.1175/JAM2492

Henderson V (2002) Urbanization in developing countries. The world bank research observer 17(1), 89-112

Hidalgo J, Masson V, Baklanov A, Pigeon G, Gimenoa L (2008) Advances in urban climate modeling: trends and directions in climate research. Annals of the New York Academy of Sciences 1146:354-374

Hien WN, Ignatius M, Eliza A, Jusuf SK, Samsudin R (2012) Comparison of STEVE and ENVI-met as temperature prediction models for Singapore context. International Journal of Sustainable Building Technology and Urban Development, 3(3), 197-209

Hong SY, Lim KSS, Lee YH, Ha JC, Kim HW, Ham SJ, Dudhia J (2010) Evaluation of the WRF double-moment 6-class microphysics scheme for precipitating convection. Advances in Meteorology 2010

Höppe P (1997) Aspects of human biometerology in past, present and future. International journal of biometeorology 40, 19-23

Huff FA (1986) Urban Hydrological Review. Bulletin of the American Meteorological Society 67:703–712. CrossRef

Huff FA, Changnon SA (1972) Climatological assessment of urban effects on precipitation at St. Louis. Journal of Applied Meteorology 11:823–842. CrossRef

Hung T & Yoshifumi Y (2005) MODIS Applications in Environmental Change Researches in the Southeast-Asian Region. International Journal of Geoinformatics 1(1):117-123

Hunh T, Daisuke U, Shiro O, Yoshifumi Y (2006) Assessment with satellite data of the urban heat island effects in Asian mega cities. International Journal of Applied Earth Observation and Geoinformation 8:34-48. doi:10.1016/j.jag.2005.05.003

Imamura IR (1991) Observational studies of urban heat island characteristics in different climate zones. Dissertation, University of Tsukuba

Imhoff ML, Bounoua L, DeFries R, Lawrence WT, Stutzer D, Tucker CJ (2004) The consequences of urban land transformation on net primary productivity in the United States. Remote Sensing Environment 89:434-443.

Ioannides YM, Rossi-Hansberg E (2005) Urban Growth. Working Paper Dept. of Economics Tufts University. Medford, MA

Iqbal N, Ravan M, Jamshed A, Birkmann J, Somarakis G, Mitraka Z, Chrysoulakis N (2022) Linkages between typologies of existing urban development patterns and human vulnerability to heat stress in Lahore. Sustainability 14(17), 10561

Jain M (2023) Two decades of nighttime surface urban heat island intensity analysis over nine major populated cities of India and implications for heat stress. Frontiers in Sustainable Cities 5, 1084573

Jallu SB, Shaik RU, Srivastav R, Pignatta G (2022) Assessing the effect of COVID-19 lockdown on surface urban heat island for different land use/cover types using remote sensing. Energy Nexus 5, 100056

Jamsran BE, Lin C, Byambakhuu I, Raash J, Akhmadi K (2019) Applying a support vector model to assess land cover changes in the Uvs Lake Basin ecoregion in Mongolia. Information processing in agriculture 6(1), 158-169

Jauregui E (1997) Heat island development in Mexico City. Atmospheric Environment 31:3821–3831

Jáuregui E (1973) The urban climate of Mexico City. Erdkunde 27, 298–307. Crossref

Jin M, Shephard M, Peters-Lidard CD (2007) Development of a parameterization for simulating the urban temperature hazard using satellite observations in climate model. Natural Hazards 43(2):257-271

Jing S, Li B, Tan M, Liu H (2013) Impact of relative humidity on thermal comfort in a warm environment. Indoor and Built Environment 22(4), 598-607

Joyce RJ, Janowiak JE, Arkin PA, Xie P (2004) CMORPH: A Method that Produces Global Precipitation Estimates from Passive Microwave and Infrared Data at High Spatial and Temporal Resolution. Journal of Hydrometeorology 5:487 - 503

Kafy AA, Al Rakib A, Akter KS, Jahir DMA, Sikdar MS, Ashrafi TJ, ... Rahman MM (2021) Assessing and predicting land use/land cover, land surface temperature and urban thermal field variance index using Landsat imagery for Dhaka Metropolitan area. Environmental Challenges 4, 100192

Kaufmann RK, Seto KS, Schneider A, Liu Z, Zhou L, Wang W (2007) Climate response to rapid urban growth: evidence of a human-induced precipitation deficit. Journal of Climate 20:2299-2306. doi: 10.1175/JCLI4109.1

Ketterer C, Matzarakis A (2014) Human-biometeorological assessment of the urban heat island in a city with complex topography–The case of Stuttgart, Germany. Urban Climate 10, 573-584

Khan A, Chatterjee S, Wang Y (2020) Urban heat island modeling for tropical climates. Elsevier

Khan A, Chatterjee S, Filho WL, Khatun R, Dinda A, Minhas A (2020) City-scale Modeling of Urban Heat Islands for Kolkata. Climate Change, Hazards and Adaptation Options: Handling the Impacts of a Changing Climate 89-133

Khan A, Khorat S, Doan QV, Khatun R, Das D, Hamdi R, Carlosena L, Santamouris M, Georgescu M, Niyogi D (2023) Exploring the meteorological impacts of surface and rooftop heat mitigation strategies over a tropical city. Journal of Geophysical Research: Atmospheres 128(8), e2022JD038099

Kim YH, Baik JJ, (2002) Maximum urban heat island intensity in Seoul. Journal of Applied Meteorology 41:651–659

Kim SW, Brown RD (2021) Urban heat island (UHI) variations within a city boundary: A systematic literature review. Renewable and Sustainable Energy Reviews 148, 111256

Kishtawal CM, Niyogi D, Tewari M, Pielke Sr. RA, Shepherd JM (2010) Urbanization signature in the observed heavy rainfallclimatology over India,Int. J. Climatol. 30, 1908–1916

Kjelgren R, Montague T (1998) Urban tree transpiration over turf and asphalt surfaces. Atmospheric Environment 32:35–41

Koc CB, Osmond P, Peters A, Irger M (2017) Mapping Local Climate Zones for urban morphology classification based on airborne remote sensing data. In 2017 Joint Urban Remote Sensing Event (JURSE) (pp. 1-4). IEEE

Kotharkar R, Bagade A (2018) Evaluating urban heat island in the critical local climate zones of an Indian city. Landscape and Urban Planning 169, 92-104

Kotharkar R, Ghosh A (2021) Review of heat wave studies and related urban policies in South Asia. Urban Climate 36, 100777

Kotharkar R, Ramesh A, Bagade A (2018) Urban heat island studies in South Asia: A critical review. Urban climate 24, 1011-1026

Kubota H, Shirooka R, Matsumoto J, Cayanan EO, Hilario FD (2017) Tropical cyclone influence on the long-term variability of Philippine summer monsoon onset. Progress in earth and planetary science 4, 1-12

Kumar Dash S, Jenamani RK, Mohapatra M (2022) India's prolonged heatwave linked to record poor summer rains

Kumar S, Prasad T, Sasidharan NV, Nair S (2001) Heat Island intensities over Brihan Mumbai on a cold winter and hot summer night. Mausam 52:703-708. CrossRef

Kummerow C, Barnes W, Kozu T, Shiue J, Simpson J (1998) The tropical rainfall measuring mission (TRMM) sensor package. Journal of Atmospheric and Oceanic Technology 5:809-817. CrossRef

Kurbarskii AF (2001) Computational Modeling of the Turbulent Penetrative Convection above the Urban Heat Island in a Stably Stratified Environment. Journal of Applied Meteorology 40. CrossRef

Kusaka H, Kimura F (2004) Coupling a Single-Layer Urban Canopy Model with a Simple Atmospheric Model: Impact on Urban Heat Island Simulation for an Idealized Case. Journal of the Meteorological Society of Japan 82(1):67-80

Kusaka H, Kimura F (2004) Thermal Effects of Urban Canyon Structure on the Nocturnal Heat Island: Numerical Experiment Using a Mesoscale Model Coupled with an Urban Canopy Model. American Meteorological Society 43:1899-1910

Landsberg HE (1981) The Urban Climate. Int. Geophys. Ser., 28-, Academic Press, New York, 275. CrossRef

Landsberg, H. E. (1981). The urban climate Academic Press, New York and London

Lao K K-L, Ren C, Shi Y, Zheng V, Yim S, Lai D (2015) Determining the optimal size of local climate zones for spatial mapping in high density cities. ICUC9 - 9th International Conference on Urban Climate jointly with 12th Symposium on the Urban Environment Toulouse, France. International Association for Urban Climate (IAUC) and American Meteorological Society (AMS)

Lapola DM, Braga DR, Di Giulio GM, Torres RR, Vasconcellos MP (2019) Heat stress vulnerability and risk at the (super) local scale in six Brazilian capitals. Climatic Change 154, 477-492

Laue F, Adegun OB, Ley A (2022) Heat stress adaptation within informal, low-income urban settlements in Africa. Sustainability 14(13), 8182

Lei M, Niyogi D, Kishtawal C, Pielke RA, Beltrán-Przekurat A, Nobis TE, Vaidya SS (2008) Effect of explicit urban land surface representation on the simulation of the 26 July 2005 heavy rain event over Mumbai, India. Atmospheric Chemistry and Physics Discussions, European Geosciences Union, 2008, 8 (3):8773-8816

Lemonsu A, Grimmond CSB, Masson V (2003) Modeling the Surface Energy Balance of the Core of an Old Mediterranean City: Marseille. Journal of Applied Meteorology 43:312-327

Lemonsu A, Masson V (2002) Simulation of a summer urban breeze over Paris. Boundary-Layer Meteorology 104, 463-490

Lemonsu A, Masson V, Shashua-Bar L, Erell E, Pearlmutter D (2021) Inclusion of vegetation in the Town Energy Balance model for modelling urban green areas. Geoscientific Model Development 5, no. 6 (2012): 1377-1393

Li X, Mitra C, Dong L, Yang Q (2017) Understanding land use change impacts on microclimate using Weather Research and Forecasting (WRF) model. Physics and Chemistry of the Earth 103. http://dx.doi.org/10.1016/j.pce.2017.01.017

Li XX, Koh TY, Panda J, Norford LK, (2016) Impact of urbanization patterns on the local climate of a tropical city, Singapore: An ensemble study. Journal of Geophysical Research Atmosphere 121:4386–4403. doi: 10.1002/2015JD024452.

Liang Y, Song W, Cao S, Du M (2023) Local Climate Zone Classification Using Daytime Zhuhai-1 Hyperspectral Imagery and Nighttime Light Data. Remote Sensing 15(13), 3351

Liao J, Wang T, Wang X, Xie M, Jiang Z, Huang X, Zhu J, (2014) Impacts of different urban canopy schemes in WRF/Chem regional climate and air quality in Yangtze River Delta, China. Atmospheric Research 145-146:226-243. hhttp://dx.doi.org/10.1016/j.atmosres.2014.04.005

Lim YK, Shin DW, Cocke S, LaRow TE, Schoof JT, O'Brien JJ, Chassignet EP (2007) Dynamically and statistically downscaled seasonal simulations of maximum surface air temperature over the southeastern United States. Journal of Geophysical Research 112(D24102). doi: 10.1029/2007JD008764. CrossRef

Lin C, Su C, Kusaka H, Akimoto Y, Sheng Y, Huang J, Hsu H (2016) Impact of an improved WRF urban canopy model on diurnal air temperature simulation over northern Taiwan Atmospheric Chemistry and Physics 16:1809–1822. doi: 10.5194/acp-16-1809-2016

Lin YL, Smith RB (1986) Transient dynamics of airflow near a local heat source. Jornal of Atmospheric Science 43:40-49

Liu Y, Chen F, Warner T, Basara J (2005) Verification of a Mesoscale Data-Assimilation and Forecasting System for the Oklahoma City Area during the Joint Urban 2003 Field Project. Journal of Applied Meteorology and Climatology 45:912-929

Liu J, Niyogi D (2019) Meta-analysis of urbanization impact on rainfall modification. Scientific reports 9(1), 7301

Liu L, Li J, Wang J, Liu F, Cole J, Sha J, ... Zhou J (2022) The establishment of an eco-environmental evaluation model for southwest China and eastern South Africa based on the DPSIR framework. Ecological Indicators 145, 109687

Liu Z, Cheng W, Jim CY, Morakinyo TE, Shi Y, Ng E (2021) Heat mitigation benefits of urban green and blue infrastructures: A systematic review of modeling techniques, validation and scenario simulation in ENVI-met V4. Building and Environment 200, 107939

Liu Z, He C, Zhou Y, Wu J (2014) How much of the world's land has been urbanized, really? A hierarchical framework for avoiding confusion. Landscape Ecology 29, 763-771

Liu Z, Lai J, Zhan W, Bechtel B, Voogt J, Quan J, ... Li J (2022) Urban heat islands significantly reduced by COVID-19 lockdown. Geophysical Research Letters 49(2), e2021GL096842

Lowry WP (1977) Empirical estimation of urban effects on climate: A problem analysis. Journal of Applied Meteorology 16:129-135. CrossRef

Luber G, McGeehin M (2008) Climate change and extreme heat events. American journal of preventive medicine 35(5), 429-435

Malik S, Pal SC, Sattar A, Singh SK, Das B, Chakrabortty R, Mohammad P (2020) Trend of extreme rainfall events using suitable Global Circulation Model to combat the water logging condition in Kolkata Metropolitan Area. Urban Climate 32, 100599

Mandal J, Fu Y, Overvig A, Jia M, Sun K, Shi N, Zhou H, Xiao X, Yu N, Yang Y (2018) Hierarchically porous polymer coatings for highly efficient passive daytime radiative cooling. Science eaat9513. https://doi.org/10.1126/science.aat9513

Marcotullio PJ, Keßler C, Fekete BM (2021) The future urban heat-wave challenge in Africa: Exploratory analysis. Global Environmental Change 66, 102190

Martilli A, Clappier A, Rotach MW (2002) An urban surface exchange parameterization for mesoscale models. Boundary Layer Meteorology 104:261–304

Masson V (2000) A physically-based scheme for the urban energy budget in atmospheric models. Boundary Layer Meteorology 94:357– 397

Masson V, Grimmond CSB, Oke TR (2002) Evaluation of the Town Energy Balance (TEB) scheme with direct measurements from dry districts in two cities. Journal of applied meteorology 41(10), 1011-1026

Matzarakis A, Muthers S, Koch E (2011) Human biometeorological evaluation of heat-related mortality in Vienna. Theoretical and applied climatology 105, 1-10

Mauree D, Nedege B, Clappier A (2018) Multi-scale modeling of the urban meteorology: Integration of a new canopy model in the WRF model. doi: 10.31223/osf.io/w89cj

Mcdonald RI, Kareiva P, Forman RTT (2008) The Implications of current and future urbanization for global protected areas and Biodiversity conservation. Biological Conservation 141(6):1695-1703 doi: 10.1016/j.biocon.2008.04.025

Mentaschi L, Duveiller G, Zulian G, Corbane C, Pesaresi M, Maes J, ... Feyen L (2022) Global long-term mapping of surface temperature shows intensified intra-city urban heat island extremes. Global Environmental Change 72, 102441

Mestayer PG, Durand P, Augustin P, et al., (2005) The urban boundary-layer field campaign in Marseille (UBL/CLU ESCOMPTE): set-up and first results. Boundary Layer Meteorology 114:315-365. CrossRef

Miao S, Chen F, Li Q, Fan S (2010) Impacts of Urban Processes and Urbanization on Summer Precipitation: A Case Study of Heavy Rainfall in Beijing on 1 August 2006. Journal of Applied Meteorology and Climatology 50:806-825

Mills G (2007) Cities as agents of global change. International Journal of Climatology 27:1849–1857. CrossRef

Mirzaei PA, Haghighat F (2010) Approaches to Study Urban Heat Island—Abilities and limitations. Building and Environment 45(10):2192-2201. doi: 10.1016/j.buildenv.2010.04.001

Mishra AK, Rajput P, Singh A, Singh CK, Mall RK (2021) Effect of lockdown amid COVID-19 on ambient air quality in 16 Indian cities. Frontiers in Sustainable cities 3, 705051

Mitra C, Shepherd JM, Jordan T (2012) On the relationship between the premonsoonal rainfall climatology and urban land cover dynamics in Kolkata city, India. International Journal of Climatology 32(9), 1443-1454

Mitra C, Shepherd JM, Jordan T (2012) On the relationship between the premonsoonal rainfall climatology and urban land cover dynamics in Kolkata city, India. International Journal of Climatology 32(9), 1443-1454

Mohammad P, Goswami A (2022) Predicting the impacts of urban development on seasonal urban thermal environment in Guwahati city, northeast India. Building and Environment 226, 109724

Mohammad P, Goswami A, Bonafoni S (2019) The impact of the land cover dynamics on surface urban heat island variations in semi-arid cities: a case study in Ahmedabad City, India, using multi-sensor/source data. Sensors 19(17), 3701

Mohan M, Kikegawa Y, Gurjar BR, Bhati S, Kolli NR (2013) Assessment of urban heat island effect for different land use-land cover from micrometeorological measurements and remote sensing data for megacity Delhi. Theoretical and Applied Climatology 112:648-658

Mohan M, Bhati S (2011) Analysis of WRF model performance over subtropical region of Delhi, India. Advances in Meteorology 2011.

Molders N, Olson MA (2004) Impact of urban effects on precipitation in high latitudes. Journal of Hydrometeorology. 5:409–429

Molnár G, Gyöngyösi AZ, Gál T (2019) Integration of an LCZ-based classification into WRF to assess the intra-urban temperature pattern under a heatwave period in Szeged, Hungary. Theoretical and Applied Climatology 138, 1139-1158

Morakinyo TE, Kong L, Lau KKL, Yuan C, Ng E (2017) A study on the impact of shadow-cast and tree species on in-canyon and neighborhood's thermal comfort. Building and Environment 115, 1-17

More R, Kale N, Kataria G, Rane RA, Deshpande S (2014) Study of the different approaches used to estimate the Urban Heat Island effect in India. J. Multidiscip. Sci. Emerg. Res. 4, 1080–1083

Moreno M (1895) Comparación de los climas de México y Tacubaya [A comparison between the climates of Mexico City and Tucabaya]. In: Memorias de la Sociedad Científica “Antonio Alzate,” Tomo IX. Imprenta del Gobierno Federal, México. Crossref

Morini E, Castellani B, Presciutti A, Filipponi M, Nicolini A, Rossi F (2017) Opticenergy performance improvement of exterior paints for buildings. Energy and Buildings 139, 690–701. https://doi.org/10.1016/j.enbuild.2017.01.060

Morris CJG, Simmonds I (2000) Associations between varying magnitudes of the Urban Heat Island and the synoptic climatology in Melbourbe, Australia. International Journal of Climatology 20:1931-1954

Morris KI, Chan A, Ooi MC, Oozeer MY, Abakr YA, Morris KJK (2016) Effect of vegetation and waterbody on the garden city concept: An evaluation study using a newly developed city, Putrajaya, Malaysia. Computers Environment and Urban Systems 58:39-51.

Mughal MO, Li X, Yin T, Martilli A, Dissegna MA, Norford LK, (2018) Urban climate study using WRF incorporating WUDAPT and remote sensing data in a tropical city. preprints

Mughal MO, Li XX, Norford LK (2020) Urban heat island mitigation in Singapore: Evaluation using WRF/multilayer urban canopy model and local climate zones. Urban Climate 34, 100714

Nadimpalli R, Patel P, Mohanty UC, Attri SD., Niyogi D (2022) Impact of urban parameterization and integration of WUDAPT on the severe convection. Computational Urban Science 2(1), 41

Nakamura Y, Oke TR (1988) Wind, temperature and stability conditions in an east-west oriented urban canyon. Atmospheric Environment (1967), 22(12), 2691-2700. Crossref

Nakayoshi M, Moriyaki R, Kawai T, Kanda M (2009) Experimental study on rainfall interception over an outdoor urban-scale model. Water Resources Research 45(4). doi: 10.1029/2008WR007069. CrossRef

Nanda D, Mishra DR, Swain D (2021) COVID-19 lockdowns induced land surface temperature variability in mega urban agglomerations in India. Environmental Science: Processes & Impacts 23(1), 144-159

Nath B, Ni-Meister W, Choudhury R (2021) Impact of urbanization on land use and land cover change in Guwahati city, India and its implication on declining groundwater level. Groundwater for Sustainable Development 12, 100500

Navinya C, Patidar G, Phuleria HC (2020) Examining effects of the COVID-19 national lockdown on ambient air quality across urban India. Aerosol and Air Quality Research 20(8), 1759-1771

Nikolopoulou M, Vasilikou C (2019); Outdoor thermal comfort for pedestrians in movement: thermal walks in complex urban morphology. International Journal of Biometeorology https://doi.org/10.1007/s00484-019-01782-2

Niyogi D, Pyle P, Lei M, Arya SP, Kishtawal, CM, Shepherd M, Chen F, Wolfe B (2011) Urban modification of thunderstorms: an observational storm climatology and model case study for the Indianapolis urban region. Journal of Applied Meteorology and Climatolology 50:1129–1144. https://doi.org/10.1175/2010JAMC1836.1

Oke T R (1995) The heat island of the urban boundary layer: Characteristics, causes and effects. In: Cermak JE, Davenport AG, Plate EJ, Viegas DX (ed.) Wind climate in cities. Dordrecht: Kluwer Academic 81–107 CrossRef

Oke TR (1978) Surface heat fluxes and the urban boundary layer. WMO Symposium for Boundary-Layer Physics Applied to Specific Problems of Air Pollution, WMO No. 510, Geneva: World Meteorology Organization. 63-70.

Oke TR (1981) Canyon geometry and the nocturnal urban heat island: Comparison of scale model and field observations. International Journal of Climatology 1:237-254. CrossRef

Oke TR (1987) Boundary Layer Climates. Methuen. London and New York.

Oke TR (1988) Street design and urban canopy layer climate. Energy and Buildings 11 (1-3):103-113

Oke TR (1988) The uban energy balance. Progresses in Physical Geography 12(4):471–508.

Oke TR, (1976) The distinction between canopy and boundary-layer heat islands. Atmosphere 14:268–277

Oke TR, (1982) The energetic basis of the urban heat island. Quarterly Journal of the Royal Meteorological Society 108:1–24.

Oke TR (1988) The urban energy balance. Progress in Physical geography, 12(4), 471-508

Oke TR, Mills G, Christen A, Voogt JA (2017) Urban climates. Cambridge University Press

Oke TR (1973) City size and the urban heat island. Atmospheric Environment 7, 769–779

Oke TR (1974) Review of Urban Climatology 1968–1973. WMO Technical Note No. 134, WMO No. 383. World Meteorological Organization, Geneva.

Orville RE, Huffines G, Nielsen-Gammon J, Zhang R, Ely B, Steiger S, Phillips S, Allen S, Read W (2001) Enhancement of cloud-to-ground lightning over Houston, Texas. Geophys. Res. Lett., 28, 2597-2600

Oţoiu A, Grădinaru G (2018). Proposing a composite environmental index to account for the actual state and changes in environmental dimensions, as a critique to EPI. Ecological indicators 93, 1209-1221

Otte TL, Lacser A, Dupont S, Ching JKS (2004) Implementation of an Urban Canopy Parameterization in a Mesoscale Meteorological Model. Journal of Applied Meteorology 43:1648-1665

Pal M, Foody GM (2012) Evaluation of SVM, RVM and SMLR for accurate image classification with limited ground data. IEEE Journal of Selected Topics in Applied Earth Observations and Remote Sensing 5(5), 1344-1355

Papanastasiou DK, Kittas C (2012) Maximum urban heat island intensity in a medium-sized coastal Mediterranean city. Theoretical and Applied Climatology 107(3):407-416 doi: 10.1007/s00704-011-0491-z

Parihar SM, Sarkar S, Dutta A, Sharma S, Dutta T (2013) Characterizing wetland dynamics: a post-classification change detection analysis of the East Kolkata Wetlands using open source satellite data. Geocarto International 28(3), 273-287

Parkes B, Buzan JR, Huber M (2022) Heat stress in Africa under high intensity climate change. International journal of biometeorology 66(8), 1531-1545

Pataki DE, Bowling DR, Ehleringer JR (2003) Seasonal cycle of carbon dioxide and its isotopic composition in an urban atmosphere: Anthropogenic and biogenic effects. Journal of Geophysical Research 108(D23):4735 doi:10.1029/2003JD003865. CrossRef

Patel P, Karmakar S, Ghosh S, Niyogi D (2020) Improved simulation of very heavy rainfall events by incorporating WUDAPT urban land use/land cover in WRF. Urban Climate 32, 100616

Pathirana A, Denekew HB, Veerbeek W, Zevenbergen C, Banda AT (2014) Impact of urban growth driven landuse change on microclimate and extreme precipitation - A sensitivity study. Atmospheric Research 138:50-72

Paul S, Ghosh S, Mathew M, Devanand A, Karmakar S, Niyogi D (2018) Increased Spatial Variability and Intensifcation of Extreme Monsoon Rainfall due to Urbanization. Scientific Reports 8:3918. doi:10.1038/s41598-018-22322-9

Pawe CK, Saikia A (2018) Unplanned urban growth: land use/land cover change in the Guwahati Metropolitan Area, India. Geografisk Tidsskrift-Danish Journal of Geography 118(1), 88-100

Perlewitz P (1890) Über den Einfluss der Stadt Berlin auf deren klimatische Verhältnisse [The influence of the town of Berlin on its climatic conditions]. Das Wetter 6, 97–109. Crossref

Petersen WA, Christian HJ, Rutledge SA (2005) TRMM observations of the global relationship between ice water content and lightning. Geophysical Research Letters 32:2471–2494

Pielke RA (2005) Land Use and Climate Change. Science 310:1625-1626. doi:10.1126/science.1120529

Pigeon G, Zibouche K, Bueno B, Le Bras J, Masson V (2014) Improving the capabilities of the Town Energy Balance model with up-to-date building energy simulation algorithms: an application to a set of representative buildings in Paris. Energy and buildings 76, 1-14

Prata AJ, Caselles V, Coll C, Sobrino JA (1995) Thermal remote sensing of land surface temperature from satellites: Current status and future prospects. Remote Sensing Reviews 12:175–223

Prawin B, Masilamani P, Abdul Rahaman S (2021) Performance assessment of classification algorithms for landuse/landcover change using sentinel 2 data–a case study of tiruppur. The International Archives of the Photogrammetry, Remote Sensing and Spatial Information Sciences 44, 139-142

Qin Z, Karnieli A, Berliner P (2001) A mono-window algorithm for retrieving land surface temperature from Landsat TM data and its application to the Israel-Egypt border region. International journal of remote sensing 22(18), 3719-3746

Rajagopalan P, Lim KC, Jamei E (2014) Urban heat island and wind flow characteristics of a tropical city. Solar Energy 107:159-170. http://hdl.handle.net/10536/DRO/DU:30067915

Ramamurthy P, Bou-Zeid E (2016) Heatwaves and Urban Heat Islands: A Comparative Analysis of Multiple Cities Using a High-Resolution Numerical Model: Heatwaves and Urban Heat Islands. Journal of Geophysical Research: Atmosphere.122. doi:10.1002/2016JD025357

Ramanathan V, Crutzen PJ, Kiehl JT, Rosenfeld D (2001) Aerosols, climate, and the hydrological cycle. Science 294:2119-2124

Ramankutty N, Foley JA, Norman J, McSweeney K (2002) The global distribution of cultivable lands: current patterns and sensitivity to possible climate change. Global Ecology and biogeography 11(5), 377-392

Rana A, Uvo CB, Lars B, Parthsarthi P (2012) Trend analysis for rainfall in Delhi and Mumbai, India,Clim. Dyn.,38,45–56, doi:10.1007/s00382-011-1083-4

Rasheed A (2009) Multiscale Modelling of Urban Climate. Dissertation École Polytechnique Fédérale De Lausanne

Rath SS, Panda J, Sarkar A (2022) Distinct urban land cover response to meteorology in WRF simulated pre-monsoon thunderstorms over the tropical city of Kolkata. Meteorology and Atmospheric Physics 134(4), 76

Ren C, Fung JC, Tse J, Wang R, Wong M, Xu Y, (2017) Implementing WUDAPT product into urban development impact analysis by using WRF simulation result - A case study of the Pearl River Delta Region (1980-2010). The 13th Symposium on Urban Environment 22-26 Jan 2017, Seattle, WA, US

Ren GY, Chu ZY, Chen ZH Ren YY (2003) Implications of temporal change in urban heat island intensity observed at Beijing and Wuhan stations. Geophysical Research Letters 34, L05711; doi:10.1029/2006GL027927

Renou E (1868) Différences de température entre la ville et la campagne [Temperature differences between town and country]. Annuaire, Société Météorologique de France. 16. pp. 83–97. Crossref

Ribeiro I, Martilli A, Falls M, Zonato A, Villalba G (2021) Highly resolved WRF-BEP/BEM simulations over Barcelona urban area with LCZ. Atmospheric Research 248, 105220

Rosenfeld D (2000) Suppression of rain and snow by urban air pollution. Science 287:1793-1796.

Rotach MW, Vogt R, Bernhofer C, et al., (2005) BUBBLE - an urban boundary layer meteorology project. Theoretical and Applied Climatology 81, 231-261. CrossRef

Roth M (2007) Review of urban climate research in (sub) tropical regions. International Journal of Climatology 27:1859–1873

Roth M, Oke TR, Emery W (1989) Satellite-derived urban heat islands from three coastal cities and the utilization of such data in urban climatology. International Journal of Remote Sensing 10(11):1699-1720. doi: 10.1080/01431168908904002

Saaty TL (2001) Fundamentals of the analytic hierarchy process. The analytic hierarchy process in natural resource and environmental decision making, 15-35.

Sachs JD (2001) Tropical underdevelopment. Working paper 8119. NBER Working Paper Series. National Bureau of Economic Research. Cambridge, MA, USA

Salamanca F, Krpo A, Martilli A, Clappier A (2010) new building energy model coupled with an urban canopy parameterization for urban climate simulations—part I. formulation, verification, and sensitivity analysis of the model. Theoretical and Applied Climatology 99 (3–4):331-344. http://dx.doi.org/10.1007/s00704-009-0142-9.

Salamanca F, Martilli A, Yagüe C (2012) A numerical study of the Urban Heat Island over Madridduring the DESIREX (2008) campaign with WRF andan evaluation of simple mitigation strategies. International Journal of Climatology 32:2372-2386. doi: 10.1002/joc.3398

Salamanca F, Zhang Y, Barlage M, Chen F, Mahalov A, Miao S (2018) Evaluation of the WRF-urban modeling system coupled to Noah and Noah-MP land surface models over a semiarid urban environment. Journal of Geophysical Research: Atmospheres 123:2387–2408. https://doi.org/10.1002/2018JD028377

Salamanca F, Martilli A (2010) A new building energy model coupled with an urban canopy parameterization for urban climate simulations—Part II. Validation with one dimension off-line simulations. Theoretical and Applied Climatology 99, 345-356

Salamanca F, Martilli A, Tewari M, Chen F (2011) A study of the urban boundary layer using different urban parameterizations and high-resolution urban canopy parameters with WRF. Journal of Applied Meteorology and Climatology 50(5), 1107-1128

Salata F, Golasi I, de Lieto Vollaro R, de Lieto Vollaro A (2016) Urban microclimate and outdoor thermal comfort. A proper procedure to fit ENVI-met simulation outputs to experimental data. Sustainable Cities and Society 26, 318-343

Sangiorgio V, Fiorito, F, Santamouris M (2020). Development of a holistic urban heat island evaluation methodology. Scientific reports, 10(1), 17913.

Sarmah T, Das S (2018) Urban flood mitigation planning for Guwahati: A case of Bharalu basin. Journal of environmental management 206, 1155-1165

Schmid HP, Cleugh HA, Grimmond CSB, Oke TR, (1991) Spatial variability of energy fluxes in suburban terrain. Boundary Layer Meteorology 54(3):249–276. http://dx.doi.org/10.1007/BF00183956.

Schwarz N, Lautenbach S, Seppelt R (2011) Exploring indicators for quantifying surface urban heat islands of European cities with MODIS land surface temperatures. Remote Sensing of Environment 115:3175–3186

Seino N, Aoyagi T, Tsuguti H (2018) Numerical simulation of urban impact on precipitation in Tokyo: How does urban temperature rise affect precipitation? Urban Climate 23:8-35. http://dx.doi.org/10.1016/j.uclim.2016.11.007

Seto KC, Fragkias M, Güneralp B, Reilly MK (2011) A meta-analysis of global urban land expansion. PloS one 6(8), e23777

Sharma A, Fernando HJS, Hamlet AF, Hellmann JJ, Barlage M, Chen F (2017) Urban meteorological modeling using WRF: a sensitivity study. International Journal of Climatology 37:1885-1900. doi: 10.1002/joc.4819

Shastri H, Paul S, Ghosh S, Karmakar S (2015) Impacts of urbanization on Indian summer monsoon rainfall extremes. J Geophys Res Atmos 120:496–516. doi:10.1002/2014JD022061

Shen H, Huang L, Zhang L, Wu P, Zheng C (2016) Long-term and fine-scale satellite monitoring of the urban heat island effect by the fusion of multi-temporal and multi-sensor remote sensed data: A 26-year case study of the city of Wuhan in China. Remote Sensing of Environment 172:109–125

Shephard JM (2005) A Review of Current Investigations of Urban-Induced Rainfall and Recommendations for the Future. Earth Interactions 9(12)

Shephard JM, Burian SJ (2003) Detection of Urban-Induced Rainfall Anomalies in a Major Coastal City. Earth Interactions 7(4)

Shepherd JM, Pierce H, Negri AJ (2002) Rainfall modification by major urban areas: observations from spaceborne rain radar on the TRMM satellite. Journal of Applied Meteorology 41:689–701

Shepherd, M. (2022). The curious relationship between COVID-19 lockdowns and urban heat islands. Geophysical Research Letters, 49(7), e2022GL098198.

Shiraki Y, Shigeta Y (2013) Effects of Land Surface Temperature on the Frequency of Convective Precipitation in the Tokyo Area. Journal of Geographic Information System 5:303-313

Singh J, Gairola A, Das S, (2015) Numerical Simulation of a Severe Thunderstorm over Delhi Using WRF Model. International Journal of Scientific and Research Publications 5(6)

Siu LW, Hart MA (2013) Quantifying urban heat island intensity in Hong Kong SAR, China. Environmental monitoring and assessment 185, 4383-4398

Skamarock WC, Klemp JB, Dudhia J, Gill DO, Barker DM, Wang W, Powers JG (2005) A description of the advanced research WRF version 2. No. NCAR/TN-468+STR, Mesoscale and Microscale Meteorology Division, National Center for Atmospheric Research, Boulder, CO.

Slezakova K, Pereira MC (2021) 2020 COVID-19 lockdown and the impacts on air quality with emphasis on urban, suburban and rural zones. Scientific reports 11(1), 21336

Smoliak BV, Snyder PK, Twine TE, Mykleby PM, Hertel WF (2015) Dense network observations of the Twin Cities canopy-layer urban heat island. Journal of Applied Meteorology and Climatology 54(9), 1899-1917

Sobel AH (2012) Tropical Weather. Nature Education Knowledge 3(12):2

Solecki W, Seto KC, Marcotullio PJ (2013) It's time for an urbanization science. Environment: science and policy for sustainable development 55(1), 12-17

Song J, Du S, Feng X, Guo L (2014) The relationships between landscape compositions and land surface temperature: quantifying their resolution sensitivity with spatial regression models. Landscape and Urban Planning 123:145-157

Stewart I (2011) A systematic review and scientific critique of methodology in modern urban heat island literature. International Journal of Climatology 31:200–217. doi: 10.1002/joc.2141

Stewart ID, Oke TR (2012) Local Climate Zones for Urban Temperature Studies. Bulletin of the American Meteorological Society doi: 10.1175/BAMS-D-11-00019.1

Stewart ID (2019) Why should urban heat island researchers study history?. Urban Climate 30, 100484

Stewart ID, Oke TR (2012) Local climate zones for urban temperature studies. Bulletin of the American Meteorological Society 93(12), 1879-1900

Streutker DR (2003) Satellite-measured growth of the urban heat island of Houston, Texas. Remote Sensing of Environment 85(3):282-289. CrossRef

Sultana S, Satyanarayana ANV (2019) Impact of urbanisation on urban heat island intensity during summer and winter over Indian metropolitan cities. Environmental monitoring and assessment 191(Suppl 3), 789

Sultana S, Satyanarayana ANV (2023) Impact of land use land cover on variation of urban heat island characteristics and surface energy fluxes using WRF and urban canopy model over metropolitan cities of India. Theoretical and Applied Climatology 152(1-2), 97-121

Sundersingh SD (1991) Effect of heat islands over urban madras and measures for its mitigation Energy and Buildings 15 1–2, 245–252

Swain M, Nadimpalli RR, Mohanty UC, Guhathakurta P, Gupta A, Kaginalkar A, ... Niyogi D (2023) Delay in timing and spatial reorganization of rainfall due to urbanization-analysis over India's smart city Bhubaneswar. Computational Urban Science 3(1), 8

Taha H (1988) Modifying a Mesoscale Meteorological Model to Better Incorporate Urban HeatStorage: A Bulk-Parameterization Approach. Journal of Applied Meteorology 38:466-473

Taha H (1999) Modifying a mesoscale meteorological model to better incorporate urban heat storage: A bulk-parameterization approach. Journal of Applied Meteorology and Climatology 38(4), 466-473

Takane Y, Kikegawa Y, Hara M, et al. (2017) A climatological validation of urban air temperature and electricity demand simulated by a regional climate model coupled with an urban canopy model and a building energy model in an Asian megacity. International Journal of Climatology 37(Suppl.1):1035-105

Tang B, Bi Y, Li ZL, Xia J (2008) Generalized split-window algorithm for estimate of land surface temperature from Chinese geostationary FengYun meteorological satellite (FY-2C) data. Sensors 8(2), 933-951

Tetali S, Baird N, Klima K (2022) A multicity analysis of daytime Surface Urban Heat Islands in India and the US. Sustainable Cities and Society 77, 103568

Thielen J, Wobrock W, Gadian A,Mestayer PG, Creutin J-D (2000) The possible influence of urban surfaces on rainfall development: A sensitivity study in 2D in the meso-gamma scale. Atmospheric Research 54:15–39. CrossRef

Tibrewal K, Venkataraman C (2022) COVID-19 lockdown closures of emissions sources in India: Lessons for air quality and climate policy. Journal of Environmental Management 302, 114079

Toparlar Y, Blocken B, Vos PEJ, van Heijst GJF, Janssen WD, van Hooff T, Montazeri H, Timmermans HJP (2015) CFD simulation and validation of urban microclimate: a case study for Bergpolder Zuid, Rotterdam. Building and Environment 83:79–90. http://dx.doi.org/10.1016/ j.buildenv.2014.08.004

Topolansky M (1924) Der geltungsbereich klimatologischer stationen [The representative area of climatological stations]. Zeitschrift für angewandte Meteorologie 41, 125–128. Crossref

Tran H, Uchihama D, Ochi S, Yasuoka Y (2006) Assessment with satellite data of the urban heat island effects in Asian mega cities. International journal of applied Earth observation and Geoinformation 8(1), 34-48

Tumanov S, Stan-Sion A, Lupu A, Soci C, Oprea C (1999) Influences of the city of Bucharest on weather and climate parameters. Atmospheric Environment 33:4173-4183

Ulpiani G (2021) On the linkage between urban heat island and urban pollution island: Three-decade literature review towards a conceptual framework. Science of the total environment 751, 141727

Unger J (2004) Intra-urban relationship between surface geometry and urban heat island: Review and new approach. Climate Research 27(3):253-264. CrossRef

Unger J, Sümeghy Z, Zoboki J (2001) Temperature cross-section features in an urban area. Atmospheric Research 58(2):117-127. CrossRef

United Nations, Department of Economic and Social Affairs, Population Division (2013). World Population Prospects: The 2012 Revision, Highlights and Advance Tables. Working Paper No. ESA/P/WP.228.

Veena K, Parammasivam KM, Venkatesh TN (2020) Urban Heat Island studies: Current status in India and a comparison with the International studies. Journal of Earth System Science 129, 1-15.

Vittal H, Karmakar S, Ghosh S (2013) Diametric changes in trends and patterns of extreme rainfall over India from pre-1950 to post-1950. Geophys Res Lett 40:3253–3258. doi:10.1002/grl.50631

Voogt JA, Oke TR (1997) Complete Urban Surface Temperatures. Journal of Applied Meteorology 36:1117-1132. https://doi.org/10.1175/1520-0450

Voogt JA, Oke TR (2003) Thermal remote sensing of urban climate. Remote Sensing of Environment 86:370-384

Voogt JA, Oke TR (1997) Complete urban surface temperatures. Journal of applied meteorology 36(9), 1117-1132

Wan Z (1999) MODIS land-surface temperature algorithm theoretical basis document, Version 3.3. NASA Documents. Website address: http://modis.gsfc.nasa.gov/atbd/ atbd_mod11.pdf.

Wang X, Gao P, Song C, Cheng C (2020) Use of entropy in developing SDG-based indices for assessing regional sustainable development: A provincial case study of China. Entropy 22(4), 406.

Wang Y, Yu W, Fang Z (2020) Multiple kernel-based SVM classification of hyperspectral images by combining spectral, spatial, and semantic information. Remote Sensing 12(1), 120

Weng Q, Lu D, Schubring, J (2004) Estimation of land surface temperature-vegetation abundance relationship for urban heat island studies. Remote Sensing of Environment 89:467–483

Weng Q (2009) Thermal Remote Sensing of Urban Climate and Environmental Studies: Methods, Applications, and Trends. ISPRS Journal of Photogrammetry and Remote Sensing 64, 335-344 https://doi.org/10.1016/j.isprsjprs.2009.03.007

Wong NH, Yu C (2005) Study of green areas and urban heat island in a tropical city. Habitat International 29:547–558

Xu X, Chen F, Shen S, Miao S, Barlage M, Guo W, Mahalov A (2018) Using WRF-Urban to Assess Summertime Air ConditioningElectric Loads and Their Impacts on Urban Weather in Beijing. Journal of Geophysical Research: Atmospheres. doi: 10.1002/2017JD028168

Xu Y, Ren C, Cai M, Wang R (2018) Issues and challenges of remote sensing–based local climate zone mapping for high-density cities. IEEE 978-1-5090-5808-2/17

Xu Y, Ren C, Ma P, Ho J, Wang W, Lau K, Lin H, Ng E, (2017) Urban morphology detection and computation for urban climate research. Landscape and Urban Planning 167:212 – 224

Xu H (2008) A new index for delineating built-up land features in satellite imagery. International journal of remote sensing 29(14), 4269-4276

Xu X, Chen F, Shen S, Miao S, Barlage M, Guo W, Mahalov A (2018) Using WRF-urban to assess summertime air conditioning electric loads and their impacts on urban weather in Beijing. Journal of Geophysical Research: Atmospheres 123(5), 2475-2490

Yan Y, Sun Y, Tian P, Li J (2022) Spatio-Temporal Variation of Economic Drivers of Urban Heat Island Effect in Yangtze River Delta. Frontiers in Marine Science 9, 877301

Yang L, Qian F, Song DX, Zheng KJ (2016) Research on urban heat-island effect. Procedia engineering 169, 11-18

Yin Z, Liu Z, Liu X, Zheng W, Yin L (2023) Urban heat islands and their effects on thermal comfort in the US: New York and New Jersey. Ecological Indicators 154, 110765

Yokoyama H, Ooka R, Kikumoto H (2018) Study of mobile measurements for detailed temperature distribution in a high-density urban area in Tokyo. Urban Climate 24:517-528

Yoo C, Han D, Im J, Bechtel B (2019) Comparison between convolutional neural networks and random forest for local climate zone classification in mega urban areas using Landsat images. ISPRS Journal of Photogrammetry and Remote Sensing 157, 155-170

Zhang D, Shou Y, Dickerson RR, Chen F (2011) Impact of Upstream Urbanization on the Urban Heat Island Effects along the Washington–Baltimore Corridor. Journal of Applied Meteorology and Climatology doi: 10.1175/JAMC-D-10-05008.1

Zhang Y, Zhang J, Zhang X, Zhou D, Gu Z (2020) Analyzing the characteristics of UHI (Urban heat island) in summer daytime based on observations on 50 sites in 11 LCZ (local climate zone) types in Xi'an, China. Sustainability 13(1), 83

Zhong S, Qian Y, Zhao C, Leung R,Yang X-Q (2015) A case study of urbanization impact on summerprecipitation in the Greater Beijing MetropolitanArea: Urban heat island versus aerosol effects Journal of Geophysical Research: Atmosphere 120:10,903-10,914, doi: 10.1002/2015JD023753

Zhong H, Zhang P, Li Y, Yang X, Zhao Y, Wang Z (2020) Highly Solar-Reflective Structures for Daytime Radiative Cooling under High Humidity. ACS Applied Materials & Interfaces, 12(46), 51409–51417. https://doi.org/10.1021/acsami.0c14075

Zhong S, Yang XQ (2015) Mechanism of urbanization impact on a summer cold-frontal rainfall process in the greater Beijing metropolitan area. Journal of Applied Meteorology and Climatology 54(6), 1234-1247

Zhou D, Zhao S, Zhang L, Sun G, Liu Y (2015) The footprint of urban heat island effect in China. Scientific Reports 5(11160). doi: 10.1038/srep11160

Zhou L, Dickinson RE, Tian Y, Fang J, Li Q, Kaufmann RK, Tucker CJ, Myneni RB (2004) Evidence for a significant urbanization effect on climate in China. Proceedings of the National Academy of Sciences of the United States of America 10(26):9540-9544. doi: 10.1073/pnas.0400357101

Zhou G (2020) Urban High-Resolution Remote Sensing: Algorithms and Modeling. CRC Press

Zhou X, Yamamoto M, Yan S, Ishida Y, Cai M, Ji Q, Makvandi M, Li C (2022) Exploring the impacts of heat release of vehicles on urban heat mitigation in Sendai, Japan using WRF model integrated with urban LCZ. Sustainable Cities and Society 82 103922

Zhu XX, Qiu C, Hu J, Shi Y, Wang Y, Schmitt M, Taubenböck H (2022) The urban morphology on our planet–Global perspectives from space. Remote Sensing of Environment 269, 112794.

Zou ZH, Yi Y, Sun JN (2006) Entropy method for determination of weight of evaluating indicators in fuzzy synthetic evaluation for water quality assessment. Journal of Environmental sciences 18(5), 1020-1023

APPENDICES

Appendix 3.1a: Confusion Matrix for LCZ Kolkata

	LCZ 1	LCZ 2	LCZ 3	LCZ 4	LCZ 5	LCZ 6	LCZ 7	LCZ 8	LCZ 9	LCZ 10	LCZ A	LCZ B	LCZ C	LCZ D	LCZ E	LCZ F	LCZ G
LCZ 1	**0**	0	0	0	0	0	0	0	0	0	0	0	0	0	0	0	0
LCZ 2	0	**0.42**	0.2	0.07	0.06	-	0.01	0.01	-	0.05	-	0.01	0.02	0.15	-	-	-
LCZ 3	0.01	0.27	**0.59**	-	0.01	0	0.01	0.01	0	0	-	-	0	0.06	0.04	-	-
LCZ 4	-	0.02	-	**0.6**	-	-	-	-	-	-	0.21	0.16	-	-	0.11	-	-
LCZ 5	-	0.17	-	-	**0.7**	-	-	-	-	-	-	0.02	-	0.08	0.03	-	-
LCZ 6	-	0.01	-	-	0	**0.6**	-	-	-	-	-	0.03	0.34	0.03	-	-	-
LCZ 7	-	0	0	0	0	0	**0.1**	0	0	0	0	0	0	0	0	0	0
LCZ 8	-	0.01	0.09	-	0.01	0	0.01	**0.64**	-	0.01	-	0	0.02	0.13	0.04	0.04	-
LCZ 9	-	-	-	-	-	-	-	0.1	**0.74**	-	-	-	0.01	0.15	-	-	-
LCZ 10	-	0.07	0.03	-	-	-	-	0.07	-	**0.75**	-	-	-	0.01	0.06	0.01	-
LCZ A	-	-	-	-	-	0	-	-	-	-	**0.91**	0.05	0.05	0	-	-	-
LCZ B	-	-	-	-	-	-	-	-	-	-	0.43	**0.56**	0.1	0	-	-	-
LCZ C	-	0	-	-	-	0	-	-	0	-	0.01	0.02	**0.9**	0.07	0	-	-
LCZ D	-	-	-	-	-	0	0	-	0	0	0.06	0.01	0.04	**0.85**	-	0.05	-
LCZ E	-	0.05	0.03	-	-	-	0.01	0.01	-	0.04	-	-	-	0.08	**0.7**	0.09	-
LCZ F	-	-	-	-	-	-	-	-	-	-	-	-	-	0.13	-	0.87	-
LCZ G	-	0.15	-	-	-	-	-	-	-	0	-	-	0	0	0.02	0	**0.87**

Appendix 3.1b: Confusion Matrix for LCZ Guwahati

	LCZ 1	LCZ 2	LCZ 3	LCZ 4	LCZ 5	LCZ 6	LCZ 7	LCZ 8	LCZ 9	LCZ 10	LCZ A	LCZ B	LCZ C	LCZ D	LCZ E	LCZ F	LCZ G
LCZ 1	**0**	0	0	0	0	0	0	0	0	0	0	0	0	0	0	0	0
LCZ 2	0	**0.64**	0.15	-	0.13	-	0	-	-	0	0	-	-	0.06	0.01	-	-
LCZ 3	0	0.25	**0.61**	-	0.1	-	0	0	-	-	-	-	-	0	0.03	-	-
LCZ 4	0	0	0	**0**	0	0	0	0	0	0	0	0	0	0	0	0	0
LCZ 5	-	0.01	-	-	**0.96**	-	-	-	-	-	-	-	-	0.03	-	-	-
LCZ 6	-	-	-	-	-	**0.66**	-	-	-	-	-	0.03	0.31	-	-	-	-
LCZ 7	0	0	0	0	0	0	**0**	0	0	0	0	0	0	0	0	0	0
LCZ 8	-	0.01	0.14	-	-	-	0	**0.76**	-	-	-	-	-	0	0.03	0.06	-
LCZ 9	-	-	-	-	-	-	-	-	**0.77**	-	-	0.01	0.02	0.21	-	-	-
LCZ 10	0	0	0	0	0	0	0	0	0	**0**	0	0	0	0	0	0	0
LCZ A	-	-	-	-	-	-	-	-	-	-	**0.93**	0.02	0.05	0	-	-	-
LCZ B	-	-	-	-	-	-	-	-	-	-	0.23	**0.67**	0.1	-	-	-	-
LCZ C	-	-	-	-	-	-	-	-	-	-	0.01	0.02	**0.93**	0.04	-	-	-
LCZ D	-	-	-	-	-	-	-	-	-	-	0.03	0.01	0.05	**0.88**	0	0.04	-
LCZ E	-	0.03	-	-	-	-	-	-	-	0.02	-	-	0.02	0.22	**0.69**	0.02	-
LCZ F	-	-	-	-	-	-	-	-	-	-	-	-	-	0.07	-	**0.93**	-
LCZ G	-	0.1	-	-	-	-	-	-	-	-	-	-	0	-	-	0.05	**0.85**

Appendix 3.2: LCZ-wise Urban Roughness Parameters

UCP/LCZ	LCZ-2 CMR	LCZ-3 CLR	LCZ-5 OMR	LCZ-6 OLR	LCZ-8 LLR	LCZ-9 SB
Urban Fraction	0.90	0.90	0.75	0.65	0.65	0.40
Vegetation Fraction	0.10	0.10	0.25	0.35	0.35	0.60
Avg. Building Height (m)	16.5	10	16.5	6.5	4	4
Avg. Road Width (m)	8	8	15	8	8	6

	LCZ-2 CMR	LCZ-3 CLR	LCZ-5 OMR	LCZ-6 OLR	LCZ-8 LLR	LCZ-9 SB
Surface Albedo						
Road **Roof** **Wall**	0.15	0.14	0.12	0.16	0.16	0.17
Thermal Conductivity						
Road	0.70	0.70	0.70	0.70	0.70	0.70
Roof	1.04	1.01	1.20	1.01	1.24	1.01
Wall	1.02	1.01	1.10	1.02	1.20	1.01
Heat Capacity						
Road	$1.95\text{-}10^6$	$1.98\text{-}10^6$	$1.95\text{-}10^6$	$1.98\text{-}10^6$	$1.94\text{-}10^6$	$1.95\text{-}10^6$
Roof	$1.97\text{-}10^6$	$1.97\text{-}10^6$	$1.97\text{-}10^6$	$1.97\text{-}10^6$	$1.97\text{-}10^6$	$1.97\text{-}10^6$
Wall	$1.63\text{-}10^6$	$1.62\text{-}10^6$	$1.72\text{-}10^6$	$1.62\text{-}10^6$	$1.86\text{-}10^6$	$1.61\text{-}10^6$
Emissivity						
Road	0.93	0.93	0.93	0.93	0.93	0.93
Roof	0.91	0.92	0.87	0.92	0.86	0.92
Wall	0.92	0.93	0.90	0.93	0.87	0.93

Appendix 4.1: Gridded average daily T_2 and RF 4 different time periods (1989, 1999, 2009 and 2019) over (a.) KMA and (b.) GMA regions.

(a.)

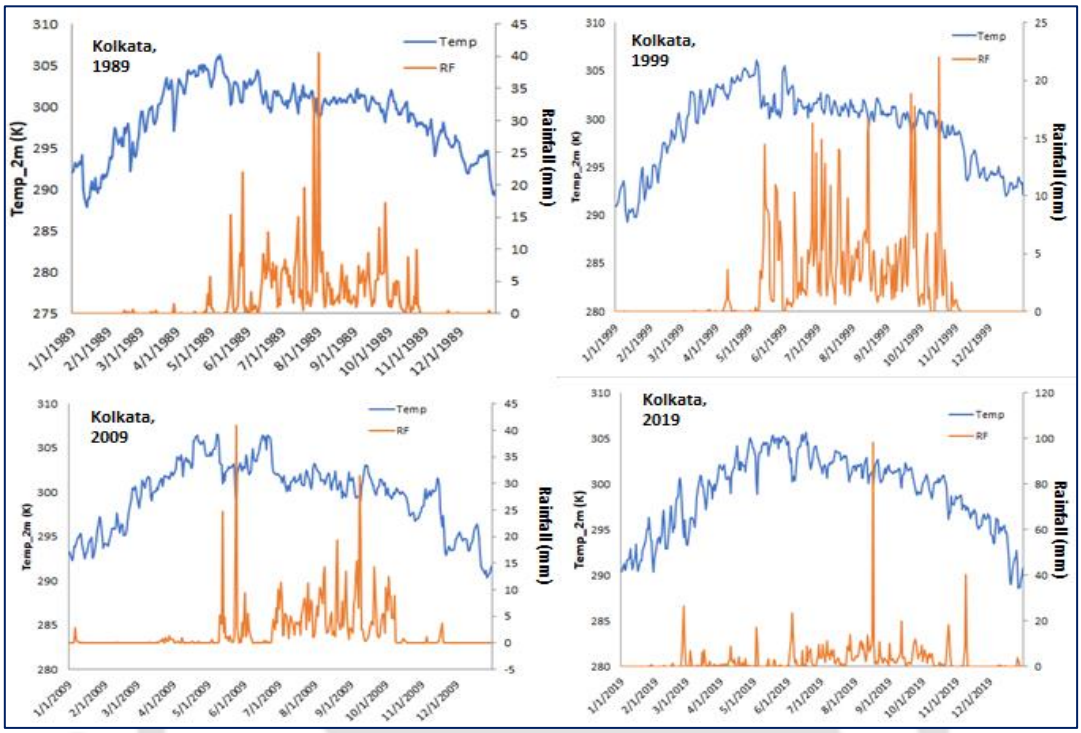

(b)

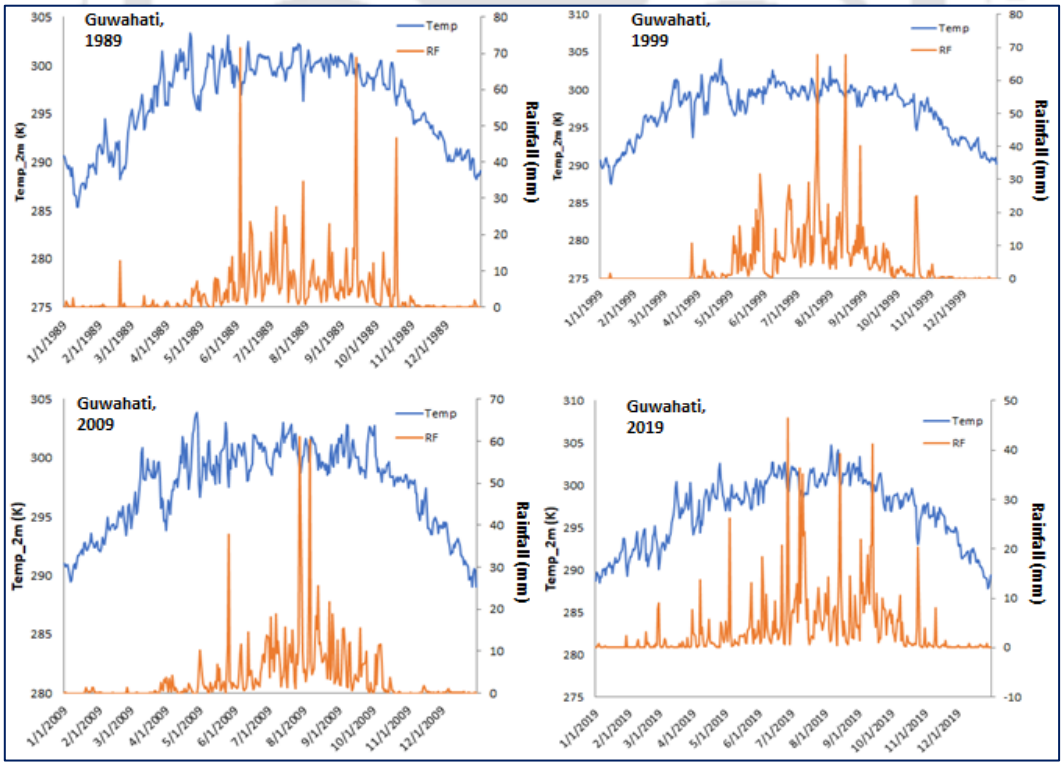

Data Source: European Center for Medium Range Weather Forecast (ECMWF) ERA5 – Land Reanalysis datasets at 9 km grid Resolution

LIST OF PUBLICATIONS

Research articles published:

1. **Bhattacharjee, S.,** Lekshmi, K., and Bharti, R. (2023). Evidences of localized coastal warming near major urban centres along the Indian coastline: past and future trends. Environmental Monitoring and Assessment. https://doi.org/10.1007/s10661-023-11214-9

2. **Bhattacharjee, S.**, Lekshmi, K., and Bharti, R. (2023). Time-series analysis of urbanization impact on the temperature variations off Mumbai coast. International Society of Photogrammetry and Remote Sensing Archives. https://doi.org/10.5194/isprs-archives-XLIII-B3-2021-31-2021

Research articles under review:

3. **Bhattacharjee, S.**, and Bharti, R., (2023). Distinct urban land cover response to the micro-meteorology of tropical cities with coupled WRF-LCZ simulations.
4. **Bhattacharjee, S.**, and Bharti, R., Application of geospatial techniques and entropy-based multi-criteria analysis to assess the eco-environment changes in a complex urban system
5. **Bhattacharjee, S.**, and Bharti, R., Exploring the meteorological impacts of different heat mitigation strategies over a dense tropical city.

Research articles to be submitted:

6. **Bhattacharjee, S.**, and Bharti, R., Impact of the increase in urban sprawls on the overall climatology of two morphologically different cities in India (*Manuscript ready).*
7. **Bhattacharjee, S.**, and Bharti, R., WRF simulated high resolution urban climate Index to analyse the meteorological health of cities (*Manuscript under preparation)*
8. **Bhattacharjee, S.**, and Bharti, R., A systematic analysis of Urban Microclimatic studies: a climatic zone perspective (*Manuscript under preparation*)

International Conferences:

1. **Bhattacharjee, S.**, and Bharti, R., Evaluating the micro-climate of two morphologically different Indian cities with coupled WRF-LCZ model during monsoon season; International Conference on Urban Climate, 2023 (Oral Presentation)

2. **Bhattacharjee, S.**, and Bharti, R., Intra-urban morphological heterogeneity and its impact on the micro-climatic variations in the Kolkata Metropolitan region of India, EGU General Assembly 2023 (Oral Presentation)

3. **Bhattacharjee, S.**, and Bharti, R., Estimation and prediction of UHI in relation to spatial variations in urban green spaces and built-up intensity using machine learning techniques, SPIE REMOTE SENSING, 2022 (Oral Presentation)

4. **Bhattacharjee, S.**, and Bharti, R., Analysing surface and atmospheric UHI of two topographically and morphologically different cities in India, GRSS/ISPRS - JOINT URBAN REMOTE SENSING EVENT (JURSE), 2022 (Oral Presentation)

5. **Bhattacharjee, S.,** Lekshmi, K., and Bharti, R., Time series analysis of urbanization impact on the temperature variations off Mumbai coast, XXIVth ISPRS Congress, 2021

6. **Bhattacharjee, S.**, and Bharti, R., The impact of covid-19 lockdown on the urban micro-climate of major coastal vs. inland cities of india, EGU General Assembly 2021